The University Of Sheffield.

Extracellular matrix stiffness and chemoresistance in breast cancer.

By: Emma Jane Grant

A thesis submitted in partial fulfilment of the requirements for the degree

of

Doctor of Philosophy

The University of Sheffield

Faculty of Science

Department of Chemistry

September 2020

Table of contents.

Acknowledgements.

I would first like to thank my two PhD supervisors; Dr Helen Bryant and Dr Barbara Ciani for their continued help and support throughout my PhD, but most particularly during my final year where both a worldwide pandemic and diagnosis of a personal chronic illness have challenged my ability to complete my PhD. Without their help, support, guidance and understanding I would not have been able to complete this work. I would also like to thank the EPSRC for the funding of this project which made it possible for me to undertake this work.

I would like to thank Dr Pete Laity, Dr Nick Peake, Dr Frederik Claeyssens and Dr Jose Ricardo Aguilar Cosme for their help and extensive expertise in the development and measurement of the *in vitro* models used in this thesis. I would also like to thank the two masters students I supervised; Lucy Ginn and Manpreet Barj for the work they have contributed towards the project.

I would not have been able to complete the work in this thesis without the friendship and support of my fellow Bryant and Ciani lab members and also members of the Collis and Thompson lab groups. Special mentions go to Rachel, Callum, Leona, Polly, Katie, Fatma, Ola, Tom, Natasha and Chris for whom the PhD would've been much less enjoyable or bearable without.

Finally, I must thank my parents and family for their continuous support and love, and Marcus for everything. I couldn't have done it without you.

Abstract.

Chemoresistance poses a great barrier in breast cancer treatment. During tumorigenesis tissue stiffness increases but the relevance of this to chemotherapy response is not fully known. We hypothesised that stiffness may influence the efficacy of chemotherapy, and that modulating stiffness and the pathways involved may be novel targets for cancer cell killing. To first investigate this, we developed a two-dimensional (2D) polyacrylamide *in vitro* stiffness model for growth of breast cancer cell lines. We observed that cell growth and size was increased at higher stiffnesses. Also increased at higher stiffnesses were the levels of replication stress and DNA damage. Interestingly, of the 8 chemotherapeutic agents tested, a differential response was only observed for one agent, gemcitabine. Resistance to gemcitabine was observed at higher stiffnesses in only 2 of the 7 breast cancer cell lines investigated, MCF-7 and T-47D. They share a common factor of progesterone receptor (PR) expression. Pre-treatment with the PR inhibitor mifepristone abolished resistance to gemcitabine at higher stiffnesses. We confirmed our findings in a three-dimensional (3D) alginate *in vitro* stiffness model. Combined treatment with PR inhibitors may therefore help in reducing resistance to gemcitabine in stiffer breast tumours which are PR positive.

List of figures.

List of tables.

Declaration.

I, the author, confirm that the Thesis is my own work. I am aware of the University's Guidance on the Use of Unfair Means (www.sheffield.ac.uk/ssid/unfair-means). This work has not previously been presented for an award at this, or any other, university.

Abbreviations.

2D	Two-dimensional
3-APTMS	3-Aminopropyl-trimethoxysilane
3D	Three-dimensional
5-FU	5-Fluorouracil
ABC transporters	ATP-binding cassette transporters
AF 1-3	Activating function domains 1-3
Akt	Protein kinase B
APS	Ammonium persulphate
ATCC	American Type Culture Collection
ATR	Ataxia telangiectasia and Rad3 related
Bcl-2	B-cell lymphoma 2
Bcl-xL	B-cell lymphoma-extra large
BRCA	Breast cancer susceptibility gene
BrdU	5-Bromo-2'-deoxyuridine
BSA	Bovine serum albumin
CaM	Calmodulin
CldU	5-Chloro-2'-deoxyuridine
CTPS	Cytidine triphosphate synthetase
DAPI	4',6-Diamidino-2-phenylindole
DBD	DNA binding domain
dCDA	Deoxycytidine deaminases
DCIS	Ductal carcinoma in situ
dCK	Deoxycytidine kinase
ddH_2O	Ultra-pure deionised water
dFdCDP	Gemcitabine diphosphate
dFdCMP	Gemcitabine monophosphate
dFdCTP	Gemcitabine triphosphate
dFdU	Difluorodeoxyuridine
dFdUMP	2’2’-Difluorodeoxyuridine monophosphate
DIAPH1	Diaphanous homolog 1
DMEM	Dulbecco's Modified Eagle Medium
DMSO	Dimethyl sulphoxide
dNTP	Deoxyribonucleotide
DSMZ	Deutsche Sammlung von Mikroorganismen und Zellkulturen
E-cadherin	Epithelial cadherin
ECL	Enhanced chemiluminescence
ECM	Extracellular matrix
EDTA	Ethylenediaminetetraacetic acid
EdU	5-Ethynyl-2'-deoxyuridine
EGFR	Epidermal growth factor receptor
EMT	Epithelial to mesenchymal transition
ER (ERα)	Oestrogen receptor alpha
ERBB2/HER2	Human epidermal growth receptor-2
ERK	Extracellular signal-related kinase

FA	Focal adhesion
FAK	Focal adhesion kinase
FCS	Foetal calf serum
GAPDH	Glyceraldehyde 3-phosphate dehydrogenase
GEF	Guanine exchange factors
Gemcitabine/dFdC	2',2'-Difluorodeoxycytidine
H	Hinge domain
H3K27ac	Histone H3 acetylation at K27
H3K4me3	Histone H3 trimethylation at K4
H3K9me3	Histone H3 trimethylation at K9
HEPES	4-(2-Hydroxyethyl)-1-piperazineethanesulphonic acid
HIPE	High internal phase emulsion
HRP	Horse radish peroxidase
HSP	Heat shock protein
HU	Hydroxyurea
IBC	Invasive breast cancer
IdU	5-Iodo-2’-deoxyuridine
IF	Immunofluorescence
IMS	Industrial methylated spirits
IPH	Immunophilins
IR	Ionising radiation
LAD	Lamina associated domain
LBD	Ligand binding domain
LINC	Linker of nucleoskeleton and cytoskeleton
LOX	Lysyl oxidase
MAPK	Mitogen-activated protein kinase
MBC	Metastatic breast cancer
MBS	Myosin-binding subunit
MGMT	O^6-methylguanine-DNA methyltransferase
MLC	Myosin light chain
MLCK	Myosin light chain kinase
MMC	Mitomycin C
MMP	Matrix metalloproteinase
MN	Micronuclei
MP	Myosin phosphatase
mPR	Membrane associated progesterone receptor
mTOR	Mammalian target of rapamycin
NEAA	Non-essential amino acids
NSCLC	Non-small cell lung cancer
NTPs	Ribonucleotides
OD	Optical density
Pa	Pascals
PARP	Poly (ADP-ribose) polymerase
PAX	Paclitaxel
PBS	Phosphate buffered saline
PCR	Polymerase chain reaction

PEG	Polyethylene glycol
PGR	Progesterone receptor gene
pH3	Phosphorylated histone 3
PI3K	Phosphoinositide 3-kinase
PIPES	Piperazine-N,N′-bis(2-ethanesulphonic acid)
PMSF	Phenylmethanesulphonyl fluoride
PR	Progesterone receptor
PRE	Progesterone responsive element
pRPA	Phosphorylated replication protein A
RANKL	Receptor activator of nuclear factor kappa-B ligand
RGD ligands	Arginine-glycine-aspartic acid ligands
Rho A	Ras homolog gene family member A
RIPA	Radioimmunoprecipitation assay
Rn	Normalised reporter value
RNR	Ribonucleotide reductase
ROCK	Rho-associated coiled coil-containing protein kinase
ROX	6-Carboxyl-rhodamine
RPA	Replication protein A
RPM	Revolutions per minute
RPMI	Roswell Park Memorial Institute
RT-q-PCR	Reverse transcriptase quantitative polymerase chain reaction
SD	Standard deviation
SDS	Sodium dodecyl sulphate
SEM	Standard error of the mean
ssDNA	Single stranded DNA
STAT3	Signal transducer and activator of transcription 3
Sulfo-SANPAH	Sulphosuccinimidyl 6-(4′-azido-2′-nitrophenylamino)hexanoate
TAZ	Transcriptional co-activator with PDZ binding motif
TBS	Tris-buffered saline
TBS-T	0.05% v/v Tween-20 in TBS
TCP	Tissue culture plastic
TEAD	Transcriptional enhanced associated domain
TEMED	Tetramethylethylenediamine
TK2	Thymidine kinase 2
TNBC	Triple negative breast cancer
TRP	Transient receptor potential
TS	Thymidylate synthase
UV	Ultraviolet
VE-cadherin	Vascular endothelial cadherin
VEGFR	Vascular endothelial growth receptor
WB	Western blotting
WBP-2	WW domain binding protein-2
wt	Wild type
YAP	Yes kinase-associated protein
γH2AX	Phosphorylated H2A histone family member X

1. Introduction.

1.1. Breast cancer.

In women, breast cancer is the leading cause of cancer deaths responsible for 15% of all 4.2 million female cancer deaths in 2018 (Bray et al., 2018). It is the most commonly diagnosed cancer in women, accounting for 24.2% of all newly diagnosed female cancers (Bray et al., 2018). Although the use of hormone receptor targeting agents has led to large improvements in survival in the last few decades, current breast cancer treatments are still not adequate and more specific therapy may improve treatment success.

1.1.1. Breast cancer subtypes.

Breast cancer is divided into several subtypes, the three major subtypes are based on the presence or absence of hormone receptors; oestrogen receptor alpha (ER/ERα), PR and human epidermal growth factor receptor-2 (ERBB2/HER2) (Waks & Winer, 2019). The majority of breast cancers (70%) are classified as the hormone receptor (ER and PR) positive but ERBB2 negative subtype. The remaining 30% are halved with 15% classified as the ERBB2 positive subtype and 15% classified as triple negative breast cancer (TNBC) (not expressing ER, PR or ERBB2) (Waks & Winer, 2019). TNBCs show a poorer prognosis with a higher chance of recurrence, where 5-year survival rates for stage 1 tumours are 85% vs 94% and over in the other two subtypes (Waks & Winer, 2019).

The receptor positive subtypes can be further sub-divided into luminal A and B molecular subtypes. Luminal A is classified as being ER and/or PR positive but ERBB2 negative and shows low levels of cell proliferation (Fragomeni et al., 2018). Whereas luminal B shows higher levels of cell proliferation and is ER and/or PR positive but can also be ERBB2 positive or negative (Fragomeni et al., 2018).

Receptor positivity is quantified clinically via immunohistochemical staining, where tumour samples with 1-100% of cells staining positive for ER or PR classified as positive (Allison et al., 2020). Staining for PR is optional however, where it is mainly used for prognostic purposes (Allison et al., 2020). PR positivity is most commonly seen alongside ER positivity where 55% of 138,322 breast cancers were ER+/PR+/ERBB2− and 9.9% were ER+/PR+/ERBB2+ (Parise & Caggiano, 2014). However, there are a small proportion of breast cancers which are PR positive and ER negative where 0.79% of 138,322 breast cancers are ER−/PR+/ERBB2− and 0.41% were ER−/PR+/ERBB2+ (Parise & Caggiano, 2014).

Receptor positive breast cancers typically respond well to specific endocrine therapy. Both ER and PR act as transcription factors which affect the expression of genes, leading to downstream signalling that results in increased tumorgenicity. Typically, treatment is directed towards the ER, via the use of specific inhibitors such as tamoxifen, owing to the large percentage of breast cancers that are ER positive (80%). In contrast PR receptors are present in 55-60% of all breast cancers (Fragomeni et al., 2018), but to date inhibition of these receptors is not used clinically in breast cancer treatment. However, clinical trials are currently underway for PR inhibition as a monotherapy (ClinicalTrials.gov, 2020). With a large proportion of breast cancers being PR positive it is clear that use of PR inhibitors may improve treatment for many patients.

ERBB2 is a tyrosine kinase receptor which contributes to increased cellular proliferation and survival through the mammalian target of rapamycin (mTOR) and mitogen-activated protein kinase (MAPK) pathways. ERBB2 positive breast cancer patients are typically

responsive to targeted therapy in the form of trastuzumab and pertuzumab, monoclonal antibodies targeting the receptor (Fragomeni et al., 2018).

TNBC and cancers that have become resistant to targeted therapies are for the most part treated with conventional chemotherapy which is discussed in section 1.3.1.

This thesis investigates tissue stiffness and breast cancer response to chemotherapy. In this regard the PR has been linked to stiffness responses and therefore will be discussed in detail below.

1.1.2. Development of breast cancer.

Development of cancer occurs due to the influence of genetic and environmental factors. In normal cells growth is controlled but is derailed in cancers due inheritance of genetic defects in certain genes or through damage and mutation of DNA by environmental factors. Five to 10 percent of breast cancers occur due to inherited gene mutations (Feng et al., 2018). Examples include mutations in breast cancer susceptibility (BRCA) 1 and 2 genes where those with a mutation have a 70% chance of developing breast cancer in their lifetime (Feng et al., 2018). Environmental factors include; age, weight and lifestyle factors.

Proto-oncogenes genes, such as *MYC,* are often switched on in breast cancer (Berns et al., 1995) which promotes cell growth and drives cell cycle progression. Tumour suppressor genes such *TP53* are often switched off in breast cancer (Shahbandi, Nguyen, & Jackson, 2020). This prevents the induction of programmed cell death in the

event of high levels of replication stress and DNA damage, to allow for uncontrolled cell growth. Increased cell growth can also be promoted via hormone receptors (Lee et al., 2019; Louie & Sevigny, 2017).

In the breast, epithelial cells are arranged into ducts, which deliver milk and lobules, which produce milk. They are surrounded by extracellular matrix (ECM) tissue. Breast cancer types include ductal carcinoma in situ (DCIS), invasive breast cancer (IBC) and metastatic breast cancer (MBC). In DCIS the epithelial cells which line the breasts ducts become cancerous and cells infiltrate the lumen of the ducts. When the cancerous cells leave the ducts or lobules and spread to other parts of the breast IBC is developed. MBC is developed once the cancerous cells invade other tissues within the body (Feng et al., 2018). Alongside changes to epithelial cells, the surrounding tissue of the breast is also modified, where increased production of matrix components and modification to these components leads to stiffening and tissue degradation to facilitate the availability of nutrients to aid cancer survival (Cox & Erler, 2011).

1.1.3. Progesterone receptors and breast cancer.

The lack of direct targeting of the PR, despite its prevalence in breast cancer, indicates it as a key area of development for future treatments. Inhibitors of the PR are currently in clinical trials as a monotherapy (ClinicalTrials.gov, 2020), indicating the potential for use as a future treatment regimen. The PR acts as a transcription factor which modulates the expression of progesterone responsive genes in the classical pathway but also plays a role in other pathways in a non-classical role as detailed further below.

1.1.3.1. Progesterone receptor gene and protein structure.

The PR gene, *PGR*, is comprised of 8 exons (Figure 1.1.a) and is located in chromosome 11 (Misrahi et al., 1993). From the gene two main PR isoforms are transcribed, PR-A and PR-B. The transcription start sites for both these isoforms are within the first exon, where the PR-A site is downstream of B as indicated in Figure 1.1.a. A third less common isoform, PR-C, has been observed in pregnancy (Taylor, McParland, Taylor, & Bell, 2009) but its presence as a naturally occurring isoform in the breast or breast cancer is not well determined. It is also encoded by the *PGR* gene and it s transcription start site is located within the second exon (Rękawiecki, Kowalik, & Kotwica, 2011). A schematic of the protein structure of these isoforms is shown in Figure 1.1.b. PR-B is the largest isoform (116 kDa in humans) (Wei, Norris, & Baker, 1997). It contains a ligand binding domain (LBD) which facilitates progesterone binding, a DNA binding domain (DBD) which facilitates DNA binding to progesterone responsive elements (PRE), 3 transcription activating function domains (AF-1-3) which bind transcriptional activators required for promotor activation and also modulate receptor dimerization and a hinge (H) which provides flexibility but also plays a role in DNA binding (Hill, Roemer, Churchill, & Edwards, 2012; Rękawiecki et al., 2011). PR-A is 94 kDa protein (Wei et al., 1997) that is similar to PR-B apart from a truncation at the N-terminus that results in lack of AF-3. PR-C is a 60 kDa protein (Wei et al., 1997) which lacks the DBD, AF-1 and AF-3 but retains its LBD and H (Hill et al., 2012).

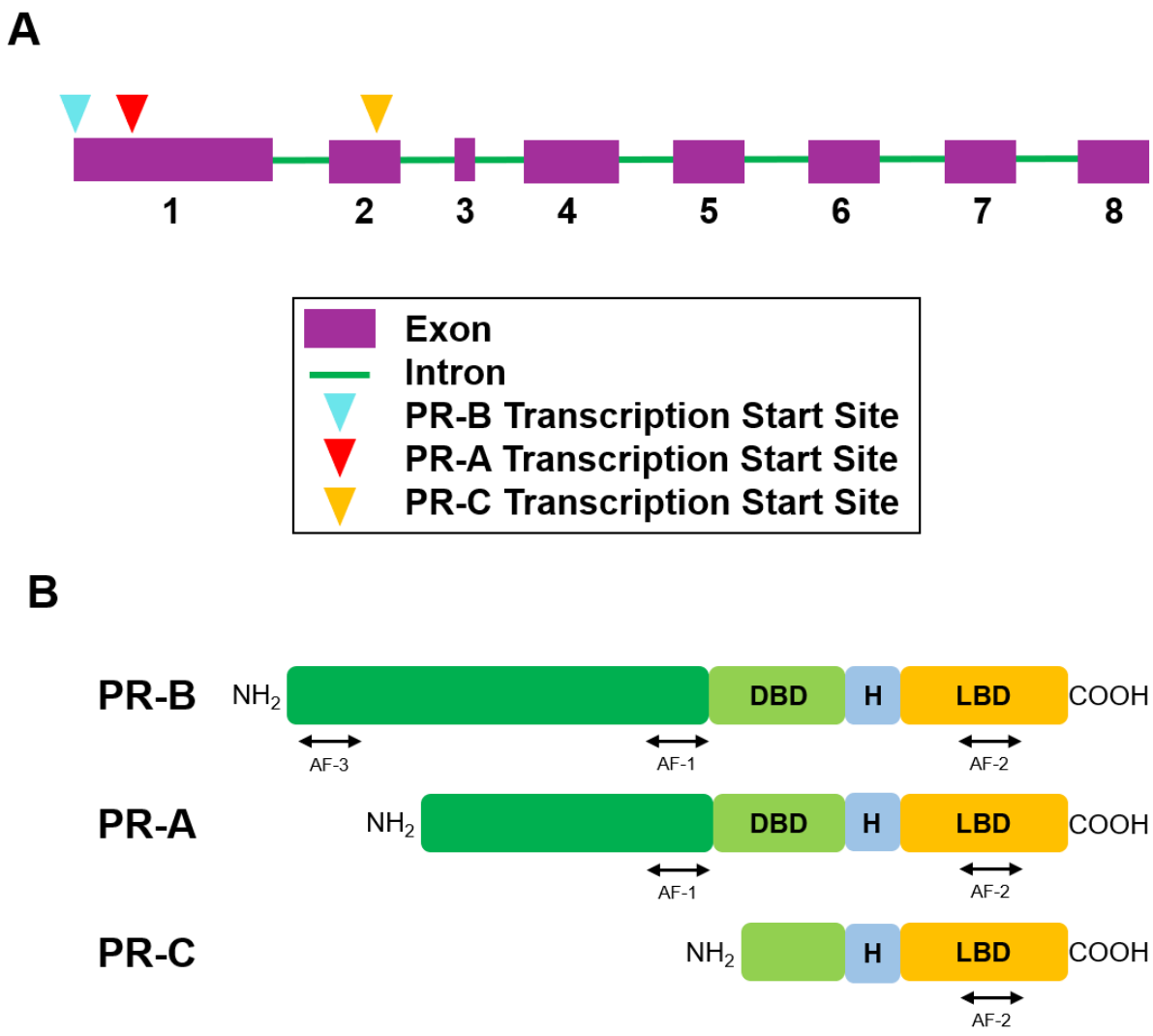

Figure 1.1. The human progesterone receptor gene and protein isoforms. (A) Schematic of the human progesterone receptor gene (*PGR*). The general location of the transcription start sites of the three isoforms are indicated. (B) Protein structure of the three progesterone receptor isoforms derived from the transcripts. The N (NH_2) and C (COOH) terminals are indicated. The B and A isoforms both contain a DNA binding domain (DBD), a hinge (H) and a ligand binding domain (LBD) as indicated. The C isoform only contains the LBD and the H. The activation function domains (AF1-3) are also indicated.

PR isoform modulation of different downstream targets can be attributed to the to the AF-3 domain, which is present in PR-B but not PR-A. AF-3 is required for PR-B interaction with co-activators and other ligands required for target gene modulation (Tung et al., 2006). It is thought that this difference in the N-terminal structure of the two isoforms

contributes to their differential binding to different DNA sequences in PREs or to different translational co-activators or repressors (Jacobsen & Horwitz, 2012).

1.1.3.2. Classical progesterone receptor pathway.

PR-A and B can form hetero and homodimers (A:B, A:A and B:B) (Jacobsen & Horwitz, 2012). The function or dimerization ability of PR-C is not well defined. PR-A and B are expressed in equimolar amounts within normal tissue (Mote, Bartow, Tran, & Clarke, 2002) as such it is predicted that PR dimers are composed of 25% A:A, 25% B:B and 50% A:B (Jacobsen & Horwitz, 2012). The different dimerization combinations provide diversity in the downstream response, although this is not well defined for A:B and is understood more for homodimers from cell lines expressing a singular isoform (Richer et al., 2002). Dimerization occurs upon binding of progesterone and displacement of chaperone proteins (Figure 1.2.) (Demarzo, Beck, Onate, & Edwards, 1991). This allows for binding to PRE and transcription of downstream genes with the help of co-activators (Rękawiecki et al., 2011). PR has been found to upregulate the expression of several proteins including c-Src, MAPK/cyclin D1, Wnt-1, epidermal growth factor receptor (EGFR) (Faivre & Lange, 2007), receptor activator of nuclear factor kappa-B ligand (RANKL) (Trabert, Sherman, Kannan, & Stanczyk, 2020), $p21^{cip1/WAF1}$ (Diaz Flaqué et al., 2013) and signal transducer and activator of transcription (STAT3) (Proietti et al., 2005), highlighting the proliferative impact of PR signalling.

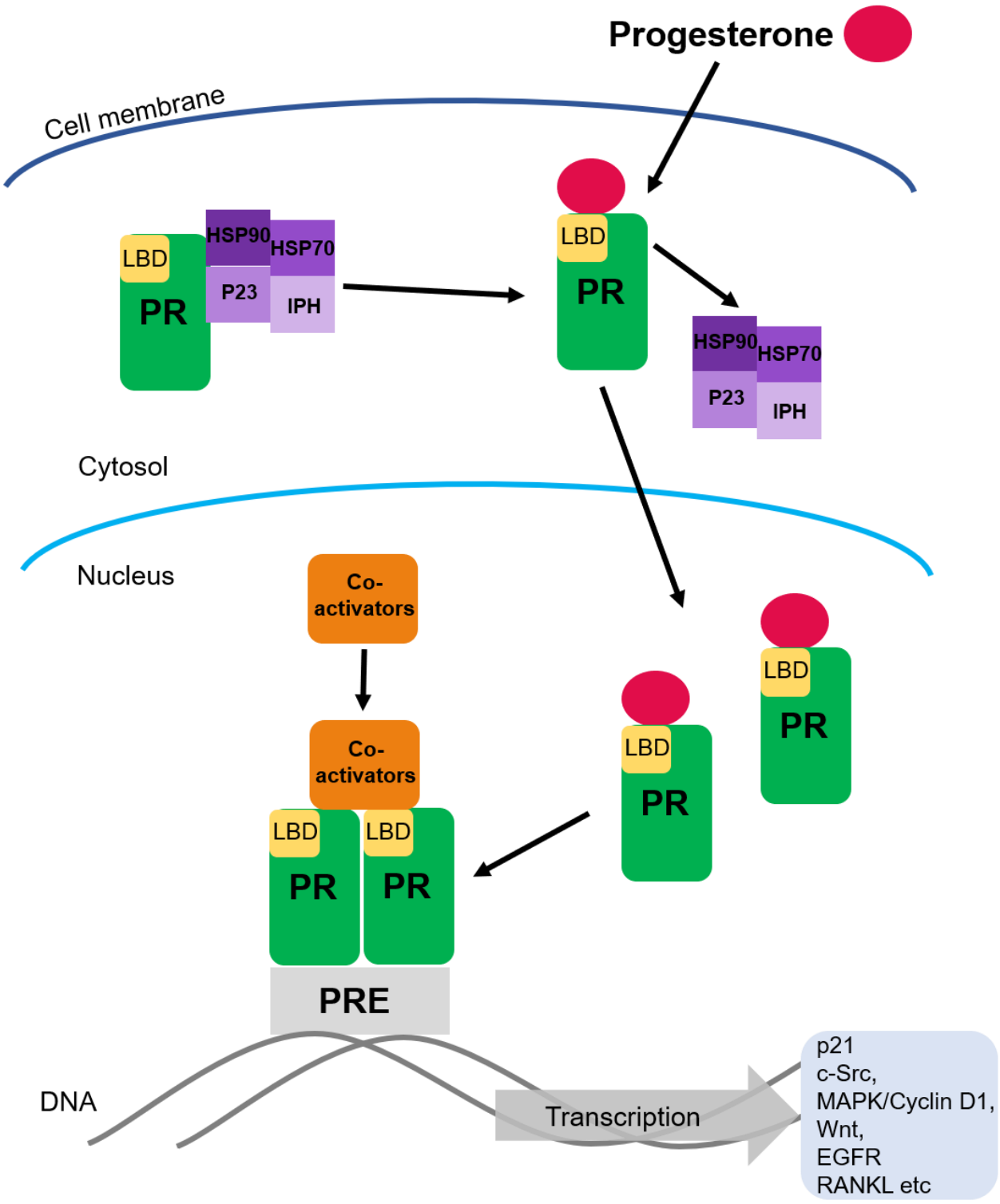

Figure 1.2. The classical PR pathway. The progesterone receptor (PR) remains inactive within the cytoplasm when bound to its chaperone proteins; heat shock proteins (HSP) 90 and 70, p23 and immunophilins (IPH). Upon progesterone binding to PR at its ligand binding domain (LBD) the chaperone proteins are displaced, and the progesterone-PR complex can translocate to the nucleus. Here it forms dimers with other progesterone bound PR and then binds to DNA at progesterone responsive elements (PRE). Co-activators bind to PR allowing for promotor activation and gene transcription.

1.1.3.3. Progesterone receptor regulation and deregulation in breast cancer.

The two PR isoforms are differentially regulated through expression from two different promoters (Kastner et al., 1990). PR expression is regulated by ER (Lim, Palmieri, & Tilley, 2016) owing to the presence of oestrogen response elements and binding sites of other ER interacting transcription factors within the PR promoters (Jacobsen & Horwitz, 2012). ER regulation of PR isoforms is also varied between BC cell lines (Vienonen, Syvälä, Miettinen, Tuohimaa, & Ylikomi, 2002), indicating the complexities of PR regulation. ER regulation of PR is a well-known feature of breast cancer and as such the presence of PR is often used to predict response to ER hormone therapies. However, ER-/PR+ breast cancers are a known subtype, which are more aggressive and show a poorer prognosis (Rakha et al., 2007). Therefore, PR expression is not only controlled by ER and phenotypes of breast cancer such as these constitute a significant treatment issue. With relevance here, it has been observed that WW domain binding protein-2 (WBP-2) and Yes kinase-associated protein (YAP) are factors that can co-activate expression of PR (Dhananjayan et al., 2006). YAP functions as a stiffness sensor, therefore we can suggest that stiffness may contribute to modulation of PR expression. PR levels can also be also be modulated at the protein level through various post translational modifications (Jacobsen & Horwitz, 2012).

The expression of PR isoforms A and B are also regulated by the presence of progesterone (Misao, Nakanishi, Iwagaki, Fujimoto, & Tamaya, 1998; Rękawiecki et al., 2011). High levels of progesterone induce expression of PR-A, which inhibits PR-B expression. The opposite expression pattern is observed with low levels of progesterone. This balance is thought to modulate the effects of progesterone, as PR-B has a higher level of transcriptional activity able to induce proliferative capacity compared to PR-A. As such PR-B is thought to increase more progesterone signalling in comparison to PR-A

(Conneely, Mulac-Jericevic, Lydon, & De Mayo, 2001; Kariagina, Aupperlee, & Haslam, 2008). In the normal breast PR-A and B are expressed in equimolar amounts. However, in cancer the expression ratio is often shifted, with a higher PR-A to B ratio due to reduction in PR-B levels (Graham et al., 2005). Whilst PR-B is thought of as a proliferative driver including its specific induction of cyclin D1 expression, (Boonyaratanakornkit et al., 2007), PR-A is thought to contribute to the aggressive nature of breast cancers through alterations in the expression of cell-cell and cell-matrix proteins (Graham et al., 2005) and through upregulation of anti-apoptotic proteins such as B-cell lymphoma-extra large (Bcl-xL) (Richer et al., 2002).

1.1.3.4. Non-classical functions.

Secondary to the function of the PR as a transcription factor, other non-classical PR functions have been established. These include membrane associated PRs (mPRs) signalling to downstream pathways in the cell, non-genomic signalling by PR to other cell signalling pathways and potential mechanical modulation of PR (Garg, Ng, Baig, Driggers, & Segars, 2017). Some of these pathways are observed to be activated in breast cancer, for example, c-Src and EGFR are over expressed in breast cancer and are associated with breast cancer development (Biscardi, Ishizawar, Silva, & Parsons, 2000). The activation of both is observed by non-classical PR functions. PR is reported to activate c-Src in a rapid, non-genomic method independent of transcriptional activation (Boonyaratanakornkit et al., 2001). Here, PRs rapidly activate c-Src through displacement of its SH3 domain which leads to downstream activation of MAPK. Secondly, a mPR has been reported to stabilise EGFR and thus maintain its functions in growth control within cancer cells (including breast) (Ahmed, Rohe, Twist, & Craven, 2010).

Of relevance to this study, non-classical PR signalling has been linked to tissue stiffness. Progesterone signalling is thought to be connected to a non-classical pathway leading to production of ECM components. Treatment of rats with progesterone reduced production of fibronectin and laminin but maintained levels of collagen III expression (Shynlova, Mitchell, Tsampalieros, Langille, & Lye, 2004). Secondly Shynlova et al., (2004) reported that increased ECM tension was correlated with increased production of basal membrane components but decreased progesterone, although the mechanisms surrounding this are uncharacterised. Whilst this has been observed primarily in the uterus it may extend to changes in the stiffness of other tissues and highlights a link between ECM tension, progesterone signalling and synthesis of ECM components.

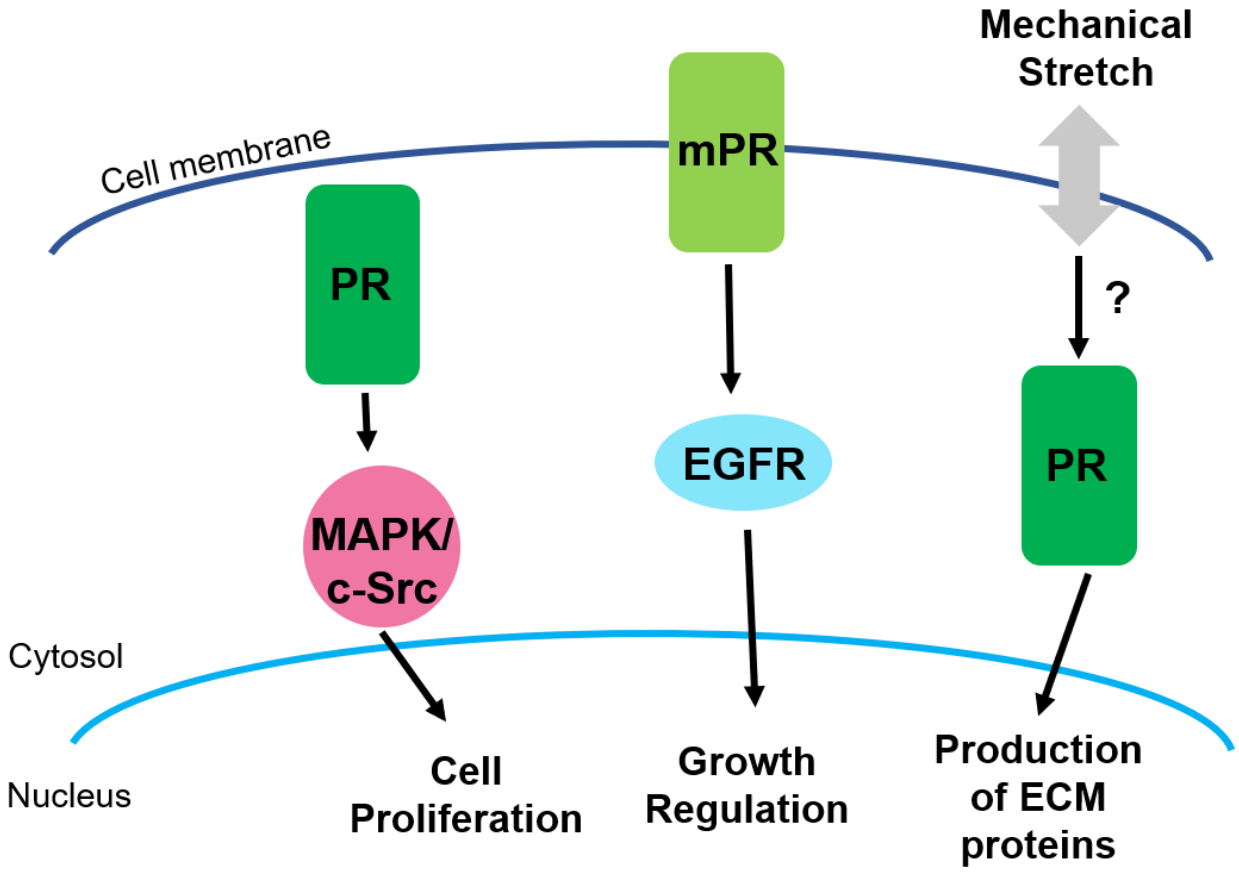

Figure 1.3. Non-classical functions of the PR. Schematic representation of some of non-classical functions mediated by PR. Cytoplasmic PR has been shown to directly activate c-Src and downstream MAPK signalling through displacement of c-Src SH3 domains. PR signalling has also been linked to changes in the expression of ECM proteins and may also be modulated by changes in tension. Membrane bound PRs (mPR) are reported to stabilise epidermal growth factor receptor (EGFR) in the membrane and thus allow for maintained EGFR signalling.

1.2. The extracellular matrix.

1.2.1. Components of the extracellular matrix.

The non-cellular component of tissues is termed the ECM. It is comprised of various classes of glycosaminoglycans such as hyaluronan and fibrous proteins such as collagens and elastins which vary greatly between tissues and during development (Bruce et al., 2002). These components provide mechanical structure and a biochemical network for communication between cells and the ECM. The majority of these components are secreted by fibroblast cells which reside within the ECM. The ECM is not

a static entity; it is remodelled by specific enzymes including matrix metalloproteinases (MMPs) and serine proteases (Theocharis, Skandalis, Gialeli, & Karamanos, 2016). The ECM can be categorised into two distinct subtypes; the basement membrane and the interstitial matrix (Figure 1.4.).

The basement membrane interacts directly with cells and is located between epithelial cells and the surrounding stroma (Bonnans, Chou, & Werb, 2014). It is composed of a collagen IV network and other ECM components including laminins which facilitate epithelial cell – ECM interactions. Cells which are in contact with the basement membrane form physical contacts with the ECM including focal adhesions (FAs) and hemidesmosomes. These structures are facilitated through integrins, transmembrane proteins which interact intracellularly with actin filaments in FAs and with intermediate filaments in hemidesmosomes.

The interstitial matrix is composed of collagen fibrils, other proteins such as elastin and fibroblasts which secrete ECM components. Both subgroups contain collagens, with them being the main component of the interstitial matrix (Theocharis et al., 2016). All higher order collagen structures are composed of collagen α-helical chains which combine to form a triple helix (Shoulders & Raines, 2009). Not all collagens arrange in the same structures, allowing different collagens to provide different structural properties to different matrices. The fibrillar collagens, including types I, II, III, V and XI, combine collagen triple helices into sheet like collagen fibrils which are strengthened and stiffened by crosslinking of collagen molecules (Buehler, 2006). Crosslinking of collagens is facilitated by lysyl oxidases (LOX) which also crosslink other ECM components (Frantz, Stewart, & Weaver, 2010). These collagen fibrils are then tightly packed into rope like collagen fibres. Another

type of collagen formation is the network forming collagens which includes types IV and X. These types have interruptions in their α-helical chains and form into dimers and then tetramers. This results in formation of loosely packed networks which are mesh like in appearance (Theocharis et al., 2016). Alongside collagens, two other distinct groups of ECM fibres exist. Elastins associate with collagens and provide recoil function to a tissue. The third group are fibronectins which organise the ECM and aid in attachment of cells to the ECM. Fibronectin is also a force responsive fibre whereby it can undergo force induced unfolding resulting in exposure of binding sites facilitating signalling pathways (Smith et al., 2007).

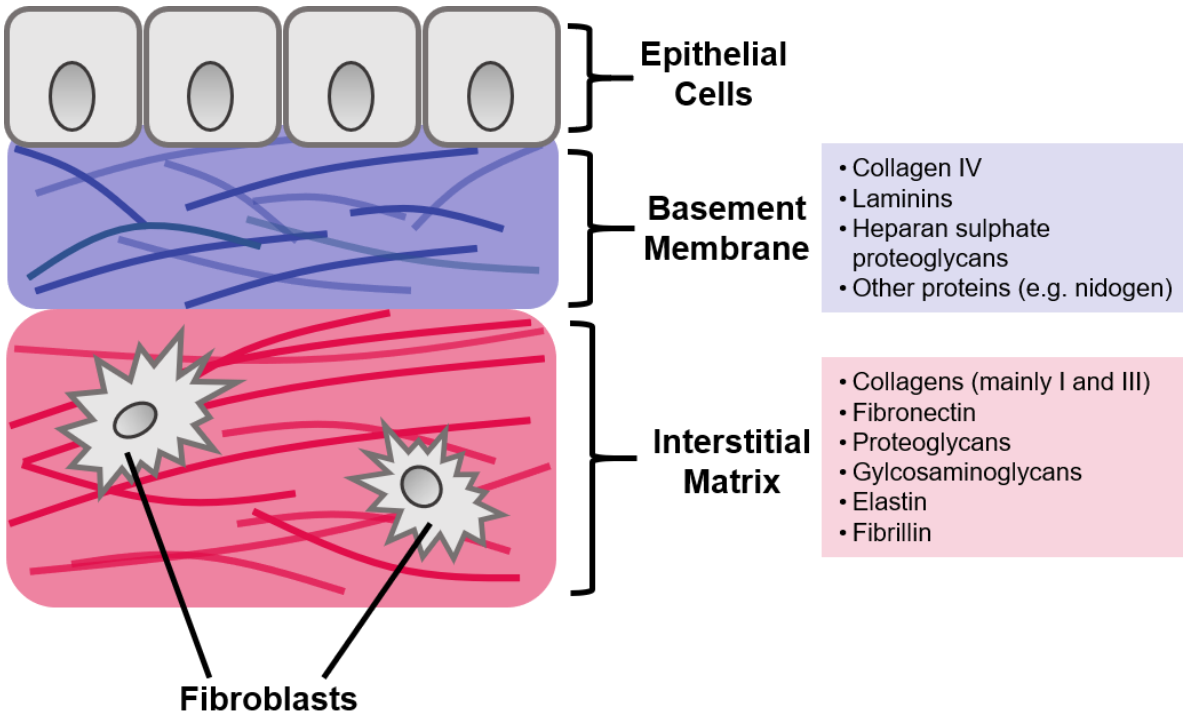

Figure 1.4. Overview of the extracellular matrix. The extracellular matrix is defined as the non-cellular component of tissues and occurs in two distinct forms; basement membrane which occurs directly adjacent to epithelial cells and the interstitial or stromal matrix which surrounds the basement membrane.

1.2.2. ECM stiffness.

1.2.2.1. Stiffness in human tissues.

Maintaining a homeostatic environment within a tissue requires dynamic conversation between epithelial cells and the cells which reside within the surrounding interstitial matrix. This includes fibroblasts which excrete ECM components allowing ECM modulation. This fine tuning of ECM content and structure provides an important balance of tension within the tissue. In glandular tissues, such as the breast, the tensional homeostasis is that of a compliant nature where the breast has an elastic modulus somewhere in the region of 100-200 Pascals (Pa) (Paszek et al., 2005). Firmer tissues such as muscle have a higher elastic modulus of around 5-12 kPa (Butcher, Alliston, & Weaver, 2009) and the skin is around 420-850 kPa (Agache, Monneur, Leveque, & De Rigal, 1980). More rigid structures such as the bone have a much higher stiffness within the range of Giga Pa (Zysset, Guo, Hoffler, Moore, & Goldstein, 1999).

A mechanically compliant tissue is much more resilient to increases in tension, as the network of fibrous proteins within the interstitial matrix are formed into a relaxed structure with limited crosslinking. This is important as tension within the ECM is transduced to localised cells influencing intracellular stiffness. In cancer however, stiffness is often heightened where breast stiffness is increased from 100-200 Pa to ~4 kPa (Paszek et al., 2005). Thus suggesting that treatment tailored towards increased ECM stiffness may be a key therapeutic window in specific treatment of cancer vs normal cells. Note that it is likely that significant patient heterogeneity exists (Plodinec et al., 2012), but this has not been extensively studied.

1.2.2.2. ECM stiffness measurements.

In order to determine the stiffness of matrix, a force needs to be applied to allow the viscous and elastic properties to be established. If a substance is completely elastic the energy of the force applied will be completely stored within the substance and then released completely with no deformation of the substance. If a substance is completely viscous however, the sample will deform when a force is applied to it and retain this deformation using the energy applied for movement (Janmey, Georges, & Hvidt, 2007). The directional application of force allows different information about a substance to be determined (Figure 1.5.a-c). In biological systems an application of shear stress, parallel to the surface of the substance is often used (Figure 1.5.a) as it closely mimics the pressures encountered by cells and tissues exerted by fluids flowing along membranes (Janmey et al., 2007).

Two key rheological terms are stress: the force applied per unit area and strain: the measurable deformation of the substance. The relationship between stress and strain provides information about a substance's modulus. It is measured in Pascals and is used to indicate a materials' stiffness. Due to the elastic nature of hydrogels, the majority of stiffness values are reported as elastic moduli, which is calculated as detailed in Figure 1.5.d.

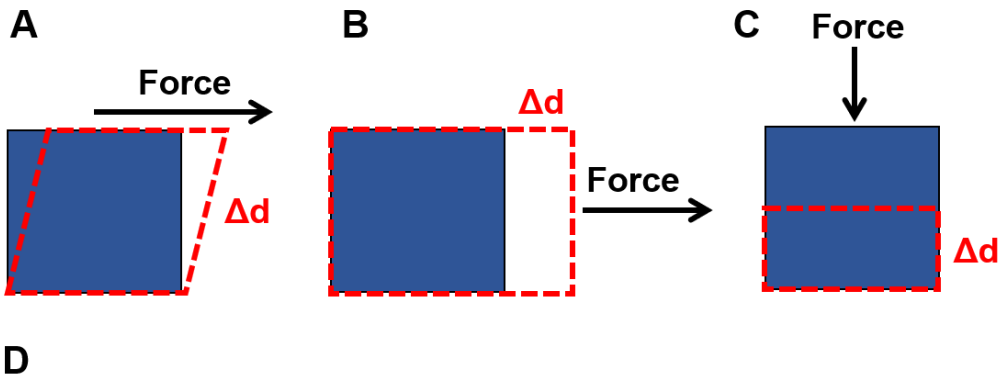

$$Elastic\ Modulus = Stress/Strain$$

Figure 1.5. Measuring stiffness. (A) Application of a shear force as depicted deforms the object Δd and allows calculation of a shear modulus. (B) Application of a tensile force as indicated deforms the object Δd and allows calculation of a tensional modulus. (C) Application of a compressive force as indicated deforms the object Δd and allows calculation of a compressive modulus. (D) Calculation of elastic modulus from the stress (applied force) and the measured strain (deformation).

In human studies, breast cancer stiffness is measured whilst the tumour is *in situ* and therefore a non-invasive measurement is used such as ultrasound (Chen et al., 2019), elastography (L. Huang, Ma, Du, Liu, & Gong, 2019) or through area and deformation calculations (Boyd et al., 2014). Breast density is sometimes used as a comparative measurement for stiffness. However, it has recently been reported that tissue stiffness shows no correlation to density in breast tissue (Chen et al., 2019).

1.2.2.3. ECM stiffness alters cellular phenotype.

In cancer increased stiffness is often observed and changes in local stiffness have been observed to modulate many cellular phenotypes, including the hallmarks of cancer. This is known as mechanotransduction, the communication of stiffness from the matrix into localised cells. Both physical and chemical connections are involved as is summarised in Figure 1.6. The matrix is physically tethered to the cell and the nucleus through integrins,

actin stress fibres and the linker of nucleoskeleton and cytoskeleton (LINC) complexes (Figure 1.6.a). The nuclear lamina are directly connected to the LINC complex and DNA at lamina attachment domains (LADs) (Shevelyov & Ulianov, 2019). Forces applied to the ECM have been shown to propagate through actin stress fibres at a rapid speed which can result in physical rearrangements of DNA and changes in gene expression (Tajik et al., 2016).

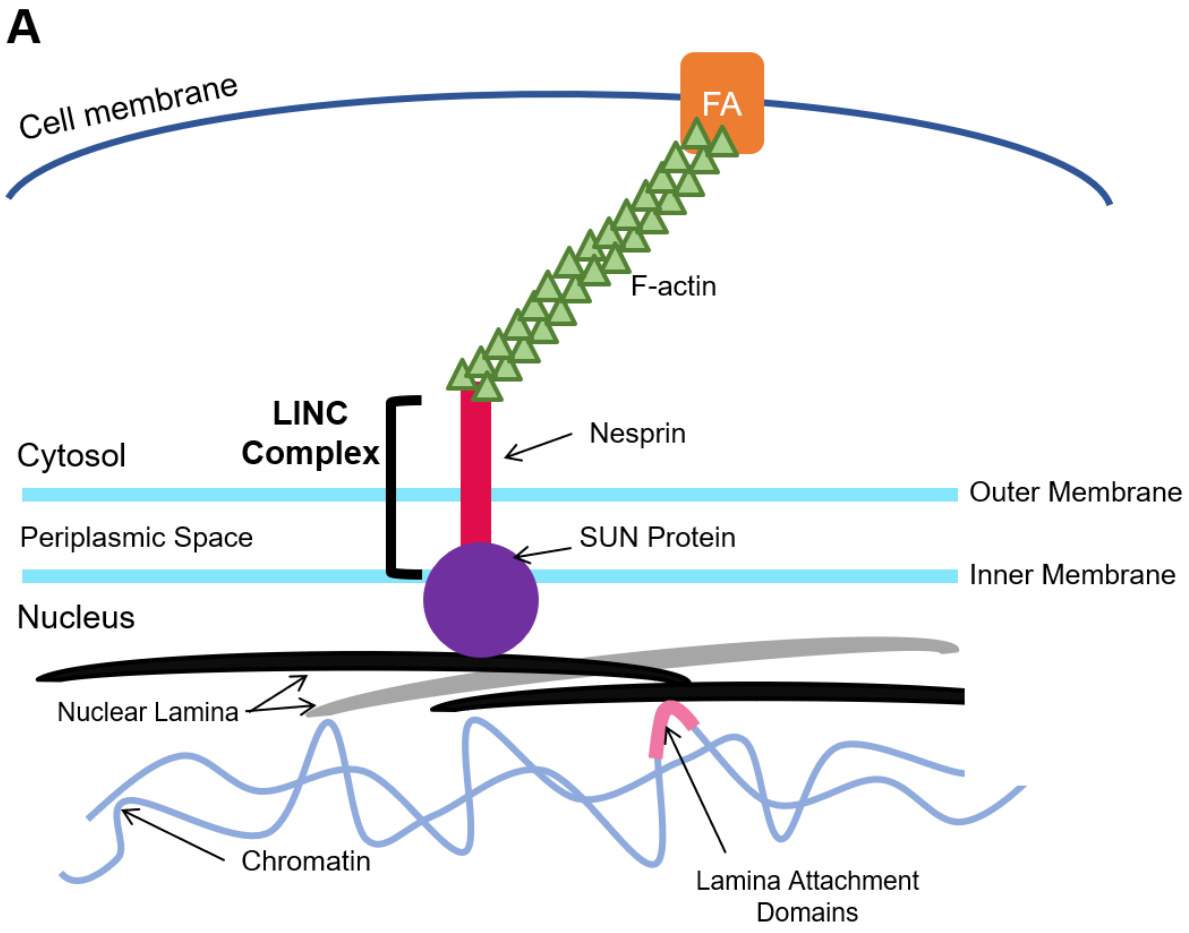

Figure 1.6. Key mechanotransduction pathways. Legend overleaf.

Biochemical pathways are activated following increased FA formation which results in formation of stress fibres. FA signalling activates downstream signalling pathways resulting in further transduction of stiffness as is summarised in Figure 1.6.b. These changes result in modifications to cell phenotype as discussed in the following sections.

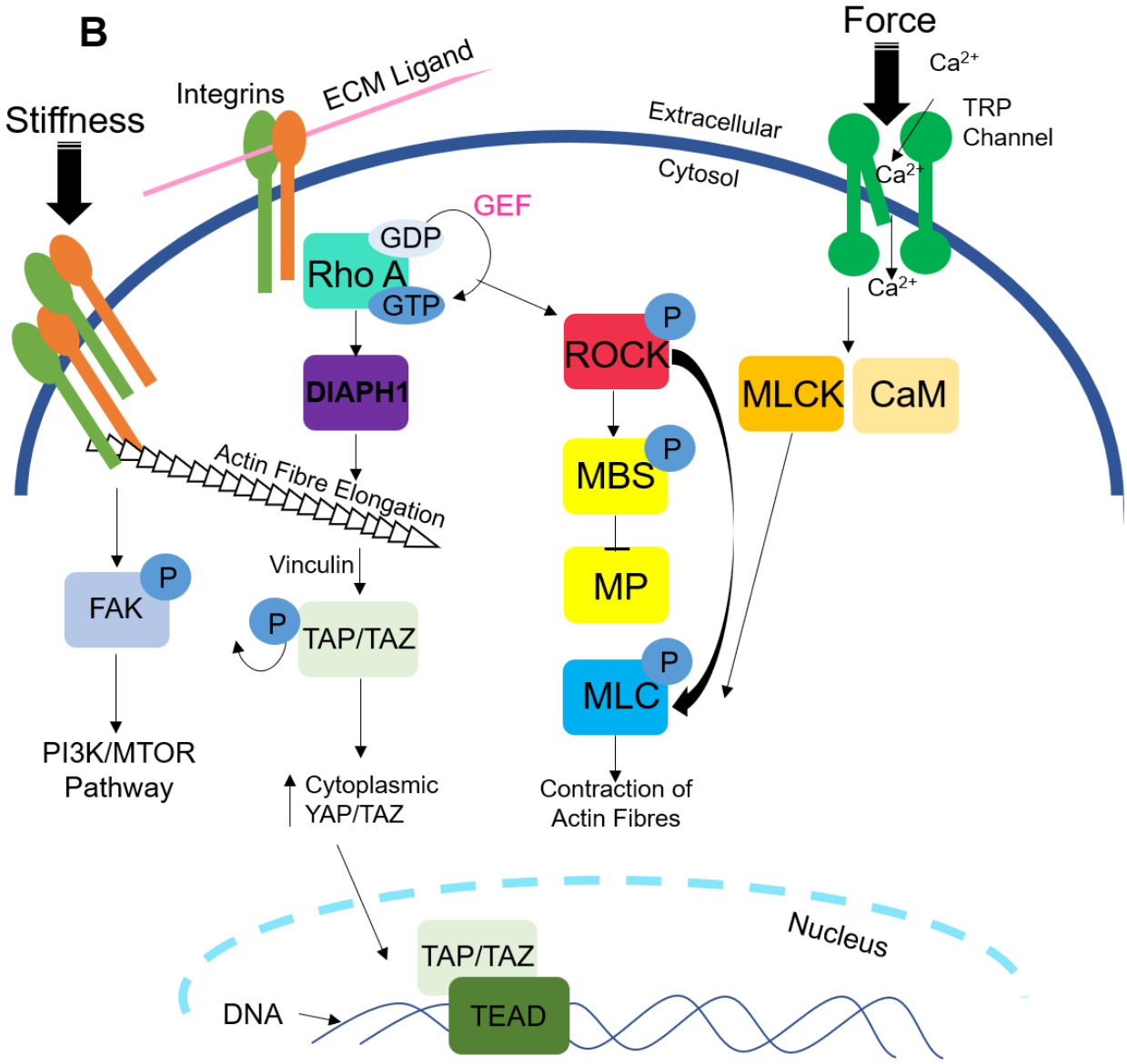

Figure 1.6. Key mechanotransduction pathways. Legend overleaf.

Figure 1.6. Key mechanotransduction pathways. Stresses exerted in the extracellular matrix (ECM) are conferred to attached cells in a number of ways. (A) Physical attachment of ECM to the nucleus allows for rapid transduction of force and changes to gene expression. The nuclear envelope is comprised of two membranes separated by a periplasmic space. Nuclear lamina supports this structure from within the nucleus and facilitates attachment to chromatin through lamina associated domains. Cytoplasmic actin filaments are connected physically to the nuclear envelope by the linker of nucleoskeleton and cytoskeleton (LINC) complex and to the cytoplasm through focal adhesions (FA). (B) Increased stiffness leads to increased formation of FAs. Binding of ECM ligands to integrins results in guanine exchange factors (GEF) converting Ras homolog gene family member A (RhoA) to its activated GTP bound state. Activated RhoA can then go on to bind to diaphanous homolog 1 (DIAPH1), which in turn binds to nascent actin fibres and promotes their elongation. Activated RhoA can also activate Rho-associated coiled coil-containing protein kinase (ROCK) by phosphorylation. This results in inactivation of myosin phosphatase (MP) through phosphorylation of its myosin-binding subunit (MBS). This allows for activation of myosin light chain (MLC) resulting in actin fibre contraction. Application of force to transient receptor potential (TRP) channels within the plasma membrane results in channel opening and calcium ion influx. These ions activate proteins including calmodulin (CaM) and myosin light chain kinase (MLCK) which can also phosphorylate MLC and result in actin fibre contraction. Increased FA signalling through focal adhesion kinase (FAK) results in activation of downstream mitogen-activated protein kinase (MAPK) and phosphoinositide 3-kinases (PI3K) pathways. On stiff substrates, increased vinculin binding promotes nuclear translocation of YAP/transcriptional co-activator with PDZ binding motif (TAZ) which modulates gene transcription through transcriptional enhanced associate domains (TEAD). Both these pathways stimulate cell proliferation.

1.2.2.3.1. Cellular morphology.

Increased heterogeneity in cellular and nuclear size is associated with cancer and is used clinically as a measure for tumorgenicity (Kumar, Srivastava, & Srivastava, 2015). Increased matrix stiffness is also associated with modulation of cellular size. In the MDA-MB-231 TNBC cell line, cellular spreading was measured following culture on polyacrylamide hydrogels at stiffnesses of 0.5, 1.1, 4.5, 32.5 and 102.5 kPa (Syed, Schober, Blanco, & Zustiak, 2017). Cellular spreading increased over the range of stiffnesses but was only found to be significant over large stiffness ranges; 0.5 vs 32.5/102.5 kPa. However, a significant increase in cellular area was observed between 1.1 and 4.5 kPa, similar to the stiffness ranges observed in the breast *in vivo.* Others have observed a similar responses in the MDA-MB-231 breast cancer cell line, with significantly increased cellular spreading between 1 vs 100 kPa (Zustiak, Nossal, & Sackett, 2014) and between more physiologically relevant stiffnesses of 0.15 and 4.8 kPa

(Tilghman et al., 2010). These studies all used 2D polyacrylamide hydrogels, however in 3D stiffness models different changes in cellular shape are frequently reported. For example, MCF-7 breast cancer cells were rounder when cultured in alginate in comparison to tissue culture plastic (TCP) (Cavo et al., 2016). Others have reported reduced cell size and increased cellular deformation with increasing stiffness in mouse mammary cancer cell lines (Khavari, Nydén, Weitz, & Ehrlicher, 2016). This highlights some of the striking differences observed between *in vitro* models. It may also indicate why only increased variation in shape and size is observed clinically rather than an absolute change in one direction.

The relationship between cell size and matrix stiffness is varied in different cancer cell lines. In lung, renal, neuroblastoma and liver cancer cell lines a positive correlation between ECM stiffness and cell size has been observed in a 2D model. However, when colorectal, prostate and pancreatic cancer cell lines were investigated no change in cell size was observed following culture at different stiffnesses (Schrader et al., 2011; Tilghman et al., 2010; Zustiak et al., 2014). This suggests that different tissues and cancers show varying sensitivities to changes in stiffness in regard to morphological changes.

Changes in the nucleus are also observed, where cells cultured on stiffer matrices are reported to express more of the nuclear envelope component lamin A (Swift et al., 2013). In metastatic cancers, low levels of lamin A aid migration through tissues by allowing the nucleus to remain malleable, deform through small gaps and then regain their previous morphology (Harada et al., 2014). However higher expression of lamin A is reportedly more advantageous in cellular survival following migrational stress (Denais et al., 2016).

Combined with the knowledge of heterogenous expression of lamin A in cancer (Capo-chichi et al., 2011), this suggests that subpopulations with increased lamin A aid in maintaining growth on stiff substrates and those with reduced lamin A may facilitate metastasis, another hallmark of cancer.

Other pathways have been implicated in altering nuclear stiffness dependant on extracellular stiffness. Application of mechanical stress is reported to reduce nuclear stiffness through modulation of chromatin packing (Nava et al., 2020), where a reduction in tightly wound DNA in the form of heterochromatin was observed. An increase in nuclear stiffness via increased chromatin condensation is reported to aid in cell migration and is promoted via focal adhesion kinase (FAK) signalling (B. Zhang et al., 2016).

The mechanisms behind changes in cellular spreading are not clear. When cellular adhesion is compared between stiffnesses it does not indicate that a difference in adhesion contributes to a change in cellular area (Tilghman et al., 2010; Zustiak et al., 2014). However, when mouse embryonic fibroblasts were cultured on soft and stiff polyacrylamide hydrogels an increase in FA size and number was observed (Kim & Wirtz, 2013). This may suggest that, whilst overall adhesion is not altered in the context of cell culture, changes in the number and intensity of FA may allow for increased FA signalling which allows for increased cell spreading. For example, Rac, a Rho family GTPase member, is a well-known remodeller of the cytoskeleton which transduces extracellular stiffness into the cell from FAs (Bae et al., 2014). Therefore, increased FAs would theoretically allow for increased Rac signalling and increased cytoskeletal remodelling to increase cell size.

1.2.2.3.2. Proliferation and angiogenesis.

An increased replicative potential is another hallmark of cancer which is observed with increased ECM stiffness. Interestingly the same breast, lung, renal, neuroblastoma and liver cancer cell lines which are reported to be responsive to stiffness through changes in cell size also showed increased growth at higher stiffnesses (Tilghman et al., 2010; Zustiak et al., 2014). Similarly, the same colorectal, prostate and pancreatic cancer cell lines which did not show changes in cell size also showed no differences in cell growth with stiffness. This further suggests that only some tissues alter their phenotype in response to stiffness.

An increase in cell proliferation on stiffer matrices has been attributed to activation of FAK (Paszek et al., 2005), which associates with FAs and is phosphorylated upon application of stress (Tang, Mehta, & Gunst, 1999; Yano, Geibel, & Sumpio, 1996) and downstream pro-proliferative MAPK/extracellular signal-regulated kinase (ERK) signalling (Paszek et al., 2005). FAK phosphorylation is also associated with increased cyclin D1 expression, which is required for initiation of S-phase in the cell cycle (Bae et al., 2014). Similarly FAK, MAPK/ERK, phosphatidylinositol 3-kinase (PI3K)/protein kinase B (Akt) and STAT3 signalling has also been implicated in increased proliferation of hepatocellular carcinoma cells grown on stiffer matrices (Schrader et al., 2011).

Changes in ECM stiffness are associated with changes in cellular nature, including stemness and mesenchymal transformation. Cancer stem cells are a sub-population of cancer cells which pose a huge barrier in chemotherapeutic resistance and disease recurrence (Aponte & Caicedo, 2017). It has been reported that reduced ECM stiffness results in significantly increased expression of stem cell markers including NANOG and

OCT4 (Schrader et al., 2011). This indicates a mechanism by which lower stiffness environments such as the bone marrow can potentiate cancer recurrence following metastasis. Epithelial to mesenchymal transition (EMT) is another cellular process associated with cancer, where cells lose their epithelial nature such as cell-cell adhesions and become more migratory with a mesenchymal phenotype (Roche, 2018). This change is associated with increased chemotherapeutic resistance and is observed in breast cancer, pancreatic cancer and hepatocellular carcinoma cells cultured at higher stiffnesses (Joyce et al., 2018; Rice et al., 2017; Schrader et al., 2011). Markers of EMT include loss or mis-localisation of epithelial cadherin (E-cadherin), a protein involved with cell to cell contacts and facilitation of cellular signalling in the β-catenin/Wnt signalling pathways (Tian et al., 2011). Loss of E-cadherin is thought to result in mis-localisation of β-catenin and increased Wnt signalling leading to increased proliferation (Kam & Quaranta, 2009; Sormunen, Leong, Vääräniemi, Fernando, & Eskelinen, 1999). Secondly, an increase in nuclear YAP is also associated with EMT. YAP then promotes cellular proliferation and migration through upregulation of the transcription factor Slug and subsequent downstream downregulation of E-cadherin (Cheng, Jin, Chen, Xi, & Guo, 2020).

Angiogenesis, the growth of new vasculature, is another hallmark of cancer. It aids in survival of the newly formed tumour through supply of oxygen and nutrients. Increased stiffness has been associated with increased blood vessel growth, branching and remodelling (Zanotelli & Reinhart-King, 2018). This is reportedly owed to mechanical induction of vascular endothelial growth factor receptors (VEGFRs) allowing for increased endothelial cell growth (Coon et al., 2015; LaValley et al., 2017). Secondly, increased stiffness is reported to disrupt vascular endothelial cadherin (VE-cadherin) function (Bordeleau et al., 2017; Conway et al., 2013). VE-cadherin facilitates cell-cell connections

in blood vessels required to maintain the barrier integrity between the blood and epithelial cells. Its disruption is often observed in cancer cells resulting in leaky vasculature and cellular re-arrangement required for formation of new vasculature (Bentley et al., 2014; Gavard, 2014).

1.2.2.3.3. DNA replication, cell division and genomic stability.

Replication of DNA and cell division is a highly mechanically dependant process. Altered matrix stiffness is reported to affect DNA replication and cell division. It is reported that soft substrates (20 kPa) impaired completion of mitosis in colon cancer cells and led to an increased accumulation of chromosomal abnormalities in comparison to stiffer substrates (50 kPa) (Rabineau et al., 2013). This indicates that a stiffness threshold may be required for successful cell division. Chromosome segregation abnormalities, including chromosome bridges and lagging chromosomes where DNA is improperly connected to the mitotic spindle, are also observed at lower stiffnesses in normal cells (Leyla Kocgozlu et al., 2012). This suggests that normal and cancerous cells respond similarly to ECM stiffness in relation to cell division. However, note that compared to physiological stiffnesses of breast or breast cancer 20 kPa and 50 kPa are both very stiff.

Similarly, it has been observed that a stiffness of 200 kPa was required for efficient DNA replication in the PtK2 normal kidney cell line (L. Kocgozlu et al., 2010). DNA replication was not observed at a lower stiffness of 50 kPa, owed to a lack of vinculin assembly in FAs, however transcription still occurred in co-ordination with MAPK pathway activation (L. Kocgozlu et al., 2010). This suggests that activation of vinculin and MAPK at certain stiffness thresholds are required for DNA replication and transcription respectively.

Increases in mechanical stress on chromatin have been observed to induce DNA damage (Mayr, Hu, Hainaut, & Xu, 2002). In non-cancerous cells, issues of increased DNA damage are protected by cell cycle checkpoints which safeguard genomic stability, preventing acquisition of chromosome errors and rearrangements. Genomic instability is a hallmark of cancer owing to loss of such checkpoints (Visconti, Monica, & Grieco, 2016) and subsequently aneuploidy and chromosomal rearrangements are commonly observed in tumours (Hasty & Montagna, 2014; Sansregret & Swanton, 2017). It is reported that mammary epithelial cells cultured at higher stiffnesses in an alginate/Matrigel model had higher levels of basal DNA damage, however inhibition of proliferation reduced DNA damage at higher stiffnesses (Sun, 2019). This suggests that both an increase in direct mechanical tension on DNA and increased proliferation at higher stiffnesses may contribute to increased DNA damage. Recently it has been reported that cells reduce nuclear stiffness through reduction of chromatin condensation in response increased mechanical forces to protect DNA from damage (Nava et al., 2020). This suggests that nuclear mechanics may protect cells from critical levels of damage potentiating survival.

1.2.3. Stiffness models.

Several *in vitro* models have been developed for study of matrix stiffness. Hydrogels are water enriched polymer networks. They are often favoured for *in vitro* models as they closely mimic the composition of the ECM and ECM proteins can be attached (Caliari & Burdick, 2016). Other stiffness models include foams and electrolyte films such as those used by Kocgozlu et al., (2012) which, similarly to hydrogels, allow increases in stiffness through increased bonding or crosslinking between matrix components (Leyla Kocgozlu et al., 2012). However, these models tend be tailored to higher stiffnesses (L.-M. Wang et al., 2015), indicating a limitation of their use. Foams, such as decellularised tissues, have also been employed for *in vitro* models (Kornmuller, Brown, Yu, & Flynn, 2017) which

allow for a closer comparison to *in vivo* environments. However, they have some limitations including the extensive treatment required for cell seeding and high variability between matrices. Other foam like structures include polymer based high internal phase emulsions (HIPEs). These are emulsions formed out of the desired polymer to create a pocketed structure, which, once set, will create areas for cell seeding (Owen et al., 2016). Synthetic matrices provide consistency in stiffness and cell seeding potential.

Hydrogels are typically composed of synthetic or natural components. They can exist as 2D culture models, where cells grow on the surface of a matrix, or as 3D culture models, where cells are embedded within the matrix (Caliari & Burdick, 2016). 2D models are less representative of the *in vivo* environment, however 3D models have limitations including nutrient availability, cell recovery and imaging.

Synthetic hydrogels include polyacrylamide and polyethylene glycol (PEG). Polyacrylamide hydrogels are one of the most popular hydrogel models, therefore protocols for their use are well standardised (Caliari & Burdick, 2016). Stiffness can be finely tuned through variation in gel components and the degree of crosslinking (Figure 1.7.a). This cross-linking is permanent and allows for a maintained stiffness, plus gels can be stored for weeks in advance with only small variations in stiffness observed (Denisin & Pruitt, 2016). Biological molecules can be chemically cross-linked to the surface to facilitate cell attachment (Figure 1.7.b). However, polyacrylamide hydrogels are confined to 2D culture due to the toxicities of un-gelated reagents (Caliari & Burdick, 2016). This is an advantage of using PEG, as its inert nature allows for both 2D and 3D culture. Secondly PEG has many possibilities for chemical modifications which allows for more complex investigations. This includes modifications that allow for specific ECM

degradation using light (Kloxin, Kasko, Salinas, & Anseth, 2009) allowing study of cell migration, or non-specific degradation by MMPs (Lutolf et al., 2003) providing further recapitulation of *in vivo* environmental changes.

Naturally derived hydrogels are typically made up of ECM components such as collagens or laminins. Alginate hydrogels are another alternative, made from alginate salts derived from brown algae. The naturally derived nature of them allows for decreased toxicity to cells and therefore cells can be grown in both 2D and 3D (K. Y. Lee & Mooney, 2012). Matrices made from ECM components such as collagens are advantageous as they already have the ligands required for cell adhesion and growth. However, these components are expensive and gelation is highly temperature dependant which can result in issues with stiffness variabilities (Walters & Stegemann, 2014). Alginate hydrogels are advantageous in this respect, as stiffness can be controlled through alginate percentage and concentration of the calcium containing crosslinking solution (Figure 1.7.c) (K. Y. Lee & Mooney, 2012). However, alginate hydrogels do not readily contain ligands required for cell adhesion in some cell lines. As such chemical modifications are often required, such as the addition of RGD (arginine-glycine-aspartic acid) ligands, which aid cell attachment and growth (Rowley, Madlambayan, & Mooney, 1999). An aspect for consideration with both gel types is degradation. Whilst this is advantageous in retrieval of cells from the matrices it can also lead to matrix degradation over time, which can result in stiffness variabilities (K. Y. Lee & Mooney, 2012).

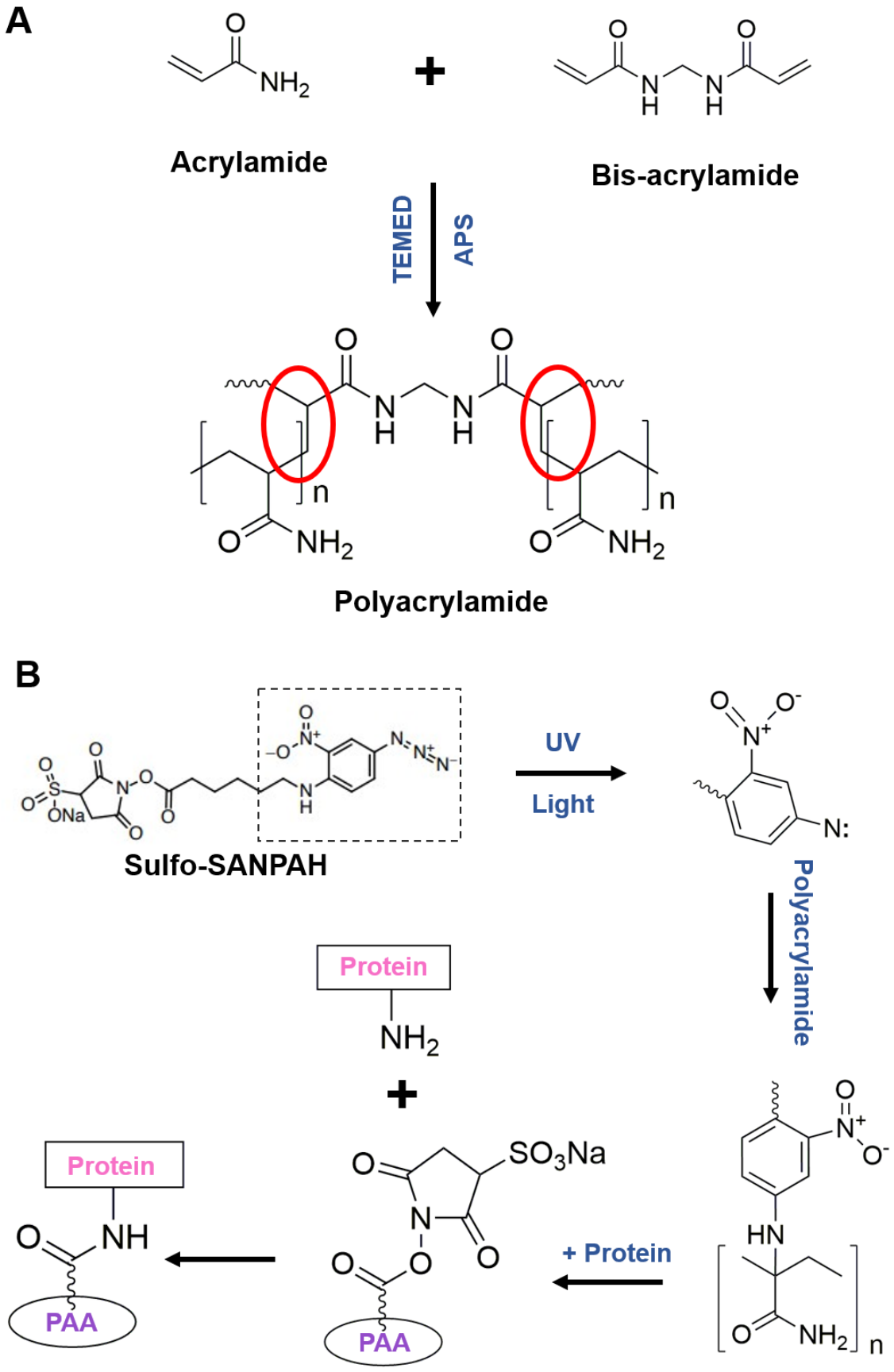

Figure 1.7. Bonding types in polyacrylamide and alginate hydrogels. Legend overleaf.

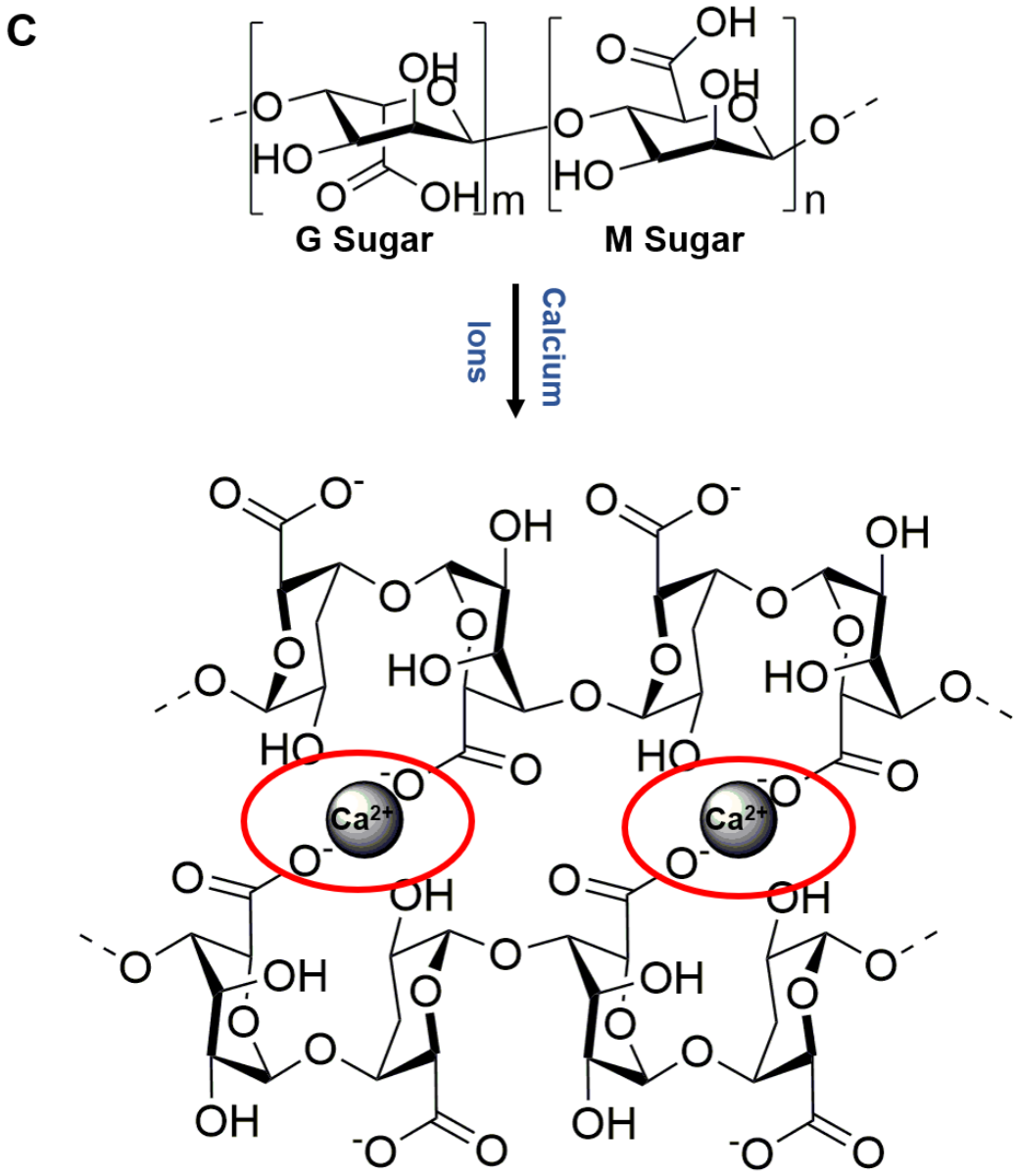

Figure 1.7. Bonding types in polyacrylamide and alginate hydrogels. (A) Polyacrylamide hydrogels are formed from acrylamide and bis-acrylamide monomers. The reaction is initiated through the addition of TEMED (Tetramethylethylenediamine) and APS (ammonium persulphate). Formation of polyacrylamide hydrogels produces a covalent bond (as circled in red) with n number of chains as indicated. (B) Crosslinking of proteins to polyacrylamide hydrogels involves the use of the ultraviolet (UV)-activated crosslinker Sulfo-SANPAH. UV treatment of Sulfo-SANPAH results in formation of a radical containing reactive end (nitrene). These react with the polyacrylamide chain as indicated forming a covalent bond. Proteins have free amine groups (-NH) at the N-terminus or on a residues' sidechain (e.g. lysine) which react with the opposite end of Sulfo-SANPAH, allowing for direct crosslinking of proteins to the polyacrylamide hydrogel. (C) Alginate is comprised of guluronic (G sugar) and mannuronic (M sugar) residues in variable quantities (m, n) as indicated. Addition of calcium ions results in formation of ionic bonding (as circled in red) between only G sugars.

This can be negated through chemical modifications to the components to allow for permanent bonding (Chuang, Lin, Melero-Martin, & Chen, 2018; Desai, Koshy, Hilderbrand, Mooney, & Joshi, 2015). Both collagen and alginate gels have been used in study of breast cancer as they allow for investigations of these lower stiffnesses (Joyce et al., 2018; Paszek et al., 2005).

1.3. Chemotherapeutics.

1.3.1. Traditional chemotherapeutics in breast cancer.

Chemotherapeutic agents are used in breast cancer either alongside surgery, radiotherapy or hormone therapies to aid in tumour shrinkage (Pathak et al., 2018). However, they are also used in receptor negative breast cancers, breast cancers where hormone directed treatments have not been successful or where resistance has arisen. The most commonly used agents are taxanes and anthracyclines either as monotherapies or in combination (Moreno-Aspitia & Perez, 2009). Taxanes, examples of which include paclitaxel (PAX) and docetaxel, function by stabilising microtubules in their polymerised state, thus preventing depolymerisation required for cell division, resulting in apoptosis (Abal, Andreu, & Barasoain, 2003). They act non-specifically but play on the nature of rapid growth observed in cancers. Treatments which include a taxane increase survival and reduce the chance of recurrence (Willson et al., 2019). However, taxane treatment is associated with unpleasant side effects including nerve damage (Willson et al., 2019). As taxanes and anthracyclines are often used as a first choice of therapy, resistance is often observed in disease recurrence thus indicating a limitation of their treatment range (Moreno-Aspitia & Perez, 2009). Anthracyclines, such as doxorubicin and epirubicin, are DNA intercalating agents which bind to both DNA and topoisomerases (Beretta & Zunino, 2008). Topoisomerases make DNA breaks to allow for the relaxation of DNA torsions (Lodish et al., 2000). Anthracyclines prevent topoisomerases from being

released from the DNA, therefore preventing DNA repair leading to cell death via p53 mediated apoptosis. Another mechanism of action of anthracyclines is through creation of reactive oxygen species which can also lead to DNA damage (Beretta & Zunino, 2008). Anthracyclines act non-specifically, although the aberrant DNA repair pathways in cancer cells provides somewhat of a targeted approach. Treatment of breast cancers with anthracyclines improves disease free survival rate and overall survival (Ding et al., 2018), but long term cardiovascular toxicity is a key issue with its use (McGowan et al., 2017).

The use of ionising radiation (IR) alone or alongside chemotherapeutic agents is advantageous for treatment of breast cancer. IR functions by causing DNA damage through direct ionisation or through the generation of reactive oxygen species (Borrego-Soto, Ortiz-Lopez, & Rojas-Martinez, 2015). If the DNA lesion load is too high, it will result in cell death. Therefore, IR acts somewhat specifically towards cancer cells which typically harbour aberrant DNA repair mechanisms.

If treatment with anthracyclines or taxanes is unsuccessful, or has previously been used prior to cancer recurrence, a different chemotherapy regime will be used. This often involves the use of antimetabolites such as 5-fluorouracil (5-FU) and gemcitabine. Antimetabolites are typically similar in structure to DNA bases allowing them to incorporate into replicating DNA (Tiwari, 2012). This incorporation leads to an increase in replicative stress, the slowing or stalling of replication. Another way antimetabolites can further perturbate this effect is by inhibiting enzymes which are involved in production of deoxyribonucleotide (dNTP) bases. This depletes the pool of available dNTPs and increases replicative stress. If the increase in replicative stress passes a critical threshold then cell death will occur. They are often used as a monotherapy or in combination with

other chemotherapeutics such as taxanes or alkylating agents (Moreno-Aspitia & Perez, 2009). Due to the increased basal levels of replicative stress and errors in DNA repair in cancerous cells, antimetabolites are somewhat selectively targeted. They are the most widely used chemotherapeutics in all cancers, hence resistance is often observed (Peters, 2014).

Alkylating agents such as cyclophosphamide and cisplatin are often used in combination with anthracyclines, taxanes and antimetabolite agents in treatment of breast cancer (Moreno-Aspitia & Perez, 2009). They function by creating DNA crosslinks between guanine bases resulting in increased replicative stress and DNA damage (Colvin, 2003). They show some selectivity towards cancer cells, similarly to antimetabolites, owing to the higher basal levels of replication stress and faulty DNA repair processes in cancers. Treatment of breast cancers with alkylating agents is reported to be less successful where high levels of O^6-methylguanine-DNA methyltransferase (MGMT) are observed (Isono et al., 2014), indicating some limitations of their use.

Other groups of chemotherapies used in treatment of breast cancers are vinca alkaloids and epothilones which both function similarly to taxanes by disrupting microtubule function. Vinca alkaloids, such as vinorelbine, function by preventing polymerisation of tubulin into microtubules, which is required for cell division, therefore resulting in mitotic arrest and cell death (Moudi, Go, Yien, & Nazre, 2013). They are typically used as a monotherapy where previous exposure to taxanes and anthracyclines has been unsuccessful (Moreno-Aspitia & Perez, 2009). Issues with neurotoxicity are observed with some vinca alkaloids but have been improved upon in newer derivatives (Martino et al., 2018). Epothilones function similarly to taxanes by acting as microtubule stabilisers, thus

leading to a halt in mitosis and cell death (Goodin, 2008). Ixabepilone is an epothilone used in breast cancers, commonly in combination with antimetabolites where taxane and anthracycline use has been unsuccessful (Moreno-Aspitia & Perez, 2009).

The tyrosine kinase inhibitor lapatinib is also used in breast cancers which are ERBB2 positive (Higa & Abraham, 2007). Lapatinib inhibits tyrosine kinases, molecular switches, involved in EGFR and ERBB2 pathways thus turning off the stimulation of cancer cell growth. It is used in recurrent breast cancers, which are resistant to taxanes and anthracyclines, in combination with antimetabolites (Moreno-Aspitia & Perez, 2009).

Some newer chemotherapeutic agents directly target the increased replicative stress in cancers, where replicative stress is increased beyond the point of cell survival. Under higher replicative stress, the poly (ADP-ribose) polymerase (PARP) prevents fork collapse and facilitates replication restart (Bryant et al., 2009). Ataxia telangiectasia and Rad3-related protein (ATR) is also important for cell survival in response to replicative stress through its role in single stranded DNA (ssDNA) break repair (Saldivar, Cortez, & Cimprich, 2017). The PARP inhibitor olaparib acts by trapping PARP on DNA, preventing ssDNA break repair, resulting in formation of double strand breaks (Caulfield, Davis, & Byers, 2019). Olaparib is particularly effective in treating BRCA mutated/deficient tumours, where cell killing is specific to these tumours due to a deficiency in homologous recombination (Bryant et al., 2005). Use of olaparib in BRCA mutated breast cancers increases progression free survival in comparison to traditional chemotherapeutics (Griguolo, Dieci, Guarneri, & Conte, 2018; Marsh & Williamson, 2019). Similarly, ATR inhibitors prevent signalling of ssDNA damage which results in increased replication stress. For this reason, they have shown promising potential for use in breast cancer in

combination with DNA damaging agents (Thomas et al., 2018; Vendetti et al., 2015) and radiation (Tu et al., 2018). Use of ATR inhibitors in cancers including the breast are currently in clinical trials and show efficacy where PARP inhibitor treatment was unsuccessful (Mei, Zhang, He, & Zhang, 2019).

All of these chemotherapeutic agents typically play on the common characteristics of cancers; increased replicative stress, rapid cell growth and aberrant DNA repair mechanisms. However, non-cancerous cells can still be affected leading to numerous side effects. Resistance is often developed, especially in disease recurrence. As such, the need for tailored combination therapies and prognostic markers would be advantageous.

1.3.2. Gemcitabine.

Gemcitabine (2',2'-difluorodeoxycytidine/dFdC), sold commercially as Gemzar, is an antimetabolite chemotherapeutic agent. It is an analogue of deoxycytidine, where 2 fluorine atoms have been added at position 2 of the cyclopentane ring (Figure 1.8.). It was first synthesised in the 1980's by Hertel et al., for investigation as an antiviral or anticancer agent (Hertel, Kroin, Misner, & Tustin, 1988).

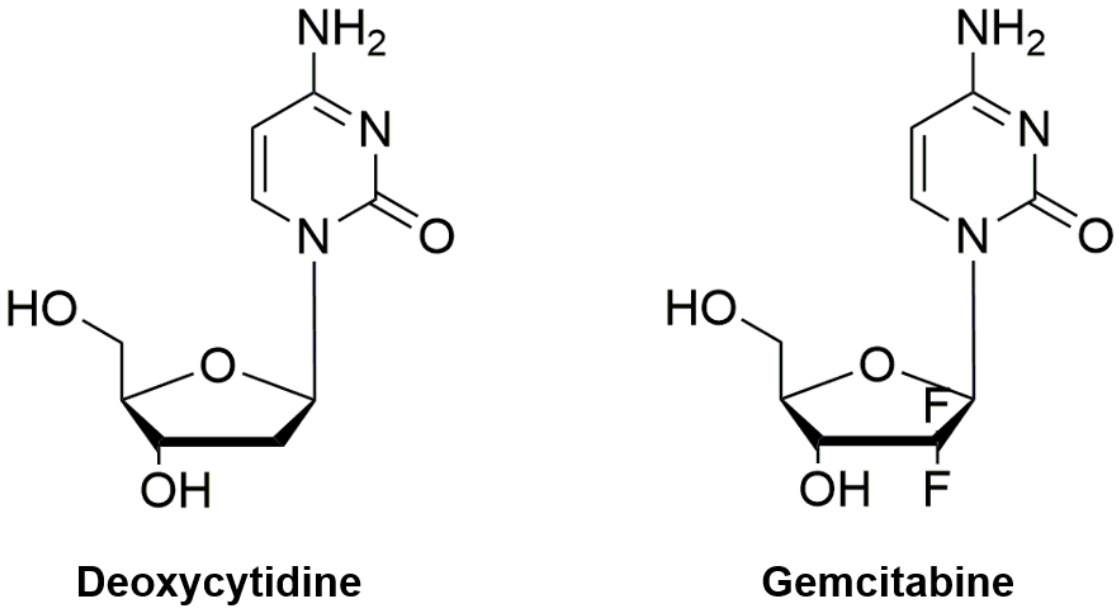

Figure 1.8. Structures of deoxycytidine and gemcitabine. Figures drawn in ChemDraw.

It was found to be effective in the treatment of cancer and was approved for clinical treatment of pancreatic cancer in 1996 (Lilly, 1996), non-small cell lung cancer (NSCLC) in 1998 (ThePharmaLetter, 1998), and breast cancer in 2004 (Lilly, 2004).

1.3.2.1. Metabolites and mechanism of action.

Gemcitabine is up taken into the cell by nucleoside transporters within the plasma membrane (Mackey et al., 1998). Upon entry into the cell, gemcitabine undergoes several transformations to become its active metabolites (Figure 1.9.a). Firstly, gemcitabine is phosphorylated by deoxycytidine kinase (dCK) or thymidine kinase 2 (TK2) to form gemcitabine monophosphate (dFdCMP). It then undergoes further phosphorylation by the same kinases to form gemcitabine diphosphate and triphosphate (dFdCDP and dFdCTP respectively), which are the active drug metabolites (Mini, Nobili, Caciagli, Landini, & Mazzei, 2006). dFdCMP can also be deaminated to form difluorodeoxyuridine monophosphate (dFdUMP). Both dFdUMP and gemcitabine can be deaminated by

deoxycytidine deaminases (dCDA) to form difluorodeoxyuridine (dFdU) initially thought to be an inactive metabolite that is then excreted from the cell. It has recently been shown to be an active metabolite alongside dFdUMP (Honeywell, Ruiz Van Haperen, Veerman, Smid, & Peters, 2015).

Each metabolite elicits different inhibitory affects which contribute to an increase in replicative stress (Figure 1.9.b). dFdCTP incorporates into replicating DNA and leads to termination of DNA synthesis (P. Huang, Chubb, Hertel, Grindey, & Plunkett, 1991) and DNA damage (Ewald, Sampath, & Plunkett, 2007; Jones, Kotsantis, Stewart, Groth, & Petermann, 2014). It can also weakly inhibit the function of DNA polymerase (Gandhi & Plunkett, 1990) and incorporate into RNA and inhibit RNA synthesis (Ruiz Van Haperen, Veerman, Vermorken, & Peters, 1993). Alongside direct incorporation, gemcitabine analogues also inhibit enzymes which produce dNTPs, therefore depleting the available nucleotide pools, slowing DNA replication and increasing replicative stress. Ribonucleotide reductase (RNR) converts ribonucleotides (NTPs) into dNTPs and is inhibited by dFdCDP (Heinemann et al., 1990). Thymidylate synthase (TS) converts deoxyuridine monophosphate into deoxythymidine monophosphate and is inhibited by dFdUMP and dFdU (Honeywell et al., 2015). Cytidine triphosphate synthetase (CTPS) is required for pyrimidine nucleotide biosynthesis and is inhibited by dFdCTP (McCluskey, Mohamady, Taylor, & Bearne, 2016).

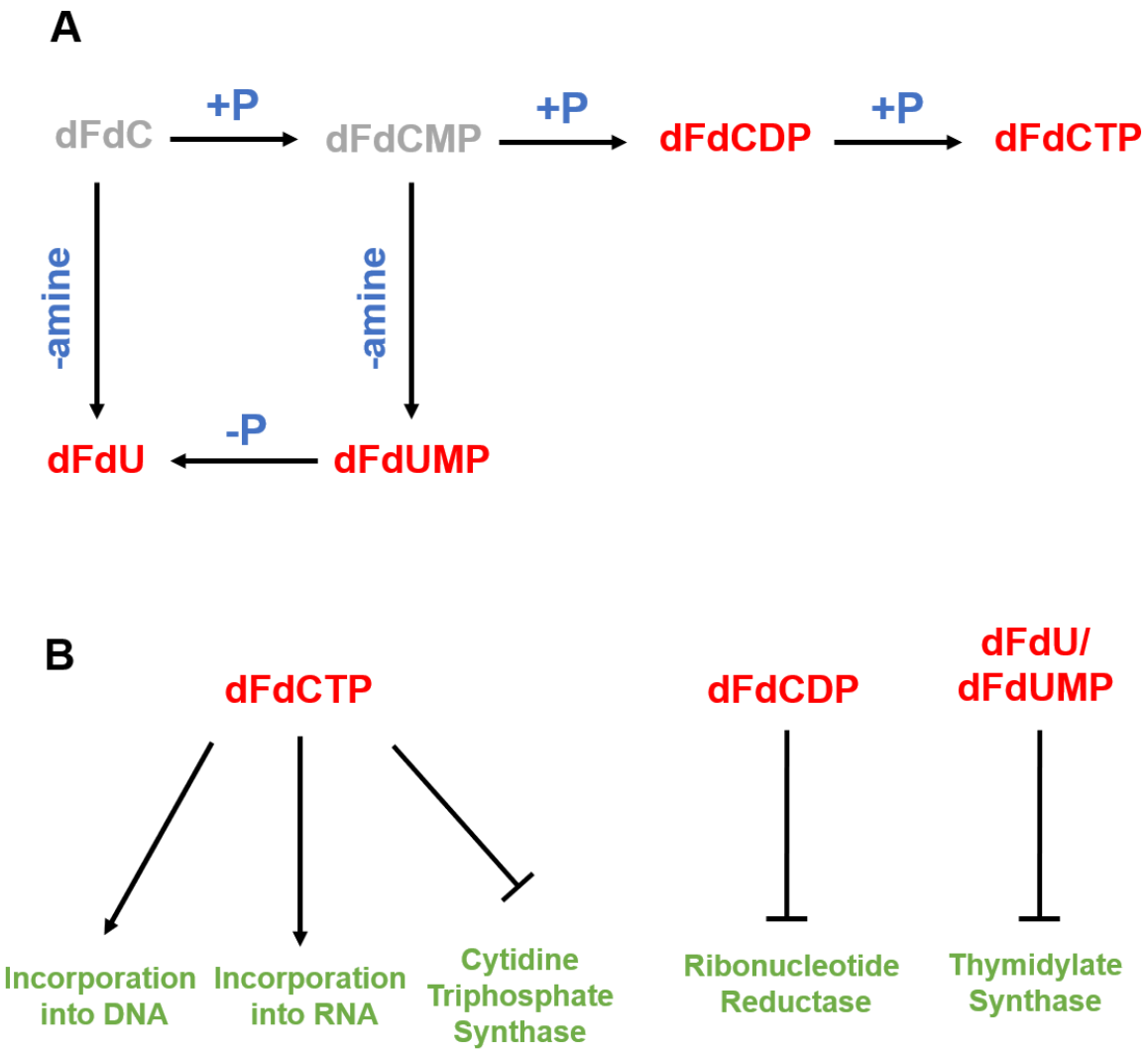

Figure 1.9. Metabolites and mechanisms of action of gemcitabine. (A) Metabolites of gemcitabine (dFdC); gemcitabine monophosphate (dFdCMP), gemcitabine diphosphate (dFdCDP) and gemcitabine triphosphate (dFdCTP) form through phosphorylation (+P) as depicted in the figure. Secondly deamination can form other metabolites difluorodeoxyuridine monophosphate (dFdUMP) and difluorodeoxyuridine (dFdU). The active metabolites are highlighted in red text. (B) Mechanism of action of the gemcitabine metabolites.

If the increase in replicative stress and subsequent DNA damage induced by gemcitabine cannot be overcome by the cell, programmed cell death (intrinsic apoptosis) occurs (Chandler, Canete, & Callery, 2004; Ferreira, Span, Peters, Kruyt, & Giaccone, 2000; Zheng, Hu, Sui, Ma, & Jiang, 2014). Recently gemcitabine has also been shown to

induce autophagy, however it is thought to act in a cytoprotective role rather than to induce cell death (Ming Chen et al., 2014; Papademetrio et al., 2014).

1.3.2.2. Clinical uses of gemcitabine and resistance.

Gemcitabine is used clinically for the treatment of a variety of solid tumours, including breast cancer. Typically, it is used in advanced breast cancers where disease recurrence or metastasis has occurred, as a monotherapy or in combination with PAX or docetaxel (Moreno-Aspitia & Perez, 2009). Gemcitabine is commonly used clinically in combination with cisplatin in NSCLC, breast cancer and ovarian cancer (Moreno-Aspitia & Perez, 2009; Toschi, Finocchiaro, Bartolini, Gioia, & Cappuzzo, 2005). This combination is thought to be efficacious due to the increased DNA crosslinking by cisplatin which is aided by gemcitabine's DNA modifications (Moorsel et al., 1999). In the treatment of advanced breast cancer, regimens including gemcitabine resulted in an improved overall survival and chemotherapeutic response (Xie, Zhang, Jin, & Fu, 2018).

Breast cancer subtype is reported to correlate with response to gemcitabine containing therapies. Combination treatment of gemcitabine and carboplatin resulted in lower overall patient survival in luminal A breast cancers in comparison to luminal B or TNBC subtypes (Nelli et al., 2013). This may be owed to the lower cell proliferation rates observed in luminal A breast cancers, which would limit gemcitabine incorporation. Treatment of metastatic TNBC with cisplatin and gemcitabine found 62.5% of cancers to be responsive (Zhang et al., 2015).

Resistance to gemcitabine is observed and poses a major problem to its use clinically. Resistance is commonly found to be due to overexpression of RNR (Jordheim, Guittet,

Lepoivre, Galmarini, & Dumontet, 2005), therefore requiring higher doses of gemcitabine for continued activity. Resistance is also observed due to upregulation of Wnt, Hedgehog and Notch pathways which upregulate anti-apoptotic proteins, increase expression of drug efflux pumps and increase growth of cancer stem cells, allowing for disease recurrence (Jia & Xie, 2015).

1.3.3. ECM stiffness alters chemotherapeutic response.

Increased ECM stiffness is associated with increased resistance to chemotherapies. In the context of gemcitabine, stiffness is typically investigated in pancreatic cancer, where it is a first line of therapy in advanced disease (Saung & Zheng, 2017). BxPC-3 and MiaPaCa-2 cell lines are reported to be more resistant to gemcitabine when cultured at an increased stiffness (1 kPa vs 500 Pa) (Puls, Tan, Whittington, & Voytik-Harbin, 2017). However, no difference in gemcitabine sensitivity was observed in BxPC-3 cells when cultured at 1, 4 and 25 kPa (Rice et al., 2017), highlighting the effect small stiffness changes can impart on gemcitabine sensitivity.

In breast cancer, patients with a lower breast elastography responded better to neoadjuvant chemotherapy than those with a higher measured elastography (50% response vs 14% respectively) (Hayashi et al., 2012). The chemotherapy regime included anthracyclines and/or taxanes in combination with other chemotherapeutics including 5-FU, epirubicin, cyclophosphamide and trastuzumab for ERBB2 positive tumours. The same stiffness pattern was observed by Jing et al., (2016) and others (Evans et al., 2013; Falou et al., 2013) for patients who underwent a similar chemotherapy regime, further confirming the relationship. When elastography was evaluated before and after treatment of breast cancer, a significant reduction in stiffness was only observed in tumours which

responded to therapy (stiffness reduction of 42% vs 26% respectively) (Jing et al., 2016). These and other studies (Fang & Yang, 2019; Fernandes et al., 2019; Katyan, Mittal, Mani, & Mandal, 2019) indicate that measurement of stiffness during chemotherapeutic treatment is a predictor of overall response. Interestingly, Jing et al., (2016) also observed that ER and PR negative tumours showed a greater change in stiffness following neoadjuvant therapy than ER and PR positive tumours. This indicates that ER and PR signalling may play a role in stiffness modulation and chemotherapeutic resistance in this context.

In agreement with this, *in vitro* stiffness models have indicated that breast cancer cell lines are more resistant to chemotherapeutics on stiffer matrices compared to compliant matrices. The MCF-7 cell line is reported to be more resistant to PAX at higher stiffnesses (100 kPa vs 1 kPa) (Zustiak et al., 2014). Similarly, MCF-7 cells were more resistant to cisplatin when cultured on stiff collagen coated plastic vs soft collagen gels (Domura, Sasaki, Ishikawa, & Okamoto, 2017). MDA-MB-231 TNBC cells, but not MCF-7 cells, are also reported to be more resistant to doxorubicin when cultured in stiffer alginate hydrogels (2 kPa vs 200 Pa) (Joyce et al., 2018).

This indicates that stiffness modulates breast cancer response to chemotherapy. However, the reasons for this and the relationship to breast cancer subtype is not well known. Further investigations are therefore warranted and will be investigated in this thesis.

1.4. Hypothesis and aims.

The first hypothesis of this thesis is that breast cancer cell lines grown on stiffer matrices will be more resistant to chemotherapeutic agents.

The second hypothesis of this thesis is that inhibition of stiffness pathways or PR activity will reduce resistance to chemotherapeutics at higher stiffnesses.

The aims of this thesis are to:

1. Optimise and validate 2D and 3D *in vitro* stiffness models suitable for growth of breast cancer cell lines.
2. Determine chemotherapeutic response of breast cancer cell lines in these models and the molecular responses which go alongside resistances.
3. Investigate the effect of stiffness pathway inhibition and PR inhibition on chemotherapeutic resistance at higher stiffness.

2. Materials and methods.

2.1. Materials.

2.1.1. General lab equipment.

2.1.1.1. Lab equipment.

Item Name	Supplier
Autoclave	Scientific Laboratory Supplies
Balance	Fischer Scientific
Belly dancer	Stovall Life Science
Benchtop centrifuge – accuSpin Micro	Fischer Scientific
Biological safety cabinet	Envair
Criterion blotter	Bio-Rad
DeltaVision microscope	GE Healthcare Life Sciences
Film processor	Konica
Film scanner	EPSON
Fluorescent plate reader - SpectraMax M5e multi-mode microplate reader	Molecular Devices
Fluorescent microscope – TE200 inverted fluorescent microscope	Nikon Instruments
Haemocytometer	Hawksley
Heat block	Grant Instruments
Heated magnetic stirrer	The Northern Media Supply Ltd
Hoefer SE250 mighty small II system	Amersham Biosciences
Hoefer DE250 miniVE vertical electrophoresis unit	Amersham Biosciences
Tissue culture incubator	Sanyo
Light microscope	Optika
Mid bench centrifuge – Heraeus MegaFuge 16	Thermo Scientific
Mr. Frosty™ freezing container	Thermo Fischer Scientific
Multichannel F1-ClipTip Pipette	Thermo Fischer Scientific
Multiskan™ FC microplate photometer	Thermo Scientific
Nanodrop ND-1000 UV-vis spectrophotometer	Thermo Fischer Scientific
pH meter	Jenway
Pipette aid	Drummond
Pipettes	Gilson
Power pack	Biometra
Rheometer - Bohlin Gemini 200	Malvern Instruments
Ultraviolet radiation crosslinker - CX-2000 8 Watt 254nm	UVP
Ultraviolet radiation lamp – 36 Watt USND-3601 365nm	USpicy
Vortex	Scientific Industries
Water baths	Grant Instruments
2700 GeneAmp polymerase chain reaction (PCR) machine	Applied Biosciences
7900 Real-time PCR machine	Applied Biosciences

2.1.1.2. Glassware, plastics and disposables.

Item Name	Supplier
0.2 µM Sterile syringe filter	Fisher Scientific
Centrifuge tubes – 15 mL	SARSTDEDT
Centrifuge tubes – 50 mL	Fischer Scientific
Coverslip – Rectangular 22 x 50 mm	Thermo Fischer Scientific
Coverslip – Circular 13 mm	VWR
Coverslip – Circular 25 mm	Scientific Laboratory Supplies
Cryovials	SARSTDEDT
Culture plates – 6 well	STARLAB
Culture plates – 24 well	Corning Incorporated
Culture plates - 96 well	Corning Incorporated
Eppendorfs – 0.5 mL, 1.5 mL and 2 mL	SARSTDEDT
Gel loading tips	Fischer Scientific
Glass bottles	Fischer Scientific
Glass bottomed Petri dishes	Ibidi
Glass plates	Web Science
KimWipes	VWR
Microlance needles	Becton Dickinson (BD)
Microscope slides - 76 x 26 mm	Thermo Fischer Scientific
Pipette tips	SARSTDEDT
Plastic pipettes –10 mL	Fischer Scientific
Plastic pipettes – 5 mL and 25 mL	SARSTDEDT
Sterile cotton buds	Heinz Herenz
Sterile syringes	BD
Tissue culture dish – 10 cm and 14.5 cm	CELLSTAR
Tissue culture flask – T25 and T75	SARSTDEDT
Universal vials	SARSTDEDT

2.1.1.3. Purified water.

A Triple Red System produced Type 1 Ultra-pure deionised water (ddH_2O).

2.1.1.4. Sterilisation.

Glassware and solutions were sterilised by autoclaving at 15 p.s.i and 120 °C for 15 minutes. Solutions that could not be autoclaved were filter sterilised using a sterile syringe and a 0.2 µM filter. Polyacrylamide hydrogels were sterilised with 8-Watt 254 nm ultraviolet (UV) radiation for 30 minutes.

2.1.2. Chemicals.

Chemical Name	Supplier
40% Acrylamide	Sigma Aldrich
alamarBlue	Thermo Fischer Scientific
Alginic acid sodium salt (Cat No. 1809F)	Sigma Aldrich
Amersham enhanced chemiluminescence (ECL) Western blotting reagent	GE Life Sciences
Ammonium persulphate (APS)	Sigma Aldrich
3-Aminopropyl-trimethoxysilane (3-APTMS)	Sigma Aldrich
Benzonase endonuclease	Merck Millipore
2% Bis-acrylamide	Bio-Rad
Bovine serum albumin (BSA)	Sigma Aldrich
Bromophenol blue	Sigma Aldrich
Calcium chloride	Fischer Scientific
Chloroform	Fisher Scientific
Collagen type I from rat tail	Sigma Aldrich
Crystal violet	Sigma Aldrich
4',6-Diamidino-2-phenylindole (DAPI)	Sigma Aldrich
Dimethyl sulphoxide (DMSO)	Fisher Scientific
Diphenyl(2,4,6-trimethylbenzoyl)phosphine oxide/2-hydroxy-2-methylpropiophenone, blend	Sigma Aldrich
DNA-free™ DNA removal kit	Invitrogen
Dried skimmed milk powder	Marvel
Ethanol	Fisher Scientific
Ethanolamine	Sigma Aldrich
Goat serum	Sigma Aldrich
25% Glutaraldehyde	Sigma Aldrich
Glycerol	Fischer Scientific
Glycine	Fischer Scientific
4-(2-Hydroxyethyl)-1-piperazineethanesulphonic acid (HEPES)	Sigma Aldrich
High capacity cDNA reverse transcription kit	Applied Biosystems
Hydrochloric acid	Sigma Aldrich
Shandon™ Immu-Mount™	Thermo Fischer Scientific
Industrial methylated spirits (IMS)	Fischer Scientific
Isopropanol	Fisher Scientific
Magnesium chloride	BDH Laboratory Supplies
Methanol	Fischer Scientific
Methylene blue	Sigma Aldrich
NP-40 Alternative	Merck
4% Paraformaldehyde in PBS	Boster Bio
Phosphate buffered saline (PBS)	VWR
Phalloidin 488 conjugate (1000x)	Santa Cruz Biotechnologies
Phenylmethanesulphonyl fluoride (PMSF)	Sigma Aldrich
Phosphatase inhibitor cocktail tablets	Roche
Piperazine-N,N′-bis(2-ethanesulphonic acid) (PIPES)	Sigma Aldrich
Pluronic F68	Sigma Aldrich
Precision plus protein standard	Bio-Rad
Protease inhibitor cocktail tablets	Roche
Protein assay dye reagent concentrate	Bio-Rad

Chemical Name	Supplier
ProtoGel (30% acrylamide, 0.8% w/v bis-acrylamide stock solution)	Geneflow
Rain-X	ITW Global Brands
Resazurin sodium salt high purity biological stain	Sigma Aldrich
RNeasy plus mini kit	Qiagen
RT^2 first strand kit	Qiagen
RT^2 SYBR® green qPCR master mix	Qiagen
Sodium chloride	Fisher Scientific
Sodium citrate dihydrate	Sigma Aldrich
20% Sodium dodecyl sulphate (SDS)	Fisher Scientific
Sodium deoxycholate	Sigma Aldrich
Sodium hydroxide	Fischer Scientific
Sucrose	Fischer Scientific
Sulphosuccinimidyl 6-(4′-azido-2′-nitrophenylamino)hexanoate (Sulfo-SANPAH)	Thermo Fischer Scientific
TaqMan universal PCR master mix	Applied Biosystems
Tetramethylethylenediamine (TEMED)	VWR
Toluene	Fisher Scientific
Tris Base	Fisher Scientific
Triton-X-100	Fischer Scientific
Triton-X-405	Sigma Aldrich
Trizol™ reagent and phasemaker™ tubes complete system	Invitrogen
Tween-20	Acros Organics
Universal X-ray developer	Champion Photochemistry
Universal X-ray fixer	Champion Photochemistry
β-Mercaptoethanol	Sigma Aldrich

2.1.2.1. PCR probes.

Gene Target	Assay ID	Technology	Supplier
Total progesterone receptor (PGR)	PPH01007F	SYBR® Green	Qiagen
β-actin	PPH00073G	SYBR® Green	Qiagen
Total *PGR*	Hs01556702_m1	TaqMan	Thermo Fisher Scientific
PGR-B isoform	Hs4419616_s1	TaqMan	Thermo Fisher Scientific
Glyceraldehyde 3-phosphate dehydrogenase (GAPDH)	Hs02786624_g1	TaqMan	Thermo Fisher Scientific

2.1.2.2. Cytotoxic agents.

Cytotoxic Agent	Mechanism of Action	Diluent	Supplier
5-Fluorouracil (5-FU)	Pyrimidine analogue, inhibits thymidylate synthase, incorporates into DNA and RNA	DMSO	Sigma Aldrich
5-Iodo-2'-deoxyuridine (IdU)	Nucleoside analogue, incorporates into DNA	DMEM	Sigma Aldrich
Gemcitabine	Nucleoside (cytidine) analogue, incorporates into DNA and RNA, inhibits ribonucleotide reductase, cytidine triphosphate synthetase and thymidylate synthase	ddH_2O	Sigma Aldrich
Hydroxyurea (HU)	Inhibits ribonucleotide reductase and thymidylate synthase	DMEM	Sigma Aldrich
Mitomycin C (MMC)	Forms inter-strand DNA crosslinks	DMSO	Sigma Aldrich
Paclitaxel (PAX)	Inhibits microtubule function by hyper-stabilisation	DMSO	Sigma Aldrich

2.1.2.3. Pathway inhibitors.

Inhibitor name	Target	Mechanism of Action	Diluent	Supplier
FAKi 14	Focal adhesion kinase (FAK)	Inhibits FAK autophosphorylation at Y397	ddH_2O	Sigma Aldrich
Mifepristone	Progesterone receptor (PR)	Progesterone receptor antagonist	Ethanol	Sigma Aldrich
NVP-Bez 235	Phosphoinositide 3-kinase (PI3K)/ mammalian target of rapamycin (MTOR)	Inhibits kinase activity through competitive binding to their ATP-binding site	DMSO	Cayman Chemical Company
Olaparib	Poly (ADP-ribose) polymerase (PARP)	Traps PARP on DNA and inhibits PARP enzymatic activity	DMSO	Adooq Bioscience
Pazopanib	Yes-associated protein (YAP)	Multi-kinase inhibitor	DMSO	Apex Bio
VE821	Ataxia telangiectasia and Rad3 related (ATR)	ATP analogue, inhibits ATR kinase activity	DMSO	Tocris
Y-27632	Rho-associated coiled coil-containing protein kinase (ROCK)	Inhibits ROCK I kinase activity	PBS	Sigma Aldrich

2.1.3. Irradiation.

Cells were irradiated using a CIB/IBL 437 CS-137 irradiator in a 3.8 L irradiation canister.

This was performed on cells directly in a 6-well plate.

2.1.4. Antibodies.

2.1.4.1. Primary antibodies.

Antibody Name	Host Animal	Manufacturer (Catalogue Number)	Application (Dilution)
β-catenin	Mouse	Santa Cruz Biotechnology (sc-7963)	IF (1:200)
Phosphorylated H2A histone family member X (γH2AX) S139	Mouse	Millipore (JBW301)	IF (1:500)
γH2AX S139	Rabbit	Cell Signalling Technology (2577)	IF (1:500)
5-Bromo-2'-deoxyuridine (BrdU) (Clone B44)	Mouse	BD Bioscience (347580)	IF (1:750)
Epithelial cadherin (E-cadherin)	Rabbit	Cell Signalling (24E10)	IF (1:200)
Glyceraldehyde 3-phosphate dehydrogenase (GAPDH)	Mouse	Proteintech (60004-1-Ig)	WB (1:20,000)
Phosphorylated histone 3 (pH3) S10	Rabbit	Millipore (06-570)	IF (1:500)
H3K9me3 (Histone H3 trimethylation at K9)	Mouse	Novus (NBP1-30141)	IF (1:200) WB (1:2000)
H3K4me3 (Histone H3 trimethylation at K4)	Rabbit	Novus (NB21-1023)	IF (1:500) WB (1:500)
H3K27ac (Histone H3 acetylation at K27)	Mouse	Millipore (MABE670)	WB (1:500)
Ki67	Mouse	Santa Cruz Biotechnology (sc-23900)	IF (1:100)
Lamin A/C	Rabbit	Abcam (ab26300)	IF (1:1000) WB (1:1000)
Lamin B1	Rabbit	Proteintech (12987-1-AP)	WB (1:1000)
p53	Mouse	Santa Cruz Biotechnology (sc-126)	WB (1:1000) IF (1:100)
Phosphorylated replication protein A (pRPA) T21	Rabbit	Abcam (ab61065)	IF (1:250)
Replication protein A 34 (RPA34)	Mouse	Calbiochem (NA19L)	IF (1:500)
Vinculin	Mouse	R & D Systems (MAB68961)	IF (10 µg/mL) WB (1:1000)
Yes kinase-associated protein (YAP)	Rabbit	Santa Cruz (sc-154-07)	IF (1:100)

IF: Immunofluorescence, WB: Western blot

2.1.4.2. Secondary antibodies.

Antibody Name	Host Animal	Manufacturer (Catalogue Number)	Application (Dilution)
Anti-mouse Alexa 488	Goat	Thermo Fischer Scientific (A11017)	IF (1:1000)
Anti-mouse Alexa 594	Goat	Thermo Fischer Scientific (A11005)	IF (1:500)
Anti-rabbit Alexa 488	Donkey	Life Technologies (A21206)	IF (1:500)
Anti-rabbit Alexa 594	Goat	Thermo Fischer Scientific (A11037)	IF (1:1000)
Anti-mouse IgG horse radish peroxidase (HRP)	Horse	Cell Signalling Technology (7076)	WB (1:2000)
Anti-rabbit IgG HRP	Goat	Cell Signalling Technology (7074)	WB (1:2000)

2.1.5. Cell lines.

Cell Line Name	Supplier	Genotype	Receptor Expression
CAL-51	DSMZ	Human mammary gland adenocarcinoma, derived from metastatic site: pleural effusion	ER- PR- ERBB2-
MCF-7	ATCC	Human mammary gland adenocarcinoma, derived from metastatic site: pleural effusion	ER+ PR+ ERBB2-
MDA-MB-231	ATCC	Human mammary gland adenocarcinoma, derived from metastatic site: pleural effusion	ER- PR- ERBB2-
MDA-MB-468	ATCC	Human mammary gland adenocarcinoma, derived from metastatic site: pleural effusion	ER- PR- ERBB2-
SK-BR-3	ATCC	Human mammary gland adenocarcinoma, derived from metastatic site: pleural effusion	ER- PR- ERBB2+
ZR-75-1	ATCC	Human mammary gland ductal carcinoma, derived from metastatic site: ascites	ER+ PR- ERBB2-
T-47D	ATCC	Human mammary gland ductal carcinoma, derived from metastatic site: pleural effusion	ER+ PR+ ERBB2-

ATCC: American Type Culture Collection, DSMZ: Deutsche Sammlung von Mikroorganismen und Zellkulturen

2.1.6. Cell culture reagents.

2.1.6.1. Foetal calf serum (FCS).

Virus, endotoxin and mycoplasma free FCS was provided by Life Science Production and stored at -20 °C prior to use.

2.1.6.2. Cell culture medium.

CAL-51, MCF-7, MDA-MB-231 and ZR-75-1 cell lines were cultured in high glucose Dulbecco's Modified Eagle Medium (DMEM) containing L-glutamine supplied by Sigma Aldrich. The MDA-MB-468 and T-47D cell lines were cultured in Roswell Park Memorial Institute (RPMI)-1640 medium containing L-glutamine supplied by Sigma Aldrich. The SK-BR-3 cell line was cultured in high glucose McCoy's 5A (modified) medium containing L-glutamine supplied by Lonza. All medias were supplemented with 10% foetal calf serum and 1x non-essential amino acids (NEAA) supplied by Sigma Aldrich.

2.1.6.3. Trypsin.

Trypsin ethylenediaminetetraacetic acid (EDTA) comprised of 0.5 g/L trypsin and 0.2 g/L Versene (EDTA) was supplied by Sigma Aldrich.

2.1.7. Buffers and stock solutions.

2.1.7.1. Phosphate buffered saline (PBS).

Oxoid PBS tablets were dissolved into ddH_2O at a concentration of 1 tablet per 100 mL. This was then sterilised by autoclave and stored at room temperature.

2.1.7.2. Tris-buffered saline (TBS).

Ten times TBS was produced by dissolving 24.2 g tris base (200 mM) and 80 g NaCl (1.4 M) in 700 mL ddH_2O. The pH was adjusted to 7.6 with 5 M HCl and finally topped up to 1 L with ddH_2O. Ten times TBS was diluted 1 in 10 with ddH_2O to produce 1x solution. Both solutions were stored at room temperature.

2.1.7.3. 1 M Tris pH 6.8 and 8.0.

One molar tris solution was produced by dissolving 121.1 g of tris base in 700 mL ddH_2O. The pH was adjusted to 6.8 or 8.0 using 5 M HCl and finally topped up to 1 L with ddH_2O. Both solutions were stored at room temperature.

2.1.7.4. 1.5 M Tris pH 8.8.

One point five molar tris solution was produced by dissolving 181.7 g of tris base in 700 mL ddH_2O. The pH was adjusted to 8.8 using 5 M HCl and finally topped up to 1 L with ddH_2O. It was stored at room temperature.

2.1.7.5. 10% SDS.

Ten percent SDS solution was made by mixing 500 mL 20% SDS solution with 500 mL ddH_2O. The solution was stored at room temperature and heated to 60 °C upon presence of precipitation until the precipitated SDS had dissolved.

2.1.7.6. 5x Radioimmunoprecipitation assay (RIPA) cell lysis buffer.

One hundred mL 5x RIPA buffer was made by adding 25 mL 1 M tris pH 8.0 (250 mM), 15 mL 5 M NaCl (750 mM), 5 mL 10% SDS (0.5%), 5 ml NP-40 alternative (5%), 2.5 g sodium deoxycholate (2.5%) and ddH_2O to a total volume of 100 mL. Five times RIPA buffer was autoclaved and then stored at room temperature.

2.1.7.7. 5x SDS sample buffer.

One hundred mL 5x SDS sample buffer was made by adding 25 mL 1 M tris pH 6.8 (250 mM), 10 g SDS (10%), 50 mL glycerol (50%), 5 mL β-mercaptoethanol (5%), 20 mg bromophenol blue (0.02%) and ddH_2O to a total volume of 100 mL. The solution was stored at room temperature.

2.1.7.8. SDS-polyacrylamide gel electrophoresis (SDS-PAGE) running buffer.

Ten times SDS-PAGE running buffer was made by dissolving 30 g tris base (250 mM) and 144 g glycine (1.9 M) in 900 mL ddH_2O. One hundred mL of 10% SDS (1%) was added to bring the volume up to 1 L. One times SDS-PAGE running buffer was produced by diluting 100 mL 10x SDS-PAGE running buffer with 900 mL ddH_2O. Both solutions were stored at room temperature.

2.1.7.9. Towbin transfer buffer.

Ten times Towbin transfer buffer was made by dissolving 30.3 g tris base (250 mM) and 144 g glycine (1.9 M) with 700 mL ddH_2O. Once the solute was fully dissolved the solution was brought to a final volume of 1 L with ddH_2O. One times Towbin transfer buffer was produced by mixing 100 mL 10x Towbin buffer and 700 mL of ddH_2O. This solution was then brought up to 1 L with 200 mL methanol and mixed again. One times Towbin transfer buffer was chilled to 4 °C on day of use.

2.1.7.10. 0.1 M Sodium hydroxide.

Nought point one molar sodium hydroxide solution was made by dissolving 4 g of sodium hydroxide pellets in 1 L of ddH_2O. The solution was stored at room temperature and sterile filtered prior to use.

2.1.7.11. 0.5% v/v 3-APTMS.

Nought point five percent v/v 3-APTMS solution was made by mixing 1 mL of 3-APTMS into 200 mL of ddH_2O through gentle inversion. The solution was stored at room temperature and sterile filtered prior to use.

2.1.7.12. 0.5% v/v Glutaraldehyde.

Nought point five percent v/v glutaraldehyde solution was made by adding 4 mL of 25% glutaraldehyde solution to 200 mL ddH_2O.

2.1.7.13. Sulfo-SANPAH.

A stock solution of 2.5 mg/mL Sulfo-SANPAH was made by dissolving 50 mg of Sulfo-SANPAH in 2 mL of DMSO. The solution was then aliquoted into 1.5 mL Eppendorfs at a volume of 40 µL. These aliquots were snap frozen using dry ice and 100% ethanol and stored promptly at -80 °C for up to one year. At the time of use, an aliquot was quickly thawed at room temperature and diluted to a concentration of 0.00625% with the addition of 15,960 µL PBS.

2.1.7.14. 1% Ethanolamine in 50 mM HEPES pH 8.5.

Fifty millimolar 4-(2-hydroxyethyl)-1-piperazineethanesulphonic acid (HEPES) buffer pH 8.5 was made by dissolving 5.96 g of HEPES free acid in 300 mL ddH_2O.The pH was adjusted to 8.5 using 1 M sodium hydroxide (4 g sodium hydroxide pellets in 100 mL of ddH_2O) before the final solution was brought to 500 mL total volume with ddH_2O. The solution was sterilised by autoclaving and stored at 4 °C in the dark.

On the day of use 30 mL of 50 mM HEPES pH 8.5 was moved into a falcon tube. 300 µL of ethanolamine was added to the HEPES and the solution mixed well. The volume of HEPES and ethanolamine was scaled up or down according to the volume of gels being made on the day. The solution was filter sterilised prior to use.

2.1.7.15. 0.15 M Sodium chloride.

Nought point one five molar sodium chloride solution was made by dissolving 8.77 g of sodium chloride in 1 L of ddH_2O. The solution was sterilised by autoclaving and then stored at room temperature.

2.1.7.16. 200 mM Calcium chloride.

Two hundred millimolar calcium chloride solution was made by dissolving 29.4 g calcium chloride dihydrate in 1 L of ddH_2O. The solution was sterilised by autoclaving and then stored at room temperature.

2.1.7.17. 0.3 mg/mL Resazurin in TBS.

Nought point three mg/mL resazurin in TBS was made by dissolving 30 mg of high purity resazurin sodium salt in 100 mL of 1x TBS. The solution was sterile filtered and stored at 4 °C protected from light for up to 6 months.

2.2. Methods.

2.2.1. Mammalian cell culture.

2.2.1.1. Passaging cells.

All cell lines were maintained in T75 flasks at 37 °C with 5% CO_2. For cell passaging culture medium was removed and cells washed twice with 10 mL PBS. One mL of trypsin EDTA was then added to the cells followed by incubation at 37 °C for 3-5 minutes to allow the detachment of cells from the flask. Following detachment 9 mL of warm medium was added to the flask and the cells resuspended. The resulting cell solution was then seeded into new culture flasks. Experiments were performed when cells were 60-80% confluent to ensure that they were in a logarithmic growth phase.

2.2.1.2. Freezing cells.

Cells which were 60-80% confluent were trypsinised, resuspended in fresh medium and then centrifuged in a falcon tube at 1200 revolutions per minute (RPM) for 3 minutes. The cell pellet was resuspended in culture medium containing DMSO at a concentration of 10% for the CAL-51 cell line and at 5% for MCF-7, MDA-MB-231, MDA-MB-468, SK-BR-3, T-47D and ZR-75-1 cell lines. Each flask pellet was resuspended in 2 mL of medium containing DMSO and then distributed into 1 mL cryovials. These were stored overnight at -80 °C in a Mr. Frosty™ freezing container. Frozen cells were then kept at -80 °C for short term storage (< 1 year) and in liquid nitrogen for long term storage (> 1 year).

2.2.1.3. Thawing cells.

Frozen cells were thawed by a short incubation at 37 °C just until all ice crystals had disappeared. Cells were transferred into a 15 mL falcon tube and 9 mL of warm culture medium was added. Cells were then centrifuged at 1200 RPM for 3 minutes. The cell

pellet was resuspended in 10 mL warm culture medium and then transferred into a T25 flask.

2.2.2. Formation of polyacrylamide hydrogels.

2.2.2.1. Activation of bottom coverslips.

Twenty-five millimetre and 13 mm diameter glass coverslips or 10 cm^2 glass plates were activated prior to pouring of polyacrylamide gels to facilitate chemical attachment of the gel to the glass surface. A volume of 1 mL was used for each solution on 25 mm coverslips, 300 µL for 13 mm coverslips and 10 mL on glass plates respectively. Coverslips/glass plates were first sterilised with 70% industrial methylated spirits (IMS) (700 mL IMS mixed with 300 mL water) and allowed to air dry. Coverslips/glass plates were then cleaned to reveal hydroxyl groups on the glass surface by incubation with 0.1 M sodium hydroxide solution for 3 minutes. Following aspiration and disposal of sodium hydroxide, coverslips/glass plates were incubated with 0.5% v/v 3-aminopropyl-trimethoxysilane for 3 minutes. This solution was then aspirated and the coverslips were washed 3 times in ddH_2O. Coverslips/glass plates were blotted dry with a KimWipe and then incubated with 0.5% v/v glutaraldehyde for 30 minutes. Following incubation this solution was aspirated and coverslips/glass plates were washed 3 times in ddH_2O and then allowed to dry on a KimWipe.

2.2.2.2. Treatment of top coverslips.

To allow for effective removal of top coverslips from set polyacrylamide gels coverslips were treated to become water-repellent. Twenty-five millimetre and 13 mm diameter glass coverslips and 10 cm^2 glass plates were sterilised with a 70% IMS solution and allowed to air dry. A thin film of Rain-X was applied to the surface of each coverslip / glass plate with

a sterile cotton bud and allowed to air dry in a sterile laminar flow hood. They were stored at room temperature prior to use in a sterile sealed Petri dish and re-treated with Rain-X on the day of each gelation.

2.2.2.3. Gelation of polyacrylamide hydrogels.

Polyacrylamide gels were comprised of varying acrylamide, bis-acrylamide and phosphate buffered saline volumes as detailed in Table 2.1. These volumes were added to a 1.5 mL Eppendorf tube with 3 µL TEMED and the solution gently mixed by inversion.

One Eppendorf of gel solution was used per 4x 25 mm coverslips or 12x 13 mm coverslips. Ten microlitres of 10% APS solution (1 g APS diluted in 10 mL ddH_2O made fresh on the day of polyacrylamide gelation and stored at 4 °C) was added to each tube prior to gel pipetting onto coverslips. Volumes were scaled up by a factor of 10 for gels formed on glass plates. Gel solutions were pipetted at a volume of 200 µL onto 25 mm diameter coverslips and 50 µL onto 13 mm diameter coverslips. Top coverslips were placed treated side down on top of the gels to provide a smooth topology and even gel thickness. For 10 cm^2 glass plates gels were set between the activated and Rain-X treated side of the two plates using SDS-PAGE gel casting equipment and 1 mm spacers. Gel solution was pipetted in between the plates until it reached the top of the plates. Gels were set in the laminar flow hood where coverslips were housed in lidded Petri dishes for 30 minutes. The gel sandwiches were hydrated in PBS for 20 minutes prior to removal of the top coverslip through careful application of pressure. Gels were washed 3 times in PBS.

Predicted Stiffness				
30% Acrylamide (µL)	76 (2.25%)	183 (5.42%)	252 (7.46%)	347 (10.27%)
2% Bis-acrylamide (µL)	35 (0.07%)	38 (0.07%)	103 (0.2%)	132 (0.26%)
PBS (µL)	889	779	645	521

Table 2.1. Component ratios for polyacrylamide hydrogels.

2.2.2.4. Conjugation of collagen to the polyacrylamide hydrogel surface.

The top surface of hydrogels were treated with 0.00625% Sulfo-SANPAH by direct pipetting onto the gel surface. This solution was photoactivated by application of 365 nM UV radiation with a 36 W USND-3601 UV lamp for 10 minutes. Gels were then washed 3 times in PBS prior to overnight incubation with 0.1 mg/mL collagen type I ECM ligand at 4 °C. Gels were washed 3 times in PBS and then UV sterilised with a UVP CX-2000 UV crosslinker with 8 W 254 nm UV radiation for 30 minutes. Gels were stored in PBS prior to plating of cells for up to 3 weeks at 4 °C.

2.2.2.5. Preparation of gels for cell plating.

Collagen I coated polyacrylamide hydrogels were incubated with filter sterilised 1% ethanolamine in 50 mM HEPES pH 8.5 for 30 minutes at 4 °C to block any remaining unreacted Sulfo-SANPAH. A volume of 2 mL was used for 6 well plates, 500 µL for 24 well plates and 20 mL for 10 cm^2 glass plates in Petri dishes. Gels were washed 3 times in PBS and then soaked in serum free DMEM for at least 1 hr at 37 °C. After soaking gels were then seeded with cells appropriate for each assay.

2.2.3. Formation of alginate hydrogels.

2.2.3.1. Preparation of alginate stocks.

A stock solution of 3% alginate was made by dissolving 3 g of alginic acid sodium salt (cat no. 1809F) in 100 mL of 0.15 M sodium chloride solution. The solution was sterilised by autoclaving. The 3% alginate stock was diluted 1:3 and 2:3 with complete DMEM to form stock solutions of 1% and 2% alginate respectively. All three solutions were stored at 4 °C prior to use.

2.2.3.2. Formation of alginate beads.

Alginate solutions were warmed to 37 °C in the incubator for 15-30 minutes prior to use. Cells were trypsinised and pelleted by centrifugation at 1200 RPM for 3 minutes. The pellet was resuspended in 1 mL of complete medium per 20 mL of original cell solution prior to pelleting. Cells were mixed with the alginate by gentle pipetting at a concentration of 500,000 cells/mL of alginate for the MCF-7 cell line and 2,000,000 cells/mL of alginate for the MDA-MB-231 cell line. Alginate cell solutions were then transferred to square Petri dishes and pipetted dropwise into 1 mL of 200 mM calcium chloride solution in a 24 well plate using a multichannel pipette and low retention pipette tips. The 24 well plates were incubated at 37 °C for 10 minutes to allow alginate gels to set. The calcium chloride solution was then removed with a 5 mL stripette and four washes with 1 mL of complete DMEM were undertaken for each well. The gels were then left in complete DMEM at 37 °C prior to downstream assays.

2.2.4. Attempting to form polyacrylamide high internal phase emulsion (poly HIPEs).

Attempts to form polyacrylamide polyHIPEs were undertaken at the Kroto Research Institute with the help of Dr Frederik Claeyssens and Dr Jose Ricardo Aguilar Cosme. A solution containing 1512 µL 30% acrylamide, 618 µL 2% bis-acrylamide, 5724 µL PBS, 60 µL 10% APS, 2.4 g Triton-X-405 and 0.72 g Pluronic F68 was gently mixed. Thirty millilitres of toluene were then added dropwise to the acrylamide mixture with continuous mixing at 350 RPM, to create an emulsion. Once all the toluene was added and an emulsion formed 18 µL of TEMED was added and stirring continued at 100 RPM for 3 minutes. The emulsion solution was placed in a glass Petri dish and then placed in a 45 °C oven overnight for setting. Setting was also attempted after the addition of TEMED through the addition of the photoinitiator, diphenyl(2,4,6-trimethylbenzoyl)phosphine oxide/2-hydroxy-2-methylpropiophenone blend, at a concentration of 4% (0.2 g photoinitiator was added to 5 g of the emulsion). We then attempted to photo-crosslink the gel with exposure to UV light.

2.2.5. Rheological measurements.

The stiffnesses (elastic modulus) of polyacrylamide and alginate hydrogels were measured by Rheology. This was undertaken with the help of Dr Pete Laity (University of Sheffield) on a Bohlin Gemini 200 rheometer fitted with a 25 mm diameter flat plate for polyacrylamide gels and a 10 mm diameter flat plate for alginate gels. The Peltier heating stage where samples were mounted was set at a temperature of 37 °C to mimic incubator temperatures. Hydrogel samples were measured with applied forces of 0.2-5 N (20-509 g). The hydrogel was flooded with distilled water and covered with an environmental cuff to prevent the sample from drying. A frequency sweep from 10 to 0.01 Hz was implemented for a total of 11 frequency steps at an oscillatory strain of 0.02%.

Rheological measurements were made of 3 different gels made on the same day for each percentage measured. Means were calculated for each repeat at a measured frequency of 1 Hz for each different gel condition. For measurements of gels and cells, 60,000 cells were plated onto polyacrylamide gels and cells were plated into alginate beads at a density of 500,000 cells/mL for MCF-7 cells and 2,000,000 cells/mL for MDA-MB-231 cells. Rheological measurements were made in the same way.

2.2.6. Cell viability measurements.

2.2.6.1. alamarBlue / Resazurin.

The alamarBlue assay is a cell viability assay based on the reactant resazurin which changes from a non-fluorescent blue to resorufin, a fluorescent red substrate, due to reduction by living cells. The reaction occurs in the medium and can be measured immediately on a fluorescent plate reader. It is beneficial over other viability assays such as MTT due to increased sensitivity and lack of cell killing (Hamid, Rotshteyn, Rabadi, Parikh, & Bullock, 2004). As such viability can be measured at multiple time points in the same cells. We used it in our models for measurement of cell growth overtime and for determination of chemotherapeutic sensitivity.

For measuring cell growth cells were plated on 25 mm diameter polyacrylamide hydrogels at a density of 60,000 cells/mL or into alginate hydrogels at a density of 500,000 cells/mL for MCF-7 cells or 2,000,000 cells/mL for MDA-MB-231 cells. Cell viability was measured by alamarBlue assay 24, 72, 96, 120, 144 hrs after cell plating. To undertake an alamarBlue reading cell medium was removed from the cells and replaced with fresh medium containing resazurin or alamarBlue reagent diluted 1:10. The cells were incubated for 3-4 hrs with this solution at 37 °C protected from light. After incubation 100

µL of the solution that was incubated with cells was moved to a 96 well and then read on SpectraMax M5e multi-mode microplate reader at an excitation of 570 nm and an emission of 600 nm using SoftMax Pro software. If cells were to be measured again at a separate time point alamarBlue was washed off the cells and gels with three 10-minute PBS washes at 37 °C prior to re-addition of medium and the relevant cytotoxic compounds or inhibitors. alamarBlue was freshly added for each time point measured.

2.2.6.2. Treating cells with cytotoxic agents for analysis of chemotherapeutic sensitivity.

Cells were plated on 25 mm diameter polyacrylamide hydrogels at 60,000 cells/mL or set into alginate beads at 500,000 cells/mL for MCF-7 cells and at 2,000,000 cells/mL for MDA-MB-231 cells and incubated in complete culture medium at 37 °C for 24 hrs. Medium was then removed and fresh medium added followed by addition of the cytotoxic agent (gemcitabine, PAX, MMC, 5-FU, HU, olaparib or VE821)/IR treatment or vehicle control at the appropriate concentration. The cells were incubated at 37 °C for 48 hrs with cytotoxic agents before the medium was removed and replaced with fresh medium plus the re-addition of the cytotoxic agent / IR treatment or vehicle control to replenish this within the medium. Cells were then incubated at 37 °C for 24 hrs prior to the measurement of cell viability by alamarBlue assay as detailed in 2.2.6.1.

2.2.6.3. Treating cells with inhibitor compounds and gemcitabine for analysis of sensitivity.

Cells were plated on polyacrylamide hydrogels or set into alginate beads at the cell densities detailed in 2.2.6.2. and incubated in complete culture medium at 37 °C for 24 hrs. This medium was then removed, and fresh medium added followed by addition of the

inhibitor compound (mifepristone, FAKi 14, Y-27632, NVP-Bez 235 or pazopanib) or vehicle control at the appropriate concentration. The cells were incubated at 37 °C for 24 hrs with inhibitors prior to the addition of a vehicle control or gemcitabine at a concentration of 5 or 10 nM. Cells were incubated at 37 °C for a further 48 hrs. The medium was then removed and replaced with fresh medium plus the re-addition of inhibitor compounds and gemcitabine or vehicle controls to replenish them within the medium. Cells were then incubated at 37 °C for 24 hrs prior to the measurement of cell viability by alamarBlue assay as detailed in 2.2.6.1.

2.2.7. Immunofluorescent staining.

2.2.7.1. Actin, DAPI and vinculin.

2.2.7.1.1. Staining methods.

Cells were plated onto 13 mm diameter glass coverslips coated with and without polyacrylamide hydrogels at a cell density of 10,000 cells/well in 24 well plates. For the alginate model cells were seeded at 500,000 cells per mL into alginate beads. Cells were cultured under these conditions at 37 °C for 16-24 hrs. Cells were then washed 2 times in 500 µL PBS and fixed with 500 µL 4% paraformaldehyde in PBS for 10 minutes at room temperature. Cells were then washed 3 times in 500 µL PBS for 5 minutes. Cells were permeabilised with 200 µL 0.2% v/v Triton-X-100 in PBS and then washed 3 times in 500 µL PBS for 5 minutes. Subsequently cells were blocked for 1 hr at room temperature with 200 µL 3% w/v bovine serum albumin (BSA) in PBS. Cells were then washed 2 times in 500 µL PBS for 5 minutes. Cells were incubated with vinculin primary antibody diluted in 100 µL 1% w/v BSA in PBS for 16 hrs at 4 °C in a humidified chamber. Cells were then washed 3 times in 500 µL PBS for 10 minutes and then incubated with 100 µL of Alexa Fluor® 594–conjugated goat anti-rabbit IgG secondary antibody diluted in 1% w/v BSA in PBS with 1 µg/mL 4',6-diamidino-2-phenylindole (DAPI) and 1x Phalloidin 488 conjugate.

Coverslips were then washed 2 times in 500 µL PBS and stored in PBS at 4 °C protected from light prior to imaging.

2.2.7.1.2. Analysis.

For polyacrylamide gels, cells were imaged in a µ-Dish, 35 mm high glass bottomed Petri dishes gel side down at the Wolfson light microscopy facility, using the Applied Precision deconvolution DeltaVision microscope (GE Healthcare Life Sciences). A UPlanSAPO 40x oil objective lens was employed to image z-stack images using SoftWorks software. Eighteen to 25 cells were analysed for each condition on one occasion. For each cell the cytoplasmic area was measured using FIJI software (Schindelin et al., 2012). Images were deconvoluted prior to analysis.

Alginate beads were squashed between a coverslip and a slide and mounted using Shandon™ Immu-Mount™. Cells were imaged on a Nikon TE200 inverted fluorescent microscope using a 60x/1.4 oil immersion objective lens with Volocity software (Perkin Elmer). At least 30 cells were imaged per condition per independent repeat and the nuclear and cytoplasmic area were measured in FIJI.

2.2.7.2. Lamin A and DAPI.

2.2.7.2.1. Staining methods.

Cells were plated onto 13 mm diameter glass coverslips coated with and without polyacrylamide hydrogels at a cell density of 15,000 cells/well in 24 well plates. Cells were cultured under these conditions at 37 °C for 24 hrs to allow for cells to adhere and spread onto the underlying matrix substrate. Cells were then washed once in 500 µL PBS and fixed with 500 µL 4% paraformaldehyde in PBS for 10 minutes at room temperature.

Cells were then washed twice in 500 µL PBS for 5 minutes. Cells were permeabilised with 200 µL 0.2% v/v Triton-X-100 in PBS for 10 minutes and then washed 3 times in 500 µL PBS for 5 minutes. Subsequently cells were blocked for 1 hr at room temperature with 200 µL 3% w/v BSA in PBS. Cells were then washed 3 times in 500 µL PBS for 5 minutes. Cells were incubated with lamin A primary antibody diluted in 100 µL 1% w/v BSA in PBS for 16 hrs at 4 °C in a humidified chamber. Cells were then washed 3 times in 500 µL PBS for 5 minutes. Cells were incubated with 100 µL of Alexa Fluor® 594–conjugated goat anti-rabbit IgG secondary antibody diluted in 1% w/v BSA in PBS with 1 µg/mL DAPI for 1 hr at room temperature protected from light. Coverslips were then washed 2 times in 500 µL PBS and stored in PBS at 4 °C protected from light prior to imaging.

2.2.7.2.2. Analysis.

Cells were imaged in a µ-Dish, 35 mm high glass bottomed Petri Dishes gel side down at the Wolfson light microscopy facility, using the Applied Precision deconvolution DeltaVision microscope (GE Healthcare Life Sciences). A UPlanSAPO 40x oil objective lens was employed to image z-stack images using SoftWorks software. Twenty-one to 33 cells were imaged for each condition. The nuclear area and circularity were measured in FIJI for the centre slice of each nuclei. The z-stacks were collated into a 3D projection and the lamin A stain was inspected for each cell from all angles for any holes or areas of thinning. Images were deconvoluted prior to analysis.

2.2.7.3. YAP.

2.2.7.3.1. Staining methods.

Cells were plated onto 13 mm diameter glass coverslips coated with and without polyacrylamide hydrogels at a cell density of 30,000 cells/well in 24 well plates. Cells were cultured under these conditions at 37 °C for 24 hrs to allow for cells to adhere and spread onto the underlying matrix substrate. Cells were then washed once in 500 µL PBS and fixed with 500 µL 4% paraformaldehyde in PBS for 10 minutes at room temperature. Cells were then washed 2 times in 500 µL PBS for 5 minutes. Cells were blocked and permeabilised with 200 µL 0.1% v/v Triton-X-100 with 1% BSA in PBS for 10 minutes and then washed 3 times in 500 µL PBS for 5 minutes. Cells were washed 3 times in 500 µL PBS for 5 minutes. Cells were incubated with YAP primary antibody diluted in 100 µL 1% w/v BSA in PBS for 16 hrs at 4 °C in a humidified chamber. Cells were then washed 3 times in 500 µL PBS for 10 minutes. Cells were incubated with 100 µL of Alexa Fluor® 594–conjugated goat anti-rabbit IgG secondary antibody diluted in 1% w/v BSA in PBS with 1 µg/mL DAPI for 1 hr at room temperature protected from light. Coverslips were then washed 3 times in 500 µL PBS for 5 minutes and then mounted onto glass slides with a solution of 90% glycerol (90 mL glycerol mixed with 10 mL ddH_2O) as depicted in Figure 2.1. Slides were stored at 4 °C protected from light prior to analysis.

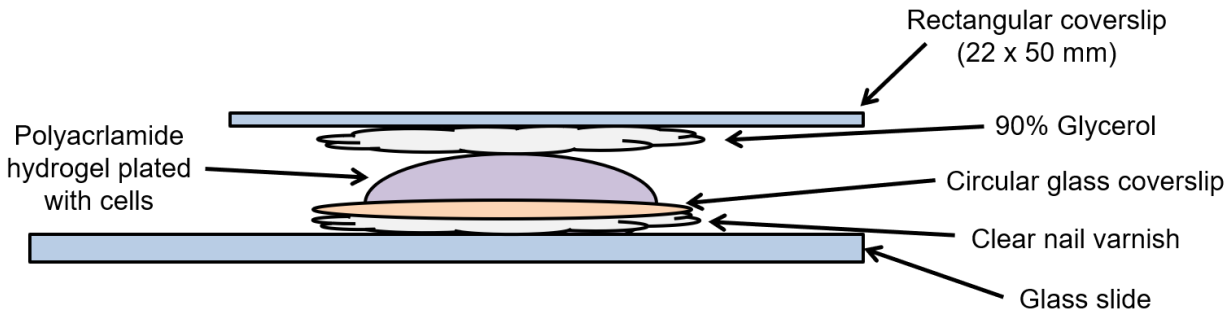

Figure 2.1. Schematic of the polyacrylamide gel mounting sandwich onto glass slides.

2.2.7.3.2. Analysis.

Images of 100 cells per condition per repeat were acquired on a Nikon TE200 inverted fluorescent microscope using a 60x/1.4 oil immersion objective lens with Volocity software (Perkin Elmer). Nuclear YAP intensity was determined by measuring the integrated density of the YAP staining using a thresholded image of the corresponding DAPI image in FIJI software.

2.2.7.4. E-cadherin and β-catenin.

2.2.7.4.1. Staining methods.

Cells were plated onto 13 mm diameter glass coverslips coated with and without polyacrylamide hydrogels at a cell density of 30,000 cells/well in 24 well plates. Cells were cultured under these conditions at 37 °C for 24 hrs. Cells were then washed once in 500 µL PBS and fixed with 500 µL 4% paraformaldehyde in PBS for 10 minutes at room temperature. Cells were washed 2 times in 500 µL PBS for 5 minutes. Cells were permeabilised with 200 µL 0.1% v/v Triton-X-100 with 2% BSA in PBS for 10 minutes at room temperature and then incubated with E-cadherin and β-catenin primary antibodies diluted in 100 µL 2% w/v BSA in PBS for 1 hr at room temperature in a humidified chamber. Cells were washed 3 times in 500 µL PBS for 5 minutes. Cells were then incubated with 100 µL of Alexa Fluor® 594–conjugated goat anti-mouse IgG secondary antibody and Alexa Fluor® 488–conjugated donkey anti rabbit IgG secondary antibody diluted in PBS with 1 µg/mL DAPI for 1 hr at room temperature protected from light. Coverslips were then washed 2 times in 500 µL PBS and then mounted onto glass slides with a solution of 90% glycerol as depicted in Figure 2.1.

2.2.7.4.2. Analysis.

Images of 30 cells per condition were acquired on a Nikon TE200 inverted fluorescent microscope using a 60x/1.4 oil immersion objective lens with Volocity software. Fluorescent channels of corresponding images were merged using FIJI and the localisation of E-cadherin and β-catenin assessed for each condition.

2.2.7.5. Ki67.

2.2.7.5.1. Staining methods.

Cells were plated onto 13 mm diameter glass coverslips coated with and without polyacrylamide hydrogels at a cell density of 10,000 cells/well in 24 well plates. Cells were cultured under these conditions at 37 °C for 96 hrs. Cells were then fixed with 500 µL 4% paraformaldehyde in PBS for 15 minutes at room temperature. Cells were washed 3 times in 500 µL PBS for 5 minutes, permeabilised with 200 µL 0.2% v/v Triton-X-100 in PBS for 10 minutes and then washed 3 times in 500 µL PBS for 5 minutes. Subsequently cells were blocked for 1 hr at room temperature with 200 µL 3% w/v BSA in PBS. Cells were incubated with Ki67 primary antibody diluted in 100 µL 1% w/v BSA in PBS for 2 hrs in a humidified chamber, then washed 3 times in 500 µL 0.2% Tween-20 in PBS for 5 minutes. Cells were then incubated with 100 µL of Alexa Fluor® 594–conjugated goat anti-mouse IgG secondary antibody diluted in 1% w/v BSA in PBS with 1 µg/mL DAPI for 1 hr at room temperature protected from light. Coverslips were then washed 3 times in 500 µL 0.2% Tween-20 in PBS and stored in PBS at 4 °C protected from light prior to imaging.

2.2.7.5.2. Analysis.

Images of 9 random fields of view per condition per repeat were acquired on a Nikon TE200 inverted fluorescent microscope using a 20x/0.45 objective lens with Volocity software. Images were acquired by imaging through the plate. Fluorescent channels of corresponding images were merged using FIJI and the number of nuclei that were stained with Ki67 counted to allow calculation of percentage of cells stained.

2.2.7.6. pH3.

2.2.7.6.1. Staining methods.

Cells were plated onto 25 mm diameter glass coverslips coated with and without polyacrylamide hydrogels at a cell density of 30,000 cells/well in 6 well plates. Cells were cultured under these conditions at 37 °C for 120 hrs. Cells were washed 2 times in 1 mL TBS for 5 minutes then fixed with 1 mL 4% paraformaldehyde in PBS for 10 minutes at room temperature. Cells were then washed 2 times in 500 µL TBS for 5 minutes. Cells were permeabilised with 200 µL 0.2% v/v Triton-X-100 in TBS for 10 minutes and then washed 3 times in 500 µL TBS for 5 minutes. Subsequently cells were blocked for 1 hr at room temperature with 200 µL 3% w/v BSA in TBS. Cells were then washed 2 times in 500 µL TBS for 10 minutes. Cells were incubated with phosphorylated histone 3 (pH3) primary antibody diluted in 100 µL 1% w/v BSA in TBS for 16 hrs in a humidified chamber at 4 °C. Cells were then washed 3 times in 500 µL TBS for 10 minutes. Cells were incubated with 100 µL of Alexa Fluor® 594–conjugated goat anti-rabbit IgG secondary antibody diluted in 1% w/v BSA in PBS with 1 µg/mL DAPI for 1 hr at room temperature protected from light. Coverslips were then washed 3 times in 500 µL TBS and then mounted onto glass slides with a solution of 90% glycerol as depicted in Figure 2.1.

2.2.7.6.2. Analysis.

Images of 9 random fields of view per condition per repeat were acquired on a Nikon TE200 inverted fluorescent microscope using a 20x/0.45 objective lens with Volocity software. Fluorescent channels of corresponding images were merged using FIJI and the number of cells positive for pH3 were counted and divided by the total number of cells to give the mitotic index.

2.2.7.7. Incorporation of IdU.

2.2.7.7.1. Staining methods.

Cells were plated onto 13 mm diameter glass coverslips coated with and without polyacrylamide hydrogels at a cell density of 30,000 cells/well in 24 well plates. Cells were cultured under these conditions at 37 °C for 24 hrs. Cells were then incubated with 25 μM of 5-iodo-2'-deoxyuridine (IdU) for 10 minutes at 37 °C. Cells were then washed in PBS for 1 minute before being pre-extracted with ice-cold pre-extraction buffer (10 mM HEPES, 1.5 mM magnesium chloride, 0.34 M sucrose, 10% glycerol, 0.1% Triton-X-100, 1 mM phenylmethanesulphonyl fluoride (PMSF)) for 5 minutes at 4 °C. Cells were then fixed with 500 μL 3% paraformaldehyde with 2% sucrose in PBS for 10 minutes at room temperature. Cells were then washed 3 times in 500 μL PBS for 5 minutes. Cells were permeabilised with 200 μL 0.5% v/v Triton-X-100 in PBS for 5 minutes at 4 °C and then washed 2 times in 500 μL PBS for 5 minutes. DNA was denatured by adding 200 μL of 2 M HCl to cells for 40 minutes at room temperature. Cells were then soaked in 500 μL PBS for 5 minutes then washed 3 times in 500 μL PBS for 10 minutes. Subsequently cells were blocked for 1 hr at room temperature with 200 μL blocking buffer (0.1% Tween 20 with 1% w/v BSA in PBS). Cells were incubated with 5-bromo-2'-deoxyuridine (BrdU) (clone B44) primary antibody diluted in 100 μL of blocking buffer for 1 hr at room temperature in a humidified chamber. Cells were then washed 3 times in 500 μL PBS for

5 minutes. Cells were then incubated with 100 µL of Alexa Fluor® 488–conjugated goat anti-mouse IgG secondary antibody diluted in blocking buffer with 1 µg/mL DAPI for 1.5 hrs at room temperature protected from light. Coverslips were then washed 2 times for 5 minutes in 500 µL PBS and then mounted onto glass slides with a solution of 90% glycerol as depicted in Figure 2.1.

2.2.7.7.2. Analysis.

Images of 100 cells per condition per repeat were acquired on a Nikon TE200 inverted fluorescent microscope using a 60x/1.4 oil immersion objective lens with Volocity software. Nuclear IdU intensity was determined by measuring the mean grey value of the IdU staining using a thresholded image of the corresponding DAPI image in FIJI software. As the background fluorescence was high in these samples stained with IdU an average background measurement was made. The mean grey value was measured for five background spots per image and averaged for each condition and each repeat. The average background mean grey value of each condition was subtracted from the nuclear IdU mean grey value of each cell to normalise for the background in each sample for each repeat.

2.2.7.8. Heterochromatin and euchromatin.

2.2.7.8.1. Staining methods.

Cells were plated onto 13 mm diameter glass coverslips coated with and without polyacrylamide hydrogels at a cell density of 30,000 cells/well in 24 well plates. Cells were cultured under these conditions at 37 °C for 24 hrs. Cells were then washed in PBS for 5 minutes before being fixed with 500 µL 100% ice-cold ethanol for 15 minutes at -20 °C. Cells were washed 3 times in 500 µL PBS for 5 minutes. Cells were permeabilised

with 200 µL 0.5% v/v Triton-X-100 in PBS for 30 minutes at room temperature and then washed 3 times in 500 µL PBS for 5 minutes. Subsequently cells were blocked for 1 hr at room temperature with 200 µL 10% v/v goat serum in PBS. Cells were then washed 3 times in 500 µL PBS for 5 minutes. Cells were incubated with H3K4me3 and H3K9me3 primary antibodies diluted in 100 µL of 3% goat serum in PBS for 16 hrs at 4 °C in a humidified chamber. Cells were then washed 3 times in 500 µL PBS for 10 minutes. Cells were incubated with 100 µL of Alexa Fluor® 488–conjugated donkey anti-rabbit IgG and Alexa Fluor® 594–conjugated goat anti-mouse secondary antibody diluted in 3% goat serum in PBS with 1 µg/mL DAPI for 1 hr at room temperature protected from light. Coverslips were then washed 3 times for 5 minutes in 500 µL PBS and stored in PBS at 4 °C protected from light prior to imaging.

2.2.7.8.2. Analysis.

Cells were imaged in a µ-Dish, 35 mm high glass bottomed Petri Dishes gel side down at the Wolfson light microscopy facility, using the Applied Precision deconvolution DeltaVision microscope. A UPlanSAPO 40x oil objective lens was employed to image z-stack images using SoftWorks software. At least 15 cells were analysed for each condition. The middle slice of each nuclei was analysed for each cell. Nuclear H3K4me3 and H3K9me3 intensity was determined by measuring the integrated density using a thresholded image of the corresponding DAPI image in FIJI software. Intensity was also measured for each condition in FIJI for a cross-nuclear profile by drawing a line across the longest axis of the nucleus for each stain to allow for investigation of foci distribution. An intensity plot was generated for each nucleus for each condition.

2.2.7.9. γH2AX and pRPA T21.

2.2.7.9.1. Staining methods.

Cells were plated onto 13 mm diameter glass coverslips coated with and without polyacrylamide hydrogels at a cell density of 30,000 cells/well in 24 well plates. Cells were cultured under these conditions at 37 °C for 16 hrs. The medium was then removed from cells and then washed once in 500 µL TBS for 5 minutes. Cells were fixed with 500 µL 4% paraformaldehyde in PBS for 10 minutes at room temperature and then washed 2 times in 500 µL TBS for 5 minutes. Cells were then washed 3 times with 500 µL 0.2% v/v Tween-20 in TBS for 10 minutes and then blocked for 1 hr at room temperature with 200 µL 3% w/v BSA in TBS. Cells were then washed 2 times with 500 µL 0.2% v/v Tween-20 in TBS for 10 minutes and then incubated with phosphorylated H2A histone family member X (γH2AX) ser139 (S139) and phosphorylated replication protein A (pRPA) thr21 (T21) primary antibodies diluted in 100 µL 0.5% w/v BSA with 0.25% Triton-X-100 in TBS for 16 hrs in a humidified chamber at 4 °C. Cells were washed 3 times in 500 µL 0.2% v/v Tween-20 in TBS for 5 minutes. Cells were then incubated with 100 µL of Alexa Fluor® 488–conjugated donkey anti-rabbit IgG secondary antibody and Alexa Fluor® 594–conjugated goat anti-mouse IgG secondary antibody diluted in 0.5% w/v BSA with 0.25% Triton-X-100 in with 1 µg/mL DAPI for 1 hr at room temperature protected from light. Coverslips were then washed 2 times in TBS prior to being mounted onto glass slides with a solution of 90% glycerol as depicted in Figure 2.1.

2.2.7.9.2. Analysis.

Images of 100 cells per condition per repeat were acquired on a Nikon TE200 inverted fluorescent microscope using a 60x/1.4 oil immersion objective lens with Volocity software. The nuclear γH2AX and pRPA T21 foci number per nuclei were counted using a foci counter macro provided by Dr Darren Robbinson (Wolfson Light Microscopy

Facility) using FIJI software for each condition. The number of micronuclei per cell were also counted and scored for γH2AX positivity from the same images.

2.2.7.10. RPA34.

2.2.7.10.1. Staining methods.

Cells were plated onto 13 mm diameter glass coverslips coated with and without polyacrylamide hydrogels at a cell density of 15,000 cells/well in 24 well plates. Cells were cultured under these conditions at 37 °C for 24 hrs prior to treatment with or without gemcitabine for a further 24 hrs. The medium was then removed from cells and they were incubated on ice with 300 µL ice-cold extraction buffer (100 mM NaCl, 300 mM sucrose, 3 mM magnesium chloride, 10 mM piperazine-N,N′-bis(2-ethanesulphonic acid) (PIPES) pH 6.8, 0.5% Triton-X-100) for 2 minutes. Cells were then washed once with 500 µL TBS and then fixed with 500 µL 4% paraformaldehyde in PBS for 10 minutes at room temperature. Cells were washed 2 times in 500 µL TBS for 5 minutes. Cells were washed 3 times with 500 µL 0.2% v/v Triton-X-100 in TBS for 10 minutes and then blocked for 30 minutes at room temperature with 200 µL 3% w/v BSA in TBS. Cells were incubated with RPA34 primary antibody diluted in 100 µL 1% w/v BSA in TBS for 1.5 hrs in a humidified chamber at room temperature. Cells were then washed 3 times in 500 µL 0.2% v/v Triton-X-100 in TBS for 5 minutes. Cells were incubated with 100 µL of Alexa Fluor® 488–conjugated goat anti-mouse IgG secondary antibody diluted in 1% w/v BSA in PBS with 1 µg/mL DAPI for 1 hr at room temperature protected from light. Coverslips were then washed 3 times in 0.2% v/v Triton-X-100 in TBS and then once in 500 µL TBS prior to being mounted onto glass slides with a solution of 90% glycerol as depicted in Figure 2.1.

2.2.7.10.2. Analysis.

Images of 100 cells per condition per repeat were acquired on a Nikon TE200 inverted fluorescent microscope using a 60x/1.4 oil immersion objective lens with Volocity software. Nuclear RPA34 intensity was determined by measuring the integrated density of the RPA34 staining using a thresholded image of the corresponding DAPI image in FIJI software.

2.2.7.11. γH2AX and p53.

2.2.7.11.1. Staining methods.

Cells were plated onto 13 mm diameter glass coverslips coated with and without polyacrylamide hydrogels at a cell density of 15,000 cells/well in 24 well plates. Cells were cultured under these conditions at 37 °C for 24 hrs prior to treatment with or without gemcitabine for a further 24 hrs. Cells were then washed once with 500 µL TBS and then fixed with 500 µL 4% paraformaldehyde in PBS for 10 minutes at room temperature. Cells were then washed 2 times in 500 µL TBS for 5 minutes. Cells were then permeabilised with 500 µL 0.5% v/v Triton-X-100 in TBS for 10 minutes at room temperature and then washed 3 times with 500 µL TBS for 5 minutes. Cells were blocked for 1 hr at room temperature with 200 µL 3% w/v BSA in TBS. Cells were then washed two times with 500 µL TBS for 10 minutes before being incubated with γH2AX and p53 primary antibodies diluted in 100 µL 1% w/v BSA in TBS for 16 hrs in a humidified chamber at 4 °C. Cells were then washed 4 times in 500 µL TBS for 10 minutes. Cells were incubated with 100 µL of Alexa Fluor® 488–conjugated goat anti-mouse IgG secondary antibody and Alexa Fluor® 594–conjugated goat anti-rabbit IgG secondary antibody diluted in 1% w/v BSA in PBS with 1 µg/mL DAPI for 1 hr at room temperature protected from light. Coverslips were then washed 3 times in TBS for 5 minutes prior to being mounted onto glass slides with a solution of 90% glycerol as depicted in Figure 2.1.

2.2.7.11.2. Analysis.

Images of 100 cells per condition per repeat were acquired on a Nikon TE200 inverted fluorescent microscope using a 60x/1.4 oil immersion objective lens with Volocity Software. Nuclear γH2AX and p53 intensity was determined by measuring the integrated density of the staining using a thresholded image of the corresponding DAPI image in FIJI software.

2.2.8. Western blotting.

2.2.8.1. Lysate production.

2.2.8.1.1. Cells cultured on plastic.

One million MCF-7 cells were plated in a 10 cm Petri dish and incubated at 37 °C for 72 hrs. Cells were washed twice with ice-cold PBS and the cells dislodged by cell scraping. The plate was washed in 10 mL of ice-cold PBS and collected in a 15 mL falcon tube. Cells were pelleted at 1,200 RPM for 3 minutes. The resultant pellet was washed twice in ice-cold PBS and then moved to a 1 mL Eppendorf tube and pelleted once more at 2,000 RPM for 3 minutes. The pellet was resuspended in one pellet volume of 1x lysis buffer (700 µL ddH_2O, 200 µL 5x RIPA lysis buffer, 10 µL 100 mM PMSF, 10 µL 100x protease inhibitor, 10 µL 100x phosphatase inhibitor and 2 µL Benzonase per 1 mL). The resuspended pellet was incubated on ice and periodically vortexed every 10 minutes for 30 minutes and then passed through a 25G needle 10 times. This solution was then centrifuged for 10 minutes at 13,400 RPM at 4 °C. The supernatant was removed into a new 1 mL Eppendorf tube and stored at -20 °C prior to protein quantification and analysis via Western blot.

2.2.8.1.2. Cells cultured on polyacrylamide hydrogels.

Three million cells were plated onto a 10 cm^2 polyacrylamide gel in a 14.5 cm Petri dish with 30 mL of medium and incubated at 37 °C for 72 hrs. All extract production was undertaken at 4 °C. Gels were washed twice in ice-cold PBS and then inverted onto 200 µL of 1x lysis buffer as detailed in section 2.2.8.1.1. for 1 minute. The resultant lysis solution was removed into a 1 mL Eppendorf tube and then vortexed, passed through a needle and centrifuged as detailed in section 2.2.8.1.1.

2.2.8.2. Protein quantification.

Quantification of protein content of RIPA lysates was performed by first producing a standard curve of known BSA concentrations in 1.5 mL Eppendorf tubes as detailed in Table 2.2. One microlitre of each lysate was diluted in 799 µl of ddH_2O followed by addition of 200 µl of Bio-Rad protein assay dye reagent concentrate in 1.5 mL Eppendorf tubes. Diluted lysates and BSA standards were mixed by inversion and then 200 µL of each solution moved to a 96 well plate. The optical density (OD) was measured using a Multiskan™ FC microplate photometer at a wavelength of 595 nm. ODs of BSA standards were plotted against their known concentrations to produce a standard curve. From this the total protein concentration within sample lysates was calculated.

Total Protein (µg)	0.1 mg/mL BSA (µL)	ddH_2O (µL)	Bio-Rad Protein Assay Dye Reagent Concentrate (µL)
0	0	800	200
1	10	790	200
5	50	750	200
10	100	700	200
15	150	650	200
20	200	600	200

Table 2.2. Volumes for BSA standard curve.

2.2.8.3. SDS-PAGE.

A polyacrylamide gel of the desired percentage (8, 10 or 12%) was made as is detailed in Table 2.3. Volumes were scaled up and down as required to produce multiple gels. Once the resolving gel was set 5 mL of stacking gel was poured on top and a comb of desired well number placed into it. The wells were washed with water following setting to ensure that they were clear of any debris. Lysates achieved by RIPA lysis were loaded at a protein concentration of 30-60 µg per lane with 1x SDS sample buffer. One lane containing 5 µL of Precision Plus protein standard was run parallel to the samples. Samples were separated in 1x SDS-PAGE running buffer at 180 V for 45 minutes to 1 hr 30 minutes until the proteins of interested were sufficiently separated.

Resolving gel (10 mL)				Stacking gel (5 mL)	
Solution	**8%**	**10%**	**12%**	**Solution**	**5%**
	Volume (mL)				**Volume (mL)**
ddH_2O	4.6	4.0	3.3	ddH_2O	3.4
30% Acrylamide/0.8% Bis-acrylamide mix	2.7	3.3	4.0	30% Acrylamide/0.8% Bis-acrylamide mix	0.83
1.5 M Tris pH 8.8	2.5	2.5	2.5	1.5 M Tris pH 6.8	0.63
10% SDS	0.1	0.1	0.1	10% SDS	0.05
10% APS	0.1	0.1	0.1	10% APS	0.05
TEMED	0.006	0.004	0.004	TEMED	0.005

Table 2.3. Volumes for resolving and stacking gel recipes.

2.2.8.4. Protein transfer.

Following SDS-PAGE proteins were then transferred from the gels onto 0.45 µm Protran nitrocellulose transfer membrane (GE Healthcare) using a Criterion blotter and 1x pre-chilled Towbin transfer buffer on ice. A current of 85 V was used for 2 hrs.

2.2.8.5. Membrane blocking and probing.

Following protein transfer membranes were blocked with 5% w/v skimmed milk powder in TBS for 1 hr at room temperature. Membranes were then probed with primary antibody diluted in 5% w/v skimmed milk powder in TBS at 4 °C for 16-24 hrs. Membranes were

washed three times with 0.05% v/v Tween-20 in TBS (TBS-T) every 10 minutes. Membranes were then incubated with the appropriate HRP-labelled secondary antibody diluted in 5% w/v skimmed milk powder in TBS for 1 hr at room temperature. Following secondary antibody incubation membranes were washed three times with TBS-T every 10 minutes prior to chemiluminescent detection.

2.2.8.6. Enhanced chemiluminescence (ECL).

Equal volumes of reagent 1 and reagent 2 of the Amersham ECL Western blotting detection reagent kit were mixed in a falcon tube and then incubated with the membrane for 1 minute at room temperature with gentle agitation to ensure full coverage of the membrane. The membrane was then moved to a developing cassette and exposed to X-ray film in a dark room for varying amounts of time to acquire different exposures. The signal was developed and fixed in the film processor using RG universal X-ray developer and using RG universal X-ray fixer respectively.

2.2.8.7. Western blot quantification.

Developed films were scanned in on an EPSON EXPRESSION 1680 pro scanner in JPEG format at 1600 dpi. Relative protein expression levels in each sample were determined by first quantifying the band densitometry of the target protein in FIJI software. This value was then normalised to the band densitometry of glyceraldehyde 3-phosphate dehydrogenase (GAPDH) for the same sample. A medium exposure was chosen for each protein to ensure it was within the detection range and that signals were not saturated.

2.2.9. Quantitative reverse transcriptase polymerase chain reaction.

Reverse transcriptase quantitative polymerase chain reaction (RT-q-PCR) allows for the mRNA expression level of a gene of interest to be quantified. The extracted mRNA is first transcribed into cDNA before it is then detected using a polymerase chain reaction (PCR) probe against the genes of interest and a house keeping gene control. You will then acquire a cycle threshold number also known as the Ct value which is the quantified number of PCR cycles required for the gene of interest to have reached a detection threshold. Therefore, if a sample has a lower Ct value it took less cycles for the gene to pass the given threshold indicating that there is more of it present within the sample compared to a sample with a higher Ct. A delta Ct value is achieved by normalising the Ct value of the gene of interest to that of the housekeeping gene.

We used RT-q-PCR to confirm total progesterone receptor gene (*PGR)* expression of the breast cancer cell lines used in our gemcitabine sensitivity assays. This was undertaken by Fatma Bucklain.

We also used RT-q-PCR to determine the levels of total *PGR* and the *PGR-B* isoform in MCF-7 cells cultured on 500 Pa and 4 kPa stiffness polyacrylamide hydrogels following treatment with mifepristone and gemcitabine alone or in combination using TaqMan technology.

2.2.9.1. RNA extraction from mammalian cell lines.

For determination of cell line total *PGR* levels Qiagen technology was used. RNA was extracted from MCF-7, T-47D, ZR-75-1, CAL-51, MDA-MB-231 and MDA-MB-468 cell

lines using a Qiagen RNeasy Plus Mini kit following the manufacturers protocol and stored at -80 °C. Three samples were collected for each cell line.

For investigations in our polyacrylamide model into total *PGR* and *PGR-B* isoform expression MCF-7 cells were plated on 500 Pa or 4 kPa stiffness polyacrylamide hydrogels or a glass control at 150,000 cells/well in a 6-well plate for 24 hrs. Ten micromolar mifepristone or a vehicle control was added to cells for 24 hrs prior to the addition of 5 nM gemcitabine or a vehicle control for a further 24 hrs. Cells were washed in PBS then RNA was extracted using Trizol and Phasemaker technology. Each coverslip was moved to a new plate then 500 µL Trizol was added to the top of each gel. Cells were agitated in the Trizol solution by pipetting and then incubated for a further 3 minutes. The Trizol solution from each well was moved to a pre-centrifuged Phasemaker tube with the addition of 100 µL of chloroform. The solutions were mixed in the Phasemaker tubes for 3 minutes and then centrifuged at 12,000 RPM for 5 minutes at 4 °C. The aqueous phase was transferred to a new RNAse free Eppendorf tube. Two hundred and fifty microlitres of isopropanol was added to each tube and then mixed by inversion. The samples were left overnight at 4 °C to allow RNA to precipitate. RNA was then pelleted by centrifugation at 12,000 RPM for 10 minutes at 4 °C. RNA was then resuspended in 500 µL 75% ethanol by vortex. RNA was then pelleted by centrifugation at 7,500 RPM at 4 °C. The supernatant was discarded, and the pellet allowed to air dry for 10 minutes at room temperature. Finally, the RNA was resuspended in 30 µL RNAse free water and heated at 55 °C for 10 minutes. RNA quantity and quality were measured by nanodrop on the RNA-40 setting, where an A260/A280 ratio of 2.0 was used to determine RNA purity. RNA samples were then stored at -80 °C prior to DNAse treatment. One sample was collected for each condition.

2.2.9.2. DNAse treatment of polyacrylamide gel harvested samples.

The RNA samples harvested from polyacrylamide gels were to be probed with a primer which did not cross an exon-exon boundary. We therefore undertook a separate DNAse treatment of each sample to ensure any genomic DNA was removed to allow for only the measurement of cDNA during the RT-q-PCR. DNAse treatment was undertaken using a DNA-free™ DNA removal kit. Briefly samples were incubated with DNAse at 37 °C for 20 minutes prior to the addition of DNase inactivation reagent for 2 minutes at room temperature. The RNA samples were retrieved via centrifugation at 10,000 RPM for 1.5 minutes and harvested to a new RNAse free Eppendorf. RNA concentration was checked via nanodrop using the RNA-40 setting and then the sample was stored at -80 °C.

2.2.9.3. Reverse transcription of RNA into cDNA.

Cell line samples for determining total *PGR* expression levels were reverse transcribed from RNA into cDNA by use of a Qiagen RT^2 first strand kit following the manufactures protocol, by Fatma Bucklain.

RNA samples harvested from polyacrylamide gels were reverse transcribed into cDNA by use of a high capacity cDNA reverse transcription kit. Briefly, 2 µg of RNA was added to 10 µL of reverse transcription master mix (containing 1x dNTP mix, 1 x MultiScribe Reverse Transcriptase and 1x random primers) and brought up to 20 µL with nuclease free water. Samples were gently mixed by pipetting and then reverse transcribed in an Applied Biosystems 2700 GeneAmp PCR machine for 10 minutes at 25 °C, 120 minutes at 37 °C, 5 minutes at 85 °C and then finally kept indefinitely at 4 °C. The cDNA and remaining RNA samples were stored at -80 °C.

2.2.9.4. Quantitative-polymerase chain reaction.

cDNA samples from cell lines were quantified using Qiagen RT^2 SYBR® Green qPCR master mixes following the manufacturers protocol. Primers were used against total *PGR* (PPH01007F) and a *β-actin* control (PPH00073G).

cDNA samples from polyacrylamide gel cultured cells were quantified by use of TaqMan technology. One times TaqMan universal master mix was mixed with 1x TaqMan probe for either total *PGR* (Hs01556702_m1), *PGR B* (Hs04419616_s1) or a *GAPDH* control (Hs02786624_g1). The volume was made up to 10 µL with nuclease free water prior to the addition of 100 ng of cDNA to each well of a 364 well plate. For each sample of cDNA, a corresponding sample of RNA (sample prior to reverse transcriptase reaction) was also run alongside it to confirm that genomic DNA was not contaminated in the sample. Each sample of cDNA and its corresponding RNA sample were run in triplicate for each probe. A no sample control was also included to identify any possible contaminants. The plate was then sealed with a plate seal and centrifuged to remove air bubbles. Thermocycling was undertaken on an Applied Biosystems 7900 Real-Time PCR machine using recommended cycling conditions of 1 cycle of 95 °C for 10 minutes to allow for polymerase activation and an initial denaturation. Then 40 cycles of 95 °C for 15 seconds then 60 °C for 1 minute to allow for denaturation and then annealing and extension.

2.2.9.5. Analysis.

To determine the fold change in expression of our genes of interest to the house-keeping gene control we used the $2^{-\Delta\Delta Ct}$ calculation method. A normalised reporter value (Rn) value was first calculated by Applied Biosystems 7900 SDS 2.4 software by normalising

the probe fluorescence to that of an internal control, ROX (6-Carboxyl-Rhodamine – 610 nm), which is present within the master mix. The equation for this is depicted below:

$$\mathrm{Rn} = \mathrm{PCR\ Probe\ fluorescence} \div \mathrm{ROX\ passive\ reference\ based\ fluorescence}$$

From this a ∆Rn is calculated from the Rn and the baseline Rn (background + ROX fluorescence) as depicted below:

$$\Delta\mathrm{Rn} = \mathrm{Rn} - \mathrm{Baseline\ fluorescence}$$

A ∆Rn value of 0.2 was defined by the software and used as the fluorescence threshold required to establish a Ct value for each reaction.

Samples were run in triplicate for each probe and the average Ct value calculated for each sample. The delta Ct value was calculated as depicted below:

$$\Delta Ct = Ct\ value\ of\ gene\ of\ interest - Ct\ value\ of\ housekeeping\ gene$$

This value was used as the comparison point for the cell line samples.

For the samples extracted from cells cultured on polyacrylamide gels the ∆∆Ct value was calculated by normalising to the control sample as depicted below, which in this experiment was sample extracted from untreated cells cultured on glass.

$$\Delta\Delta Ct = \Delta Ct\ of\ sample\ of\ interest - \Delta Ct\ of\ control\ sample$$

Finally, the fold change in expression was then calculated for each sample relative to the control sample for each gene of interest as depicted below:

$$Fold\ change\ in\ expression = 2^{-\Delta\Delta Ct}$$

2.2.10. Statistical analysis.

For parametric data the mean ± the standard deviation (SD) are presented when one data value was obtained for each condition from each independent repeat. Parametric data is presented as the mean ± the standard error of the mean (SEM) when more than one data value was obtained from each condition from each independent repeat, where the mean of means was calculated. For non-parametric data the median is plotted.

Where only one sample required comparison to another sample an unpaired one-tailed Student's t-test was used for parametric data sets. Where more than one sample required comparing to another an ordinary one-way ANOVA test with Sidak's multiple comparisons was used for parametric data sets for the selected samples which required statistical comparison.

For non-parametric data where only one sample required comparison to another sample a one-tailed Mann-Whitney test was used. For non-parametric data which required multiple comparisons a Kruskal-Wallis test with Dunn's multiple comparisons was used for the selected samples which required statistical comparison.

Statistical tests were carried out in Microsoft Excel and in GraphPad Prism Version 8 using a cut off for statistical significance of $p = 0.05$.

3. Evaluation of polyacrylamide hydrogels as a breast cancer stiffness model.

3.1. Introduction, aims and hypothesis.

Increased tissue stiffness is associated with tumorgenicity where the normal breast has an elastic modulus of around 170 Pa and the cancerous breast has an elastic modulus of around 4 kPa (Paszek et al., 2005). TCP commonly used in laboratories has a stiffness of 3 gigapascals (GPa) and glass coverslips have a stiffness of nearly 70 GPa (Paszek et al., 2005). Therefore, commonly used culture surfaces do not represent the stiffnesses encountered by cancer cells *in vivo* and therefore are not fit as models to study the role matrix stiffness plays in response to chemotherapeutics. Several *in vitro* tissue stiffness models are reported, these include hydrogels based on PEG, polyacrylamide, alginate and collagen (Caliari & Burdick, 2016).

The first stiffness model investigated in this thesis are polyacrylamide hydrogels due to their compatibility with microscopy, previous optimisation within the literature and reported stiffness reproducibility. Whilst the methodology for formation of these hydrogels has been published, it has not been undertaken within our laboratory. As such, the first task was to reproduce the model. Further, this type of matrix has not frequently been used with breast cancer cells within the 170 Pa – 4 kPa stiffness range. Therefore, the model needed to be optimised and breast cancer cell growth characterised in this model. The first chapter of this thesis will investigate the suitability of polyacrylamide gels for comparison of stiffness specific responses to chemotherapeutics in breast cancer. In all experiments a glass control was implemented to allow for confirmation that the experiment was working. As the glass was not coated in collagen it could not be used as a direct comparison to the polyacrylamide hydrogel model.

The breast cancer cell line MCF-7 was chosen for optimisation steps as it is well established within the lab, is ER and PR positive and is easy to culture. The MDA-MB-231 cell line was also used alongside the MCF-7 cell line at some stages to allow for investigation of potential differences to a TNBC cell line.

The hypothesis of this chapter is:

Breast cancer cells cultured at a stiffness physiologically relevant to breast cancer tissue will exhibit differential morphological features and growth characteristics compared to breast cancer cells grown at a stiffness physiologically observed in normal breast tissue and on common *in vitro* culture surfaces such as glass.

The aims of this chapter are:

1. To make polyacrylamide hydrogels of stiffnesses which are physiologically relevant to normal and cancerous breast tissue.
2. To characterise the morphology and growth of breast cancer cell lines cultured on polyacrylamide gels of physiologically relevant stiffness.

The objectives of this chapter are to assess:

1. Whether polyacrylamide gels of stiffnesses physiologically relevant to normal and cancerous breast tissue can be made.
2. The effect of matrix stiffness on breast cancer cell morphology.
3. The effect of matrix stiffness on the localisation and expression of stiffness responsive proteins.
4. The effect of matrix stiffness on breast cancer cell growth and mitotic index.
5. The effect of stiffness on DNA replication in breast cancer cells.

3.2. Results.

3.2.1. Production of polyacrylamide hydrogels of stiffnesses physiologically relevant to normal and cancerous breast tissue.

3.2.1.1. Determining acrylamide and bis-acrylamide concentrations required to produce a relevant stiffness range.

In this polyacrylamide hydrogel model, cells are plated on top of collagen I coated polyacrylamide gels which are formed on glass coverslips as depicted in Figure 3.1.

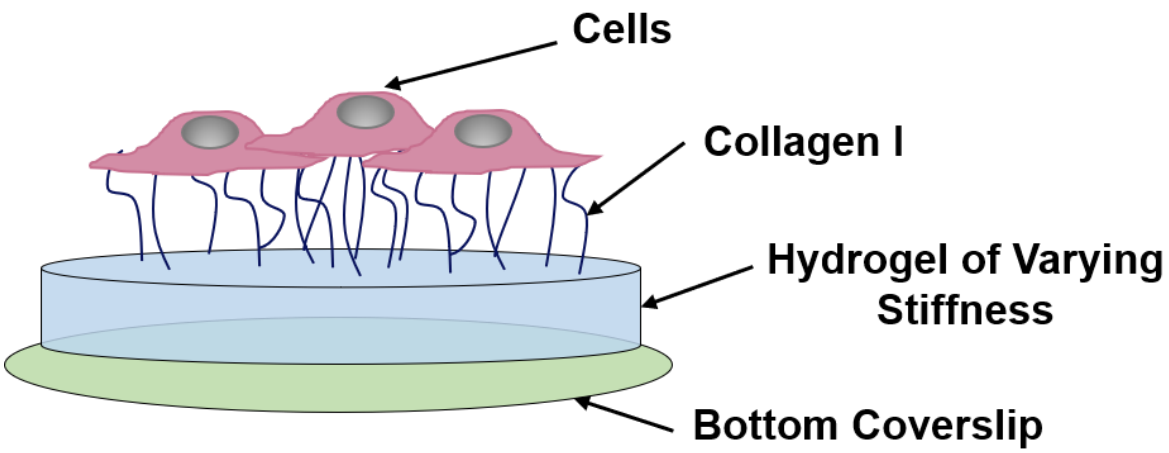

Figure 3.1. Schematic diagram of polyacrylamide hydrogels used for 2D stiffness assays. Polyacrylamide hydrogels were formed on top of a glass coverslip. Acrylamide and bis-acrylamide percentages were altered to give hydrogels of varying stiffnesses. Collagen I was chemically crosslinked to the hydrogel to facilitate cell attachment. Following gel sterilisation, cells could be seeded on top of the gels.

The acrylamide and bis-acrylamide percentages of the hydrogel can be varied to give different gel stiffnesses. For initial determination of a suitable stiffness range, four different hydrogel compositions were investigated following a protocol provided by Professor Rebecca Wells (University of Pennsylvania).

Hydrogel stiffnesses were measured using rheology with the help of Dr Pete Laity (University of Sheffield) (Figure 3.2.). Hydrogels were made complete with collagen coating and stored in PBS as they would be prior to cell seeding. Representative rheological plots for each composition are shown in Figure 3.2.a. The small phase angle observed for the 5.42, 7.46 and 10.27% acrylamide gels indicates that full gelation has occurred in these samples (Larsen, Bjørnstad, Pettersen, Tønnesen, & Melvik, 2015). Conversely the 2.25% acrylamide gel had a high variable phase angle which suggests that full gelation had not occurred. Average elastic moduli are plotted for the four gel compositions at a frequency of 1 Hz (Figure 3.2.b). A frequency of 1 Hz was chosen based on the whole body heart rate frequency which is predicted to be 1.4 Hz (Linwang, Jan, Shyu, Chiang, & Wang, 2004). The different gel percentages measured a range of elastic moduli which increased with increasing acrylamide and bis-acrylamide percentages where the 5.42% acrylamide gel measured an average of 522 ± 37 Pa, the 7.46% acrylamide gel measured an average of 4453 ± 334 Pa and the 10.27% acrylamide gel measured an average of 5736 ± 901 Pa (average ± SEM). Due to the softness of the 2.25% acrylamide gel the rheometer was unable to make a reading at higher frequencies due to destruction of the gel. To allow for comparison, average elastic moduli are also plotted for the four gel compositions at the highest frequency that the 2.25% acrylamide gel did not error at which was 0.4 Hz (Figure 3.2.c). There was very little difference in the average measured elastic moduli for the 5.42% and 7.46% acrylamide gels at 0.4 Hz compared to 1 Hz (525 ± 37 Pa and 4481 ± 342 Pa respectively). The 10.27% acrylamide gels had a slightly higher measured average elastic average modulus at 0.4 Hz of 7361 ± 649 Pa. The 2.25% acrylamide gel had a measured elastic modulus of 1.17 ± 0.37 Pa at 0.4 Hz.

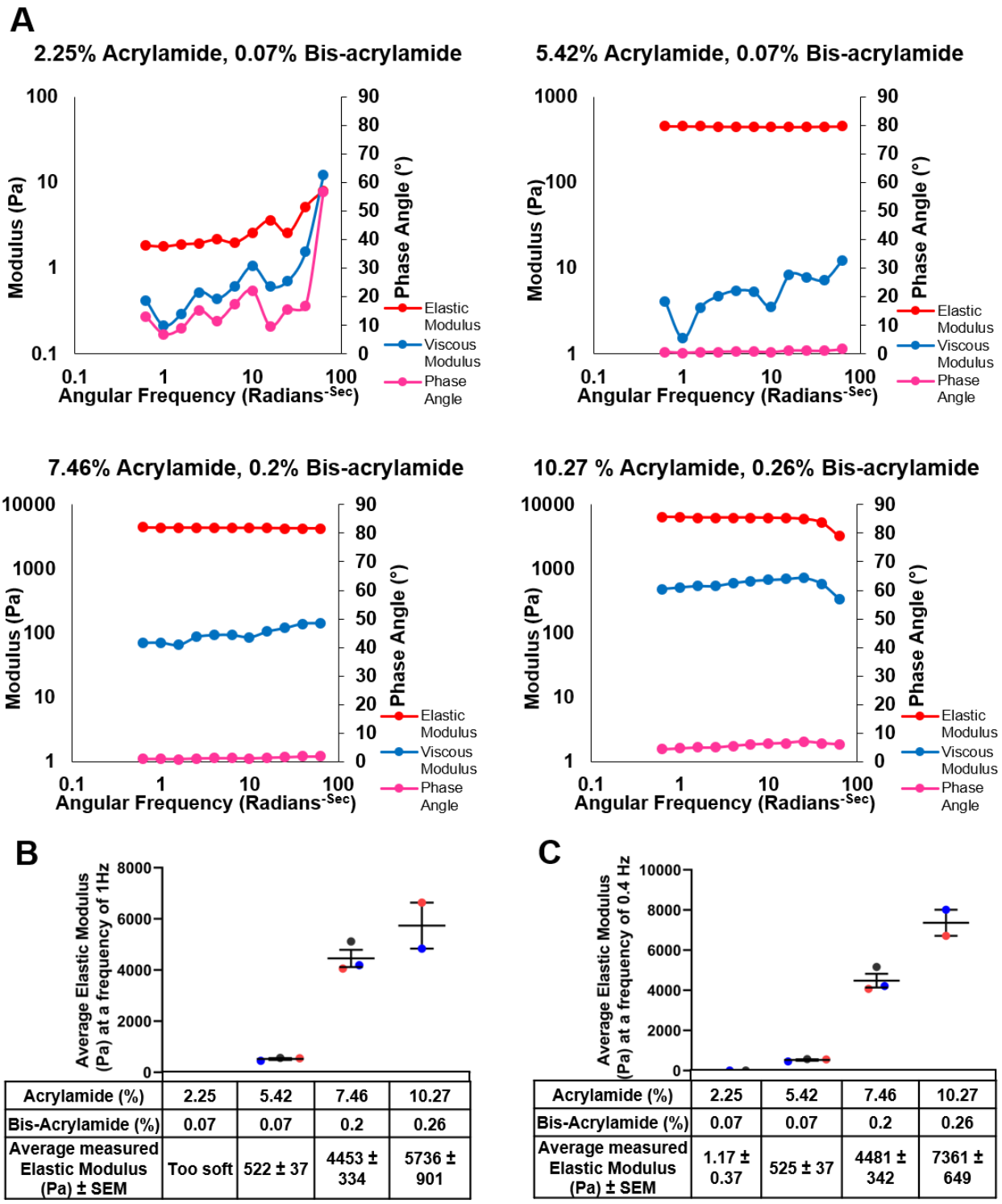

Acrylamide (%)	2.25	5.42	7.46	10.27
Bis-Acrylamide (%)	0.07	0.07	0.2	0.26
Average measured Elastic Modulus (Pa) ± SEM	Too soft	522 ± 37	4453 ± 334	5736 ± 901

Acrylamide (%)	2.25	5.42	7.46	10.27
Bis-Acrylamide (%)	0.07	0.07	0.2	0.26
Average measured Elastic Modulus (Pa) ± SEM	1.17 ± 0.37	525 ± 37	4481 ± 342	7361 ± 649

Figure 3.2. Rheological measurements of polyacrylamide hydrogels. Legend overleaf.

Figure 3.2. Rheological measurements of polyacrylamide hydrogels. (A) A representative example of rheological graphs for each gel composition showing elastic modulus, viscous modulus and phase angle. Rheological measurements were made on a Bohlin Gemini 200 rheometer fitted with a 25 mm diameter flat plate at 37 °C. A force of 0.2-5 N was applied to each hydrogel at an oscillating frequency of 10 to 0.01 Hz at a strain of 0.02%. (B) Average elastic modulus ± standard error of the mean of 3 gels measured per repeat for 2 independent repeats for the 2.25% and 10.27% acrylamide gels and 3 independent repeats for the 5.42% and 7.46% acrylamide gels at a frequency of 1 Hz. The Rheometer errored at this frequency for the 2.25% acrylamide and 0.07% bis-acrylamide gel due to the softness of this gel. Each repeat is plotted in a co-ordinating colour and the average and SEM are depicted as a black bar. (C) Average elastic modulus ± standard error of the mean of 3 gels measured per independent for 2 independent repeats for the 2.25% and 10.27% acrylamide gels and 3 independent repeats for the 5.42% and 7.46% acrylamide gels at a frequency of 0.4 Hz. Each repeat is plotted in a co-ordinating colour and the average and SEM are depicted as a black bar.

Further gel percentage combinations were investigated following a nature protocols paper (Fischer, Myers, Gardel, & Waterman, 2012). When the stiffness was measured using rheology large variations were observed in the shear moduli when different forces were applied, suggesting their unsuitability for use as a stiffness model (data not shown).

Polyacrylamide hydrogels hereafter will be referred to by their measured shear elastic moduli measured at 1 Hz for the 5.42% (500 Pa), 7.46% (4 kPa) and 10.27% (6 kPa) acrylamide gels and at 0.4 Hz for the 2.25% (1 Pa) acrylamide gel rounded to one significant figure. Following rheological measurements, we chose to focus on the 500 Pa and 4 kPa stiffnesses, due to their closeness to the normal breast tissue stiffness of 170 Pa and the cancerous breast tissue stiffness of 4 kPa respectively (Paszek et al., 2005). Exceptions to this are in the initial imaging of cells (Figure 3.4.) and in initial investigations into cell growth (Figures 3.9. and 3.12.) where all 4 stiffnesses were examined.

3.2.1.2. Assessing the effect of collagen and breast cancer cells on polyacrylamide hydrogel stiffness.

Following rheological analysis of the hydrogels alone it was important to investigate if the collagen coating or cells altered gel stiffness. Polyacrylamide hydrogels were measured uncoated, with their collagen coating as in Figure 3.2. and with both the collagen coating and plated cells for either 24 or 96 hrs, timepoints that would be relevant to future assays. The results of the measurements for 3 gels on one occasion are plotted in Figure 3.3. For 500 Pa gels neither the collagen coating nor the addition of plated cells resulted in a significant change in the average elastic modulus. For 4 kPa gels the collagen coating had no significant effect on the measured elastic modulus. However, the addition of MCF-7 cells resulted in a significant increase in the average measured elastic modulus after 24 hrs culture ($p = 0.0064$ by one-way ANOVA). Interestingly this increase in stiffness was not observed after a longer cell culture time of 96 hrs ($p = 0.2114$ by one-way ANOVA). It is important to note that although measured in triplicate the gels were only measured on one occasion and so further independent repeats would be needed to confirm the significance of this increase. Under each condition there was a significantly higher stiffness observed for the 4 kPa gel than that of the 500 Pa confirming their suitability for comparison of the effects of matrix stiffness on breast cancer cell behaviour ($p < 0.0001$, $p = 0.0004$ and $p < 0.0001$ respectively by one-way ANOVA).

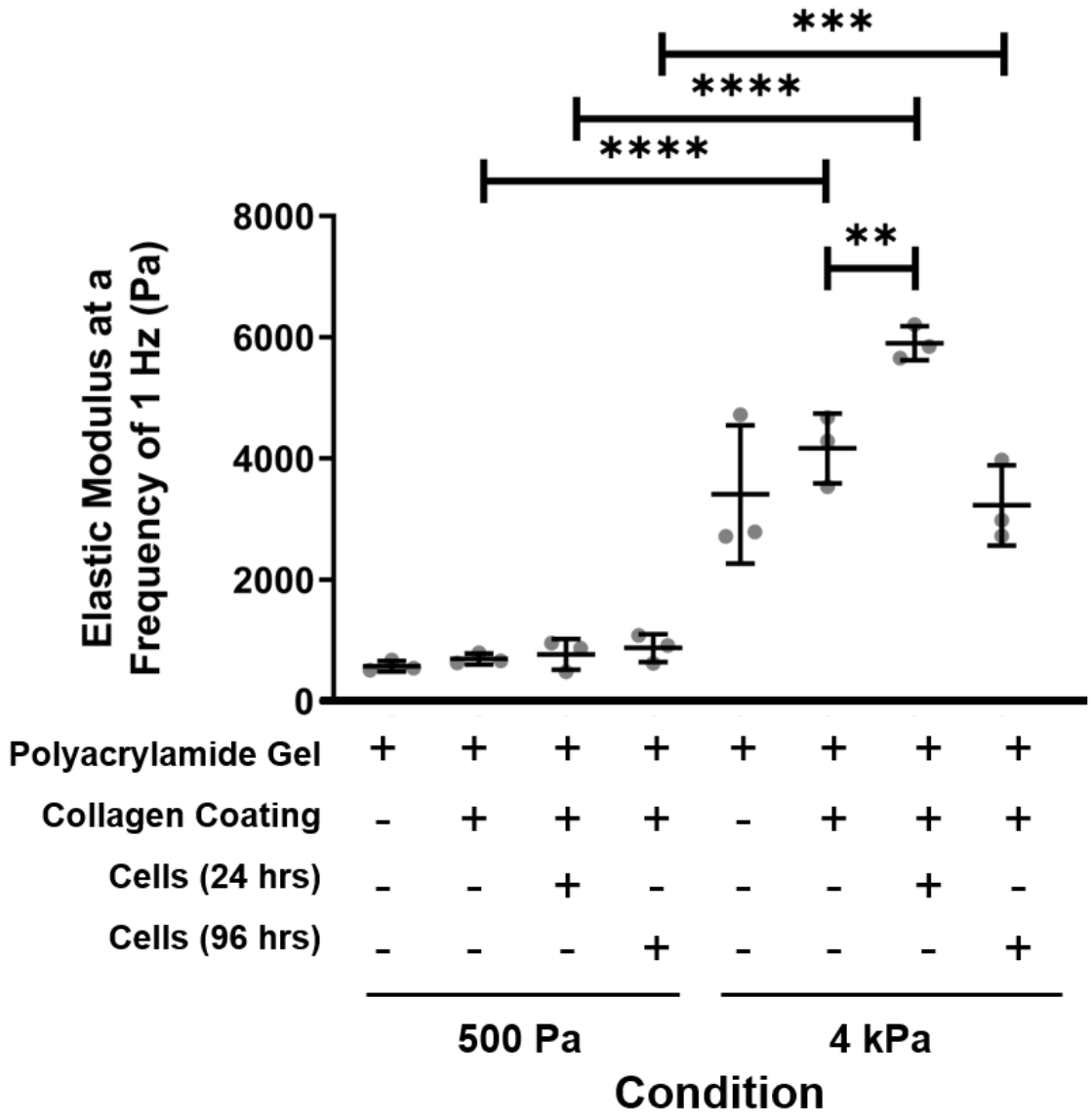

Figure 3.3. Rheological measurements of polyacrylamide hydrogels with plated cells. Measured elastic moduli of 500 Pa and 4 kPa gels without collagen coating, without cells and cultured with MCF-7 cells for 24 or 96 hrs as indicated. Averages and standard deviations of 3 gels measured on one occasion for each condition. ** indicates an ordinary one-way ANOVA p-value of < 0.01, *** of < 0.001 and **** of < 0.0001.

3.2.2. Characterisation of the morphology of breast cancer cell lines on polyacrylamide gels of physiologically relevant stiffnesses.

It is well reported that changes in matrix stiffness can change cell morphology through alterations in size and shape and in localisation of several functional proteins. In this section we set out to examine some of the most established changes in the literature. Initially brightfield imaging was undertaken to assess observable changes in cell morphology following culture of two different breast cancer cell lines cultured on the polyacrylamide hydrogels. Representative brightfield images are shown in Figure 3.4. after 48 and 120 hrs culture. Both the MCF-7 and MDA-MB-231 cell lines were rounded at 1 Pa. As stiffness increased fewer cells were rounded and instead appeared to be more spread and had several filipodia. The most striking differences were between 500 Pa and 4 kPa, supporting our decision to focus on these stiffnesses. Closer inspection of other morphological changes was undertaken through immunofluorescent staining for various markers previously reported as being altered by tissue stiffness.

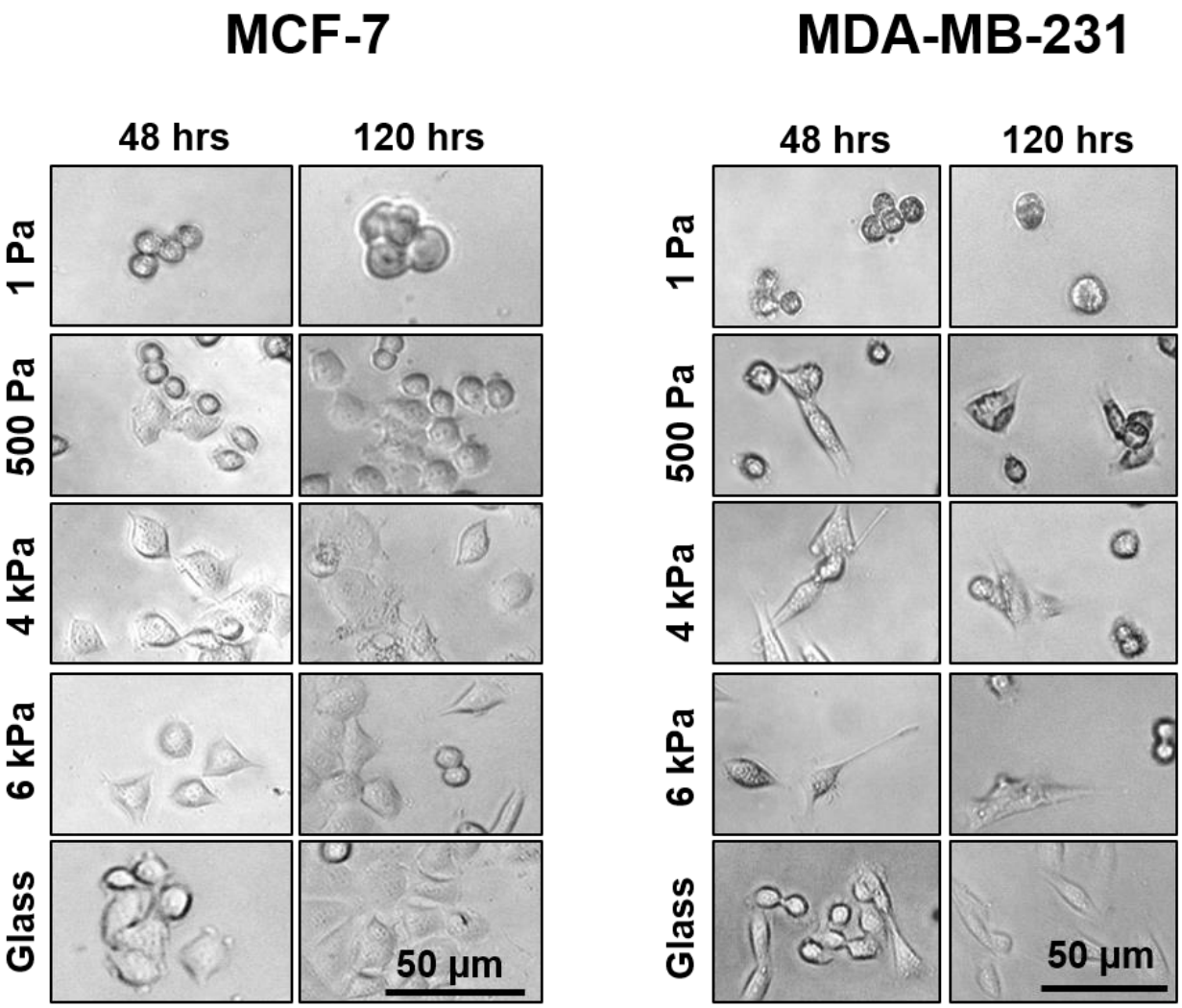

Figure 3.4. Brightfield images of MCF-7 and MDA-MB-231 cell lines cultured on polyacrylamide hydrogels. MCF-7 and MDA-MB-231 cell lines were cultured on hydrogels of increasing stiffnesses and a glass control for 120 hrs. Representative brightfield images are shown from images taken on a Nikon TE200 inverted fluorescent microscope at a magnification of 20X, 48 hrs and 120 hrs post cell plating.

3.2.2.1. Increased matrix stiffness results in an increase in cytoplasmic area.

It is well known within the literature that increasing stiffness results in increased cell spreading and formation of more FA contacts with the substrate (Bell, Redmann, & Terentjev, 2019). To determine if this was also observed in our model, cells were cultured for 16 hrs on 500 Pa and 4 kPa stiffness hydrogels and a glass control prior to fixing and staining for actin and vinculin, using immunofluorescence.

Representative images are shown in Figure 3.5.a. In the MCF-7 cell line vinculin, a component found in mature FA complexes, appeared to be patterned in foci across the whole area of the cell on the glass substrate. This suggests that the cells have several points of contact with the glass coverslip at even distributions across the cell. However, when the cells are cultured on the 500 Pa stiffness hydrogel vinculin foci were fewer in number and localised at the cell perimeter. MCF-7 cells cultured on the 4 kPa stiffness hydrogel had less distinguishable foci where more of a pan stain was observed, perhaps indicative of more FA contacts. This relationship of increased FA number with increased stiffness has been observed previously where it has been studied in depth in mouse embryonic fibroblasts (Kim & Wirtz, 2013) and in mouse mammary cells (Yeh, Ling, Chen, Lin, & Tang, 2017). Further studies in human cells and in cancer cells alongside other focal adhesion proteins are warranted to observe any specific differences. Some holes in the pan stain were observed at 4 kPa and the staining was more intense at one end than the other suggesting that some areas of the cell may be more attached to the matrix than others.

In the MDA-MB-231 cell line vinculin staining was also localised to a few bright foci at the edge of the cells but was also localised near the nucleus when cultured on glass. When cells were cultured on a 500 Pa matrix, vinculin foci were also observed. However, these foci were located in the middle of the cell rather than at the cell periphery and a pan vinculin stain was distributed across the rest of the cell. At 4 kPa vinculin foci were not observed but a pan stain was with fainter staining at the cell periphery. The distribution of vinculin foci over the whole area of the cell at 500 Pa is perhaps due to the smaller sizes of the cells, as has been observed previously in controlled cell area experiments in fibroblasts (Gallant, Michael, & García, 2005).

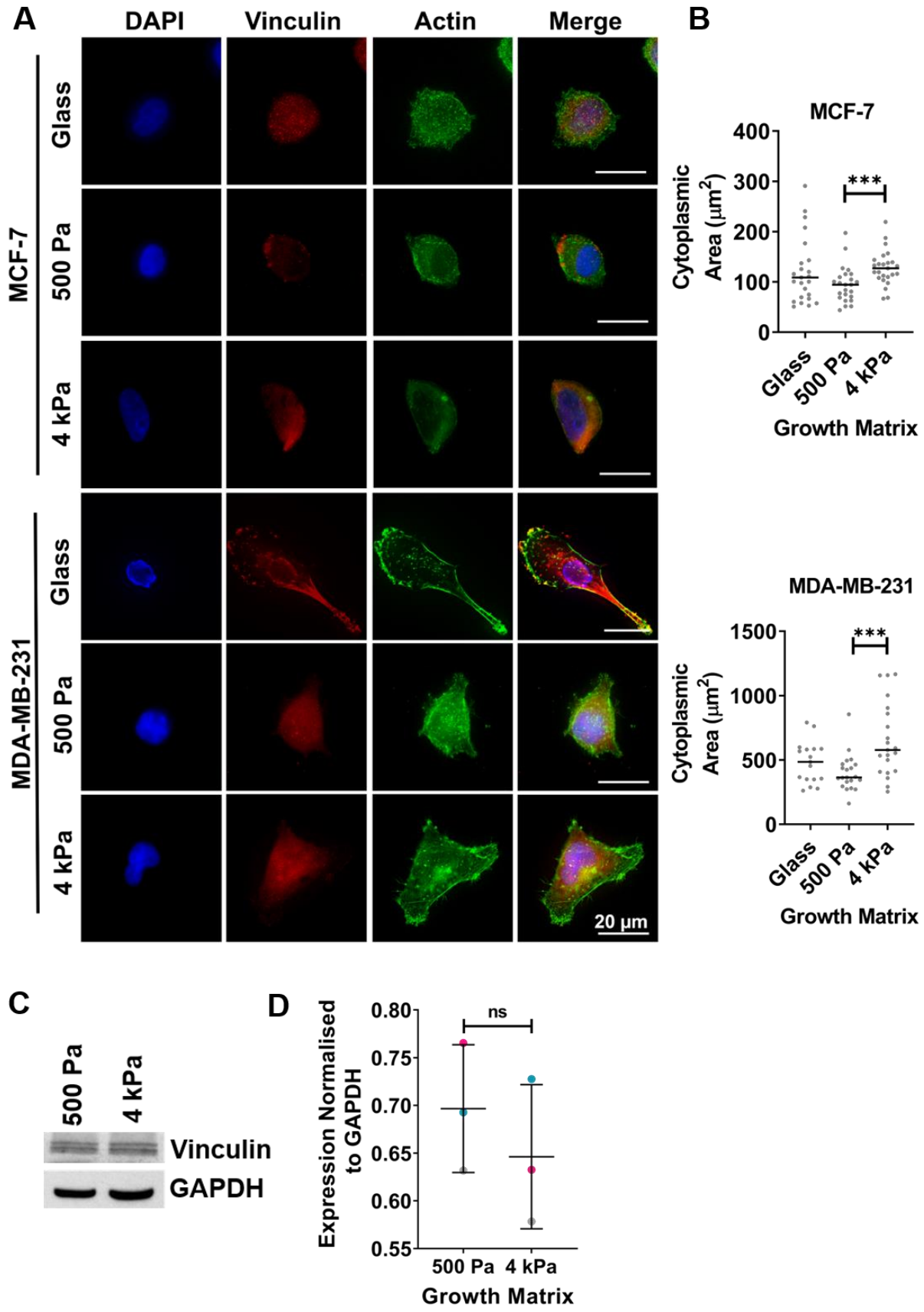

Figure 3.5. Cytoplasmic area increases with increased polyacrylamide hydrogel stiffness in MCF-7 and MDA-MB-231 cell lines. Legend overleaf.

Figure 3.5. Cytoplasmic area increases with increased polyacrylamide hydrogel stiffness in MCF-7 and MDA-MB-231 cell lines. (A) MCF-7 and MDA-MB-231 cells were cultured on 500 Pa and 4 kPa stiffness hydrogels and a glass control for 16 hrs. Cells were then fixed and stained using immunofluorescence for vinculin and actin. Representative images are shown from images taken on an Applied Precision deconvolution DeltaVision microscope at a magnification of 60X. The representative glass MDA-MB-231 image was taken on a Nikon inverted Ti microscope at a magnification of 60X. MDA-MB-231 images courtesy of Manpreet Barj and Callum Jones. (B) Cytoplasmic areas were measured in FIJI for a total of 17-25 cells per condition imaged on one occasion. The area of each cell is plotted in grey and the median in black. *** indicates a one-tailed Mann-Whitney test p-value of < 0.001. (C) Representative Western blot of whole cell extracts from MCF-7 cells cultured on 500 Pa and 4 kPa stiffness hydrogels for 72 hrs. Extracts were probed for vinculin and a GAPDH control. (D) Relative expression of vinculin compared to GAPDH expression calculated from Western blot images. Band densitometries were measured in FIJI for vinculin and normalised to the GAPDH control for each hydrogel stiffness on each occasion to give the relative expression for each of 3 independent repeats. Each repeat is plotted in a different colour and the mean and standard deviations are plotted in black. Statistical significance was determined by a one-tailed unpaired Student's t-test.

Stress fibres are bundles of filamentous actin and other proteins such as myosin that connect with the matrix in FAs. They sense matrix stiffness and convey this to the cell through the tension produced by actin and associated proteins within the stress fibres (Burridge & Guilluy, 2016). Given the changes in vinculin seen above we investigated stress fibre formation using phalloidin (a toxin that binds to actin) as a fluorescent label. The MCF-7 cell line does not produce actin stress fibres (Dube et al., 2016) and therefore it was not surprising that these were not observed when the cell line was cultured on any of the matrices. In the MDA-MB-231 cell line there was only presence of such fibres when the cells were cultured on the 4 kPa hydrogels (Figure 3.5.a.).

The actin stain was used to measure the cellular area of both cell lines cultured on each matrix. The results are plotted in Figure 3.5.b. In both the MCF-7 and MDA-MB-231 cell lines there was a significant increase in cytoplasmic area between 500 Pa and 4 kPa ($p = 0.0009$ and 0.0004 respectively by Mann-Whitney test).

As vinculin localisation appeared to change when the cell lines were cultured on the different stiffnesses, with some areas of low vinculin coverage at 4 kPa, it was next investigated if stiffness altered vinculin expression. A representative Western blot for vinculin for MCF-7 cells cultured on 500 Pa and 4 kPa hydrogels is shown in Figure 3.5.c. Densitometric analysis of three independent Western blots is shown in Figure 3.5.d. This indicated that there was no difference in vinculin expression with increased stiffness from 500 Pa to 4 kPa ($p = 0.2179$ by Student's t-test). This indicates that the changes in localisation are not due to altered expression levels.

3.2.2.2. Increased stiffness alters nuclear morphology.

As an increase in cytoplasmic area was observed with increased stiffness it was next investigated if stiffness altered nuclear morphology. To determine the effect of stiffness on nuclear envelope integrity MCF-7 and MDA-MB-231 cell lines were cultured on 500 Pa and 4 kPa stiffness polyacrylamide hydrogels and a glass control for 16 hrs prior to being fixed and stained for lamin A, a component of the nuclear envelope and DAPI for nuclear content. Representative images are depicted in Figure 3.6.a.

In both cell lines there were no observations of holes in the lamina or any observable thinning. In the MDA-MB-231 cell line wrinkling was observed when the cells were cultured on glass. The nuclear lamina appeared smooth in the cells cultured on both stiffnesses of hydrogels. These results suggest that at the stiffnesses investigated nuclear envelope integrity was not altered. As the cells were fixed it was not possible to investigate the dynamic nature of nuclear envelope remodelling.

To investigate the effect of stiffness on nuclear size, DAPI staining was used as a measure of nuclear area. The results are plotted in Figure 3.6.b.

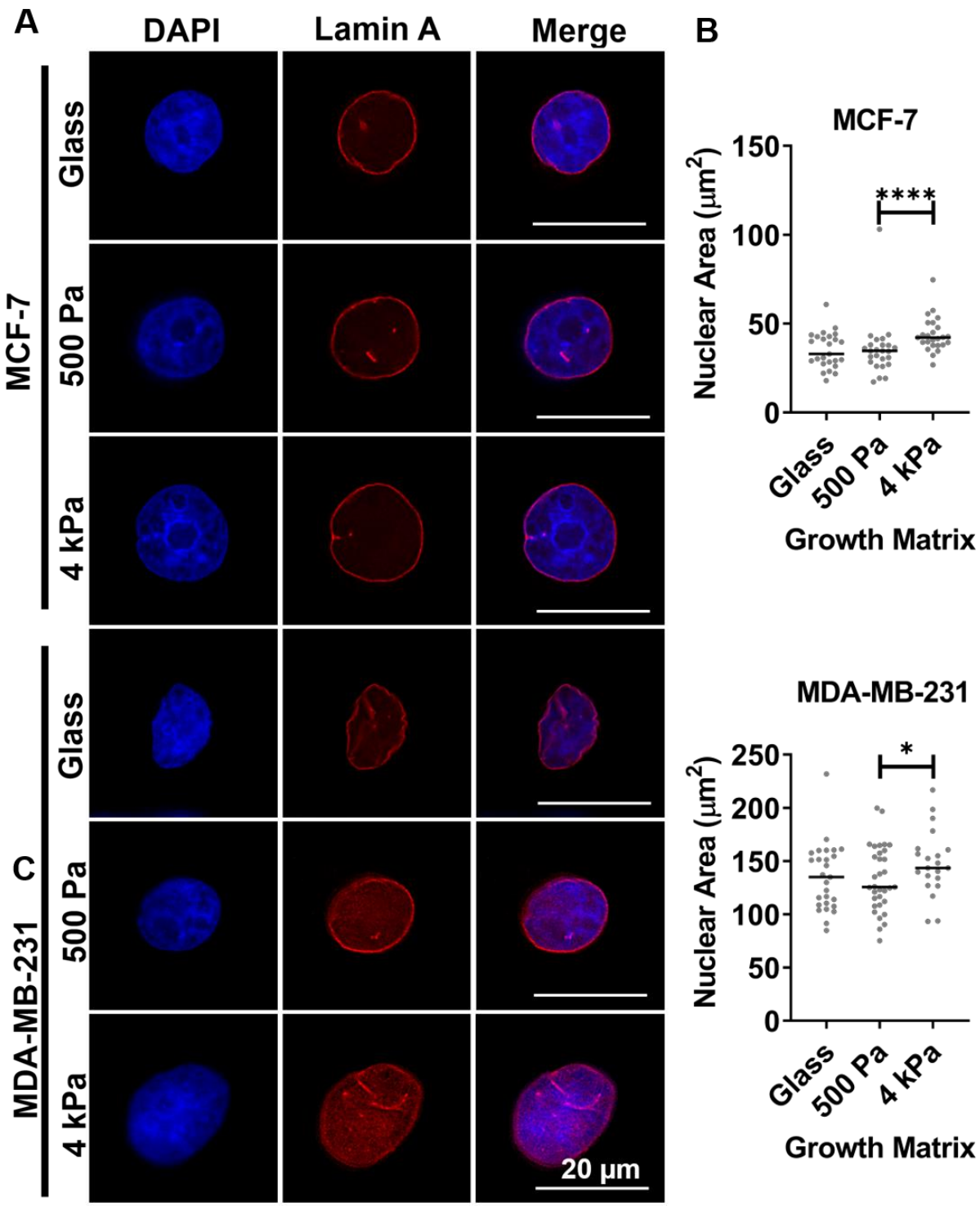

Figure 3.6. Nuclear area increases with increased polyacrylamide hydrogel stiffness in MCF-7 and MDA-MB-231 cell lines. Legend overleaf.

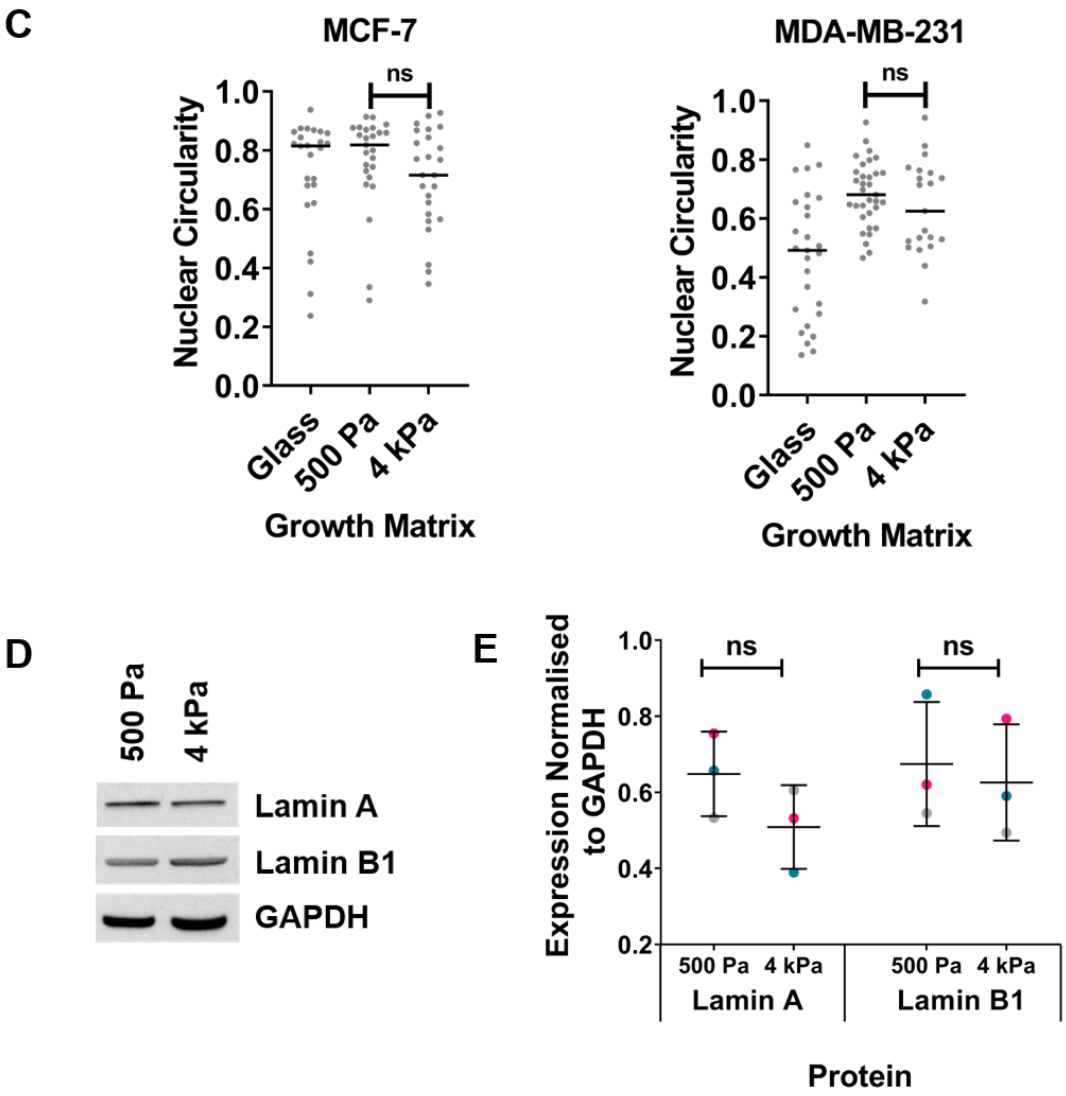

Figure 3.6. Nuclear area increases with increased polyacrylamide hydrogel stiffness in MCF-7 and MDA-MB-231 cell lines. (A) MCF-7 and MDA-MB-231 cell lines were cultured on 500 Pa and 4 kPa stiffness hydrogels and a glass control for 24 hrs at 37 °C. Cells were then fixed and stained using immunofluorescence for lamin A. Representative images are shown from images taken on an Applied Precision deconvolution DeltaVision microscope at a magnification of 60X. (B) Nuclear areas and (C) nuclear circularities were measured in FIJI for a total of 17-33 nuclei per condition pooled across 2 repeats. Each data is plotted in grey and the median in black. * indicates a one-tailed Mann-Whitney test p-value of < 0.05 and **** of < 0.0001. MDA-MB-231 images courtesy of Manpreet Barj. (D) Representative Western blot of whole cell extracts from MCF-7 cells cultured on 500 Pa and 4 kPa stiffness hydrogels for 72 hrs. Extracts were probed for lamin A, lamin B1 and GAPDH control. (E) Relative expression of lamin A and lamin B1 compared to GAPDH expression calculated from Western blot images. Band densitometries were measured in FIJI for lamin A or lamin B1 and normalised to the GAPDH control for each hydrogel stiffness on each occasion to give the relative expression for each of 3 independent repeats. Each repeat is plotted in a different colour and the mean and standard deviations are plotted in black. Statistical significance was determined by an unpaired one-tailed Student's t-test.

In the MCF-7 cell line there was a significant increase in nuclear area between 500 Pa and 4 kPa ($p < 0.0001$ by Mann-Whitney test). There was also a significant increase between 500 Pa and 4 kPa for the MDA-MB-231 cell line ($p = 0.0426$ by Mann-Whitney test). Nuclear circularity was also measured and the results are plotted in Figure 3.6.c. In both the MCF-7 and MDA-MB-231 cell line nuclear circularity was not significantly altered ($p = 0.0826$ and 0.1302 respectively by Mann-Whitney test), however the mean circularity was marginally reduced with increasing stiffness. As the results are pooled from two independent repeats a further repeat would be needed to confirm this trend. Secondly the data collected by Manpreet Barj in the MDA-MB-231 cell line were not of the same sample size for both stiffnesses. Further repeats to correct for this are also needed to confirm the statistical differences observed for these nuclear measurements.

Lamin A and lamin B protein levels were determined by Western blot (Figure 3.6.d). Consistent with the lack of observable change in lamin A by microscopy, no consistent change in protein expression was seen following band quantification (Figure 3.6.e.).

3.2.2.3. Localisation of reported stiffness sensitive proteins alters in MDA-MB-231 but not MCF-7 cells.

Several proteins are reported as altering localisation when stiffness is altered. We chose two that are associated with cancer through induction of EMT (Rice et al., 2017) a phenotypical change where cells become mesenchymal in nature, lose their cell to cell adhesions and polarity, often allowing for metastasis. It is associated with tumorigenesis and chemoresistance (Felipe Lima, Nofech-Mozes, Bayani, & Bartlett, 2016).

The first protein we investigated was E-cadherin, a transmembrane protein which locates at the cell periphery facilitating cell to cell connections (Dybdal-Hargreaves, Risinger, & Mooberry, 2018; Hartsock & Nelson, 2008). In a normal cell E-cadherin associates with β-catenin to allow for communication between cell to cell junctions and the actin cytoskeleton. Loss of E-cadherin expression is a marker of EMT and is thought to result in mis-localisation of β-catenin allowing for its interaction in the Wnt signalling pathway, therefore driving cell proliferation and migration, contributing to tumorgenicity (Tian et al., 2011).

Secondly we chose to investigate YAP, as an increased stiffness is reported to induce movement of the YAP protein to the nucleus where it acts to induce gene expression resulting in an increase in cell proliferation, EMT and suppression of apoptosis (Abylkassov & Xie, 2016). Moreover, an increased YAP expression or activity is associated with a poorer clinical prognosis (Noguchi, Saito, & Nagase, 2018).

3.2.2.3.1. A stiffness of 500 Pa or 4 kPa does not alter E-cadherin expression or localisation in the MCF-7 cell line.

To determine if changes in stiffness could induce EMT in MCF-7 cells in our model, the localisation of E-cadherin and β-catenin was assessed using immunofluorescence. Representative images are shown in Figure 3.7.a. Under all conditions both E-cadherin and β-catenin were located primarily at the cell to cell boundaries. This analysis was undertaken 24 hrs after cell plating. To determine if E-cadherin expression was changed after a longer period of culture a Western blot was run for MCF-7 cells cultured on 500 Pa and 4 kPa hydrogels for 72 hrs. A representative blot is shown in Figure 3.7.b. Densitometric analysis of three independent repeats determined that there was very little

difference in E-cadherin expression between the two stiffnesses (Figure 3.7.c). Together, these results suggest that at the stiffnesses investigated EMT was not induced in MCF-7 cells. The MDA-MB-231 cell line expresses very low E-cadherin levels (Chekhun, Bezdenezhnykh, Shvets, & Lukianova, 2013) and therefore was not analysed. It is classified as a mesenchymal - stem like subtype of TNBC (Lehmann et al., 2011).

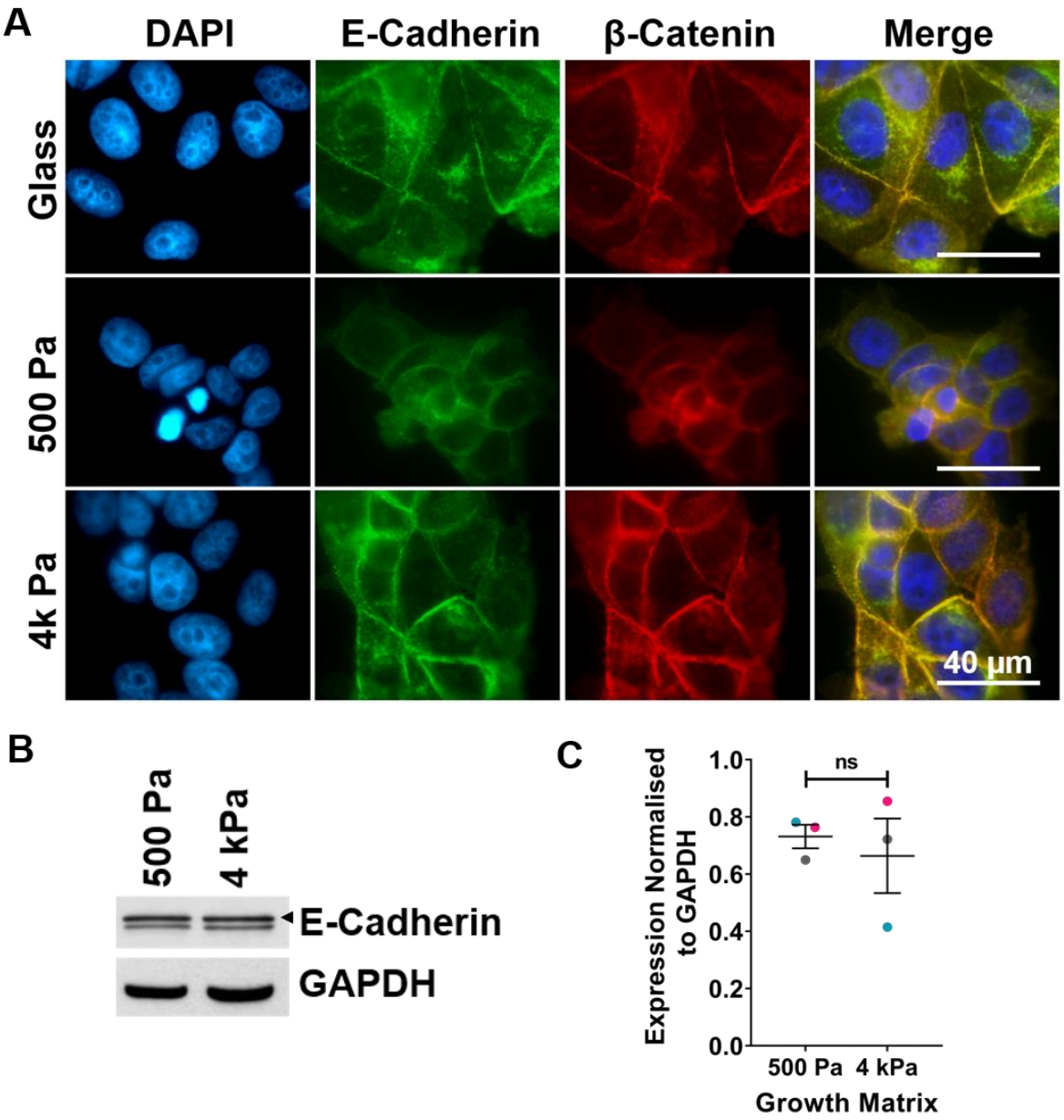

Figure 3.7. Polyacrylamide hydrogel stiffness does not alter E-cadherin or β-catenin localisation in the MCF-7 cell line. (A) The MCF-7 cell line was cultured on 500 Pa and 4 kPa stiffness hydrogels and a glass control for 24 hrs at 37 °C. Cells were then fixed and stained using immunofluorescence for E-cadherin or β-catenin. Representative images are shown from images taken on a Nikon TE200 inverted fluorescent microscope at a magnification of 60X. (B) Representative Western blot of whole cell extracts from MCF-7 cells cultured on 500 Pa and 4 kPa stiffness hydrogels for 72 hrs. Extracts were probed for E-cadherin and a GAPDH control. (C) Relative expression of E-cadherin calculated from Western blot images. Band densitometries were measured in FIJI for E-cadherin and normalised to the GAPDH control for each hydrogel stiffness on each occasion to give the relative expression for each of 3 independent repeats. Each repeat is plotted in a different colour and the mean and standard deviations are plotted in black. Statistical significance was determined by an unpaired one-tailed Student's t-test.

3.2.2.3.2. Nuclear YAP localisation is observed in MDA-MB-231 cells on stiffer matrices.

To determine if movement of YAP was occurring at the stiffness investigated, the MFC-7 and MDA-MB-231 cell lines were cultured for 24 hrs on 500 Pa and 4 kPa stiffness hydrogels and a glass control prior to staining for YAP using immunofluorescence. Representative images are shown in Figure 3.8.a. Nuclear YAP intensity was measured for each cell line under each condition for 3 independent repeats. Integrated density was used as this measurement is not biased by nuclear size (which we observed above (Figure 3.6.)). The results are shown in Figure 3.8.b. In the MCF-7 cell line there was very little difference between the average nuclear YAP intensity for cells cultured at 500 Pa or 4 kPa ($p = 0.1527$ by Mann-Whitney test). In the MDA-MB-231 cell line however the average nuclear YAP intensity significantly increased with increased matrix stiffness from 500 Pa to 4 kPa ($p < 0.0001$ by Mann-Whitney test). As the MCF-7 cell line has relatively low YAP expression in comparison to the MDA-MB-231 cell line (Shen et al., 2018), it may be that any changes which occurred in the MCF-7 cells were not detectable. These results suggest that MDA-MB-231 cells, but not MCF-7 cells, show an EMT-like phenotype at an increased stiffness of 4 kPa.

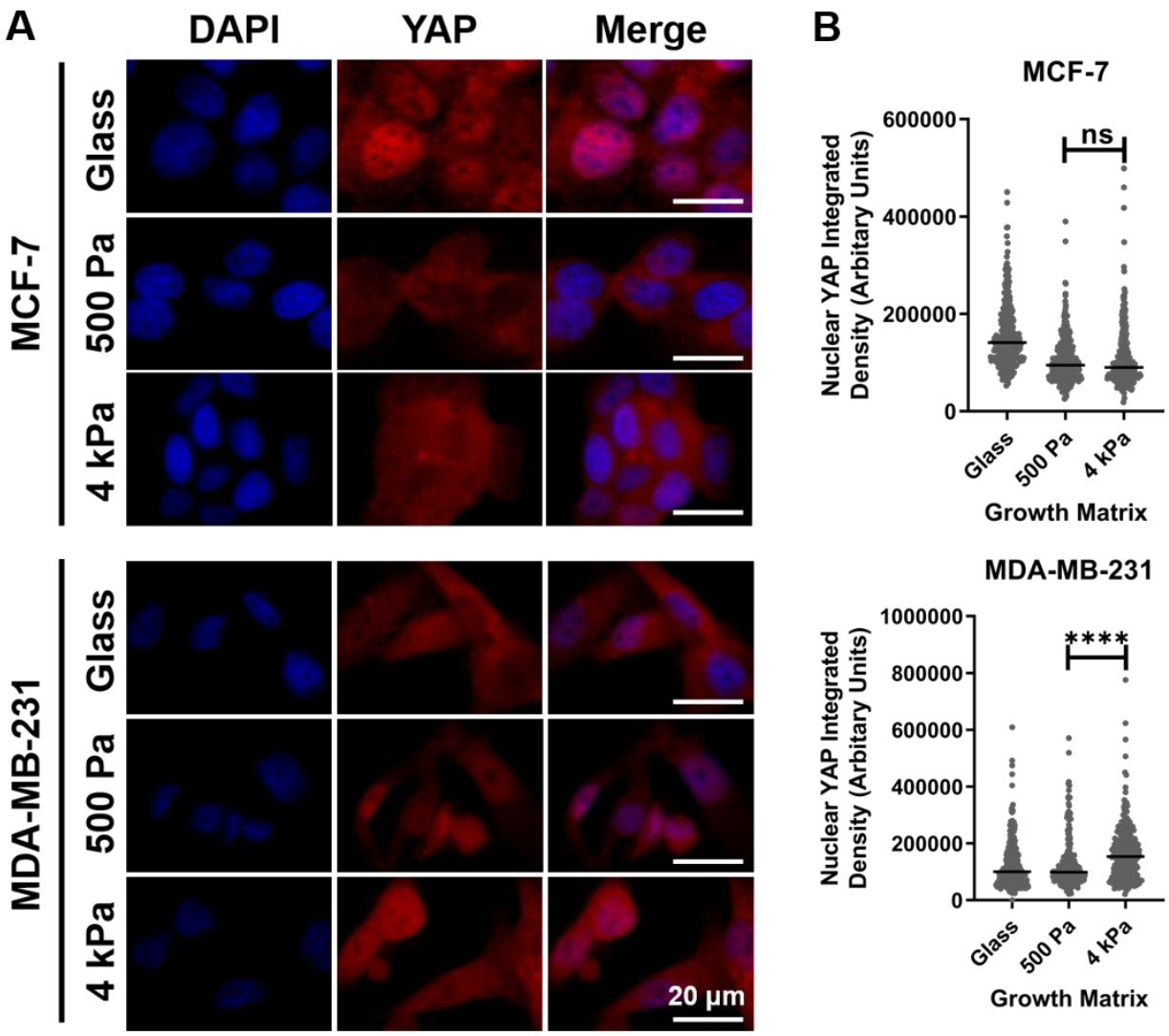

Figure 3.8. Polyacrylamide hydrogel stiffness alters YAP nuclear localisation in the MDA-MB-231 cell line but not in the MCF-7 cell line. (A) MCF-7 and MDA-MB-231 cell lines were cultured on 500 Pa and 4 kPa stiffness hydrogels and a glass control for 24 hrs at 37 °C. Cells were then fixed and stained using immunofluorescence for YAP. Representative images are shown from images taken on a Nikon TE200 inverted fluorescent microscope at a magnification of 60X. (B) Nuclear YAP intensity (integrated density) was measured for approximately 100 nuclei for each condition for each of 3 independent repeats. The pooled data is plotted in grey and the median is plotted in black. **** indicates a one-tailed Mann-Whitney test p-value of < 0.0001.

3.2.3. Increasing matrix stiffness results in increased cell growth.

In addition to altered cell shape the initial observation of cells under brightfield revealed greater numbers of cells at higher stiffnesses. To quantify this MCF-7 and MDA-MB-231 cells were plated at the same cell density on each of the hydrogel stiffnesses and a glass control for 5 days. Cells were then fixed and stained for nuclear content with DAPI in order to count the number of cells present. Representative images are shown in Figure 3.9.a. Nuclei number was counted for 9 fields of view per repeat and used as a representation of cell number. The average cell number from each repeat is plotted in Figure 3.9.b for each cell line. In the MCF-7 cell line an increase in cell number was observed with increasing matrix stiffness although appeared to plateau at 4 kPa. This increase was significant between 500 Pa and 4 kPa for the MCF-7 cell line ($p = 0.043$ by one-way ANOVA). The significant increase in growth found only between 500 Pa and 4 kPa in the MCF-7 cell line further validates our focus on these two stiffnesses for the majority of assays. In the MDA-MB-231 cell line there was no significant increase between any of the sequential steps, but a clear trend was observed of increasing cell number with increasing stiffness. It is interesting to note that for both the MCF-7 and MDA-MB-231 cell lines cell number was significantly higher on glass (70 GPa) compared to the stiffest 6 kPa matrix ($p = 0.0001$ and 0.0007 respectively by one-way ANOVA).

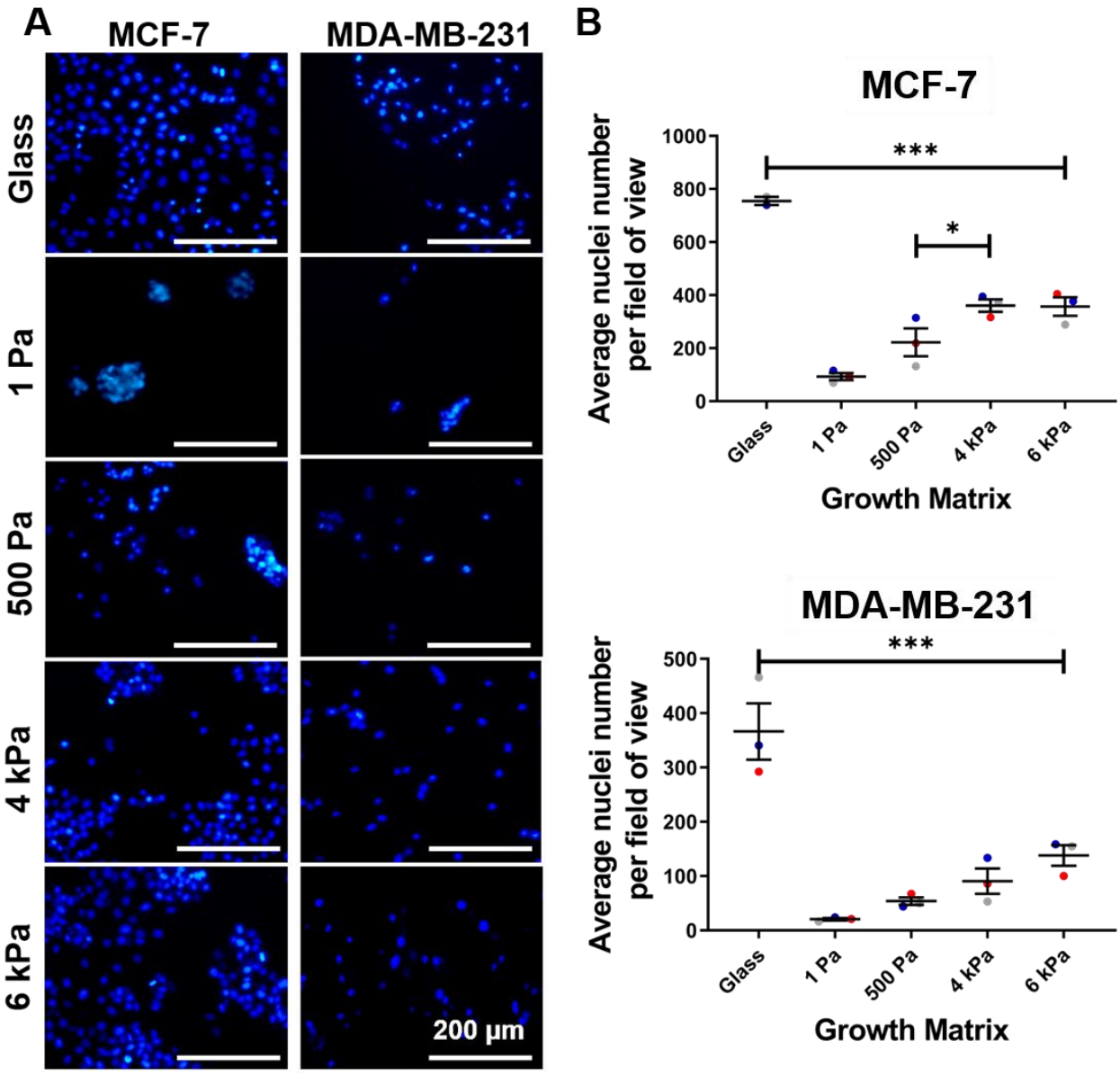

Figure 3.9. Polyacrylamide hydrogel stiffness increases cell growth in the MCF-7 and MDA-MB-231 cell lines. (A) MCF-7 and MDA-MB-231 cell lines were cultured on a range of hydrogels stiffnesses as indicated and a glass control for 120 hrs. Cells were then fixed and the nuclear content stained using DAPI. Representative images are shown from images taken on a Nikon TE200 inverted fluorescent microscope at a magnification of 20X. (B) The total number of nuclei in each image taken was counted and an average was calculated. Nine images were taken per condition for each of 3 independent repeats. The average number of cells are plotted in different colours for each repeat. The mean and standard error of the mean are plotted in black. Statistical significance was determined by a one-way ANOVA where * indicates a p-value of ≤ 0.05 and *** indicates a p-value of ≤ 0.001.

3.2.3.1. Changes in stiffness specifically effect cell growth during the first 72 hrs on a new matrix.

Having found a difference in cell number on the matrices after 120 hrs we next investigated how cell growth changed over a period of 144 hrs by making multiple cell viability readings at 24 hr time intervals. A common method for analysis of cell viability are use of metabolic assays such as alamarBlue, also known as resazurin. It can also be used as a measure of cell proliferation as an increase in the number of metabolising cells will result in an increase of conversion of resazurin into its fluorescent counterpart resorufin. It is advantageous for use with our hydrogel model as, unlike other metabolic assays, the reaction occurs within the medium and therefore does not require interaction with the cells or hydrogel. It does not result in cell killing and therefore can be used to measure the same cell sample at multiple timepoints as it can be added to the sample one day, washed out and re-added allowing incubation for the same time frame. MCF-7 cells were plated at the same density on 500 Pa and 4 kPa stiffness hydrogels. alamarBlue was added to the media and readings were taken from the samples 24, 72, 96, 120 and 144 hrs after cell plating. The average alamarBlue readings were plotted against time to produce a growth curve (Figure 3.10.a). At 24 hrs post plating there was very little difference between cells cultured at 500 Pa and 4 kPa which indicates that the plated cells adhered evenly between the two stiffnesses. However, 24-72 hrs after cell plating there was a lag in cell growth for the cells cultured on 500 Pa stiffness hydrogels comparative to those on 4 kPa hydrogels. At later time points the growth curves run parallel to each other with the estimated cell doubling times both being 34 hrs (Figure 3.10.b). The alamarBlue readings at the final time point of 144 hrs are higher for cells cultured at 4 kPa than those at 500 Pa agreeing with earlier findings of changes in cell number. This suggests that initial changes in cell doubling times are the contributing factor resulting in increased cell number at the 120 hr timepoint on 4 kPa hydrogels.

A

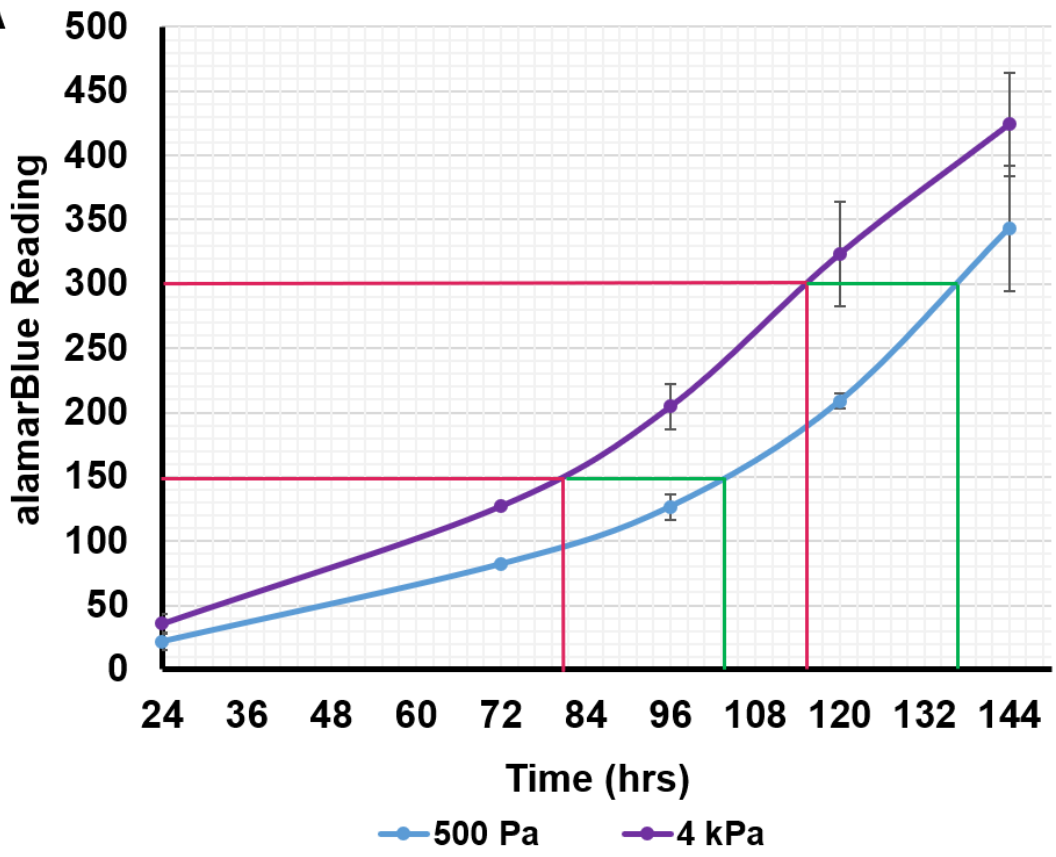

B

Matrix	Estimated (hr)		
	Time at 150 Reading	Time at 300 Reading	Cell Doubling Time
500 Pa	103	137	34
4 kPa	81	115	34

Figure 3.10. Polyacrylamide hydrogel stiffness does not alter long term cell doubling time in the MCF-7 cell line. (A) MCF-7 cells were cultured on 500 Pa and 4 kPa stiffness hydrogels for 144 hrs at 37 °C. Cells were allowed to adhere to the matrix for 24 hrs and then an alamarBlue reading made, readings were also made 48, 72 and 96 and 120 hrs after this. Three readings were made per well. From these readings a growth curve was plotted from the averages of 2 independent repeats. The standard error of the means are plotted in grey. (B) The estimated cell doubling times were calculated by estimating the time at alamarBlue values of 150 and 300 as indicated in (A) by the green and pink lines.

The alamarBlue assay has a fluorescent measurement for its read out which shows greater sensitivity over counting of cell number in Figure 3.9., as it does not introduce as much user error and allows for a distinction between viable and non-viable cells. Secondly as cell viability can be measured from the same sample at multiple timepoints it allows for a more comparative cell growth curve of the same cells, removing any gel to gel variabilities from each individual repeat. It also allows measurement of a larger sample of cells due to the convenience of the assay as the data does not have to be collected manually therefore providing a more representative readout of the whole cell population.

Having seen changes in cell growth during adaption to a new stiffness we next investigated three aspects of cells growth – proliferative index, mitotic index and DNA replication.

3.2.3.2. Stiffness does not alter proliferative index in breast cancer cells.

We have shown that cell number is altered by matrix stiffness. We next investigated if this was due to a change in the number of proliferating cells. Proliferative index is a marker of cells which are actively progressing through the cell cycle and are not quiescent. An increase in proliferation is a hallmark of cancer and the proliferative marker Ki67 is often used clinically for histological analysis of patient samples. We undertook staining for Ki67 using immunofluorescence in the MCF-7 and MDA-MB-231 cell lines cultured at 500 Pa and 4 kPa for 96 hrs. Representative images are shown in Figure 3.11.a. The percentage of nuclei staining positive for Ki67 were analysed and the results plotted in Figure 3.11.b. There was no significant difference in proliferative index in either cell line between the two stiffnesses, although there was a small trend for increased proliferation at 4 kPa.

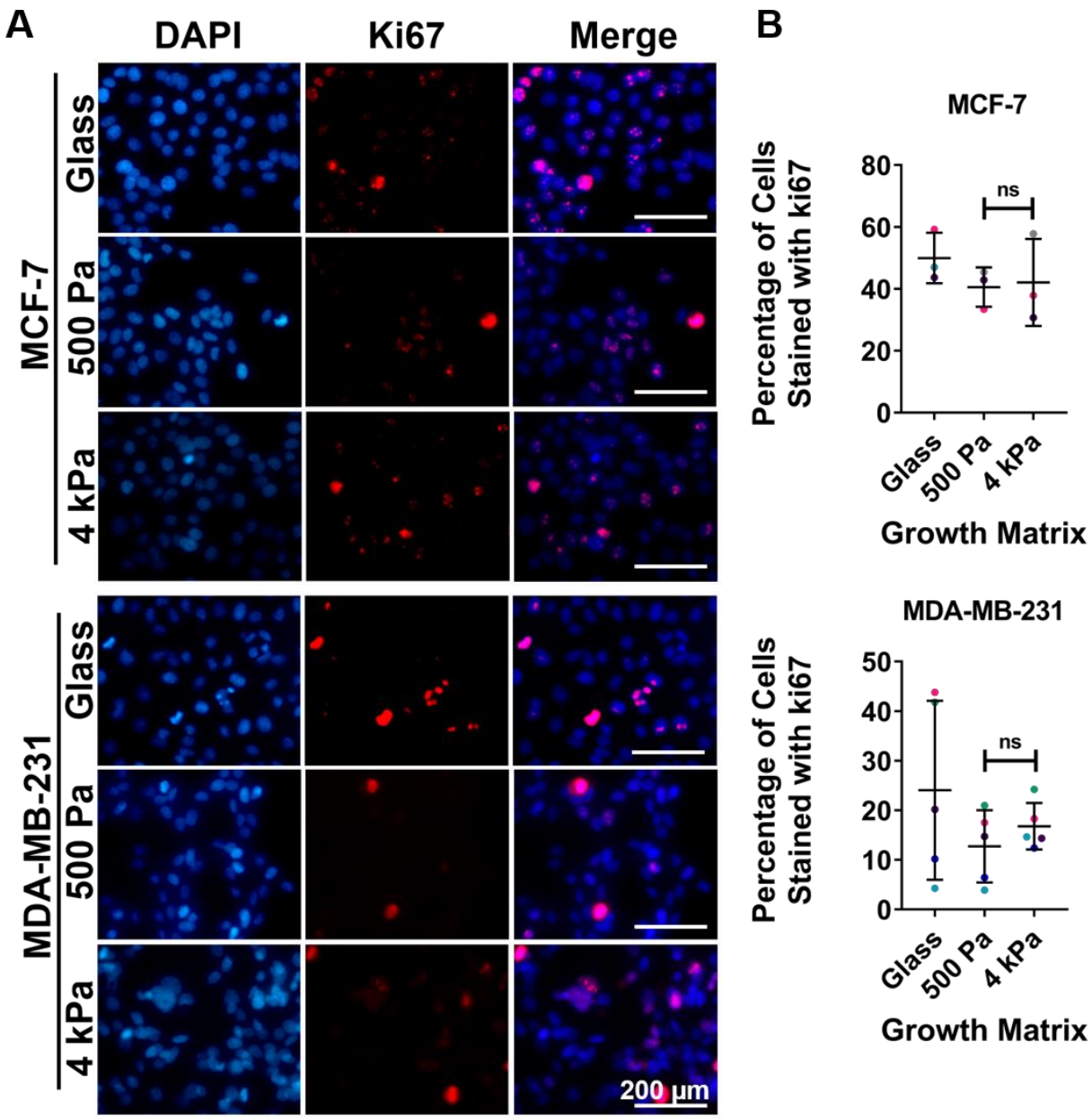

Figure 3.11. Polyacrylamide hydrogel stiffness does not alter proliferative index in the MCF-7 and MDA-MB-231 cell lines. (A) MCF-7 and MDA-MB-231 cell lines were cultured on 500 Pa and 4 kPa stiffness hydrogels for 96 hrs. Cells were then fixed and stained using immunofluorescence for Ki67. Representative images are shown from images taken on a Nikon TE200 inverted fluorescent microscope at a magnification of 20X. (B) The number of cells which stained positive for Ki67 were counted and calculated as a percentage of total cells per condition for each of 3 (MCF-7) and 5 (MDA-MB-231) independent repeats. The data is plotted in different colours for each repeat and the mean and standard deviation are plotted in black. Statistical significance was determined by an unpaired one-tailed Student's t-test. Three of the MDA-MB-231 repeats and one of the MCF-7 repeats were undertaken by Manpreet Barj.

As staining was done 96 hrs after cell plating these results are in agreement with the growth curve in Figure 3.10., where cell growth rate became equal after 72 hrs culture on each matrix. It would be interesting to repeat this experiment at earlier time points in line with those investigated in Figure 3.10. Ki67 staining does not measure cells which are quiescent, unlike the alamarBlue assay. However, the alamarBlue assays is more sensitive as it allows analysis of a larger number of cells over a range of time points as discussed above.

3.2.3.3. Stiffness has no effect on mitotic index in breast cancer cells.

It has been proposed that mechanical force can modulate mitotic speed, where application of mechanical force can result in slowed progression (Effler et al., 2006). As deregulation of mitosis is frequently observed in cancer, we decided to investigate mitosis in MCF-7 and MDA-MB-231 cells when grown on different stiffnesses. Histone 3 is specifically phosphorylated at Ser10 during mitosis and as such can be used as a marker of mitotic cells. The MCF-7 and MDA-MB-231 cell lines were plated at the same cell density on each of the hydrogel stiffnesses and a glass control for 5 days prior to being fixed and stained for pH3 and for nuclear content with DAPI. Representative images of pH3 staining are shown in Figure 3.12.a. The number of nuclei which stained positive for pH3 was divided by the total number of nuclei for each condition to give the mitotic index for three independent repeats. The independent repeats and averages are plotted in Figure 3.12.b. In neither cell line was there any significant alteration in mitotic index with increasing matrix stiffness. However, in both cell lines there was a trend of increasing mitotic index with increasing stiffness between 500 Pa and 4 kPa.

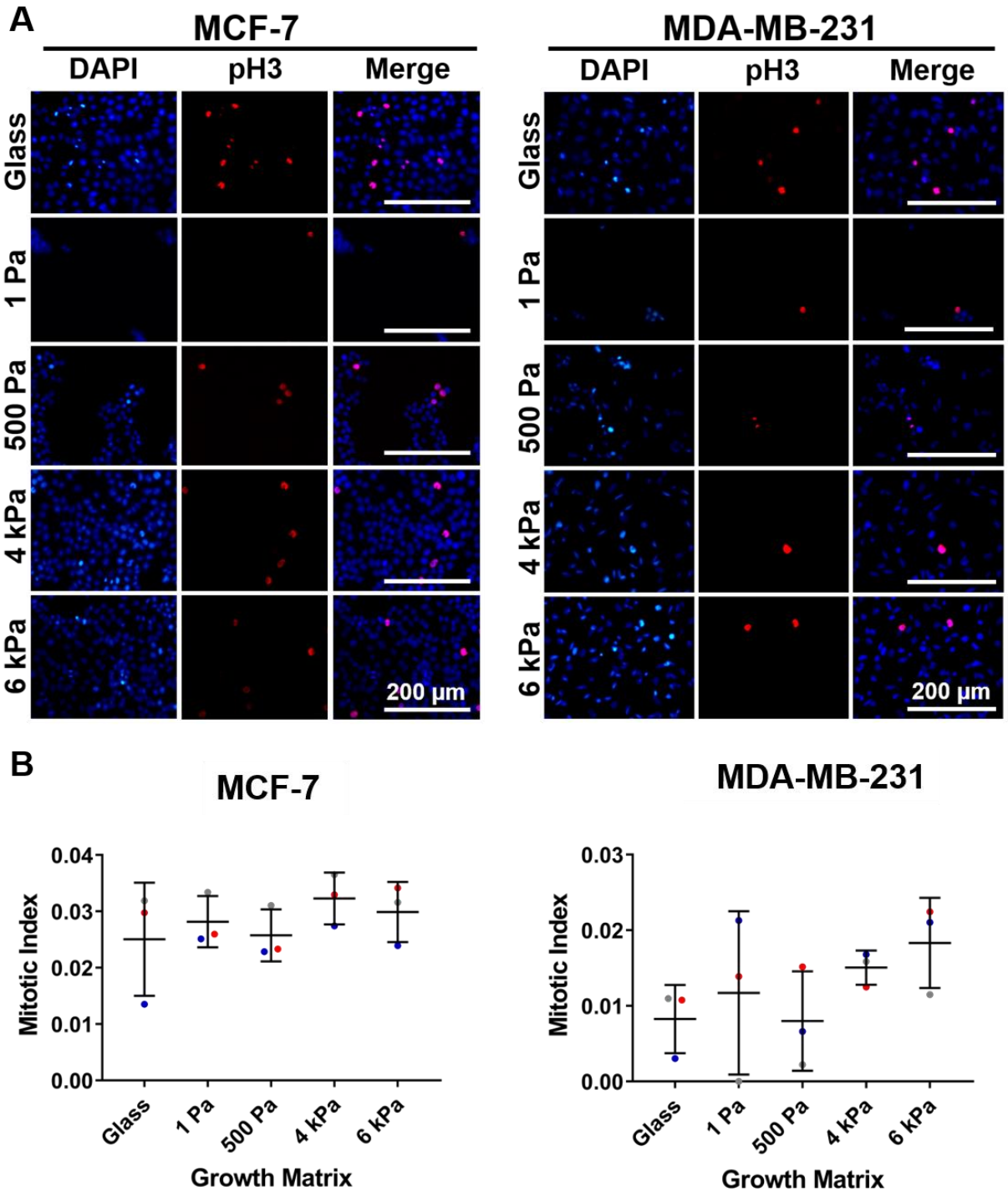

Figure 3.12. Polyacrylamide hydrogel stiffness does not affect mitotic index in the MCF-7 and MDA-MB-231 cell lines. (A) MCF-7 and MDA-MB-231 cell lines were cultured on a range of hydrogels stiffnesses as indicated and a glass control for 120 hrs. Cells were then fixed and stained for pH3 (S10) using immunofluorescence. Representative images are shown from images taken on a Nikon TE200 inverted fluorescent microscope at a magnification of 20X. (B) The number of cells which stained positive for pH3 were counted and divided by the total number of cells to give the mitotic index for each of 3 independent repeats. The data is plotted in different colours for each repeat. The mean and standard deviation are plotted in black. Statistical significance was determined by one-way ANOVA.

Mitotic index was evaluated after 120 hrs cell plating, where we observed cell growth rate to be equal between 500 Pa and 4 kPa. It would be interesting to repeat this experiment at earlier time points post plating to investigate if differences in mitotic index contributed to the observed difference in growth rate.

3.2.3.4. An increase in stiffness results in a reduction in the number of cells undergoing DNA replication.

Cell growth rate was faster in MCF-7 cells cultured on 4 kPa stiffness hydrogels than on 500 Pa stiffness hydrogels during only the first 72 hrs post plating, after which cell growth rate became equal between the two stiffnesses (Figure 3.10.). To determine if this initial change in cell growth was due to changes in DNA replication, cells were pulsed with a thymidine analogue. This analogue takes the place of thymidine during DNA replication and can then be labelled for detection of actively replicating cells. First, attempts were made using an EdU click-it kit, where cells are pulsed with the thymidine analogue 5-ethynyl-2'-deoxyuridine (EdU) for 20 minutes. This then allows detection of replicating cells by immunofluorescence using click-it technology (Figure 3.13.a). This methodology is preferential over the use of standard direct antibody labelling of the incorporated thymidine analogue as it requires lengthy acid treatment to allow for DNA double strand denaturation to provide access for binding of the large antibody.

Initial experiments gave varied results, resulting in lots of error between repeats for cells cultured on polyacrylamide hydrogels (while results on glass controls were consistent). Further insight into the click-it reaction highlighted an issue which may be occurring, details of this reaction are illustrated in Figure 3.13.b.

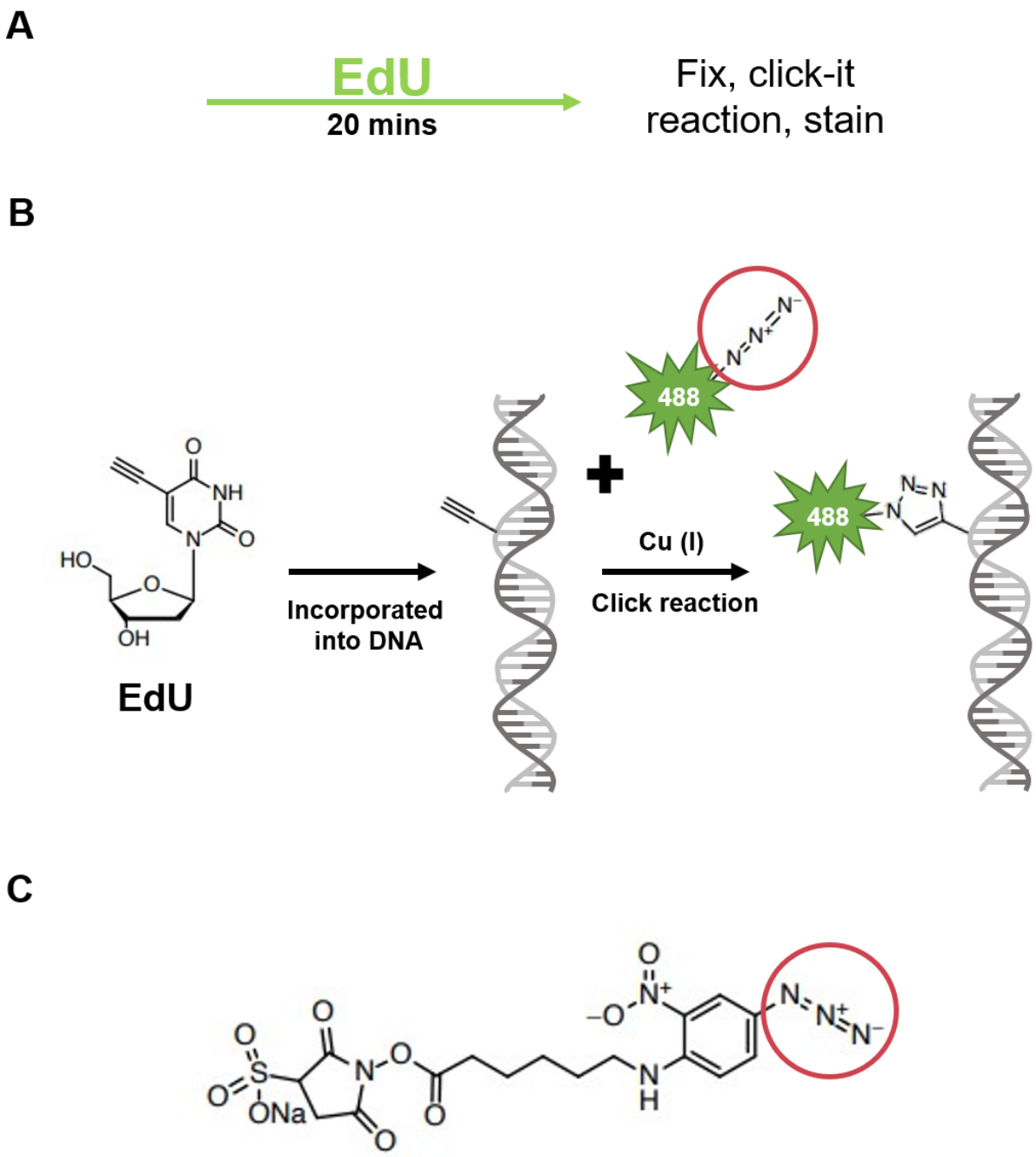

Figure 3.13. EdU Click-it kit technology is not compatible with polyacrylamide hydrogel chemistry. (A) Proposed methodology for analysis of DNA replication by measuring 5-ethynyl-2'-deoxyuridine (EdU) incorporation using a Click-it reaction. (B) Chemical reaction of the Click-it reaction allowing tagging of incorporated DNA with an Alexa-fluor labelled azide (circled in red). (C) Structure of sulphosuccinimidyl 6-(4'-azido-2'-nitrophenylamino)hexanoate (Sulfo-SANPAH), the chemical crosslinker used in polyacrylamide hydrogel gel formation with its azide group circled in red.

In the click-it reaction the ethynyl group of EdU reacts with the azide group of a fluorophore tagged azide, therefore labelling the incorporated EdU within the DNA. However, azides are also used to make polyacrylamide hydrogels in the form of sulphosuccinimidyl 6-(4'-azido-2'-nitrophenylamino)hexanoate (Sulfo-SANPAH), a chemical crosslinker used to attach collagen to the polyacrylamide gel surface (Figure 3.13.c). The azide groups in both chemicals are circled in red on the diagram. In theory, all azide groups within Sulfo-SANPAH should either be reacted with the polyacrylamide hydrogel or be washed away during the following wash steps. However, as variable results were observed, it felt sensible to try using traditional labelling of thymidine analogues with the DNA denature step and use of specific antibodies.

MCF-7 and MDA-MB-231 cell lines were cultured on 500 Pa and 4 kPa hydrogels and a glass control for 24 hrs prior to incubation with 5-iodo-2’-deoxyuridine (IdU) for 10 minutes. Cells were then fixed and stained using immunofluorescence for IdU (Figure 3.14.a). Representative images are shown in Figure 3.14.b. The intensity of IdU staining was measured in FIJI, this time the mean grey value was used as this value was more representative of overall positivity of the nuclei for IdU. When the data from three repeats was pooled, as displayed in Figure 3.14.c, there was a significant decrease in the IdU intensity at 4 kPa vs 500 Pa for both cell lines ($p < 0.0001$ by Mann-Whitney test). When the averages of each repeat were plotted as shown in Figure 3.14.d there was no significant difference but a clear trend in the same direction could be observed.

These results suggest that increased matrix stiffness causes a decrease in the proportion of cells undergoing DNA replication. Taken together with previous findings that an

increased growth rate is seen this suggests that on stiffer substrates cells are transitioning faster through S-phase.

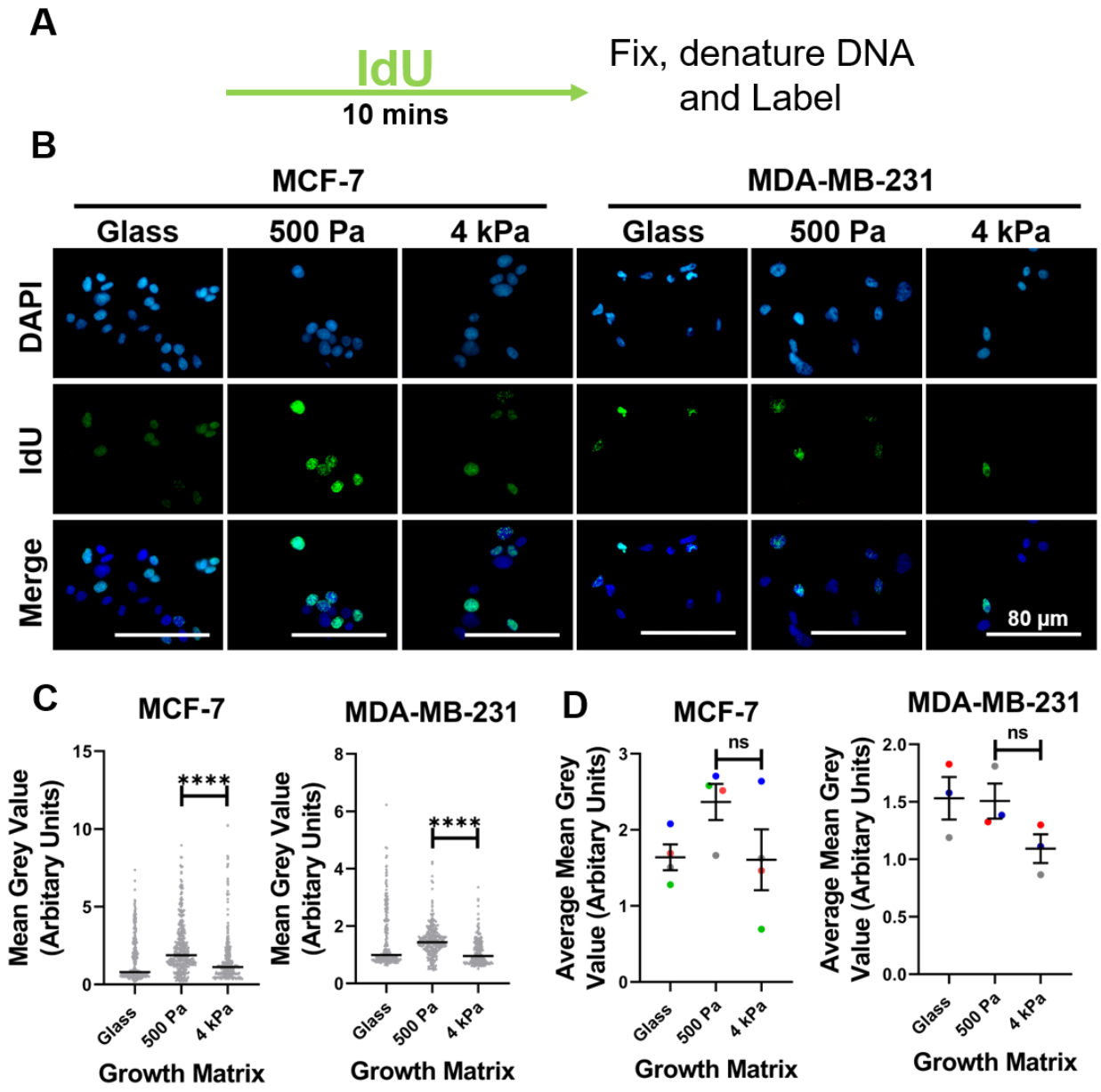

Figure 3.14. Polyacrylamide hydrogel stiffness alters DNA replication in the MCF-7 and MDA-MB-231 cell lines. (A) MCF-7 and MDA-MB-231 cell lines were cultured on 500 Pa and 4 kPa stiffness hydrogels and a glass control for 24 hrs. Cells were then incubated with 5-iodo-2'-deoxyuridine (IdU) for 10 minutes prior to being fixed and stained using immunofluorescence for IdU. (B) Representative images are shown from images taken on a Nikon TE200 inverted fluorescent microscope at a magnification of 60X. (C) Nuclear IdU intensity (mean grey area) was measured in FIJI for approximately 100 nuclei for each condition for 3 (MDA-MB-231) and 4 (MCF-7) independent repeats. The pooled data is plotted in grey and the median in black. **** indicates a one-tailed Mann-Whitney test p-value of <0.0001. The averages are plotted in different colours for each repeat in figure (D) and the mean and standard error of the mean are plotted in black. Statistical significance was determined by an unpaired one-tailed Student's t test.

3.3. Discussion.

In this chapter evidence is presented for the validity of the polyacrylamide hydrogel model to be able to determine how different ECM stiffnesses contribute to chemoresistance in breast cancer cells. After optimisation and testing two stiffnesses were decided upon (500 Pa and 4 kPa) and cells grown on these stiffnesses were shown to exhibit differences in morphology, cell growth and DNA replication. Changes seen were in general consistent with literature validating the model for testing in the next chapter.

3.3.1. A normal breast and breast cancer specific stiffness range can be achieved with polyacrylamide hydrogels.

In vivo measurements of the normal mouse mammary gland were found to have an elastic modulus of around 170 Pa and established breast tumours measured around 4 kPa (Paszek et al., 2005). The stroma around this tissue had a lower measured stiffness of around 1.2 kPa. In human studies breast cancer stiffness is measured whilst the tumour is *in situ* and therefore a non-invasive measurement is used such as ultrasound (Chen et al., 2019), elastography (L. Huang et al., 2019) or through area and deformation calculations (Boyd et al., 2014). Therefore, values obtained are often incomparable to measurements that are made *in vitro* or *in vivo* in mice experiments where direct tissue rheology can be undertaken. For example, elastography measurements obtained for the normal breast of human patients are reported to be around 20 kPa and malignant tissue in the region of 40 kPa (L. Huang et al., 2019). However, it is known that stiffnesses as high as 20-40 kPa are observed in more muscular tissues such as the heart or intestines (Butcher et al., 2009) or even the skin (Agache et al., 1980; Shaked & Gefen, 2013) which is likely to affect *in situ* measurements of the breast. Secondly it must be noted that *in situ* measurements of human breast tissue often produces stiffness values that are not reported in comparable units to pascals and that breast density, which is often used as a

surrogate for tissue stiffness, shows no correlation in breast tissue (Chen et al., 2019). It must also be noted that in our investigations, breast cancer metastasis was not explored. Breast cancer most commonly metastasises to the bone (Barney et al., 2016) which has a much higher stiffness of 2-4 GPa (Butcher et al., 2009) and the brain which has a much softer rheology of around 100 Pa (Barnes, Przybyla, & Weaver, 2017). However, the liver and lungs are also common metastatic sites of breast cancer which do have a similar stiffness to those explored in our model (around 500 Pa and 1 kPa respectively (Barnes et al., 2017)). Further investigations into the influence of stiffness of the metastatic sites on breast cancer chemoresistance is warranted but is not investigated in this thesis.

During optimisation, the softest gel we could consistently make was 500 Pa and thus this was chosen to be representative of the 'normal breast' stiffness. We could successfully make stiffer gels of 4 kPa and 6 kPa. Initial analysis of cell growth suggested little difference between 4 kPa and 6 kPa and considering the *in vivo* stiffnesses of breast cancer we focused further studies on 4 kPa as representative of cancer. In the literature, these relatively low stiffness ranges are not well represented especially by polyacrylamide models. Many studies use stiffnesses of a much higher magnitude than is observed in the cancerous breast (Ebata et al., 2017; Zustiak et al., 2014). For example the lower stiffness examined are typically 1-2 kPa and the higher stiffness are 20-100 kPa, around 10 times that observed in cancerous breast tissue (Taubenberger et al., 2019). Exceptions to this are Tilghman et al., (2010) and Joyce et al., (2018) who used 150-200 Pa and 2-4.8 kPa polyacrylamide hydrogels for comparison of MDA-MB-231 cell growth and response to chemotherapeutics. As such, it is necessary for all comparisons that the stiffness ranges used in each study are took into consideration. It is important that physiological stiffnesses are used to ensure that the correct conclusions can be determined. Our model represents the physiological stiffnesses of normal and cancerous

breast tissue but also includes the stiffnesses ranges of lung and liver which are common breast metastatic sites as discussed above.

3.3.2. An increased stiffness results in increased cytoplasmic and nuclear area in breast cancer cell lines.

Changes in cellular and nuclear size are used as markers in cancer grading of clinical samples (Kumar et al., 2015). Therefore, changes in cell size are a marker of tumorigenicity. An increase in cellular area with increased stiffness as observed in our measurements is consistent with previously published findings of 2D stiffness models of breast cancer including use of the MDA-MB-231 cell line (Tilghman et al., 2010; Zustiak et al., 2014), further validating our model. The same relationship was also observed in some other cancer cell lines (lung, renal, pancreatic, neuroblastoma and liver cancer) but not others (colorectal, prostate and pancreatic cancer) (Schrader et al., 2011; Tilghman et al., 2010; Zustiak et al., 2014) suggesting a tissue specific response to stiffness.

Previous studies of cellular morphology following growth on stiffer substrates revealed that fibroblasts required a stiffness of 4 kPa to form stress fibres (Yeung et al., 2005). This agrees with our observations in MDA-MB-231 cells, further validating our model. However, when the fibroblast cell lines made cell-cell contacts, stress fibres were able to form on the most compliant gel (180 Pa) (Yeung et al., 2005). This highlights the complex and dynamic relationship between cell morphology changes and matrix stiffness. In our experiments, cell morphology analysis was done on single cells that did not interact with neighbouring cells. Therefore, the observations made were representative of changes affected only by stiffness. Comparison is consequently not possible of the impact of cell to cell contacts on stress fibres at different stiffnesses.

Slight changes in vinculin patterning were observed, with pan staining in cells grown on 4 kPa substrates and foci at 500 Pa. Pan staining may be indicative of an increased number of cell adhesions to the matrix. However, initial measurements after 24 hrs plating on different stiffnesses showed little difference in cell metabolism. This suggests that cell number was equal after removal and replacement of the medium and indicates that adhesion is not altered by stiffness. In both cell lines the pattern of vinculin foci was different on glass vs the hydrogels, indicating the differences in cell attachment pattern between glass and a more physiologically relevant model. Previous studies show stiffness did not affect cell adhesion to the substrate in both MCF-7 and MDA-MB-231 cell lines at 150 Pa compared to 4.8 kPa and at 1 kPa compared to 100 kPa (Tilghman et al., 2010; Zustiak et al., 2014). Thus, if taken as indicative of adhesion our cell metabolism data is consistent with other models (although direct measurement of adhesion was not carried out here). Previously in the MCF-7 cell line an uneven distribution of FA complexes at one end of the cell was observed at 4 kPa, similar to our model in MCF-7 cells, which the authors state is indicative of metastasis (Nagano, Hoshino, Koshikawa, Akizawa, & Seiki, 2012). Our images appear to show lower numbers of foci at 500 Pa, which has previously been observed on softer matrices and is attributed to slower migration (Kim & Wirtz, 2013). However, it is not clear what this could mean for overall cell migration.

Stiffness has been shown previously to increase nuclear area in fibroblasts and mesenchymal stem cells, in agreement with our findings in MCF-7 and MDA-MB-231 cells (Buxboim et al., 2017; Lovett, Shekhar, Nickerson, Roux, & Lele, 2013). The nuclear lamina is mechano-responsive, showing wrinkling in mesenchymal stem cells at low stiffnesses (300 Pa) and tightening at higher stiffnesses (40 kPa) (Swift et al., 2013). This

was not observed in our model at the stiffnesses examined and with the cell lines used. Lamin A expression has also been shown to scale with stiffness, where its expression correlates positively with increasing stiffness both *in vivo* in stiffer tissues but also *in vitro* on stiffer matrices (Buxboim et al., 2017; Swift et al., 2013). We did not observe this in our data which could be due to the higher stiffness of 40 kPa used by Buxboim et al., (2017) and Swift et al., (2013). It has been reported that reduced lamina expression is associated with poor prognosis in breast cancer (Wazir et al., 2013). However, this change in expression was not observed in our experiments suggesting that the physiological stiffnesses of breast and cancerous breast tissue do not contribute to a change in lamina expression. Other errors in the lamina can occur including thinning and formation of holes which may occur due to reduced availability of repair machinery on stiffer matrices and particularly if expression levels do not provide coverage for the increase in nuclear area (King & Lusk, 2016). This was not observed in our fixed samples but as the remodelling of lamina is very dynamic it is possible that they may be observed by live cell imaging, which would be interesting to investigate. Investigations of nuclear envelope integrity at higher stiffnesses indicates that ruptures do occur but only in cells with mutations in the *LMNA* gene (Tamiello et al., 2013). Therefore, our data is not invalidated.

Most interestingly, the change in nuclear size and circularity observed in our model is suggestive of remodelling of the nuclear volume. Both an increase in nuclear size and a decrease in circularity, as observed in our model, correspond with an increased malignant phenotype in the literature (Chiotaki, Polioudaki, & Theodoropoulos, 2014; Giardina et al., 1994; Pienta & Coffey, 1991). This could indicate that LADs, points of connection between the lamina and chromatin which influence expression, may be altered affecting expression profiles of the cells (Swift et al., 2013). This warrants further investigation.

3.3.3. An increased stiffness does not induce EMT like changes in the MCF-7 breast cancer cell line but does in the MDA-MB-231 cell line.

To determine how consistent our model was with previous findings we examined the expression of two markers shown to alter in response to mechanical stress and that are associated with cancer.

A characteristic phenotype of EMT and thus tumorigenesis is loss of E-cadherin expression and signalling. The MCF-7 cell line showed no loss or movement of E-cadherin on stiffer hydrogels suggesting that EMT did not occur in this cell line. The loss of E-cadherin has been observed in a lung cancer cell line at an increased matrix stiffness of 19 kPa (Tilghman et al., 2010) and in MCF-7 and MDA-MB-231 cells in 3D stiffness model at a higher stiffness of 2 kPa (Joyce et al., 2018). Thus, our model appears inconsistent with previous data. It may be that E-cadherin levels are altered more when increased cell to cell connections are present and therefore the effect may be more pronounced in 3D culture. EMT is not always required for metastasis and as such lack of EMT at higher stiffnesses is not a depiction of lack of tumorigenicity (Petrova, Schecterson, & Gumbiner, 2016). The MDA-MB-231 cell line has a very low E-cadherin expression (Mbalaviele et al., 1996) and as such was not investigated in our model by Western blotting. Joyce et al., (2018) investigated changes in E-cadherin in their model using quantitative PCR, which is more sensitive than Western blotting, therefore allowing for the detection of its expression. Investigations with PCR in our model would be interesting to allow for a more sensitive analysis of changes in basal levels of E-cadherin expression.

An increase in nuclear YAP was observed in the MDA-MB-231 cell line. This is consistent with findings in a range of pancreatic cell lines (Rice et al., 2017) and a 3D model of MDA-MB-231 cells which compared stiffnesses of 200 Pa to 2 kPa (Joyce et al., 2018).

Protein expression of YAP can also be affected but was not examined in our model. Previous results show YAP expression is increased when cells are cultured at 40 kPa compared to 700 Pa in MDA-MB-231 cells and the normal breast cell line MCF-10A (Dupont et al., 2011). In contrast, in our model MCF-7 cells cultured at higher stiffnesses showed no change in nuclear YAP localisation. This is the opposite to data from a 3D model of MCF-7 cells where an increase in nuclear YAP intensity was observed at 2 kPa (Joyce et al., 2018).

More recently it has been seen in DCIS samples and in 3D cultures with the normal breast cell line MCF-10A that YAP movement to nucleus is not required for mechanotransduction at both physiologically relevant stiffnesses and at a higher stiffness of 20 kPa (Lee et al., 2019). This puts a question mark on the clinical relevance of nuclear YAP intensity. Taken together with our findings in the MCF-7 cell line it indicates that other mechanisms are used in breast cancers to allow for mechanotransduction and indicates that the model we have used is representative of the clinical response in regard to YAP.

3.3.4. An increased stiffness results in increased breast cancer cell growth during the initial 72 hrs post plating.

An increase in matrix stiffness has previously been associated with an increase in cell number across multiple cancer types (Tilghman et al., 2010), our data also showed this trend validating our model. Specifically, we observed increased cell growth in both MDA-MB-231 and MCF-7 cells, with growth plateauing at 4 kPa in MCF-7 cells but continuing to 6 kPa in MDA-MB-231 cells. This effect has been previously documented in MDA-MB-231 cells where increased growth was observed between 150 Pa and 4.8 kPa but

plateaued between 4.8 kPa and 9.6 kPa (Tilghman et al., 2010). Therefore, our data supports the hypothesis that increased stiffness may contribute to tumorigenesis via the promotion of cell growth. Interestingly when the extremes of stiffness were compared growth also increased in MDA-MB-231 and MCF-7 cells (25-30% increase in growth at 100 kPa vs 1 kPa) (Zustiak et al., 2014). This agrees with the increase in cell number in our model in both cell lines on glass, compared to 6 kPa, suggesting that the relationship between stiffness and cell number may be exponential. A stiffness of 100 kPa is observed in some tissues, such as skeletal muscle and the stiffness of TCP and glass is similar to the stiffnesses observed in the bone (Butcher et al., 2009). However, it is not relevant to the microenvironment experienced by the breast *in situ* as is depicted by our model, which is more relevant for investigations of chemoresistance in primary breast cancer. Interestingly this effect was not continued into the normal breast cell line MCF-10A (Tilghman et al., 2010), suggesting that the stiffness-growth relationship may be a cancer-specific effect.

This relationship between growth and stiffness does not appear limited to breast cancer cell lines as similar effects are seen in lung, renal, pancreatic, neuroblastoma and liver cancer cell lines (Schrader et al., 2011; Tilghman et al., 2010; Zustiak et al., 2014). Colorectal and pancreatic cancer cell lines appear however to have little change in cell growth with increased stiffness, suggesting that not all cancers have growth responsive to changes to matrix stiffness (Tilghman et al., 2010; Zustiak et al., 2014). Interestingly only the same cell lines which showed an increase in cellular area with stiffness also showed an increase in cell growth, indicating that some tissues are responsive to a different stiffness whilst others are not.

We observed that the change in cell growth was particularly apparent 24-72 hrs post plating perhaps reflecting cell adaptation to the changed microenvironment. This is not an abnormal finding, as cancer cells are able to readily adapt to changes in their microenvironment allowing for their survival (Poltavets, Kochetkova, Pitson, & Samuel, 2018). Converse to our findings Syed et al., (2017) observed a larger increase in cell number over a period of 9 days in MDA-MB-231 cells cultured on 103 kPa hydrogels compared to 1 kPa hydrogels. However, unlike our model, cells were continually passaged on and off the hydrogels (Syed et al., 2017), suggesting that the detachment and reattachment of cells may influence changes in proliferation on different stiffnesses. Syed et al., (2017) also used a large stiffness of 103 kPa which is not comparable to the physiological stiffnesses used in our model. Similarly to Syed at el., (2017), we investigated two breast cancer cell lines that were initially cultured on TCP and then moved to a stiffness more representative of the breast. This stiffness transition is unlikely to occur *in vivo* and indicates a limitation of our model. Use of primary breast cancer cells is more representative of how maintaining the stiffnesses observed *in vivo* influences cell proliferation. However, it has been reported that when primary breast cancer cells harvested from a mouse model were cultured on polyacrylamide hydrogels ranging from 5 kPa to 30 kPa a plateau in growth was observed in the first 4 days for all hydrogels apart from those cultured on the stiffest matrices (Medina et al., 2019). Growth rate then became even between all stiffnesses in the last 4-7 days of measurement. This pattern is similar to our results, further validating our model and indicates that it is comparable to primary breast cancer cells.

We also used Ki67 as a marker of proliferation, however we performed analysis at 96 hrs post-plating when growth kinetics were equal between the stiffnesses. It would be interesting to look at Ki67 at earlier time points post-plating when changes in cell doubling

can be observed. At these times we would expect Ki67 staining to be greater in cells grown on stiffer substrates. Indeed laryngeal squamous cancer cells cultured on 8 kPa vs 1 kPa matrices for 0, 24 and 48 hrs showed increased Ki67 staining consistent with increased proliferation during early times post-plating (Hui, Zhang, Ding, Guo, & Jiang, 2017). Further time points were not investigated by Hui et al., (2017). In liver cancer cells there was also a positive correlation between Ki67 index and stiffness (Hui et al., 2017; Schrader et al., 2011). However, it was not detailed how long cells were grown on the matrix for prior to fixing and staining for Ki67, making direct comparison with our data difficult.

Mitosis requires complete actin remodelling from the interphase cytoskeletal arrangement which occurs through cell stiffening by the Rho pathway (Théry & Bornens, 2008). As such it is reasonable to hypothesise that matrix stiffness may influence mitosis. In our results it appeared that stiffness had little effect on mitotic index. This was perhaps because of the late time point post-plating that was sampled, and as with Ki67 staining it will be important to look at earlier times. In agreement with our data it has been reported that induced pluripotent stem cells cultured on 5-60 kPa hydrogels showed no difference in mitotic index between the stiffnesses (Acevedo-Acevedo & Crone, 2015). There is little information about mitosis in cancer cells within the context of stiffness highlighting an area requiring further investigations.

In the stiffness model investigated here a stiffness of 4 kPa resulted in a lower proportion of cells incorporating IdU than cells cultured at 500 Pa. This does not agree with investigations of normal lung fibroblasts grown on polyacrylamide hydrogels for 72 hrs, where stiffness was reported to correlate positively with thymidine analogue incorporation (Mih, Marinkovic, Liu, Sharif, & Tschumperlin, 2012). This positive correlation between

stiffness and reported “DNA replication” has been observed with other normal cell lines (Klein et al., 2009) and on different matrix models (L. Kocgozlu et al., 2010). As we investigated in cancer cell lines and not normal cell lines it may suggest that the direction of the relationship between stiffness and DNA replication is dependent on the tumorgenicity of the cell line. However, in each of the previous studies the cells were incubated with thymidine analogues for a prolonged period of time (24-48 hrs), while in our study we used only a 10-minute incubation period. Long incubations will result in the thymidine analogue being present in cells undergoing S-phase at the point of fixation but also in any cell which has replicated during the incubation, such that if the cells are doubling faster more cells will be labelled. In contrast pulsing with IdU for 10 minutes prior to immediate cell fixation will give a representation of the proportion of cells in S-phase at one fixed time point. Our data therefore suggests that at any one time less cells are in S-phase when they are growing on stiffer substrates. Taken with the increase in cell number we therefore conclude that replication is faster at 4 kPa than at 500 Pa. There is a lack of investigation into the stiffness relationship with DNA replication in the context of cancer and this warrants further investigation in other cancer cell lines.

Faster replication could be indicative of inactivation of the intra-S-phase checkpoint. This checkpoint is activated during detection of DNA damage and replication stress in cells to allow for maintenance of genomic stability (Willis & Rhind, 2009). Defects in this checkpoint are associated with genomic instability and tumorgenicity. Secondly as we observed an increase in vinculin foci and in nuclear and cytoplasmic size at 4 kPa it suggests that the matrix is imparting an increasing in tension on the nucleus and therefore the DNA, which may alter replication speeds. However, it has been reported from application of direct force onto DNA that replication is decreased at higher forces (Maier, Bensimon, & Croquette, 2000). This is in disagreement with our data, however it

has also been reported that the nucleus can soften under levels of higher mechanical stress preventing tension reaching the DNA (Nava et al., 2020). As such we do not know if the direct application of force to DNA is representative of the forces felt within the nucleus of a live cell and thus it does not invalidate our data. This area is investigated in further detail in chapter 4.

Whilst we see a difference in S-phase proportion, we do not know what differences are occurring in the rest of the cell cycle. Changes in other phases of the cell cycle may further explain the differences we observe in IdU incorporation. Ideally, S-phase proportion and total cell cycle would have been investigated by flow-cytometry. However, efforts to detach breast cancer cell lines intact from our stiffness model were unsuccessful even with prolonged trypsin or collagenase treatment (data not shown). Replication speed and fork dynamics could also be analysed in further depth with successive pulses of two different thymidine analogues and DNA fibre analysis, but this also requires detachment of cells from the matrix. We did attempt to investigate immunofluorescent visualisation of the successive thymidine analogue pulses within cells. However, the antibody to 5-chloro-2'-deoxyuridine (CldU) is raised in rat and so the secondary anti-rat antibody was not compatible with collagen attached to the hydrogels, with both being of rat origin (data not shown). One previous study did manage flow cytometric analysis with MDA-MB-231 cells, where Tilghman et al., (2010) showed that stiffness had no effect on the cell cycle after 5 days growth. Again, this highlights the importance of time after cell plating and supports our hypothesis that cells adapt to their new environment during the few days following initial cell plating.

3.3.5. Summary

In summary we have generated and characterised several aspects of the basic morphology and growth of two breast cancer cell lines on two different stiffnesses. We believe these are a physiologically relevant model for the study of chemotherapeutic response that will be presented in chapter 4. For the most part our characterisation agrees with previous reports in breast cancer and several other cancers, particularly with regards to cell growth. In addition, our observations on DNA replication are novel in breast cancer although they should be expanded to other time points post-plating and other breast cancer cell lines representing other subtypes for a fuller investigation.

There are however limitations to the model. Our model generates two hydrogels with a comparative difference in stiffness. However the lowest stiffness used in our model (500 Pa) was a compromise between what could be reliably produced and the physiological stiffness found in normal breast (170 Pa) (Paszek et al., 2005) and is therefore three times stiffer than physiologically reported. It could be that substrates with stiffness lower than 500 Pa produce a different effect on cells, although we consider that the most likely scenario is that even softer gels would further exaggerate differences between 500 Pa and 4 kPa.

Secondly, the ECM is made up of a combination of different ligands which interact with the cells and each other in different ways, for simplicity we have only used collagen I. Collagen I is found in breast stroma not the basement matrix that makes direct contact with breast epithelial cells and is therefore not fully representative of physiological conditions.

The results presented in the next chapter should consider these limitations.

4. Chemotherapeutic sensitivity of breast cancer cells at different stiffnesses.

4.1. Introduction, aims and hypothesis.

Typically, two classes of drug are used as a first line of therapy to treat breast cancers. These are anthracyclines such as doxorubicin which intercalate into the DNA blocking replication and transcription, and taxanes such as PAX which stabilise microtubules and thus prevent cell division. Other agents that are less commonly used include antimetabolites such as gemcitabine, which incorporate into DNA and inhibit dNTP formation, leading to inhibition of DNA replication and induction of replication stress. DNA cross-linking agents such as mitomycin C (MMC) or cisplatin are also used. They result in the formation of covalent bonds between DNA bases, leading to inhibition of DNA replication. Whilst effective in some cases, response is variable between patients and resistance is often observed, especially in disease recurrence (Moreno-Aspitia & Perez, 2009). Greater understanding of this heterogeneous response and of resistance is needed in order to tailor treatments for individual tumours and result in better patient outcomes.

Clinical data indicates that breast stiffness predicts both breast cancer risk (Boyd et al., 2014) and correlates with chemotherapeutic resistance (Medina et al., 2019). This effect has been replicated *in vitro*, where the MDA-MB-231 breast cancer cell line was more resistant to doxorubicin when cultured at a higher matrix stiffness (Joyce et al., 2018). Prediction of response to therapeutics based upon tumour stiffness would be advantageous in determining their likely efficacy and thus optimising treatment regimes in patients. It is also important to investigate why resistance is observed at different

stiffnesses and find ways to combat this resistance to provide more effective therapies. Here we will examine the effect stiffness has on therapeutic response in breast cancer.

In chapter 3 we observed that stiffness can modulate breast cancer cell growth and DNA replication. Before looking at therapeutic response we characterised further the replication stress and DNA damage response of breast cancer cells on different stiffnesses. Following optimisation with gemcitabine, we then tested a panel of chemotherapeutic agents for their ability to inhibit cell growth at different stiffnesses. Finally, different breast cancer cell lines with a range of receptor statuses were compared to determine how this affects chemotherapeutic response.

<u>The hypothesis of this chapter is:</u>

Breast cancer cell lines grown at a physiologically relevant breast cancer stiffness (4 kPa), will be more resistant to chemotherapeutic agents in comparison to those cultured at a stiffness corresponding to that of normal breast tissue (500 Pa).

<u>The aims of this chapter are:</u>

1. To quantify the response of breast cancer cell lines to a panel of chemotherapeutic agents at the physiological stiffnesses of cancerous and normal breast tissue using the polyacrylamide hydrogel model.
2. To investigate potential mechanisms of why stiffness specific sensitivities are observed.

The objectives of this chapter are:

1. To determine if stiffness alters basal levels of replication stress and DNA damage.
2. To investigate the response of the MCF-7 cell line to a panel of chemotherapeutic agents.
3. To determine if this response is cell line specific.
4. To investigate the pathways contributing to chemotherapeutic resistance.
5. To determine if resistance can be reversed with specific pathway inhibition.

4.2. Results.

4.2.1. Basal levels of replication stress and DNA damage.

4.2.1.1. Increased stiffness induces replication stress in breast cancer cell lines.

In chapter 3 we observed a decrease in the proportion of cells undergoing DNA replication at any one time when cultured at a higher stiffness of 4 kPa. As we observed a decrease in the proportion of actively replicating cells without a reduction in cell number, we hypothesised that replication speeds could be increased. An increased replication speed can result in an increase in replication stress and DNA damage (Maya-Mendoza et al., 2018). We therefore investigated if higher stiffnesses result in increased replication stress. The MCF-7 and MDA-MB-231 cell lines were cultured for 16 hrs on 500 Pa and 4 kPa stiffness hydrogels and a glass control. Cells were then fixed and stained for a phosphorylated form of replication protein A (pRPA) (T21) using immunofluorescence. RPA coats single stranded DNA during DNA replication to protect it from damage. It is phosphorylated following replicative stress to signal that replication needs to be paused (Zou, Liu, Wu, & Shell, 2006), and therefore can be used as a marker of replication stress. Representative images of the stain are shown in Figure 4.1.a. The number of pRPA foci per cell were counted and are plotted in Figure 4.1.b.

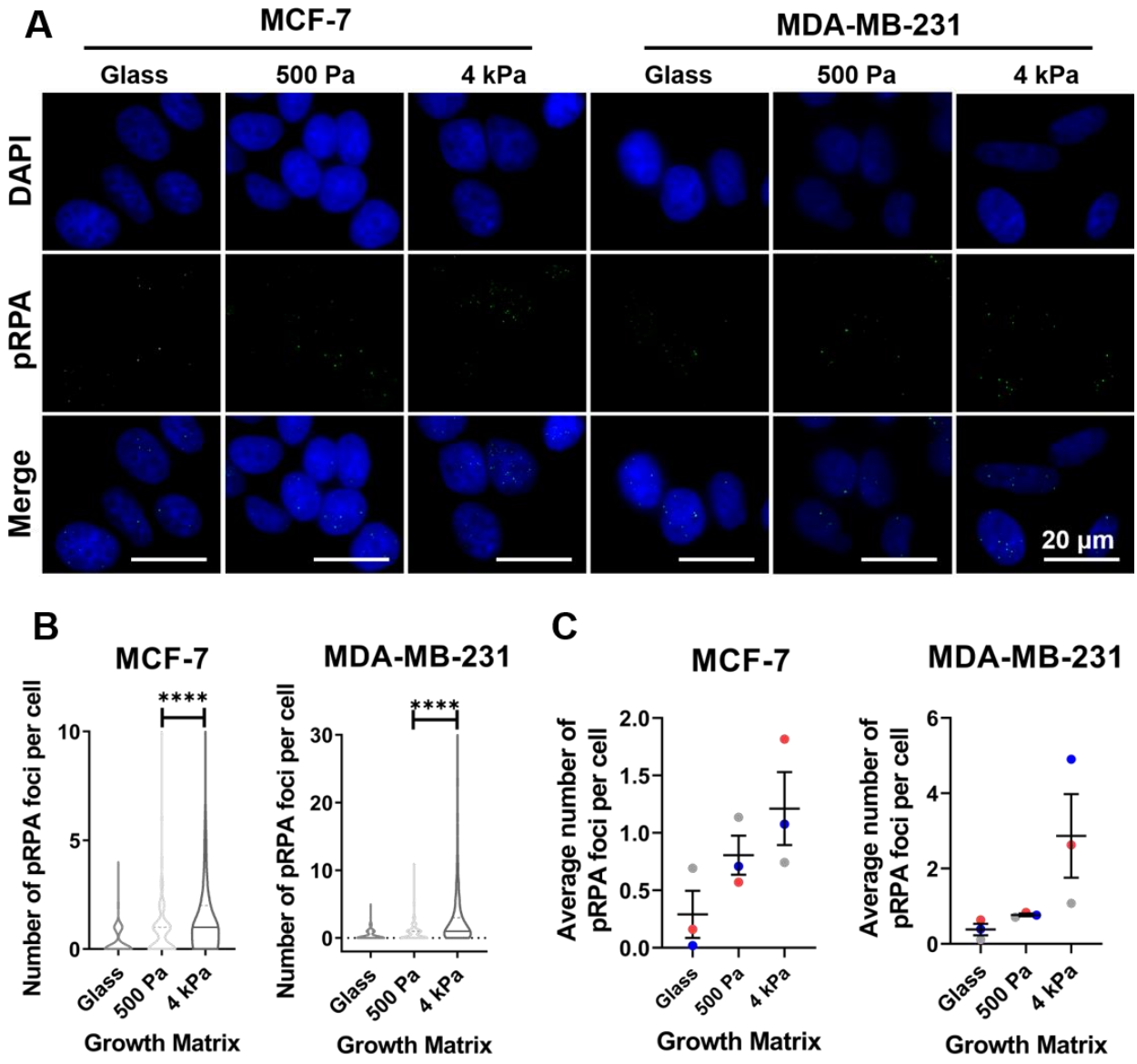

Figure 4.1. Increased polyacrylamide hydrogel stiffness increases replication stress in the MCF-7 and MDA-MB-231 cell lines. (A) MCF-7 and MDA-MB-231 cell lines were cultured on 500 Pa and 4 kPa stiffness hydrogels for 16 hrs. Cells were then fixed and stained for pRPA T21 using immunofluorescence. Representative images are shown from images taken on a Nikon TE200 inverted fluorescent microscope at a magnification of 60X. (B) The number of pRPA foci per cell were counted using FIJI. Approximately 100 cells were imaged per condition for each of 3 independent repeats. The pooled data are plotted with the median shown as a solid line and the 25% and 75% percentiles shown as dotted lines. **** indicates a one-tailed Mann-Whitney test p-value of <0.0001. (C) Mean pRPA T21 foci number per cell for each of 3 independent repeats are plotted in different colours for each repeat. The mean and standard error of the mean are plotted in black. Statistical significance was determined by an unpaired one-tailed Student's t-test.

In both the MCF-7 and MDA-MB-231 cell lines there was a significant increase in the number of pRPA foci per cell with increasing stiffness ($p < 0.0001$ by Mann-Whitney test). The mean number of pRPA foci per cell for each independent repeat are plotted in Figure 4.1.c. In both cell lines there was no significant difference, however the same trend was observed as for the pooled data. This data suggests that replication stress increases with stiffness. This agrees with our previous findings of a reduction in the number of cells undergoing active DNA replication at any one time and the hypothesis of increased replication speeds.

4.2.1.2. Increased stiffness induces DNA damage in the MDA-MB-231 cell line but not the MCF-7 cell line.

We next investigated if the increase in replication stress observed at higher stiffnesses coincided with an increase in DNA damage. Once DNA damage occurs it is signalled for repair by phosphorylation of histone H2AX at S139. This is known as γH2AX and is used as marker of DNA damage (Sharma, Singh, & Almasan, 2012). To assess endogenous levels of DNA damage MCF-7 and MDA-MB-231 cell lines were grown on 500 Pa and 4 kPa stiffness hydrogels and a glass control for 16 hrs. Cells were then fixed and stained for γH2AX using immunofluorescence. Representative images are shown in Figure 4.2.a. The number of γH2AX foci per cell were counted and the results are plotted in Figure 4.2.b. In the MCF-7 cell line there was no significant difference in the number of γH2AX foci between cells cultured at 500 Pa and at 4 kPa ($p = 0.1016$ by Mann-Whitney test). However, in the MDA-MB-231 cell line there was a significant increase in the number of γH2AX foci between cells cultured at 500 Pa and at 4 kPa ($p < 0.0001$ by Mann-Whitney test). The mean number of γH2AX foci for each repeat are plotted in Figure 4.2.c. In both cell lines there was no significant difference however there was a trend of increasing DNA damage with increasing stiffness in MDA-MB-231 cells.

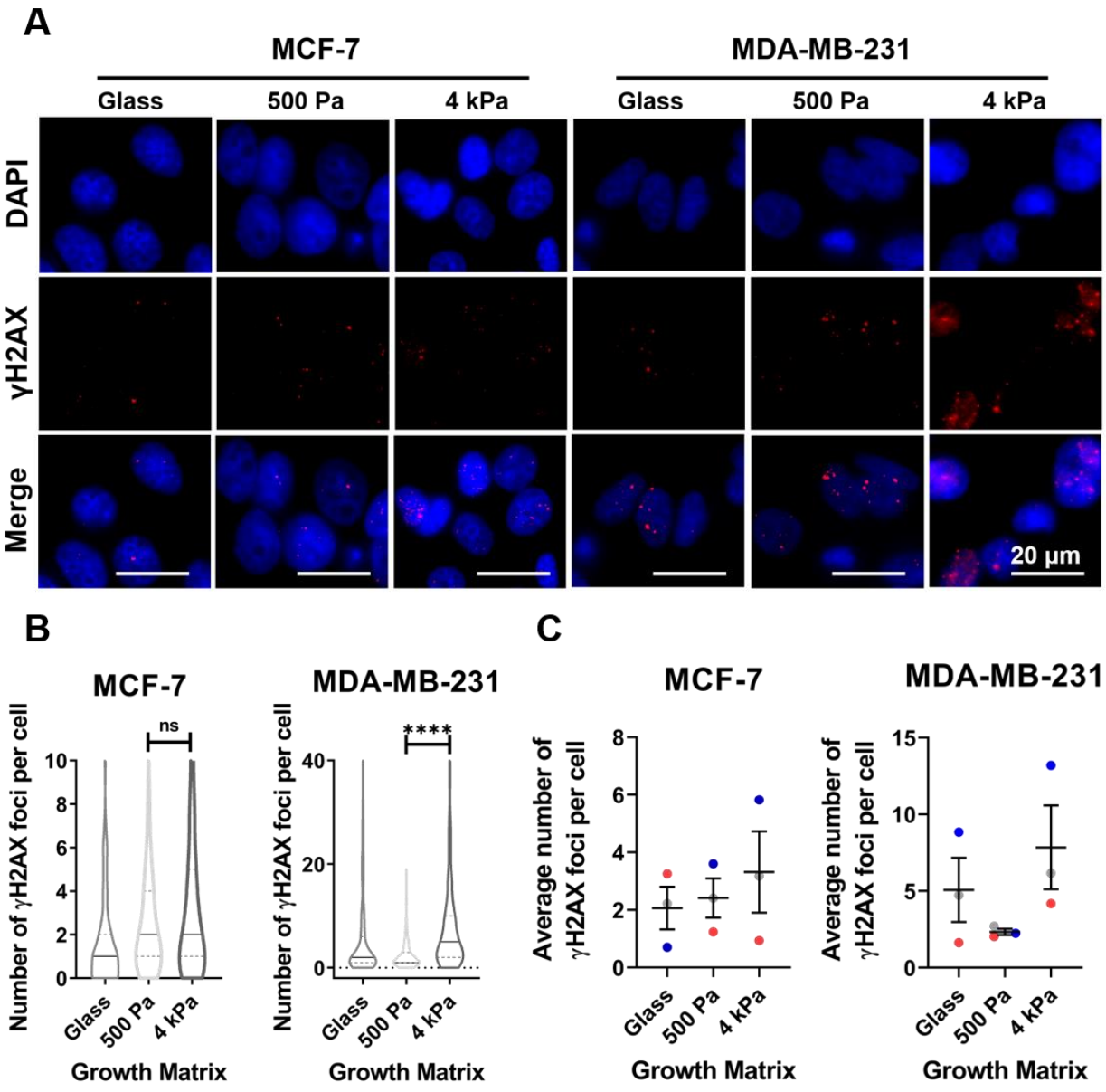

Figure 4.2. Polyacrylamide hydrogel stiffness affects DNA damage in the MDA-MB-231 cell line. Legend overleaf.

Micronuclei (MN) are segments of DNA (whole chromosomes or fragments) that form due to mis-segregation in mitosis or from genotoxic events and form their own nuclear envelope (Bakhoum et al., 2014). As such, they are a marker of genomic instability. In addition, some MN can be γH2AX positive due spontaneous MN rupture during interphase (Zhang et al., 2015) and have also been shown to be a marker of replication stress (Xu et al., 2011). As a significant increase in pRPA foci was observed at 4 kPa in both cell lines we next investigated if an increase in γH2AX positive MN was also

observed. The frequency of γH2AX positive micronuclei was determined and the results are depicted in Figure 4.2.d. There was no significant difference in the number of γH2AX positive or negative micronuclei in both cell lines between 500 Pa and 4 kPa. These findings do not agree with the replication stress differences observed from pRPA foci.

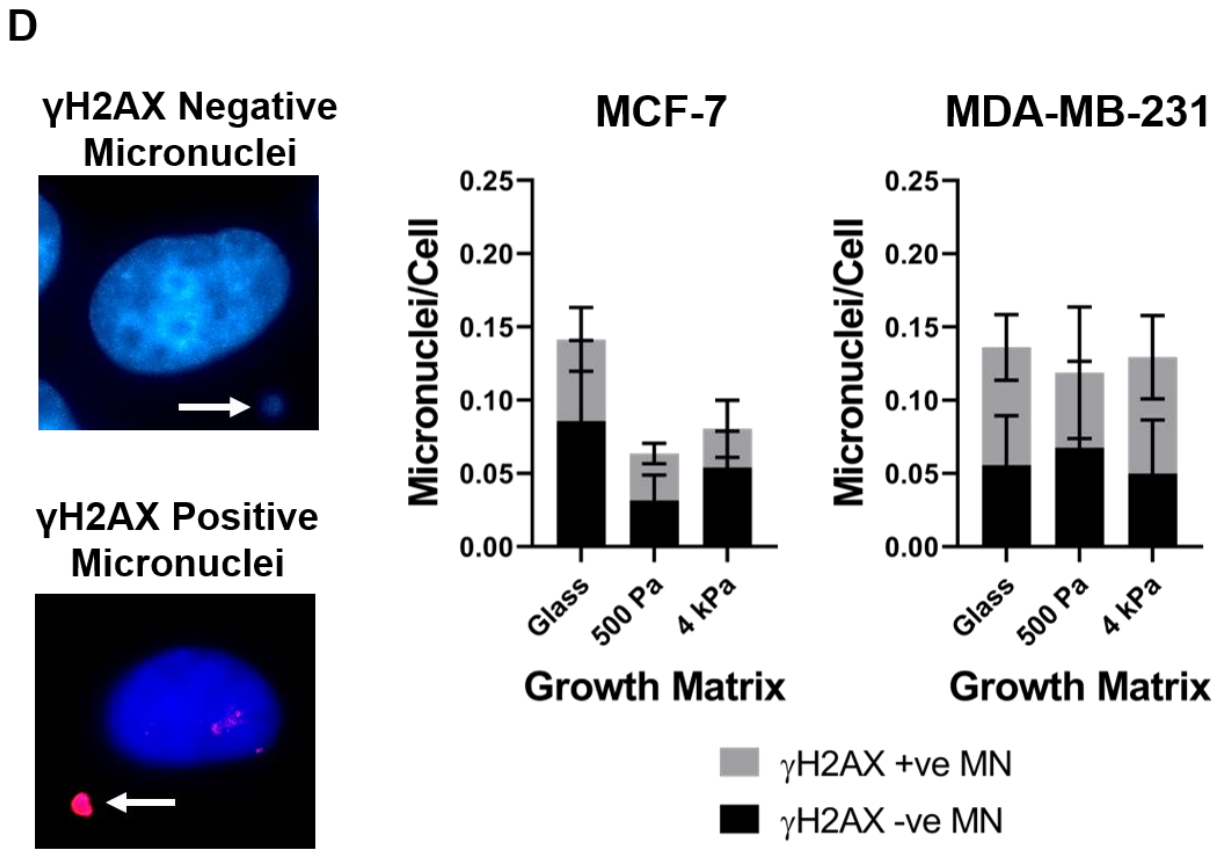

Figure 4.2. Polyacrylamide hydrogel stiffness affects DNA damage in the MDA-MB-231 cell line. (A) MCF-7 and MDA-MB-231 cell lines were cultured on 500 Pa and 4 kPa stiffness hydrogels for 16 hrs. Cells were then fixed and stained using immunofluorescence for γH2AX (S139). Representative images are shown from images taken on a Nikon TE200 inverted fluorescent microscope at a magnification of 60X. (B) The number of γH2AX foci per cell were counted in FIJI. Approximately 100 cells were imaged per condition for each of 3 independent repeats. The pooled data are plotted with the median shown as a solid line and the 25% and 75% percentiles shown as dotted lines. **** indicates a one-tailed Mann-Whitney test p-value of <0.0001. (C) Mean γH2AX foci number per cell for each of 3 independent repeats are plotted in different colours for each repeat. The mean and standard error of the mean are plotted in black. Statistical significance was determined by an unpaired one-tailed Student's t-test. (D) The number of micronuclei per cell expressed as γH2AX positive and negative for each condition. The mean and standard deviation are plotted in black. Approximately 100 cells were imaged per condition for each of 3 (MDA-MB-231) and 4 (MCF-7) independent repeats. Statistical significance was determined by an unpaired one-tailed Students t-test.

However, it has been reported that the addition of replication stressor agents are required to induce a significant difference in γH2AX positive micronuclei (Xu et al., 2011). As such the small changes in basal levels of replication stress induced by stiffness may not have been sufficient to induce a γH2AX positive micronuclei. As the results were quite varied between repeats it suggests that γH2AX positive MN were not a sensitive enough assay for determination of replication stress under the conditions used in our investigations. Secondly, the 16 hr time point used in our investigations may not have been sufficient to allow for formation of MN. However, as discussed above γH2AX positive MN can also form due to spontaneous MN rupture and as such cannot be used solely as an identification of replication stress.

4.2.2. Stiffness alters chromatin organisation in the MCF-7 cell line.

In chapter 3 we observed an increase in nuclear area with increasing stiffness. As the nuclear envelope forms direct contacts with chromatin through LADs it is possible that changes in the nuclear size may result in a re-arrangement in chromatin localisation, which could have consequences for DNA replication. One way to investigate this is to look at the localisation and amount of chromatin compaction in the form of heterochromatin. In areas of heterochromatin the DNA is tightly wound around histones which prevents gene expression in these DNA regions. In areas of euchromatin DNA is less tightly wound around histones, allowing for expression (Murakami, 2013). The differences observed in replication stress and DNA damage in Figures 4.1. and 4.2. could also be linked with this, as regions of heterochromatin are associated with maintenance of genomic stability and low levels of endogenous DNA damage (Fortuny & Polo, 2018).

We investigated chromatin structure by immunostaining for the heterochromatin marker H3K9me3 and the euchromatin marker H3K4me3. Initial attempts at staining following the manufacturers methodology using paraformaldehyde fixation produced a non-specific euchromatin stain and a pan-nuclear H3K9me3 stain (Figure 4.3.a). This was not the expected staining patterning and as such further methodological optimisation was required. Fixation with methanol and blocking with goat serum increased antibody access and specificity allowing hetero and euchromatin regions to be visualised (see glass in Figure 4.3.b). The MCF-7 cell line was then cultured on 500 Pa and 4 kPa hydrogels and a glass control for 16 hrs prior to fixation and staining for H3K9me3 and H3K4me3 by immunofluorescence. Representative images are shown in Figure 4.3.b. For cells cultured on glass and 500 Pa hydrogels H3K9me3 appeared to be localised at the nuclear periphery with a few brighter foci at the centre. For cells cultured on 4 kPa hydrogels H3K9me3 appeared to be distributed evenly across the nucleus, with a few brighter foci at the centre and the edge. There was little difference in the distribution of H3K4me3 between the cells cultured on either hydrogel, where an even distribution of H3K4me3 was observed. Whereas H3K4me3 appeared to be localised more at the nuclear periphery in cells cultured on glass.

To quantify changes in the localisation, an intensity plot was generated by measuring the intensity of each stain along the longest axis of the nucleus as depicted in Figure 4.3.c. A representative intensity plot is shown for each condition. The intensity plots are representative of the changes we observed in the images. In cells cultured on glass there are higher peaks of both H3K9me3 and H3K4me3 at the edges of the plot, with a dip in the middle, representative of the increased staining at the nuclear periphery. For cells cultured on 500 Pa and 4 kPa stiffness hydrogels the H3K4me3 staining is distributed at a low level across the whole intensity plot. In cells cultured on 500 Pa stiffness hydrogels

H3K9me3 staining is observed as a large peak at either end of the plot, with a few smaller peaks in the middle which is representative of increased staining at the nuclear periphery in Figure 4.3.b. In cells cultured on 4 kPa stiffness hydrogels however we observed a few smaller peaks distributed evenly over the entirety of the H3K9me3 plot matching with the few bright foci we observed in Figure 4.3.b.

We next assessed if stiffness affected the amount of hetero and euchromatin first by quantification of immunofluorescent intensity (Figure 4.3.d). There was no significant difference in H3K4me3 intensity but there was a significant decrease in H3K9me3 expression between 500 Pa and 4 kPa ($p = 0.0027$ by Mann-Whitney test). This suggests that an increase in stiffness results in a decrease in tightly wound chromatin which agrees with the observed increase in replication stress (Figure 4.1.). This phenomenon is thought to be due to exposure of tandem DNA repeats within DNA which poses a replication difficulty (Fortuny & Polo, 2018). However, as only fifteen nuclei were measured from one repeat, further repeats are required to confirm this result.

Further investigation into H3K9me3, H3K4me3 and H3K27ac (another euchromatin marker) protein levels by Western blot analysis found no difference between the two stiffnesses (Figure 4.3.e). Quantification of 2 and 3 repeats for each marker is shown in Figure 4.3.f. This confirmed that there was no significant difference. Western blotting is not a very sensitive technique which may suggest why little difference was seen in basal levels by this method, but was seen by immunofluorescence. However, more repeats would be needed to confirm this difference.

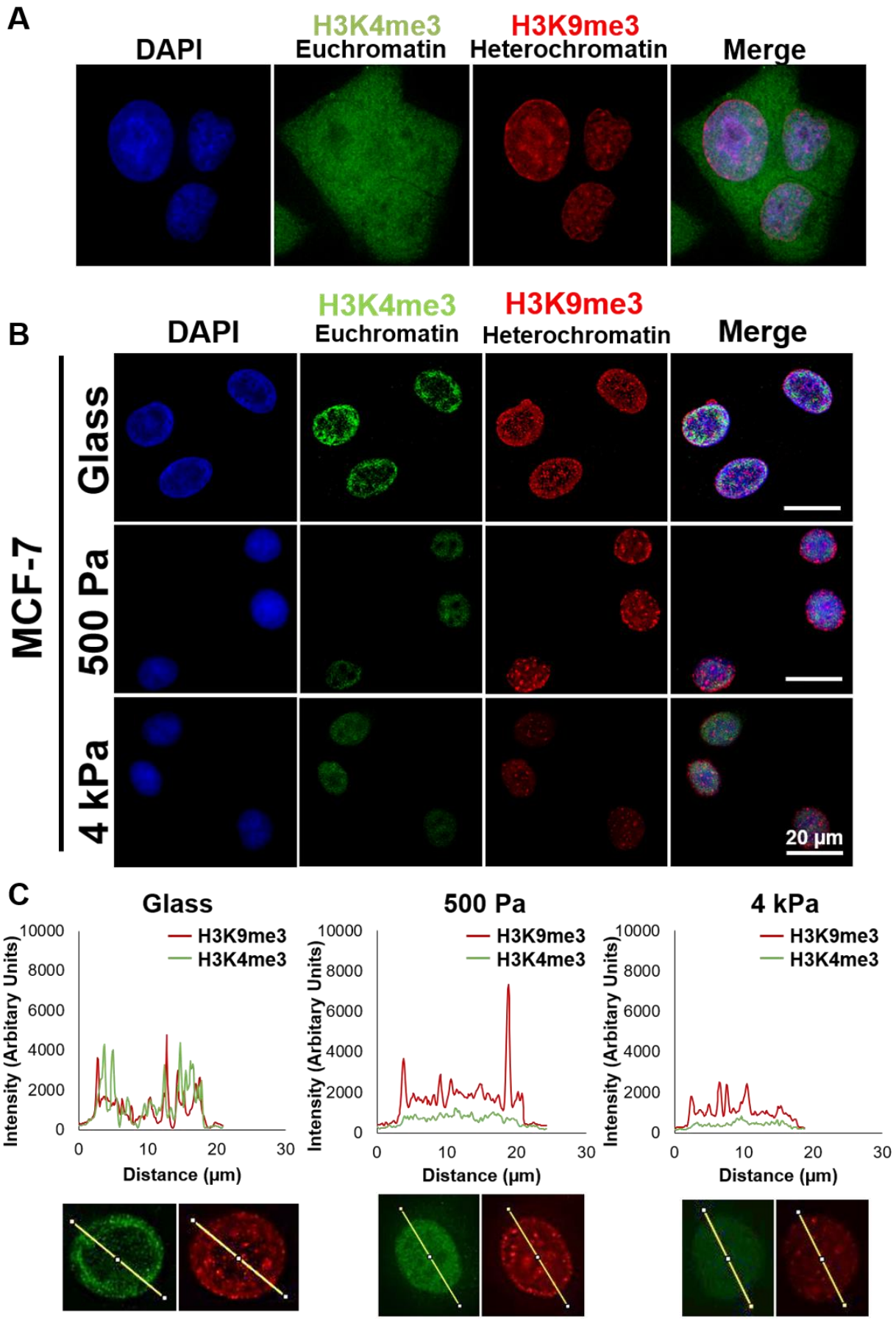

Figure 4.3. Polyacrylamide hydrogel stiffness alters heterochromatin intensity in the MCF-7 cell line. Legend overleaf.

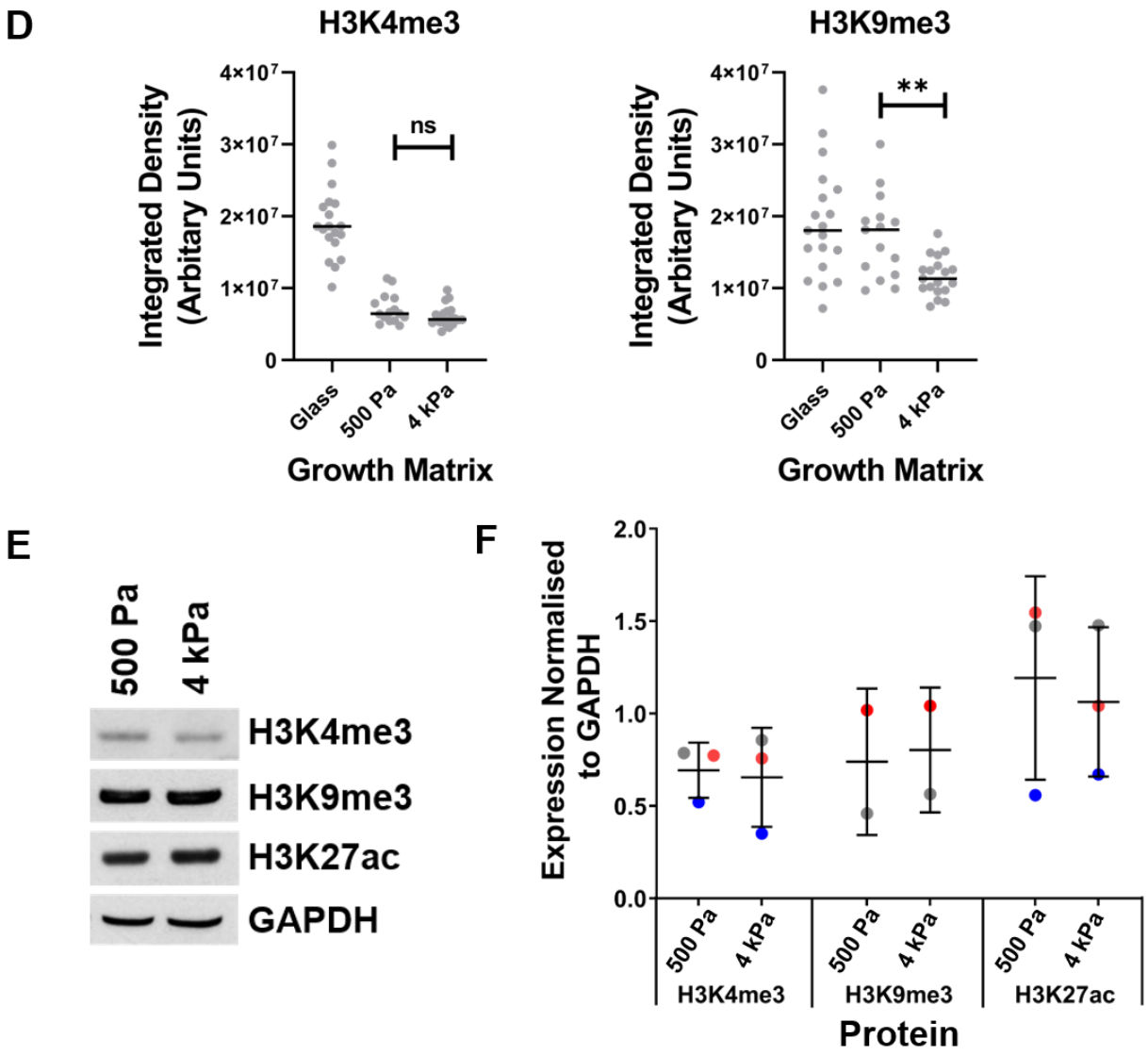

Figure 4.3. Hydrogel stiffness alters heterochromatin intensity in the MCF-7 cell line. Legend overleaf.

Figure 4.3. Hydrogel stiffness alters heterochromatin intensity in the MCF-7 cell line.
(A) Representative images of the MCF-7 cell line stained for euchromatin (H3K4me3) and heterochromatin (H3K9me3) using paraformaldehyde fixation following the antibody manufactures specifications. Images were taken on an Applied Precision deconvolution DeltaVision microscope at a magnification of 60X. (B) The MCF-7 cell line was cultured on 500 Pa and 4 kPa stiffness hydrogels and a glass control for 16 hrs. Cells were fixed using methanol and stained using the optimised immunofluorescence protocol for H3K4me3 and H3K9me3. Representative images are shown from images taken on an Applied Precision deconvolution DeltaVision microscope at a magnification of 60X. (C) Preliminary analysis of chromatin staining by measuring the intensity along the widest axis of each nuclei as pictured. From this a profile of the intensities was plotted for each chromatin stain along the line drawn, a representative plot is shown for each condition. Measurements were made in FIJI for at least 15 cells per condition for one repeat. (D) Nuclear H3K4me3 and H3K9me3 intensity (integrated density) was measured in FIJI for at least 15 cells for each condition for one repeat. Each data is plotted in grey and the median in black. ** indicates a one-tailed Mann-Whitney test p-value of <0.01. (E) Representative Western blot of whole cell extracts from MCF-7 cells cultured on 500 Pa and 4 kPa stiffness hydrogels for 72 hrs. Extracts were probed for H3K4me3, H3K9me3 and H3K27ac (another euchromatin marker) and a GAPDH control. (F) Relative expression of H3K4me3, H3K9me3 and H3K27ac compared to GAPDH expression calculated from Western blot images. Band densitometries were measured in FIJI for H3K4me3, H3K9me3 and H3K27ac and normalised to the GAPDH control for each hydrogel stiffness on each occasion to give the relative expression for each of 2 (H2K9me3) and 3 (H3K4me3 and H3K27ac) independent repeats. Each repeat is plotted in a different colour and the mean and standard deviations are plotted in black. Statistical significance was determined by an unpaired one-tailed Student's t-test.

4.2.3. Chemotherapeutic sensitivity in the MCF-7 cell line.

4.2.3.1. Sensitivity assay optimisation.

To be able to determine the response of breast cancer cells to different chemotherapeutic agents, a hydrogel compatible sensitivity assay was needed. We chose to begin with the chemotherapeutic agent gemcitabine as it has been shown to have stiffness specific resistances in pancreatic cancer cell lines (Puls, Tan, Whittington, & Voytik-Harbin, 2017). We started with the MCF-7 cell line as chemotherapeutic sensitivities had been characterised well on TCP in this cell line within our lab.

One of the first methods investigated was manual counting of cell number through DAPI staining, imaging and counting. It was used in chapter 3 to determine the changes in

growth after 5 days. Analysis and image taking was very time consuming, especially if multiple time points need to be investigated. Secondly it was not a very sensitive method as increasing doses of gemcitabine resulted in little difference between any of the stiffnesses (data not shown). This is likely due to the method not providing information about cell death or metabolic activity. Therefore, to try to investigate cell death a live annexin V and Hoechst stain was tested. This allowed for determination of cell death via necrosis or apoptosis. It did provide more sensitivity in preliminary tests on glass however the analysis was still very lengthy and variations in DAPI brightness hindered determination of whether a cell was truly necrotic, leading to false positives.

Trypan blue staining was next investigated; this agent stains only dead cells. First trypsin was used in an attempted to detach cells from the surface, this did not prove successful even with an increased trypsin concentration. Collagenase was also tried but did not detach cells at a range of attempted doses and resulted in cellular digestion with increased incubation times. On gel trypan blue staining was also attempted but the gel itself took on the stain hindering analysis. The same issue occurred when crystal violet staining was attempted (data not shown).

It became evident that a reaction which did not require intracellular readings was required. The alamarBlue assay would allow for this as the reaction occurs in the medium and can be measured immediately on a fluorescent plate reader. It is beneficial over other viability assays such as MTT as it has increased sensitivity and does not result in cell death (Hamid, Rotshteyn, Rabadi, Parikh, & Bullock, 2004). As such viability can be measured at multiple time points on the same cells. The alamarBlue assay was therefore used to investigate the cell viability of MCF-7 cells cultured on 500 Pa and 4 kPa

hydrogels and a glass control treated with 0 and 5 nM of gemcitabine. Cell viability was measured 48, 72, 96 and 120 hours after treatment with gemcitabine to determine the best time point to take measurements in future assays (Figure 4.4.). At 48 hrs no cell death was seen at 4 kPa and at 72 hrs moderate but significant cell killing was seen in all conditions. By 96 and 120 hrs low levels of survival remained, with the graph appearing to flatten between 40% and 20% survival suggesting loss of sensitivity. Thus 72 hrs was chosen as an appropriate time point, as it allowed for manipulation of survival to occur in either direction. Encouragingly in this pilot work, cells at 500 Pa were significantly more sensitive to gemcitabine than cells cultured at 4 kPa ($p = 0.0150$ by Student's t test). There was no significant difference at other time points however the same trend was observed.

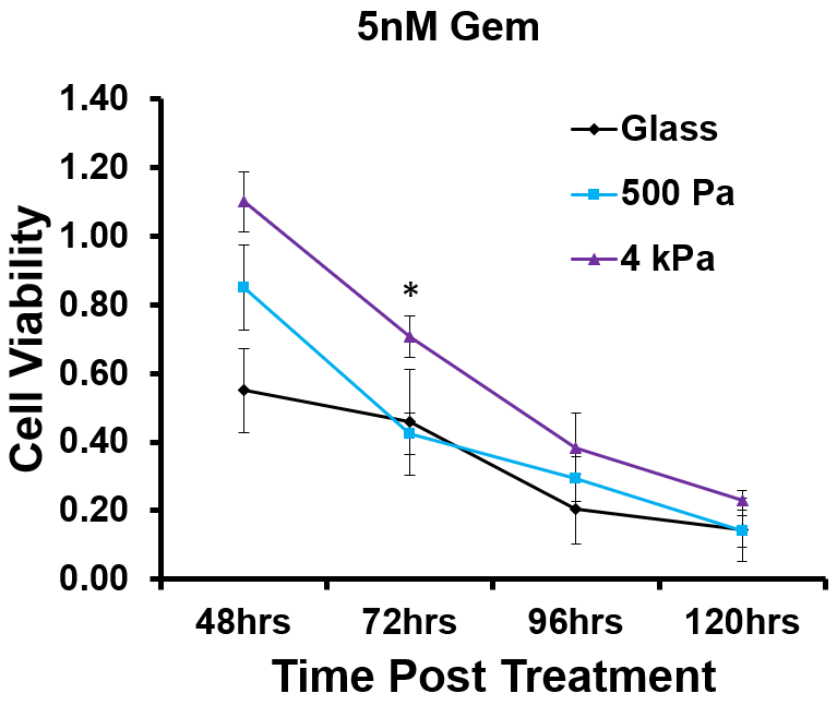

Figure 4.4. Method optimisation to determine chemotherapeutic response.
MCF-7 cells were cultured on polyacrylamide hydrogels of varying stiffnesses as indicated and a glass control for 24 hrs. Cells were then treated with 5 nM gemcitabine or a vehicle control. An alamarBlue reading was made 48, 72, 96 and 120 hrs after treatment with gemcitabine or the vehicle control. The gemcitabine or vehicle control were freshly added to the medium following removal of alamarBlue in-between readings. Cell viability was calculated by dividing the alamarBlue reading of the gemcitabine treated cells by the reading of the vehicle control treated cells for each culture matrix at each time point. The means of 2 (48 hrs) and 3 (all other time points) independent repeats are plotted with error bars depicting the standard error of the mean. Statistical significance was determined by an unpaired one-tailed Student's t-test where * indicates a p-value of ≤0.05.

4.2.3.2. Sensitivity of MCF-7 cells to a panel of chemotherapeutics at 500 Pa and 4 kPa.

Having found a compatible method and a suitable time point, other chemotherapeutic agents were then investigated. All chemotherapeutics were added for 72 hrs following plating of MCF-7 cells for 24 hrs (Figure 4.5.). Two doses were chosen for each agent based on dose curves from preliminary data on glass (data not shown) and from previous reports.

Alongside gemcitabine, two compounds, hydroxyurea (HU) and 5-FU, which also inhibit DNA replication were investigated. Gemcitabine is a cytidine analogue that incorporates into the DNA and RNA (Ruiz Van Haperen et al., 1993) but also inhibits CTPS, RNR and TS (De Sousa Cavalcante & Monteiro, 2014; Honeywell et al., 2015), which reduces the available pool of dNTPs leading to an increase in replicative stress. HU also inhibits RNR and TS (Boehm, Kreis, & Drahovsky, 1982; Yarbro, 1992). 5-FU also inhibits TS and its metabolites incorporate in DNA and RNA (Longley, Harkin, & Johnston, 2003).

Treatment with 2.5 or 5 µM 5-FU showed no significant difference in cell viability between either of the stiffnesses. Treatment with 0.1 mM or 1 mM HU also showed no significant difference. This suggests that MCF-7 cells do not show stiffness responsive drug sensitivity to HU nor 5-FU. However, when gemcitabine treatment was undertaken there was a significant increase in cell viability with an increased stiffness (4 kPa vs 500 Pa) at both 5 nM and 10 nM of gemcitabine ($p = 0.0147$ and 0.0041 respectively by Student's t test), confirming our previous findings.

PAX is a microtubule stabilising agent and thus causes cell death through prevention of cell division (Horwitz, 1994). It is used as a single agent and in combination with other drugs for treatment of breast cancer (Moreno-Aspitia & Perez, 2009). We observed in chapter 3 that stiffness altered cytoplasmic area and thus decided to investigate PAX response. At 0.5 nM and 5 nM PAX there was no significant difference in cell viability between the two stiffnesses. These results suggest that cells do not show a stiffness specific sensitivity to PAX under these conditions.

Radiotherapy treatment is used in cancer treatment, often in combination with chemotherapeutic agents. Also known as IR, it results in DNA damage through direct ionisation or through the generation of reactive oxygen species (Borrego-Soto, Ortiz-Lopez, & Rojas-Martinez, 2015). At 3 Gy and 6 Gy there was no significant difference in cell viability. These results suggest that cells do not show a stiffness specific sensitivity to IR under these conditions.

MMC is a chemotherapeutic agent that acts by alkylating DNA resulting in DNA crosslinking. It is used in treatment of metastatic breast cancer (Ospovat et al., 2009; Urruticoechea et al., 2005). There was no significant difference in cell viability between the two stiffnesses at 20 mM and 100 nM MMC. These results suggest that cells do not show a stiffness specific sensitivity to MMC under these conditions.

In cancers with higher replicative stress, PARP prevents fork collapse and facilities replication restart (Bryant et al., 2009). ATR is also important for cell survival in response to replicative stress (Saldivar et al., 2017). As we observed increased replication stress at a higher stiffness of 4 kPa in Figure 4.1., we hypothesised that cells at this stiffness might be vulnerable to inhibition of PARP or ATR. Therefore, the PARP inhibitor olaparib and the ATR inhibitor VE821 were chosen as the final two therapies to investigate. There was no significant difference in cell viability following treatment with 1 and 5 µM olaparib, however there was a trend of increasing sensitivity with an increased stiffness. There was also no significant difference in cell viability following treatment with 0.5 and 1 µM VE821, however there was a trend of increasing sensitivity with an increased stiffness. These results suggest that that cells do not show a stiffness specific sensitivity to olaparib or VE821 under these conditions. However, the trend of

increased sensitivity with increased stiffness does agree with our previous findings of an increase in replicative stress.

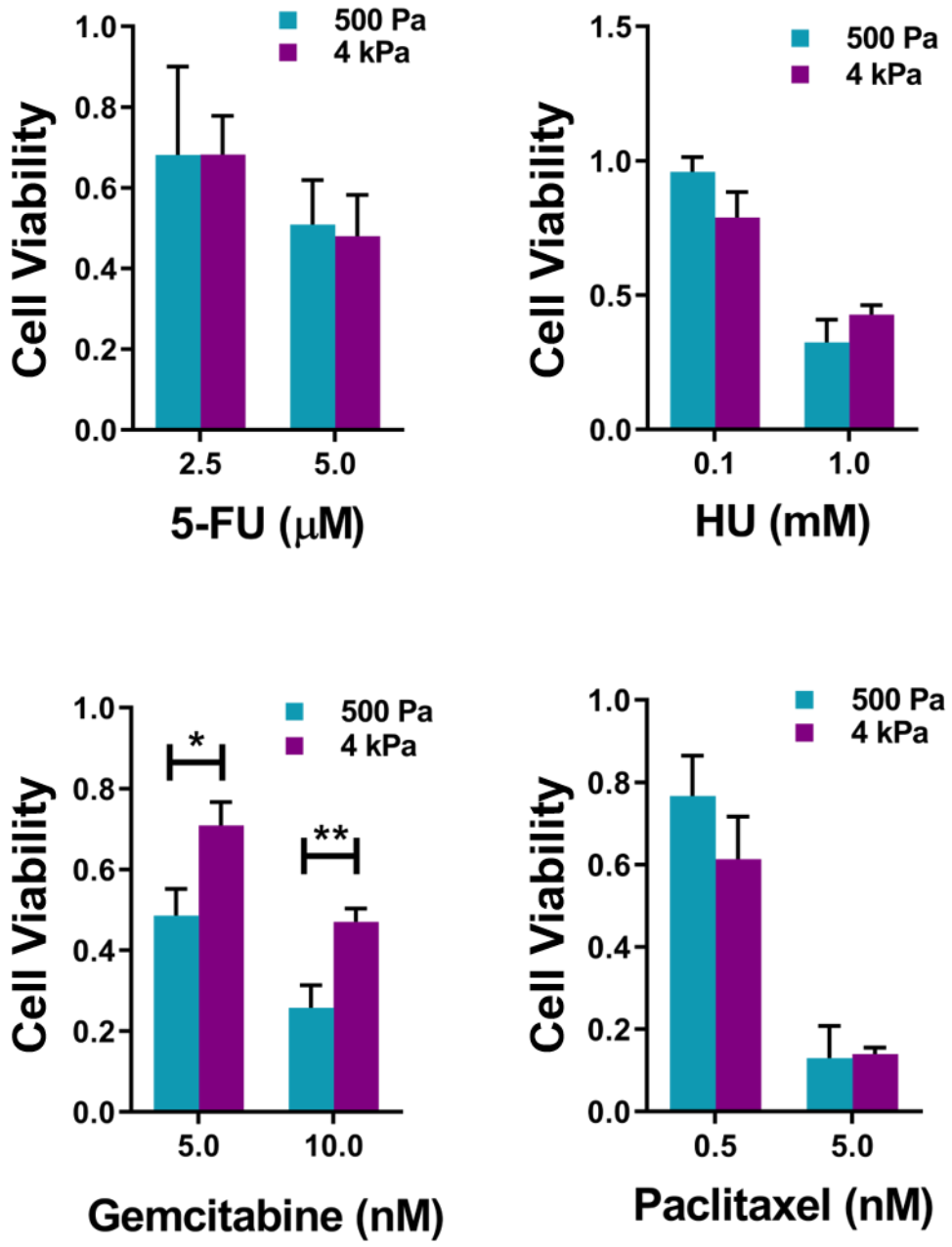

Figure 4.5. Response of the MCF-7 cell line to 8 chemotherapeutic agents when cultured on polyacrylamide hydrogels of varying stiffnesses. Legend overleaf.

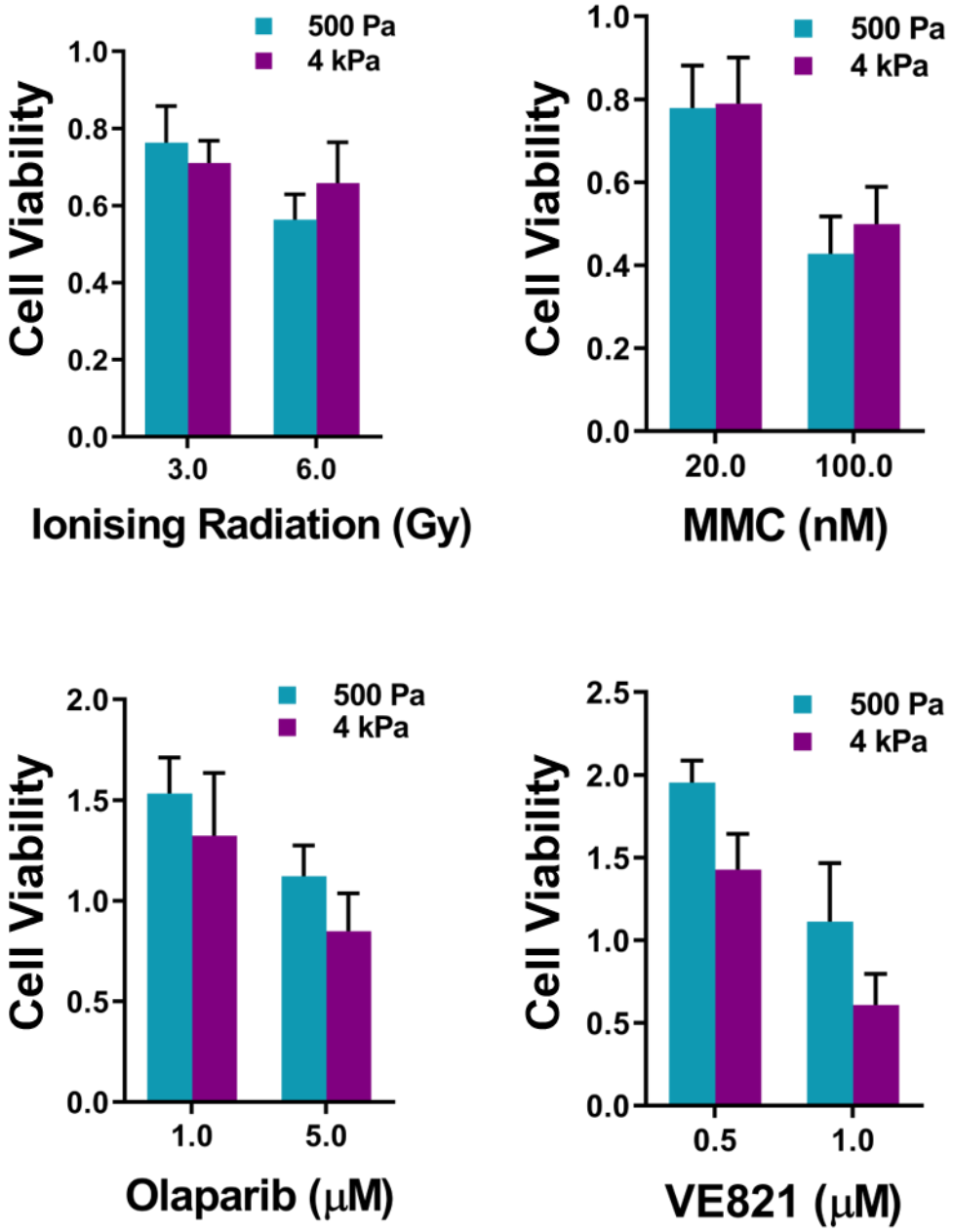

Figure 4.5. Response of the MCF-7 cell line to 8 chemotherapeutic agents when cultured on polyacrylamide hydrogels of varying stiffnesses. The MCF-7 cell line was cultured on 500 Pa and 4 kPa hydrogels for 24 hrs prior to the addition of chemotherapeutic agents at two doses as monotherapies as indicated. Eight agents were used in total; 5-fluroruracil (5-FU), hydroxyurea (HU), gemcitabine, paclitaxel (PAX), ionising radiation (IR), mitomycin C (MMC), olaparib and VE821. After 72 hrs treatment with each agent cell metabolism was measured by alamarBlue assay. The cell viability for each condition was calculated by dividing the reading of the treated sample with that of the vehicle control. Means and standard error of the means are plotted for 3 independent repeats for all agents apart from gemcitabine and VE821 where the means are from 6 and 2 independent repeats respectively. * indicates an unpaired one-tailed Student's t-test p-value of ≤0.05 and ** ≤0.01.

4.2.4. Stiffness does not affect the amount of DNA damage or replication stress induced by gemcitabine.

Having determined that stiffness caused a significant difference in response to gemcitabine only we wanted to investigate if this was linked to the differences we observed in basal levels of replication stress and DNA damage.

4.2.4.1. Replication stress.

It was initially attempted to undertake immunofluorescent staining with the same phosphorylated RPA antibody as we used in Figure 4.1. However, the staining pattern did not appear reproducible between antibody batches suggesting that the new antibody batch would not be compatible for comparison to the one used in Figure 4.1. As such, a new total RPA staining protocol was optimised. Whilst accumulation of total RPA (RPA34) is still representative of replication stress it is not as sensitive as phosphorylated RPA which must be considered when the results are being compared.

The MCF-7 cell line was cultured on 500 Pa and 4 kPa stiffness hydrogels and a glass control for 24 hrs prior to treatment with 5 nM gemcitabine or a vehicle control for a further 24 hrs. Cells were then fixed and stained using immunofluorescence for RPA34. Representative images are shown in Figure 4.6.a. The total RPA stain produces a large number of small foci which gives the appearance of a pan-nuclear stain and as such foci number could not be determined as in Figure 4.1. Instead fluorescence intensity was measured in FIJI and this was used to determine differences in the amount of replication stress. Pooled data from 3 repeats is plotted in Figure 4.6.b. The addition of gemcitabine to cells cultured on 500 Pa and 4 kPa hydrogels and the glass control resulted in a significant increase in RPA34 staining intensity ($p < 0.0001$ by Kruskal-Wallis test). This confirms that gemcitabine is working as would be expected in cells cultured on both matrices. It does not appear from these results that the culture matrix influences

gemcitabine's ability to cause replication stress as there was no significant difference between the intensity at 500 Pa and 4 kPa following treatment with gemcitabine ($p > 0.9999$ by Kruskal-Wallis test). Thus, the differences observed in cell viability following gemcitabine treatment at the two stiffnesses are likely to do with how the cell responds to the effects of gemcitabine.

However, the difference observed in chapter 3 in basal levels of replication stress between 500 Pa and 4 kPa was not observed here, as there was a non-significant difference between the vehicle control treated cells on these stiffnesses ($p = 0.2646$ by Kruskal-Wallis test). Cells were left for a total of 48 hrs prior to fixation, compared to the 16 hrs in determination of basal levels in Figure 4.1. Therefore, it could be that by 48 hrs the initial replication stress differences between the stiffnesses have begun to resolve as the cells further adapted to their substrate. It could also be due to the total RPA stain being less sensitive than phosphorylated RPA and therefore unable to detect the small changes in basal levels that were observed in Figure 4.1.

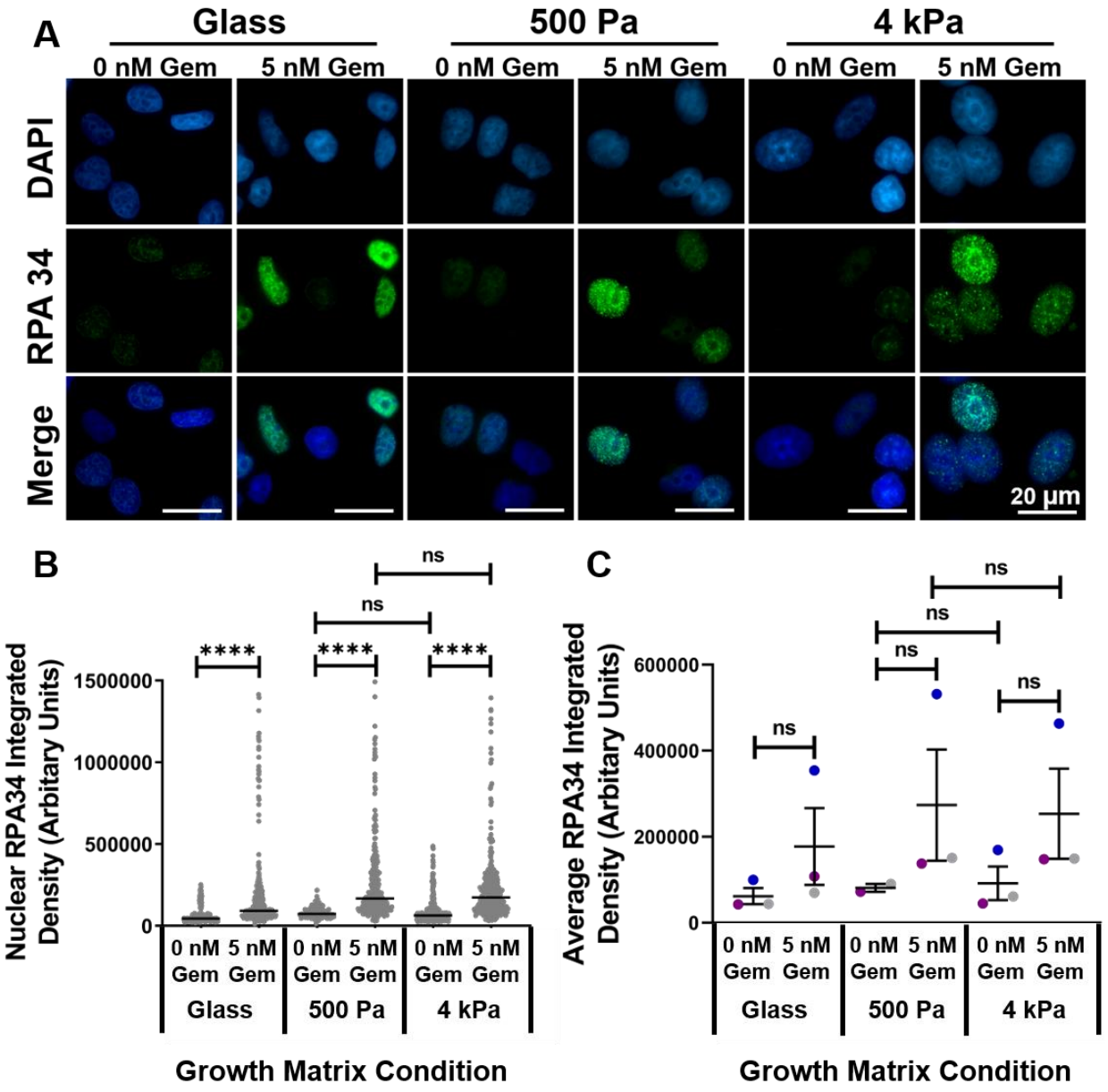

Figure 4.6. Polyacrylamide hydrogel stiffness does not alter the amount of replication stress induced by gemcitabine. (A) The MCF-7 cell line was cultured on 500 Pa and 4 kPa stiffness hydrogels and a glass control for 24 hrs prior to treatment with 5 nM gemcitabine (Gem) or a vehicle control for a further 24 hrs. Cells were then fixed and stained using immunofluorescence for RPA34. Representative images are shown from images taken on a Nikon TE200 inverted fluorescent microscope at a magnification of 60X. (B) Nuclear RPA34 intensity (integrated density) was measured in FIJI for approximately 100 nuclei for each of 3 independent repeats. Pooled data from the repeats are plotted in grey with median plotted in black. **** indicates a Kruskal-Wallis test p-value of <0.0001. (C) Mean RPA34 integrated density for each of 3 independent repeats are plotted in different colours for each repeat. The mean and standard error of the mean are plotted in black. Statistical significance was determined by one-way ANOVA.

The nuclear intensity averages from each repeat are plotted in Figure 4.6.c. Whilst not significant, the same trend is observed for these averages as for the pooled data in Figure 4.6.b.

4.2.4.2. DNA damage.

We next investigated if the amount of DNA damage caused by gemcitabine treatment was altered by stiffness. The MCF-7 cell line was cultured on 500 Pa and 4 kPa stiffness hydrogels and a glass control for 24 hrs prior to treatment with 5 nM gemcitabine (Gem) or a vehicle control for a further 24 hrs. Cells were then fixed and stained using immunofluorescence for γH2AX S139. A different γH2AX S139 antibody was used to the antibody used in Figure 4.2. due to species compatibility. Representative images are shown in Figure 4.7.a.

Addition of gemcitabine resulted in production of pan nuclear γH2AX stain which is in agreement with staining patterns observed in the literature (Moeglin et al., 2019). This type of staining is representative of lethal DNA replication stress. As such, nuclear intensity was measured to compare differences in staining as a representation of DNA damage. Pooled data from 3 repeats is shown in Figure 4.7.b. Addition of gemcitabine to MCF-7 cells cultured on glass resulted in a significant increase in nuclear γH2AX intensity ($p < 0.0001$ by Kruskal-Wallis test). This was also true for cells cultured on 500 Pa and 4 kPa hydrogels ($p < 0.0001$ and $p < 0.0001$ respectively by Kruskal-Wallis test). A larger increase in intensity was observed for cells cultured on 500 Pa hydrogels following addition of gemcitabine than for cells cultured on glass and at 4 kPa. However, there was no significant difference in the intensity of γH2AX following gemcitabine treatment for cells cultured on 500 Pa vs 4 kPa hydrogels ($p > 0.9999$ by Kruskal-Wallis test). This suggests that gemcitabine results in the same level of DNA damage on both hydrogel

stiffnesses. The difference in the amount of damage caused was due to changes in the baseline levels of DNA damage. When cells were cultured without gemcitabine there was a significant increase in the γH2AX intensity between 500 Pa and 4 kPa ($p < 0.0001$ by Kruskal-Wallis test). This difference was not observed in Figure 4.2. which may suggest that at a later time point of 48 hrs DNA damage may begin to accumulate in the MCF-7 cell line following prolonged culture at an increased stiffness. The use of a different antibody for the same epitope may also contribute to this difference, or the measure of intensity rather than foci number for this analysis.

The means of each repeat are plotted in Figure 4.7.c. The same trend was observed as in Figure 4.7.b although it was only significant following addition of gemcitabine for cells at 500 Pa ($p = 0.0228$ by one-way ANOVA).

These results suggest that hydrogel stiffness does not alter the amount of DNA damage caused by gemcitabine. The presence of a pan nuclear γH2AX stain is thought to be representative of lethal replication stress and as such these results are in agreement with the changes observed in RPA34 intensity.

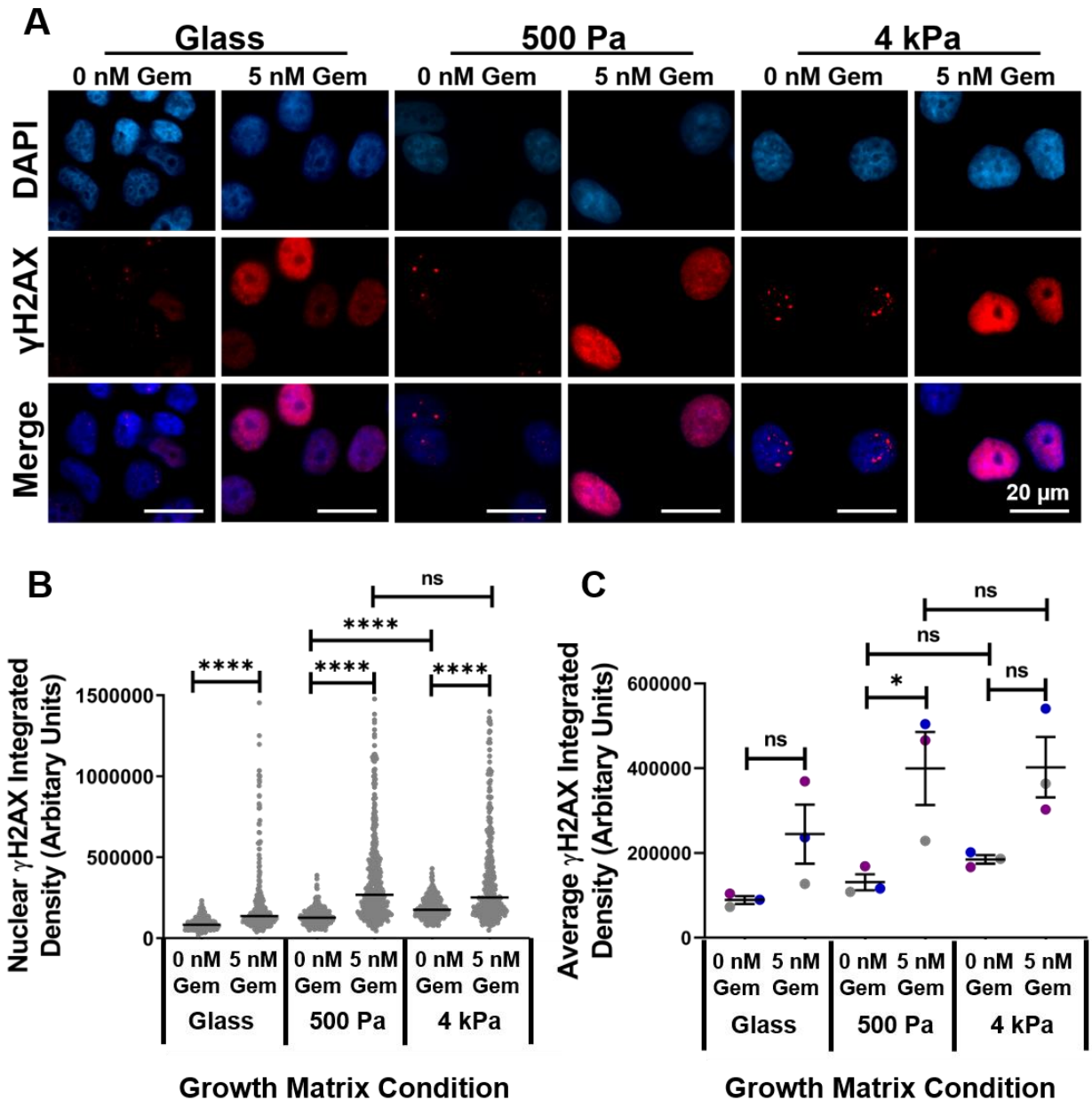

Figure 4.7. Polyacrylamide hydrogel stiffness does not alter γH2AX response to gemcitabine. (A) The MCF-7 cell line was cultured on 500 Pa and 4 kPa stiffness hydrogels and a glass control for 24 hrs prior to treatment with 5 nM gemcitabine (Gem) or a vehicle control for a further 24 hrs. Cells were then fixed and stained using immunofluorescence for γH2AX S139. Representative images are shown from images taken on a Nikon TE200 inverted fluorescent microscope at a magnification of 60X. (B) Nuclear γH2AX intensity (integrated density) was measured for approximately 100 nuclei for each of 3 independent repeats. Pooled data are plotted in grey with median plotted in black. **** indicates a Kruskal-Wallis test p-value of <0.0001. (C) Mean γH2AX integrated density for each of 3 independent repeats are plotted in different colours for each repeat. The mean and standard error of the mean are plotted in black. * indicates a one-way ANOVA p-value of <0.05.

4.2.5. Stiffness changes intracellular p53 localisation following gemcitabine treatment.

No difference in the gemcitabine-induced replication stress and DNA damage between the two stiffnesses suggests that the response downstream of the damage is altered. It has been reported that the tumour suppressor p53 has a role in mediating response to gemcitabine where cells harbouring a non-functional version are more resistant to gemcitabine (Chen, Hough, & Lawrence, 2000; Galmarini et al., 2002). Wild type (wt) p53 acts to halt cell cycle progression at the G1/S checkpoint upon induction of DNA damage. It also has a role in the initiation of apoptosis through interaction with anti-apoptotic proteins such as B-cell lymphoma 2 (Bcl-2) and Bcl-xL. Stiffness specific changes in p53 have also been observed in the p53 wt MCF-7 cell line, where low p53 levels in the nucleus conferred with resistance to the chemotherapeutic agent doxorubicin at a stiffnesses of 2 kPa (Ebata et al., 2017).

Low concentrations of wt p53 are typically observed in both the nucleus and the cytoplasm in unstressed cells (Maki, 2010). Upon DNA damage wt p53 accumulates in the nucleus but can also localise to mitochondria for induction of apoptosis. Interactions between wt p53 and cytoplasmic scaffold proteins such as actin have also been reported (Araki et al., 2015).

Therefore, we next investigated how wt p53 localisation was altered in MCF-7 cells following treatment with gemcitabine at a stiffness of 500 Pa and 4 kPa. The MCF-7 cell line was cultured on 500 Pa and 4 kPa stiffness hydrogels and a glass control for 24 hrs prior to treatment with 5 nM gemcitabine (Gem) or a vehicle control for a further 24 hrs. Cells were then fixed and stained using immunofluorescence for p53. Representative images are shown in Figure 4.8.a. The stain appears to be localised to the nucleus in

untreated cells cultured on glass and on 4 kPa stiffness hydrogels. Interestingly the stain appears to localise to the cytoplasm and the nucleus in untreated cells cultured on 500 Pa stiffness hydrogels. However, following addition of gemcitabine an observable increase in nuclear p53 is only notable in cells cultured on glass and 500 Pa stiffness hydrogels. To quantify this, nuclear p53 intensity was measured using FIJI for each condition. The pooled results from 3 independent repeats are shown in Figure 4.8.b. As expected, the addition of gemcitabine to cells cultured on glass resulted in a significant increase in p53 intensity ($p < 0.0001$ by Kruskal-Wallis test). The addition of gemcitabine to cells cultured on 500 Pa stiffness hydrogels also resulted in an increase in nuclear p53 intensity ($p < 0.0001$ by Kruskal-Wallis test). Interestingly however, the addition of gemcitabine to cells cultured on 4 kPa stiffness hydrogels did not results in a significant change in nuclear p53 intensity ($p > 0.9999$ by Kruskal-Wallis test). This agrees with the stiffness specific observations by Ebata et al., (2017) in MCF-7 cells in relation to chemoresistance. There was no significant change in the nuclear p53 intensity in cells cultured without gemcitabine at a stiffness of 500 Pa or 4 kPa ($p > 0.9999$ by Kruskal-Wallis test). However, there was a significantly higher nuclear p53 intensity in gemcitabine treated cells cultured at a stiffness of 500 Pa vs 4 kPa ($p < 0.0001$ by Kruskal-Wallis test).

The means of each repeat are plotted in Figure 4.8.c. The same trend was observed as for the pooled data in Figure 4.8.b. However, this was only significant for cells cultured on 500 Pa stiffness hydrogels following the addition of gemcitabine ($p = 0.0239$ by one-way ANOVA) and not for cells cultured at stiffness of 4 kPa ($p = 0.9575$ by one-way ANOVA). There was also a significant increase in mean nuclear p53 intensity in gemcitabine treated cells cultured at a stiffness of 500 Pa compared to 4 kPa ($p = 0.0370$ by one-way ANOVA).

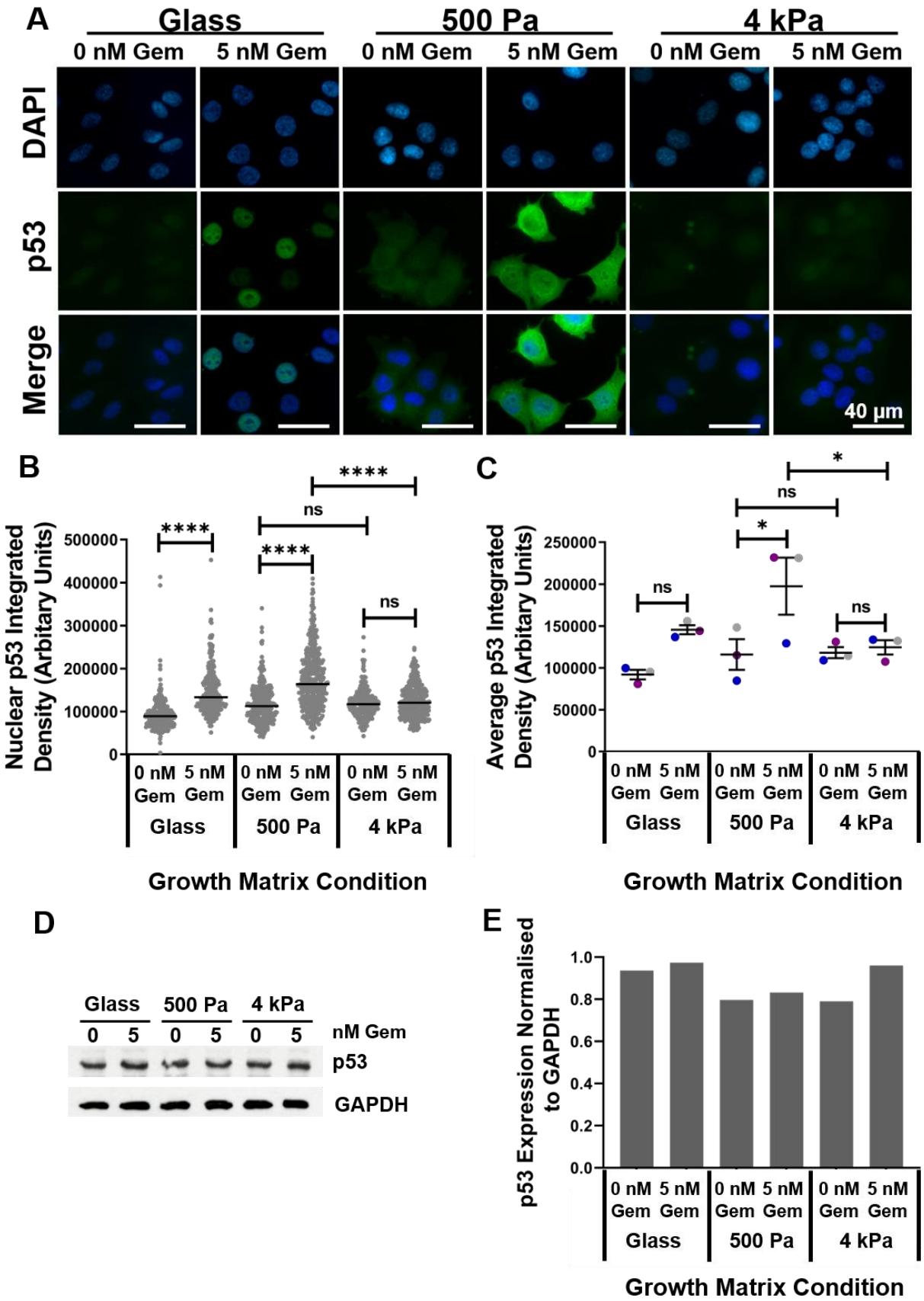

Figure 4.8. p53 accumulates in the nucleus after gemcitabine treatment in MCF-7 cells cultured at stiffness of 500 Pa but not at 4 kPa. Legend overleaf.

Figure 4.8. p53 accumulates in the nucleus after gemcitabine treatment in MCF-7 cells cultured at stiffness of 500 Pa but not at 4 kPa. (A) The MCF-7 cell line was cultured on 500 Pa and 4 kPa stiffness hydrogels and a glass control for 24 hrs prior to treatment with 5 nM gemcitabine (Gem) or a vehicle control for a further 24 hrs. Cells were then fixed and stained using immunofluorescence for p53. Representative images are shown from images taken on a Nikon TE200 inverted fluorescent microscope at a magnification of 60X. (B) Nuclear p53 intensity (integrated density) was measured for approximately 100 nuclei for each of 3 independent repeats. Pooled data from the repeats are plotted in grey with the median plotted in black. **** indicates a Kruskal-Wallis test p-value of <0.0001. (C) Mean p53 integrated density for each of 3 independent repeats are plotted in different colours for each repeat. The mean and standard error of the mean are plotted in black. * indicates a one-way ANOVA p-value of <0.05. (D) Western blot of whole cell extracts from MCF-7 cells cultured on 500 Pa and 4 kPa stiffness hydrogels with 5 nM gemcitabine or a vehicle control for 24 hrs. Extracts were probed for p53 and a GAPDH control. (E) Relative expression of p53 compared to GAPDH expression calculated from a Western blot image of one repeat. Band densitometries were measured in FIJI for p53 and normalised to the GAPDH control for each sample to give the relative expression.

These results suggest that addition of gemcitabine to MCF-7 cells cultured at a stiffness of 4 kPa does not induce the typical accumulation of p53 in the nucleus that is observed when cells are cultured at a lower stiffness of 500 Pa and on glass.

It can be observed qualitatively in the images as represented in Figure 4.8.a that in cells cultured at 500 Pa treatment with gemcitabine not only results in an increase in nuclear p53 but also in cytoplasmic p53. Conversely cells cultured at 4 kPa had no observable difference in p53 intensity following gemcitabine treatment in either the nucleus or the cytoplasm. This may suggest that the protein expression levels may be altered as well as changes in cellular localisation. To investigate this Western blotting was undertaken of MCF-7 cells cultured on 500 Pa and 4 kPa stiffness hydrogels following 24 hrs treatment with or without gemcitabine. The blot produced is displayed in Figure 4.8.d. Densitometric analysis was undertaken in FIJI to allow for quantitative measurement of the p53 band intensities relative to the GAPDH control. The results are plotted in Figure 4.8.e. The quantification showed there was little difference in p53 expression between cells cultured

at either stiffness or on the glass control. A slight increase in p53 expression can be observed in all samples following the addition of gemcitabine. These results suggest that changes in p53 expression are not likely to be responsible for the changes observed in its subcellular location, however as only one independent repeat was undertaken conclusions cannot be drawn from this repeat alone. Secondly, Western blotting is not sensitive at determining small expressional changes such as these. Therefore, further analysis into expression is needed to determine how p53 protein levels are altered due to matrix stiffness following gemcitabine treatment.

It is important to note that whilst wt p53 is expressed in the MCF-7 cell line, mutant p53 is observed in many cancers, whereby *TP53* gene mutations are the most common gene mutations observed in all cancers (Kandoth et al., 2013). This can result in either a loss or gain of function, where p53 loses its wild-type function and in the latter case can gain a new function, which is typically beneficial to cancer survival. This includes but is not limited to increased colony formation, an increased migration and drug resistance (Muller & Vousden, 2014). Therefore, it will be necessary to determine gemcitabine response in a panel of breast cancer cell lines which harbour either wt or mutant p53 to investigate potential differences in a gain of function background.

4.2.6. Progesterone receptor expression conveys resistance to gemcitabine in breast cancer cell lines at higher stiffnesses.

4.2.6.1. Progesterone receptor expression correlates to the stiffness specific response to gemcitabine in breast cancer cell lines.

We have observed a resistance to gemcitabine at higher stiffnesses in the MCF-7 cell line. To investigate if this response was observed in other breast cancer phenotypes, we compared the response of 6 more breast cancer cell lines representative of the various

subtypes of breast cancer. The 6 cell lines were cultured on 500 Pa and 4 kPa hydrogels for 24 hrs prior to the addition of gemcitabine or a vehicle control. After 72 hrs treatment, cell viability was measured by the alamarBlue assay.

The results of 3 independent repeats are plotted in Figure 4.9. The p53 statuses of each cell line were determined using the TP53 database (Leroy et al., 2013) and are detailed in the figure alongside their receptor statuses. We previously used the MDA-MB-231 TNBC cell line in Figures 4.1. and 4.2. and found that an increased stiffness led to an increased basal level of DNA damage and replication stress. As this was similar to the response of the MCF-7 cell line it suggests that the MD-MB-231 cell line may respond similarly to gemcitabine treatment across the two stiffnesses. Interestingly however, opposite to MCF-7 cells, the MDA-MB-231 cell line was more sensitive to gemcitabine at a stiffness of 4 kPa than at 500 Pa. This trend was significant at both 5 nM and 10 nM gemcitabine ($p = 0.0125$ and 0.0096 respectively by Student's t-test). They express a mutant gain of function version of p53 which has been attributed to increased survival, growth and a migratory phenotype (Muller & Vousden, 2014). The MDA-MB-468 and CAL-51 TNBC cell lines were next investigated to see if the trend observed in the MDA-MB-231 cell line was a TNBC specific effect. In the MD-MB-468 cell line, which expresses a mutant version of p53 attributed to increased proliferation, growth, survival and drug resistance (Muller & Vousden, 2014), there was no-significant difference. There was no-significant difference in the CAL-51 cell line at a 5 nM dose of gemcitabine although the trend was in agreement with MDA-MB-231 cells. At a dose of 10 nM however there was a significantly increased cell viability at 4 kPa vs 500 Pa. As n=2 for CAL-51 cells at 4 kPa with 10 nM gemcitabine, further repeats are required to confirm this trend. This is in contrast to the results observed at the lower dose of gemcitabine and to the other two TNBC cell lines. As CAL-51 is the only cell line of the three TNBC cell lines investigated to express wt p53

it indicates that wt p53 may have a role in resistance to gemcitabine at higher stiffnesses. It also suggests that the trend observed in the MDA-MB-231 and 468 cell lines may require the absence of wt p53 function. The different response between the MDA-MB-468 and MDA-MB-231 cell lines may suggest that the different mutant p53 functions gained may impact resistance to gemcitabine. This would need to be further investigated to help determine any particular phenotypes of p53 mutant cancers which could indicate a potential sensitivity to gemcitabine at higher stiffnesses. These results suggest that the same response to gemcitabine is not observed in all TNBC cell lines in a stiffness specific manner.

We next investigated the SK-BR-3 cell line which is ERBB2 positive, PR negative, ER negative. It expresses a mutant version of p53 which has been attributed to increased proliferation, growth and drug resistance (Muller & Vousden, 2014). There was no significant difference in response to either dose of gemcitabine between the two stiffnesses. Interestingly, the mutant p53 gain of functions indicated in this cell line are similar to those observed in the MDA-MB-468 cell line, which also showed no difference in gemcitabine response at the stiffnesses investigated. This may suggest that increased cell growth and drug resistance attributed to mutant p53 function does not influence survival in a stiffnesses specific manner. The ZR-75-1 cell line is ER positive and PR and ERBB2 negative. Like the MCF-7 cell line it expresses wt p53. At both doses of gemcitabine there was not any significant difference in response to gemcitabine between the two stiffnesses. As the same response was not observed for this p53 wt cell line as occurred in the MCF-7 and CAL-51 cell lines it suggests that wt p53 function alone does not contribute to gemcitabine resistance at higher stiffnesses. Investigation of this relationship at a higher concentration of gemcitabine in the ZR-75-1 cell line is warranted.

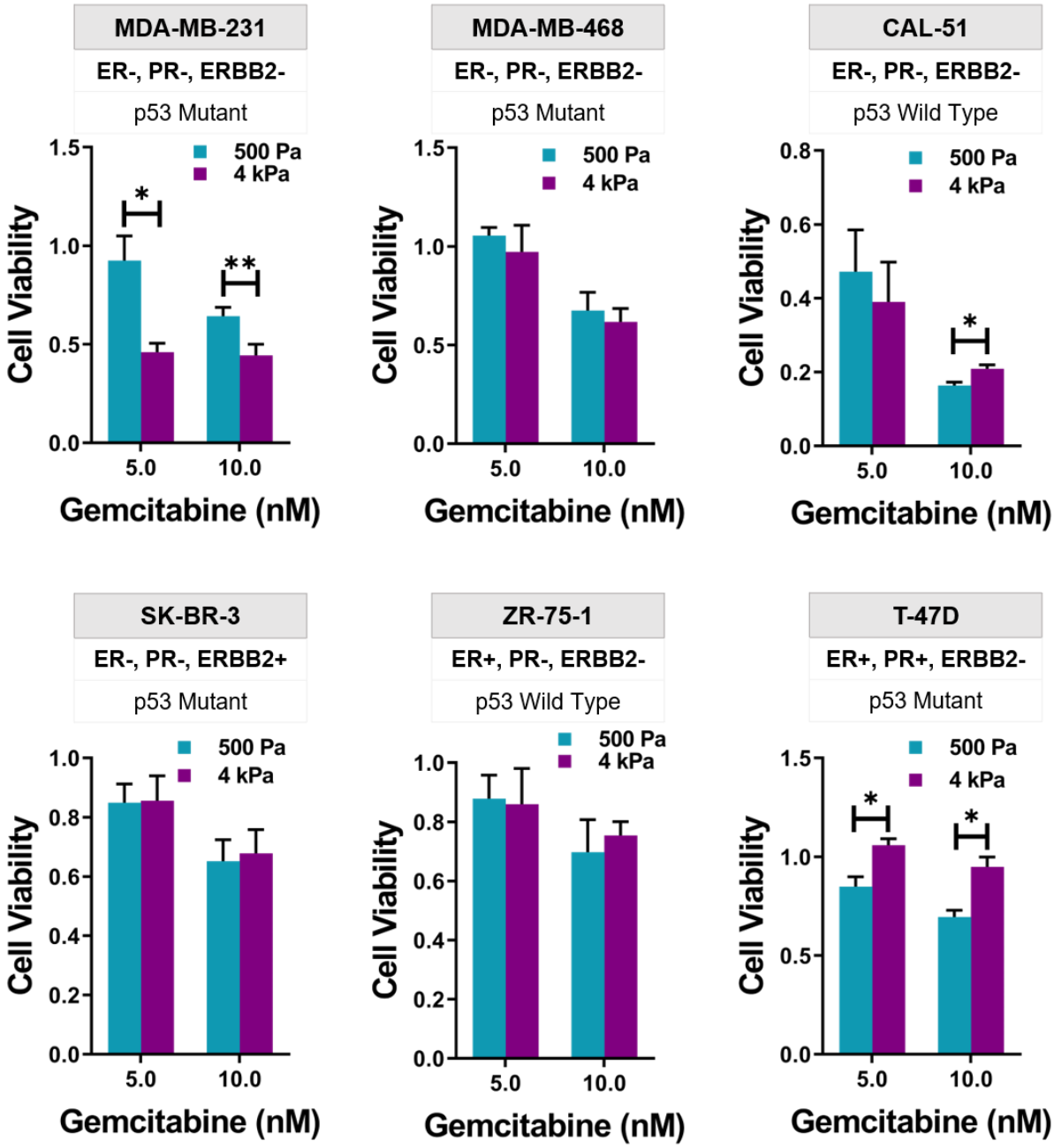

Figure 4.9. Response of 6 breast cancer cell lines to gemcitabine when cultured on polyacrylamide hydrogels of varying stiffnesses. The MDA-MB-231, MDA-MB-468, CAL-51, SK-BR-3, ZR-75-1 and T-47D cell lines were cultured on 500 Pa and 4 kPa stiffness hydrogels for 24 hrs prior to the addition of gemcitabine (gem) at two doses as indicated or a vehicle control. After 72 hrs treatment cell metabolism was measured by alamarBlue assay and the cell viability for each condition was calculated by dividing the reading of the gemcitabine treated sample with that of the vehicle control. Means and standard errors of the mean are plotted for three independent repeats (n=2 for T-47D at 500 Pa (5 and 10 nM gem) and CAL-51 at 4 kPa (10 nM gem)). * indicates an unpaired one-tailed Student's t-test p-value of ≤0.05. The oestrogen receptor (ER), progesterone receptor (PR), human epidermal growth factor receptor 2 (ERBB2) and p53 statuses are detailed for each cell line. Two of the MDA-MB-231 repeats were undertaken by Manpreet Barj.

The final cell line investigated was the T-47D cell line which is PR and ER positive but ERBB2 negative. It expresses a mutant version of p53 which has been attributed to an increased cell growth and survival. Like MCF-7 cells, T-47D cells were more sensitive to both doses of gemcitabine when cultured on softer 500 Pa matrices compared to those cultured at 4 kPa. This was significant at both 5 nM and 10 nM gemcitabine ($p = 0.0173$ and 0.0178 respectively by Student's t-test). As n=2 for cells at 500 Pa further repeats are required to confirm this trend. As the T-47D cell line is not p53 wt this suggests that p53 status is not the sole determinant of response to gemcitabine but instead highlights a correlation with PR expression as both the MCF-7 cell line and T-47D cell line share this factor in common.

It is interesting to note that the result of the MDA-MB-231 cell line is the complete opposite to the MCF-7 and T-47D cell lines. Clinically it may indicate that cells similar to MDA-MB-231 cells in stiffer tumours may respond selectively better than softer tumours to gemcitabine. The p53 mutation observed in this cell line is attributed to an increased migratory and invasive phenotype (Muller & Vousden, 2014). As this has not been observed in the other p53 mutant cell lines tested, it may suggest that migratory pathways influence gemcitabine resistance at lower stiffnesses in this cell line. This also suggests that the work below to reverse the gemcitabine resistance in the MCF-7 and T-47D cell lines could have the opposite and deleterious effect in the MDA-MB-231 cell line. Whilst our results indicate PR positivity is correlated to resistance to gemcitabine at higher stiffnesses, the interesting and individual result of the MDA-MB-231 cells therefore needs more investigation. This would allow determination of potential biomarkers to clinically determine if a tumour may be similarly sensitive to gemcitabine at higher stiffnesses. However, this will not be further investigated in this thesis.

4.2.6.2. Inhibition of the progesterone receptor re-sensitises MCF-7 cells to gemcitabine treatment at higher stiffnesses.

In Figure 4.9. we observed a trend where breast cancer cell lines which express the PR were more resistant to gemcitabine when cultured at a higher stiffness of 4 kPa. To first confirm that the cell lines used in our investigations did indeed express or not express the PR as reported in the literature we carried out RT-q-PCR for *PGR* using a Qiagen probe that detected both forms (as depicted in Figure 4.10.).

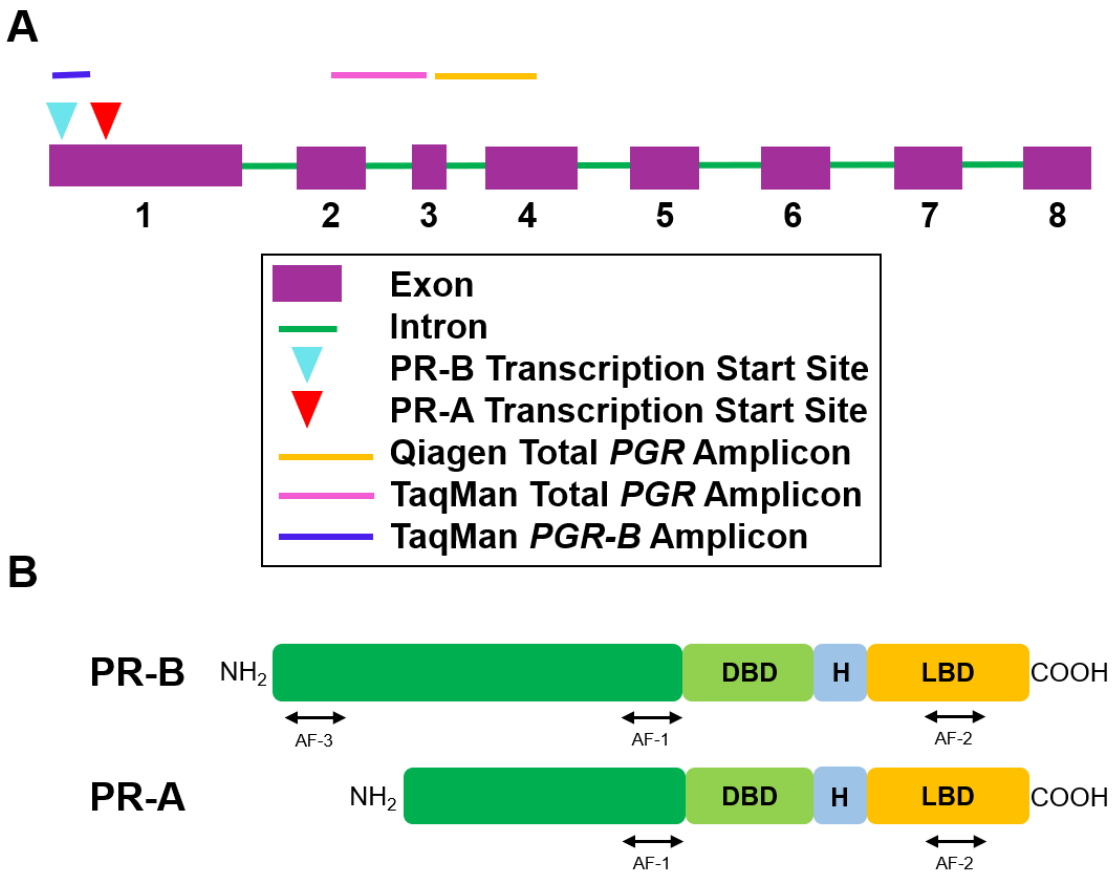

Figure 4.10. PGR gene and probe sites. (A) Schematic of the progesterone receptor gene (*PGR*) with the isoform start sites indicated. The estimated PCR probe regions are indicated. (B) Progesterone receptor A and B isoforms expressed by the *PGR* gene.

The average delta CT values relative to a β-actin control are plotted in Figure 4.11.a. The T-47D and MCF-7 cell lines both registered a delta CT value indicating that they do

express the PR. The T-47D cell line had a lower average delta CT than the MCF-7 cell line. This suggests that the T-47D cell line has a higher expression of the PR than the MCF-7 cell line consistent with previous reports (Hopp, 2004). The *PGR* delta CT value was undetermined in the ZR-75-1, Cal-51, MDA-MB-231 and MDA-MB-468 cell lines confirming that they do not express *PGR*.

Having confirmed the expression of the *PGR* in the MCF-7 and T-47D cell lines we next investigated if inhibition of PR function could reverse the resistance to gemcitabine at 4 kPa. To inhibit PR signalling we chose to use mifepristone, as it is already used clinically for treatment of unwanted pregnancy and is currently in clinical trials for use as a breast cancer therapy (ClinicalTrials.gov, 2020). Mifepristone is a PR antagonist which imparts it's inhibitory function through recruitment of co-repressors (Lanari, Wargon, Rojas, & Molinolo, 2012). Following 24 hrs culture of MCF-7 cells on 500 Pa and 4 kPa stiffness polyacrylamide hydrogels, cells were treated with mifepristone or a vehicle control for a further 24 hrs. Cells were then treated with gemcitabine or a vehicle control in combination with mifepristone or its vehicle control for a further 72 hrs. Cell viability was determined by alamarBlue assay, the results are plotted in Figure 4.11.b. In agreement with the results observed previously in Figure 4.5. cells cultured on 500 Pa stiffness hydrogels were significantly more sensitive to 5 nM gemcitabine alone than cells cultured at higher stiffness of 4 kPa ($p = 0.0116$ by Student's t-test). Interestingly however, pre-treatment with 10 µM or 15 µM of mifepristone abolished this sensitivity difference to gemcitabine, with there being no significant difference in cell viability between the two stiffnesses ($p = 0.4101$ and 0.3819 respectively by Student's t-test). This suggests that PR function contributes to resistance to gemcitabine treatment at a stiffness of 4 kPa. Combined treatment with PR inhibitors may help in reducing resistance to gemcitabine in stiffer breast tumours which are PR positive.

It is important to note that mifepristone is also an inhibitor of the glucocorticoid receptor and the androgen receptor (Fleseriu et al., 2012; Song, Coghlan, & Gelmann, 2004). Therefore, it would be important to investigate further the specificity of the interaction of PR inhibition with gemcitabine via knockdown of the PR using siRNA.

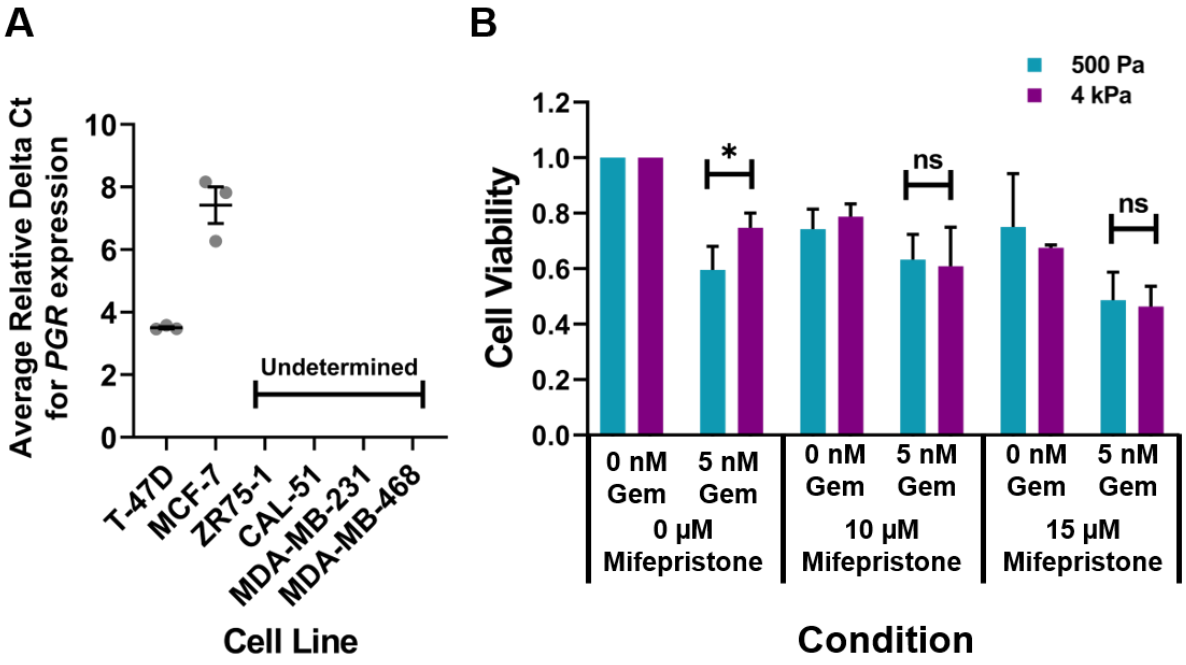

Figure 4.11. Pre-treatment with mifepristone abolishes resistance to gemcitabine at a stiffness of 4 kPa. (A) Progesterone receptor gene (*PGR*) expression in the breast cancer cell lines investigated relative to β-actin as determined by RT-q-PCR. The average relative delta CT values are plotted in grey for 3 independent cell pellets performed in triplicate. The mean and standard error of the mean are plotted in black. Results courtesy of Fatma Bucklain. (B) The MCF-7 cell line was cultured on 500 Pa and 4 kPa hydrogels for 24 hrs prior to the addition of varying doses of mifepristone or a vehicle control as indicated for 24 hrs. Gemcitabine or the vehicle control was then added in combination with mifepristone or its vehicle control for a further 72 hrs. Cell metabolism was then measured by alamarBlue assay and the cell viability for each condition was calculated by dividing the reading of the gemcitabine treated sample with the untreated vehicle control for each dose of mifepristone. Means and standard errors of the means are plotted for 3 independent repeats. * indicates an unpaired one-tailed Student's t-test p-value of ≤0.05.

4.2.6.3. Increased matrix stiffness alters progesterone receptor expression.

We observed that PR function plays a role in response to gemcitabine at a stiffness of 4 kPa. This suggests that stiffness is having a role in PR expression or function. PRs are expressed as two different isoforms in breast tissue, PR-A and PR-B. PR-B is the larger isoform and PR-A is smaller due to a downstream transcriptional start site in the first exon (Lanari et al., 2012). They can form homo and heterodimers and are typically expressed in equal concentrations within the normal breast. However, this expression balance is often skewed in cancer, with a higher concentration of PR-A than PR-B (Graham et al., 2005). This is typically due to a decrease in PR-B rather than an increase in PR-A (Graham et al., 1995). To determine if isoform expression differences were observed at the different stiffnesses we undertook Western blotting for PR-A and PR-B (Figure 4.12.a). Densitometric analysis of this blot is graphed in Figure 4.12b. In both samples cultured at a stiffness of 500 Pa and at 4 kPa there is a higher ratio of PR-A expression compared to PR-B. As MCF-7 cells are of cancerous origin this is expected. Interestingly the ratio was further skewed at a stiffness of 4 kPa compared to 500 Pa (2:1 vs 2:1.3 respectively), however further repeats would be needed to determine if this is a significant difference. Total PR expression was not altered, suggesting that there is a shift in expression from one isoform to another when cells are grown on stiffer matrices.

Western blotting however is not very sensitive for investigations into basal expression changes. Therefore, RT-q-PCR was undertaken to provide a more sensitive analysis. As the expressional start sites of both isoforms are within the same exon it is not possible to design a probe specific to *PR-A.* Therefore, total *PGR* levels and *PR-B* specific levels were determined as detailed in Figure 4.10. *PR-A* levels were calculated by subtracting the fold change in *PGR-B* expression from that of total *PGR*. We also investigated the *PGR* expression following treatment with gemcitabine and/or mifepristone. MCF-7 cells

were cultured on 500 Pa or 4 kPa stiffness hydrogels or a glass control for 24 hrs prior to the addition of mifepristone or a vehicle control for a further 24 hrs. Gemcitabine or a vehicle control was added for a further 24 hrs prior to RNA extraction. The results are plotted in Figure 4.12.c. These results are from just one biological repeat so statistical significance could not be determined. Further repeats would be needed to confirm the differences observed. Fold change in expression was calculated relative to the untreated glass cultured sample. In untreated cells there was a very similar level of expression of total *PGR* between glass and 500 Pa stiffness cultured cells. However, there was a reduction in expression (0.58-fold change relative to glass) in cells cultured at a stiffness of 4 kPa. This is different to the protein expression levels determined by Western blot, where we saw no difference in total PR expression. This could indicate that some PR protein is not translated or is degraded at 500 Pa. However, it is more likely attributed the lack of sensitivity of Western blotting as discussed above, especially as *PGR* gene expression was similar on glass and 500 Pa.

Treatment with gemcitabine or mifepristone or a combination of both, reduced expression of total *PGR* on glass and at 500 Pa but made little difference to total levels at 4 kPa. When *PGR-B* levels were examined the trend on glass and at 500 Pa mirrored what was seen at the level of total *PGR*, suggesting that the majority of the total decrease seen upon treatment with gemcitabine or mifepristone or both was due to reduction in *PGR-B* rather than any change in *PGR-A*. At 4 kPa *PGR-B* levels were also reduced by treatments. The lack of overall change in total *PGR* therefore suggests that the *PGR-A* level must have also increased. Thus, the ratios of A:B will have altered in each case. This data suggests that when grown on a 4 kPa matrix MCF-7 cells adapt and that changes in *PGR-A* can counteract the changes in *PGR-B* in 4 kPa samples allowing the levels of total *PGR* to be maintained.

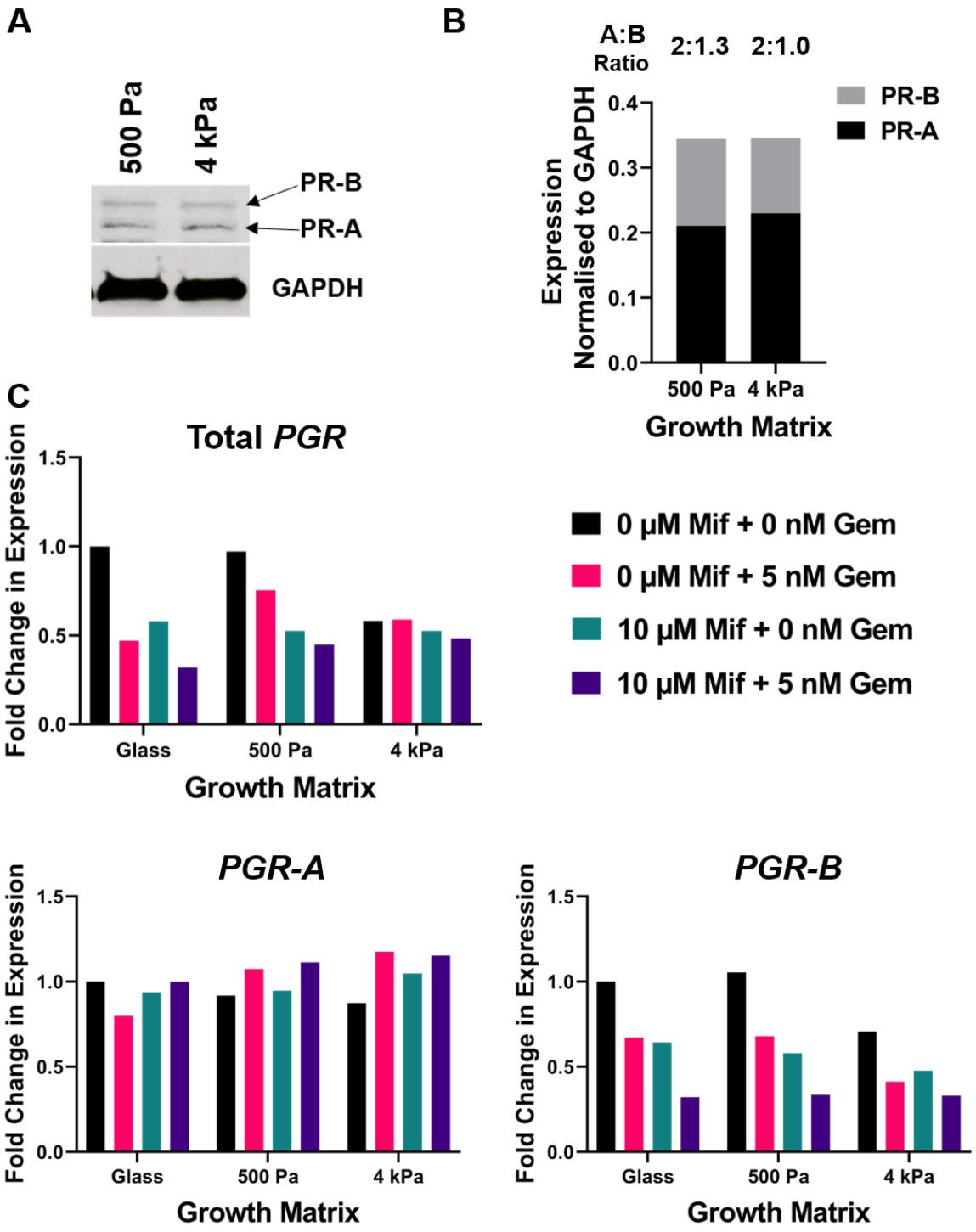

Figure 4.12. Increased stiffness alters progesterone receptor expression in the MCF-7 cell line. Legend overleaf.

Figure 4.12. Increased stiffness alters progesterone receptor expression in the MCF-7 cell line. (A) Western blot of whole cell extracts from MCF-7 cells cultured on 500 Pa and 4 kPa stiffness hydrogels for 72 hrs. Extracts were probed for PR isoforms A and B and a GAPDH control. (B) Relative expression of PR-A and B compared to GAPDH expression calculated from a Western blot image from one independent repeat. Band densitometries were measured in FIJI for PR isoforms A and B and normalised to the GAPDH control for each hydrogel stiffness to give the relative expression. (C) Expression of the total PR gene (*PGR)* and the separate A and B isoforms for MCF-7 cells by RT-q-PCR for one independent repeat. Cells were cultured on 500 Pa or 4 kPa stiffness hydrogels or a glass control for 24 hrs prior to the addition of 10 μM mifepristone or a vehicle control for a further 24 hrs. Five nanomolar gemcitabine or a vehicle control was added for a further 24 hrs prior to RNA extraction. Expression of total *PGR* and *PGR-B* were measured relative to a *GAPD* internal control. Fold change in expression was calculated relative to the untreated sample cultured on glass. *PGR-A* expression was determined by subtracting the fold expression change of *PGR-B* from that of total *PGR* expression.

4.3. Discussion.

In this chapter we present evidence that a stiffness physiologically relevant to cancerous breast tissue contributes to resistance to the chemotherapeutic gemcitabine. A relationship between PR expression and sensitivity to gemcitabine was uncovered, where inhibition of PR abolished gemcitabine resistance at a stiffness of 4 kPa.

4.3.1. Stiffness affects basal levels of replication stress but does not predict response to all antimetabolite drugs.

Here we show that culture of breast cancer cells at a stiffness physiologically relevant to breast cancer (4 kPa) results in a higher baseline of replication stress than at stiffnesses found in the normal breast (500 Pa). This was regardless of the fact that cancer cells were used which typically already have a high baseline of replicative stress (Ubhi & Brown, 2019). Had we used normal cells we may expect the differences in replicative stress to be more pronounced.

An increased replicative stress at a higher stiffness was true for both MCF-7 and MDA-MB-231 cell lines. This is consistent with our previous findings in chapter 3 of increased cell growth at 4 kPa, as replication stress often accompanies increased cellular replication in cancer cells (Maya-Mendoza et al., 2018). In the MDA-MB-231 but not the MCF-7 cell line there was also a higher amount of DNA damage at 4 kPa vs 500 Pa. DNA damage can occur during replication stress as a result of collapsed replication forks (Primo & Teixeira, 2020). Alternatively, DNA damage can arise through mechanical stresses on chromatin (Mayr et al., 2002). We may expect an increase in matrix stiffness to increase the torsional stress on DNA (Cho, Irianto, & Discher, 2017), particularly during replication. However, it has also been reported that rearrangement of chromatin occurs in response to mechanical stress to soften the nucleus and prevent DNA damage (Nava et al., 2020). The authors observed a rearrangement in H3K9me3 at the nuclear periphery which resulted in a protective softening of the nucleus. We observed a similar re-arrangement and reduction of H3K9me3 at 4 kPa in the MCF-7 cell line which could explain why an increase in DNA damage was not observed at the higher stiffness in MCF-7 cells. This could also indicate that the damage seen in MDA-MB-231 cells was not the result of DNA replication stress per se but the mechanical stress of replicating on a stiffer matrix.

It is well documented that the higher levels of replication observed in cancers makes them vulnerable to the cytotoxic effects of antimetabolite drugs (Kitao et al., 2018; Zhang, Dai, Park, & Deng, 2016). Cells can survive with low levels of replication stress however once levels reach a critical point apoptosis can be induced. One of the contributing factors to antimetabolite cytotoxicity is induction of replication stress. Therefore, in a background of increased basal replication stress low levels of antimetabolites may be selectively cytotoxic.

We investigated three antimetabolite drugs, 5-FU, HU and gemcitabine and did not observe an increased sensitivity at higher stiffnesses in the MCF-7 cell line despite higher levels of basal replication stress. The MDA-MB-231 cell line had a higher basal level of replication stress at 4 kPa than observed in the MCF-7 cell line. As the MDA-MB-231 cells were more sensitive to gemcitabine at 4 kPa than at 500 Pa it suggests that a replication stress threshold may need to be reached for sensitivity to occur. Most interestingly the response to gemcitabine in the MCF-7 cell line was opposite to the MDA-MB-231 cell line. In MCF-7 cells there was resistance to gemcitabine at 4 kPa, where more replication stress occurred. This indicates that other mechanisms are likely to be involved in the response to gemcitabine in MCF-7 cells.

Stiffness did not affect cellular sensitivity to the ATR inhibitor VE821 and the PARP inhibitor olaparib in the MCF-7 cell line, although there was a trend towards increased sensitivity at increased stiffness. This is surprising as both ATR and PARP act to promote survival during replication stress, and so inhibition during replication stress is predicted to kill cells. However, the increase in replication stress in cells grown at 4 kPa may not be large enough in the MCF-7 cell line to require ATR or PARP.

There was also no difference in sensitivity to IR, MMC or PAX. Of the three, only PAX has been previously studied in a stiffness specific context, likely due to the effects of PAX on the cytoskeleton. Zustiak et al., (2014) observed that a number of cancer cell lines, including MCF-7 cells, were more resistant to PAX at a stiffness of 100 kPa compared to 1 kPa. This disagrees with our findings, however due to the high stiffnesses used by the authors it is not comparable to our data and therefore does not invalidate it. Rice et al., (2017) reported that BxPC-3 pancreatic cancer cells were resistant to PAX at a higher

stiffness of 25 kPa compared to 1 kPa, however they saw no differences in sensitivity with the use of gemcitabine. This suggests that cancers from different tissues may respond differently to different chemotherapeutic agents. As such it is necessary that chemotherapeutic agents are tested for tissue and stiffness specificity.

It was interesting that only gemcitabine and not the other antimetabolites HU or 5-FU showed a differential effect. This suggests that the observed resistance to gemcitabine at 4 kPa in the MCF-7 cell line is likely to be due to one of the less well characterised functions of gemcitabine. HU inhibits RNR and TS, while 5-FU is incorporated into DNA and RNA and inhibits TS. Gemcitabine inhibits DNA synthesis through inhibition of RNR, TS and CTPS and through incorporation into DNA and RNA. It is possible, but unlikely, that this combined action elicits a unique response. Gemcitabine can also influence gene expression through mediation of epigenetic DNA methylation (Schäfer, Schomacher, Barreto, Döderlein, & Niehrs, 2010). DNA methylation changes have been reported after 5-FU (Fouad et al., 2018) and HU (Chondrou et al., 2018) treatment suggesting that this is not an uncommon function of antimetabolites. However, it may be specific to particular genes for the different agents. Specific expression changes influenced by gemcitabine may therefore contribute to the observed sensitivity differences between the two stiffnesses. Similar to our data the pancreatic cancer cell lines BxPC-3 and MiaPaCa-2 were also resistant to gemcitabine when grown on a stiffer matrix (1 kPa compared to 500 Pa) (Puls et al., 2017). The authors attributed the differences in sensitivity to an induction of EMT within the cells on stiffer matrices, however we observed in chapter 3 that this was not evident in our model in MCF-7 cells. In contrast, another study in the same BxPC-3 cell line, saw no difference in gemcitabine sensitivity in cells grown on stiffness of 1, 4 and 25 kPa (Rice et al., 2017). Both reports used different stiffness models, where Puls et al., (2017) used a 3D model and Rice et al., (2017) used a 2D polyacrylamide

model perhaps accounting for the contradictory results. This indicates that different models can reveal different sensitivities. Gemcitabine sensitivity has not been investigated previously in the context of stiffness in breast cancer cell lines and our data highlights this as an area which warrants further investigation.

4.3.2. Stiffness alters p53 sub-cellular localisation following gemcitabine treatment but p53 status does not correlate with stiffness specific resistance.

The p53 protein is thought to have an array of complex functions alongside its well-known function in prevention of progression of DNA damage and in cell death. It has been reported that p53 expression increases in the presence of gemcitabine, indicating it is involved in response to gemcitabine (Tolis, Peters, Ferreira, Pinedo, & Giaccone, 1999). Ebata et al., (2017) showed that resistance to doxorubicin at a stiffness of 2 kPa corresponded to a reduced nuclear accumulation of p53. This effect was also observed in our model of gemcitabine resistance in MCF-7 cells grown on a 4 kPa matrix. Ebata et al., (2017) observed abrogation of the stiffness specific response through p53 knock down suggesting that sensitivity to doxorubicin requires p53 expression. However, in our investigations with a panel of breast cancer cell lines expressing either wt or mutant p53 we did not observe a clear correlation between stiffness specific responses to gemcitabine and p53 status. This suggests that gemcitabine resistance at higher stiffnesses is not dependant on p53. Investigations using knockdown of p53 in the MCF-7 cell line and rescue of p53 in the T-47D cell line would be interesting to further explore this in the context of stiffness. Whilst we did observe a significant difference in p53 nuclear localisation we did not observe any difference in p53 expression between the stiffnesses. However, further repeats of expressional differences are required to confirm this.

4.3.3. Progesterone receptor activity contributes towards resistance to gemcitabine at higher stiffnesses.

To investigate if the sensitivity relationship with gemcitabine is observed in other cells, we tested the sensitivity of a panel of breast cancer cell lines of different receptor statuses to gemcitabine at 500 Pa vs 4 kPa. Of the seven cell lines investigated, stiffness associated resistance was observed only in the two PR positive cell lines, MCF-7 and T-47D. To my knowledge this is the first time a link between gemcitabine resistance and PRs has been observed.

The PR inhibitor mifepristone is used for treatment of unwanted pregnancy and clinical trials are currently underway for its use in PR positive breast cancer (ClinicalTrials.gov, 2020). A 10 μM dose of mifepristone was chosen as it has been shown to effectively inhibit PR function in the MCF-7 cell line (Benad, Rauner, Rachner, & Hofbauer, 2011). Secondly, lower doses of mifepristone (≤10 pM) can act as an agonist (Bottino et al., 2011) whilst higher doses of mifepristone (≥20 μM) can also kill cells irrespective of PGR expression (Tieszen, Goyeneche, Brandhagen, Ortbahn, & Telleria, 2011). However, inhibition would need to be confirmed under the conditions used in our experiments.

PR signalling shows crosstalk with gemcitabine activated pathways, including MAPK (Habiro et al., 2004; Kariagina et al., 2008) and Wnt (Faivre & Lange, 2007; Jia & Xie, 2015). Further investigation into such pathways in a stiffness specific context is warranted and may allow for determination of further links between gemcitabine and PR function. We observed a lower expression of total *PGR* in cells cultured at a higher stiffness of 4 kPa. Superficially this may suggest that increased PR signalling is not responsible for gemcitabine resistance, but PR signalling is complex so it is hard to draw this conclusion

without further investigation (see below for discussion of isoforms). However, lower expression of total *PGR* would likely increase the effectiveness of mifepristone in these cells which could contribute to the observed reduction in gemcitabine resistance following mifepristone pre-treatment.

It has been shown that the different PR isoforms may act differently such as in their response to mifepristone or their influence on gene expression (Richer et al., 2002). Little can be concluded about heterodimer pathways as studies typically involve models with just one of the isoforms expressed. As such only homodimers can form. A higher PR-A:B ratio is observed in cancer, due to a reduction in PR-B (Graham et al., 1995), similar to what we observed in our model at a higher stiffness of 4 kPa. A higher PR-A:B ratio would likely increase A:A homodimers and mifepristone has been shown to be more effective in treatment against the A isoform (Lanari et al., 2012). This may explain why only we saw a response in cells cultured at 4 kPa, where gemcitabine increased expression of PGR-A. However, a link between gemcitabine and PR has yet to be investigated.

It has been reported that both the PR-A and PR-B isoforms, which lead to down-stream activation of many PREs, can alter the expression of a different array of genes (Richer et al., 2002). Of note is the specific PR-A-induced overexpression of Bcl-xL, an anti-apoptotic protein which prevents release of cytochrome C from mitochondria (Kharbanda et al., 1997) and has also been reported to hold p53 inactive in the cytoplasm preventing activation of pro-apoptotic proteins (Amaral, Xavier, Steer, & Rodrigues, 2010). Bcl-xL expression has been shown to be reduced in MCF-7 cells treated with gemcitabine suggesting its involvement in response to gemcitabine in this cell line (Zheng et al.,

2014). Additionally it has been shown that Bcl-xL overexpression contributes to resistance to gemcitabine in colorectal cancer cell lines (Schniewind et al., 2004). Bcl-xL knockdown has also been shown to induce apoptosis independent of p53 (Strasberg Rieber, Zangemeister-Wittke, & Rieber, 2001) and as such may also contribute to gemcitabine resistance in p53 mutant cell lines, such as T-47D cells. However, further investigations are required to establish the exact mechanisms of resistance to gemcitabine in breast cancer in relation to PR expression and stiffness.

The work in this chapter highlights the importance of PR expression and inhibition as a treatment option which may offer an improved response to gemcitabine in stiffer tumours.

4.3.4. Summary.

In summary we have identified a specific relationship between response to gemcitabine in breast cancer cell lines expressing PR and the stiffness of the matrix that cells are grown on. The matrix stiffnesses used were physiologically relevant to that of breast cancer and to that of normal breast tissue, with resistance being seen in the cancer model. This relationship was specific to gemcitabine and not any of the other chemotherapeutic agents tested. This is thought to be due to a specific function of gemcitabine which warrants further investigation. Inhibition of PR function prior to treatment with gemcitabine abolished the resistance to gemcitabine in MCF-7 cells cultured at a higher stiffness of 4 kPa.

However, there are some limitations to these findings. Firstly, gemcitabine was used for timepoint optimisation for the alamarBlue viability assay. It may be possible that at other time points other chemotherapeutic agents may have shown a different response.

Furthermore, due to time constraints it was not possible to undertake combined mifepristone and gemcitabine sensitivity assays in the T-47D cell line, or to determine the effect of mifepristone on the breast cancer cell lines that did not express *PGR*. Lastly it is necessary to determine if mifepristone was effective in inhibition of PR function and to repeat *PGR* expressional analysis for a total of 3 independent repeats.

5. Developing a 3D breast cancer stiffness model for determining gemcitabine sensitivity.

5.1. Introduction, aims and hypothesis.

In the previous chapters of this thesis, a 2D polyacrylamide hydrogel model was optimised at two different stiffness physiologically relevant to the normal and cancerous breast (500 Pa and 4 kPa respectively). The response of breast cancer cell lines to chemotherapeutic agents was compared in this model. Interestingly, drug resistance was observed with gemcitabine at a stiffness of 4 kPa compared to 500 Pa. 2D stiffness models are advantageous over typical TCP or glass coverslips where responses to chemotherapeutic agents have previously been shown to differ (Medina et al., 2019). However, it has been observed that chemotherapeutic responses in 2D culture systems are not recapitulated in 3D growth environments (Joyce et al., 2018). Most importantly, the 3D environment is more representative of the cell to cell connections and metabolic issues observed in real life tissues and tumours (Breslin & O'Driscoll, 2013). Therefore, in this chapter we aim to develop a 3D model that is comparable in stiffness to the 2D polyacrylamide model and to investigate if the same response to gemcitabine is observed.

We chose an alginate hydrogel model as it is biocompatible and has previously been used to achieve stiffnesses of 200 Pa and 2 kPa (Joyce et al., 2018), similar to those reported in the normal and cancerous breast respectively. This 3D model was adapted by us from a protocol supplied by Dr Nick Peake at Sheffield Hallam University. We also tried to develop a 3D polyacrylamide model in collaboration with Dr Frederik Claeyssens at the University of Sheffield.

In this chapter, the optimisation of a 3D model and chemotherapeutic sensitivity data of MCF-7 and MDA-MB-231 cells are reported, as these cell lines showed a differential response to gemcitabine in the 2D model investigated in chapter 4.

The hypothesis of this chapter is:

The MCF-7 and MDA-MB-231 cell lines will show the same stiffness specific chemotherapeutic response to gemcitabine in a 3D model as observed in our 2D model in chapter 4.

The aims of this chapter are:

1. To develop a 3D stiffness model.
2. To determine the response of breast cancer cells to gemcitabine in 3D.

The objectives of this chapter are:

1. To optimise a protocol for formation of alginate hydrogels.
2. To determine the gemcitabine response of MCF-7 and MDA-MB-231 cell lines in this model.
3. To investigate if resistance can be reversed using PR inhibitors.
4. To develop a 3D polyacrylamide hydrogel.

5.2. Results.

5.2.1. Development of the alginate hydrogel stiffness model.

Alginate hydrogels have shown promising differences in the context of stiffness in breast cancer (Joyce et al., 2018). Therefore, we chose to investigate these first as a 3D stiffness model. In a 3D alginate model, cells are encapsulated inside the gel during the gelation phase. Alginate is derived from brown algae and is comprised of mannuronate and guluronate monomers (K. Y. Lee & Mooney, 2012), which following the addition of calcium ions crosslink to produce a gel. We began by using a protocol for the formation of a large batch of alginate beads which was kindly provided by Dr Nick Peake (Sheffield Hallam University). This was then adapted for the needs of our project to increase reproducibility and maximise cell growth. The beginning stage for formation of all alginate 3D hydrogels required mixing of an alginate solution with the cell solution, by gentle pipetting as depicted in Figure 5.1.a. Varying percentages of alginate, diluted in sodium chloride and then in cell culture medium, are used to provide different stiffnesses. The initial protocol involved slow dripping of the alginate/cell solution through a needle into an upright T25 flask containing calcium chloride solution (Figure 5.1.b). The drips form alginate beads upon contact with the solution, which undergo further gelation for 10 minutes at 37 °C. As the calcium chloride solution is relatively toxic to cells, it needed to be washed away from the beads. Beads were therefore washed twice in sodium chloride and twice in medium before being transferred to a 96 well plate. There were several aspects of this method which were not compatible with the needs of our downstream assays, most importantly the variability in droplet size which contributed to a high amount of well to well variability in cell number (data not shown). Secondly the movement of beads from the flask to the wells introduced extra potential for contamination and bead destruction. Finally, the beads appeared to be reducing in size during washing.

To overcome these problems, we tried setting the alginate directly in the wells to be used for downstream assays using a known volume of alginate/cell solution in each well to control for cell number. As depicted in Figure 5.1.c, the alginate/cell solution was placed in the bottom of each well and the calcium chloride solution pipetted gently down the side of each well. This resulted in the formation of an alginate disk/cake, each containing roughly the same number of cells. After a 10-minute incubation at 37 °C to allow for gel setting, the disks were washed in the well twice with sodium chloride and twice with medium. Whilst this method did result in increased reproducibility of cell number between wells there were issues with cell viability and complete gel setting (data not shown). A third adjustment was then tried. Here alginate beads were once again used, as the increased surface area allowed for more complete gel setting and exchange of nutrients to the cells allowing for an increased viability. The final optimised method is detailed in Figure 5.1.d. A known volume of alginate/cell solution was pipetted dropwise into each well containing calcium chloride solution. The resulting beads were set for 10 minutes at 37 °C and then washed 4 times with cell culture medium. The beads were then washed only with media as the exchange of sodium ions for the calcium ions within alginate gels has previously been observed during exposure to sodium chloride solution (LeRoux, Guilak F Fau - Setton, & Setton, 1999). We hypothesised that this may have contributed to the previously observed break-down of the beads.

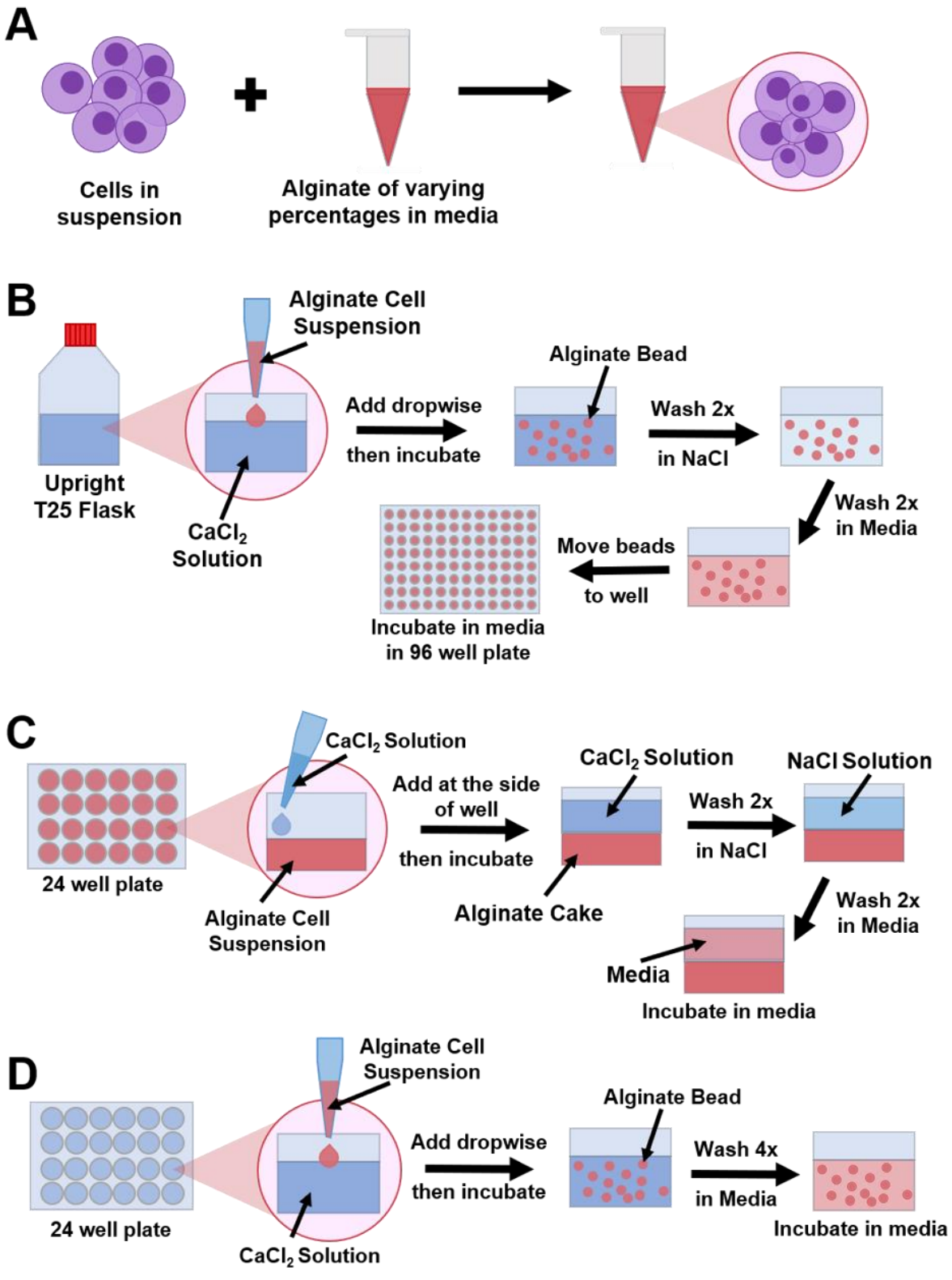

Figure 5.1. Methodological optimisation for formation of alginate hydrogels. Legend overleaf.

Figure 5.1. Methodological optimisation for formation of alginate hydrogels. (A) Simplified methodology used to create an alginate cell suspension. Different alginate percentages are used to give different stiffnesses. (B) Initial formation of alginate beads following a protocol from Dr Nick Peake (Sheffield Hallam University). Beads were initially formed in a T25 flask by dripping an alginate cell suspension into calcium chloride solution. After 10 minutes incubation at 37°C, beads were then washed in sodium chloride solution and then medium. Beads were then moved to a 96 well plate. (C) Formation of 'alginate cakes' in a 24 well plate. A known volume of alginate cell suspension is added to the bottom of the well and the calcium chloride solution is added down the side of the well. After 10 minutes incubation at 37°C, alginate was then washed in sodium chloride solution and then medium. (D) The final optimised method for alginate bead formation. Beads were formed by dropping a known volume of alginate cell suspension into each well of a 24 well plate containing calcium chloride solution. After 10 minutes incubation at 37°C alginate beads were washed in medium.

Once the method procedure had been optimised, we could then proceed to fine tune other components of the gels (Figure 5.2.a). During the optimisation stages rheological measurements were made to determine how each change was affecting the stiffness. We initially used 1 and 2% alginate set in 100 mM calcium chloride which resulted in a stiffness of 250 Pa and 1.7 kPa respectively. The lower stiffness was relevant to normal breast stiffness but the higher stiffness did not match the higher stiffnesses of the cancerous breast that we had achieved in polyacrylamide. We therefore investigated the use of 3% alginate. Although this did increase the alginate stiffness to a more cancer relevant 1.9-2.9 kPa (depending on calcium chloride concentration), it did not allow for cell growth in either cell line unlike the growth we observed in 1% alginate (Figure 5.2.b). We also tried using high viscosity alginate which surprisingly resulted in lower stiffnesses than the previously tested low viscosity alginate (data not shown).

Thus, we compromised and settled on using 1% and 2% alginate models formed of low viscosity alginate. During optimisation, MCF-7 cells grew similarly in 1% and 2% alginate when cakes of alginate were compared (Figure 5.2.c). It seems reasonable to assume

that MCF-7 cells will also grow at both these stiffnesses in alginate beads. However, it would be necessary to repeat cell growth data for the MCF-7 cell line in 1% and 2% alginate beads to confirm that cell growth is supported over time.

It has been reported that altering the calcium chloride concentration used in alginate gel setting can result in a differing gel stiffness (Tabriz, Hermida, Leslie, & Shu, 2015). We therefore investigated the effect of increasing the calcium concentration from 100 mM to 200 mM. Consistent with previous reports, gel stiffness was increased at higher calcium concentrations to 300 Pa and 1.9 kPa at 1% and 2% alginate respectively. Further we saw no drop in cell viability at these higher concentrations. Thus 200 nM was used in the final model for both gel percentages.

After the chemical components of the gels had been optimised, we then optimised the cellular component (Figure 5.2.d). Interestingly, we found that the MCF-7 cell line grew well in the model, but the TNBC MDA-MB-231 cell line showed a slower increase in growth, potentially limiting the use of this model. Therefore, we tested the growth of a different TNBC cell line and varied the concentration of cells added to the alginate. We determined that the MDA-MB-231 cell line showed the best growth of the cell lines investigated but this could be improved by increasing cell number up to 2 million per mL of alginate as is depicted in Figure 5.2.e. However, growth of MDA-MB-231 cells was still poor in comparison to MCF-7 cells. The reason for this is not clear.

A

	Alginate Method Component		
	Alginate	**Calcium Chloride**	**Sodium Chloride Washes**
Issue	Gels were not as stiff as polyacrylamide gels for comparison.	Gels were not as stiff as polyacrylamide gels for comparison.	Gels were becoming softer over time and visibly disappearing in the well.
Changes Made	1. Increase alginate percentages up to 3%. 2. Try a higher viscosity of alginate.	Compare use of 100 mM and 200 mM calcium chloride solution for gel setting.	As sodium ions may displace calcium ions bonding the gel together try washing in medium which contains a lower concentration of sodium and also contains calcium.
Result	1. Cell growth was slowed at 3% alginate but not at 2%. 2. Higher viscosity alginate produced lower stiffness alginate beads.	The use of 200 mM calcium chloride produced a higher stiffness gel without altering cell viability.	Gels did depreciate in stiffness over time but were still within a comparable range within the time scale. Cell viability was not affected.

B

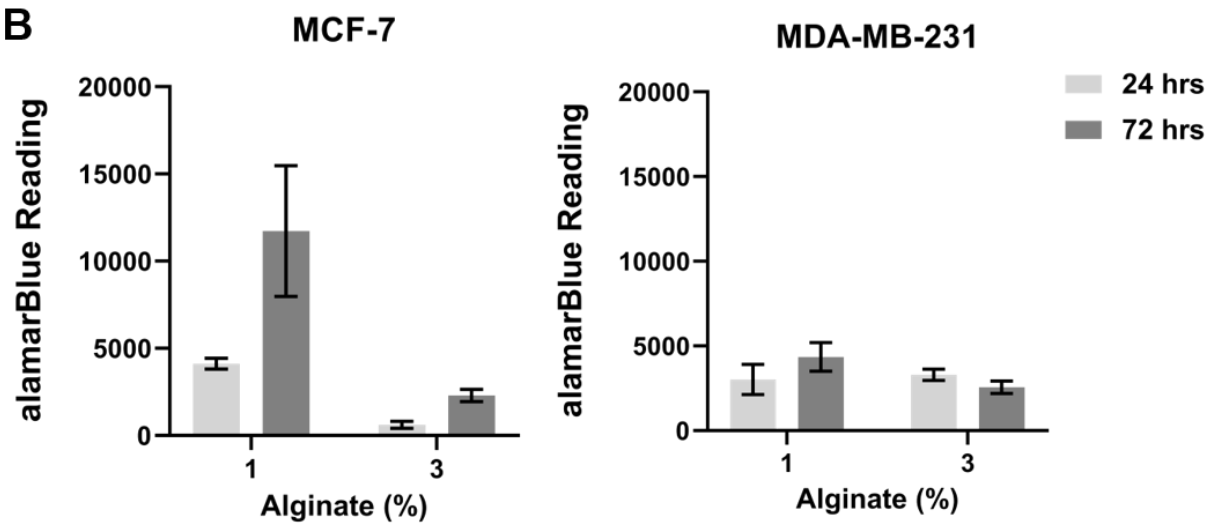

Figure 5.2. Further optimisation for formation of alginate hydrogels. Legend overleaf.

C

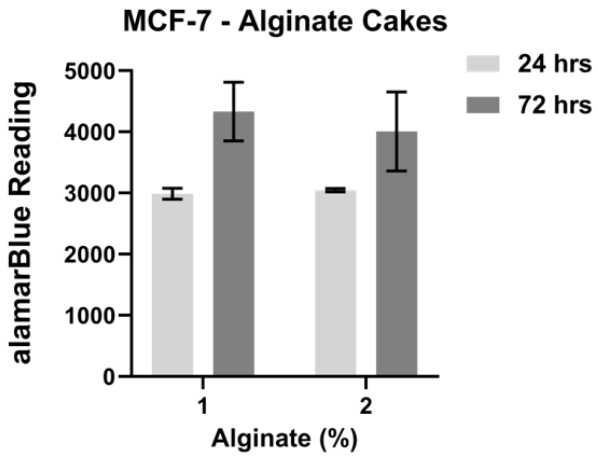

D

	Alginate Method Component	
	Cell Lines Used	**Cell Number**
Issue	The MCF-7 cell line grows well in alginate over time but MDA-MB-231 are a lot slower.	The MCF-7 cell line grows well in alginate over time but MDA-MB-231 are a lot slower.
Changes Made	Investigate using another triple negative breast cancer cell line (CAL-51) in the alginate model to assess suitability.	Try different cell concentrations of the MDA-MB-231 cell line in alginate.
Result	The MDA-MB-231 cell line were more proliferative than the CAL-51 cell line in alginate.	Increasing cell concentration from 500,000 cells/mL of alginate to 2,000,000 cells/mL of alginate improved proliferation over time.

E

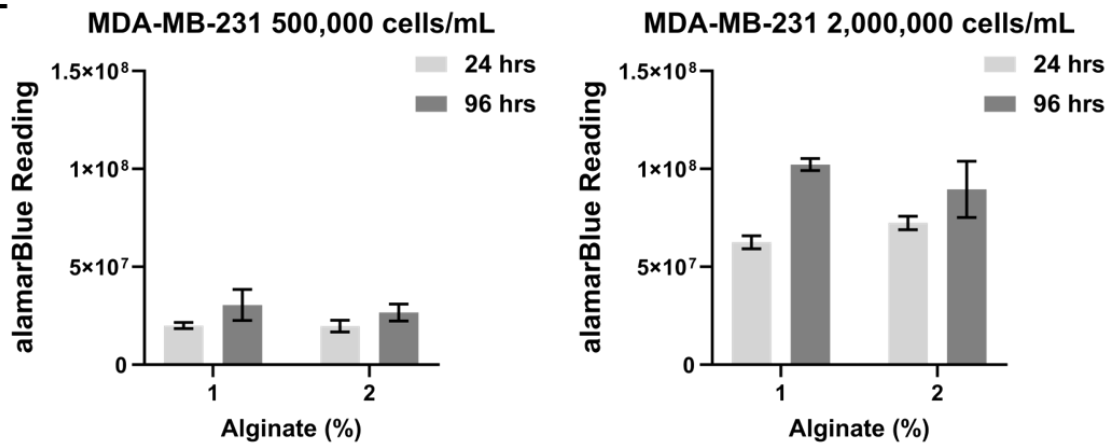

Figure 5.2. Further optimisation for formation of alginate hydrogels. Legend overleaf.

Figure 5.2. Further optimisation for formation of alginate hydrogels. (A) Table detailing the further issues of the alginate model and the optimisation steps undertaken by the adjusting chemical components. The results of the changes are detailed. (B) Optimisation of growth in different alginate percentages. MCF-7 and MDA-MB-231 cell lines were cultured in 1 and 3% alginate beads set with 200 mM calcium chloride (except for MDA-MB-231 cells using 1% alginate where 100 mM was used) at 500,000 cells/mL. The cell metabolism was measured by alamarBlue assay after 24 and 72 hrs. Means and standard deviations are plotted for 3 experimental repeats on one occasion. (C) Cell growth in alginate cakes at 1 and 2% alginate concentrations, set with 100 mM calcium. MCF-7 cells were cultured at 125,000 cells/mL and the cell metabolism measured by alamarBlue assay after 24 and 72 hrs. Means and standard deviations are plotted for 3 experimental repeats on one occasion. (D) Table detailing the further issues of the alginate model and the optimisation steps undertaken by adjusting the cell lines and numbers used in alginate bead formation. The results of the changes are detailed. (E) Optimisation of MDA-MB-231 cell number in the different alginate percentages. Cells were cultured in 1 and 2% alginate beads set with 200 mM calcium chloride at 500,000 cells/mL and 2,000,000 cells/mL. Cell metabolism was measured by alamarBlue assay after 24 and 96 hrs. Means and standard deviations are plotted for 3 experimental repeats on one occasion. For all graphs, MDA-MB-231 data was provided by Lucy Ginn.

5.2.2. Rheology of alginate hydrogels.

Having optimised the methodology for the formation of alginate hydrogels we next examined the stability of stiffness and the effect inclusion of cells had on this. One and 2% alginate hydrogels were made in 200 mM calcium chloride without cells and allowed to set for 10 minutes prior to 4 washes in medium. To observe changes over time, gels were then incubated in medium at 37 °C for 1 hr or 144 hrs and their stiffness was measured by rheology with the help of Dr Peter Laity (University of Sheffield). Representative rheological plots for each composition are shown in Figure 5.3.a. The small phase angle observed for all gels indicates that full gelation had occurred (Larsen et al., 2015). To allow for comparison to the polyacrylamide hydrogel model the average elastic moduli are plotted at a frequency of 1 Hz for the two gel compositions at both time points (Figure 5.3.b).

As seen during the optimisation, one hour after gelation, stiffness was increased at higher alginate percentages where the 1% alginate hydrogel had an average stiffness of 319 ± 58 Pa and the 2% alginate hydrogel had an average stiffness of 1919 ± 303 Pa. This difference is significant ($p < 0.0001$ by one-way ANOVA). These values are in agreement with those reported in the literature for these percentages of alginate and calcium concentrations (Cavo et al., 2016). The 1% alginate stiffness of 300 Pa is a little higher than the normal breast stiffness of 170 Pa and the 2% stiffness of 1.9 kPa is lower than the cancerous breast stiffness of 4 kPa. However, as there was a significant difference in stiffness between the 1% and 2% alginate beads and as 3% alginate was not compatible with cell viability, these were considered the best compromise between stiffness and cell viability.

We next investigated how stable bead stiffness was with time. After 144 hrs, gel stiffness was reduced for both gel compositions with an average stiffness of 275 ± 59 Pa for 1% alginate hydrogels and an average stiffness of 1175 ± 262 Pa for 2% alginate hydrogels. The reduction in stiffness was only significant for the 2% hydrogels ($p < 0.0001$ by one-way ANOVA). However, there was still a significant difference between the stiffness of the 1 and 2% hydrogels at 144 hrs ($p < 0.0001$ by one-way ANOVA), confirming their suitability for comparison of the effects of 3D stiffness on gemcitabine sensitivity in breast cancer cell lines.

Finally, we investigated how the addition of cells to the alginate hydrogels altered their stiffness (Figure 5.3.c). When comparing the beads containing cells to those without cells at the same alginate percentage and time point, cells made no significant difference to stiffness.

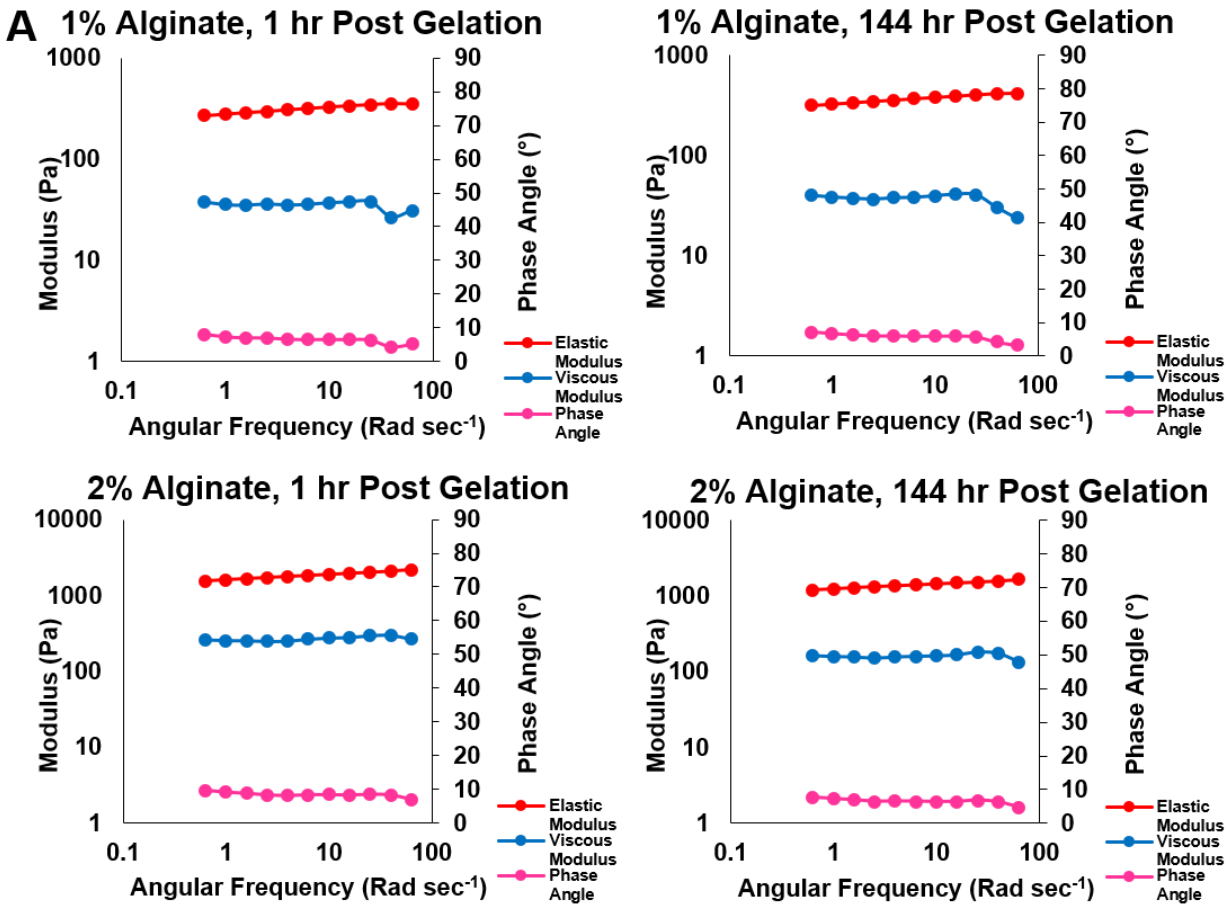

B

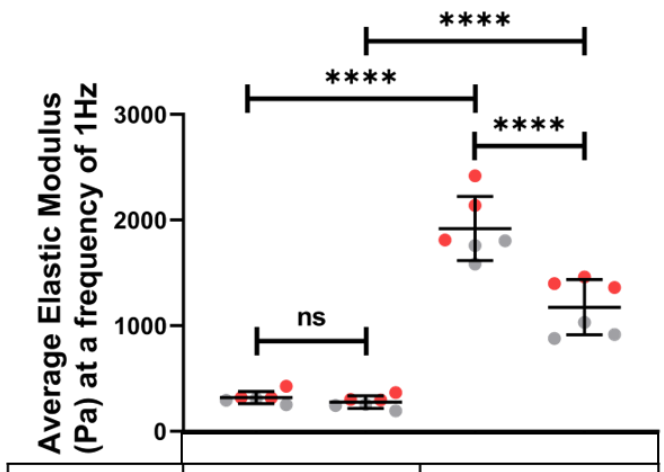

Alginate (%)	1		2	
Time post gelation (hr)	1	144	1	144
Average measured Elastic Modulus (Pa) ± SD	319 ± 58	275 ± 59	1919 ± 303	1175 ± 262

Figure 5.3. Rheological measurements of optimised alginate beads. Legend overleaf.

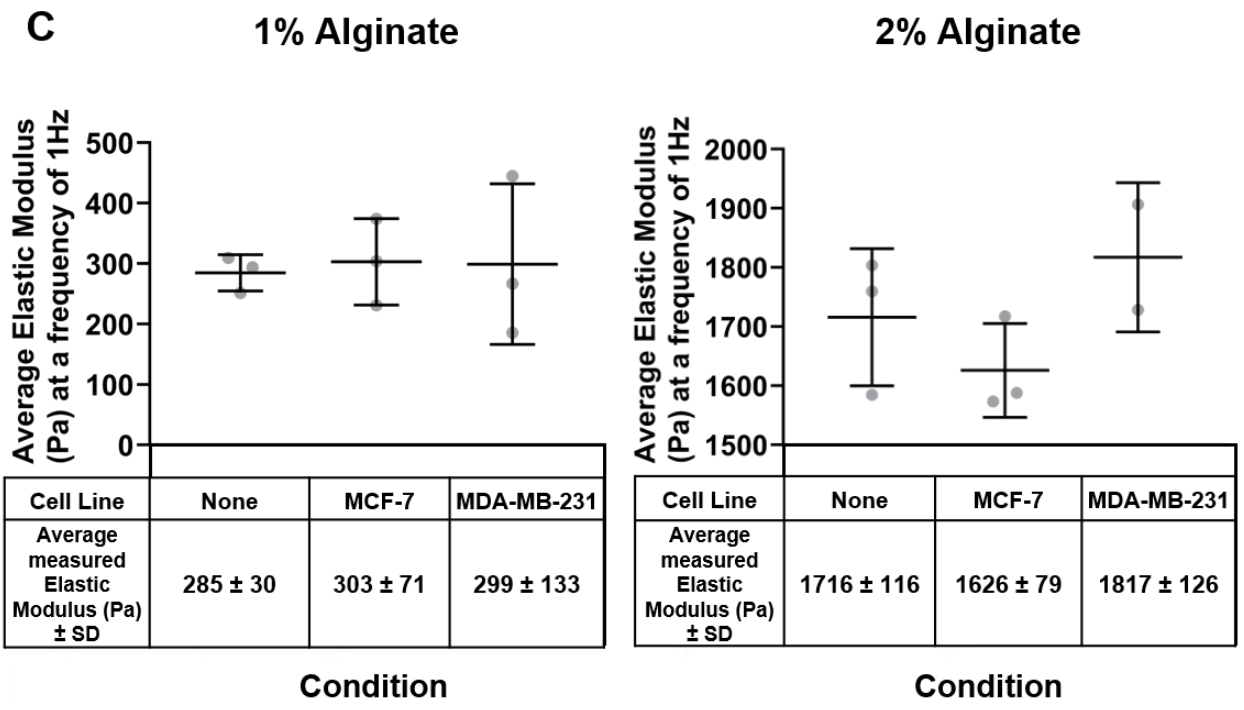

Figure 5.3. Rheological measurements of final optimised alginate beads. (A) A representative example of rheological graphs for each alginate percentage at 1 and 144 hrs post gelation showing elastic modulus, viscous modulus and phase angle. Rheological measurements were made on a Bohlin Gemini 200 rheometer fitted with a 10 mm diameter flat plate at 37 °C. A force of 0.2 - 5 N was applied to each hydrogel at an oscillating frequency of 10 to 0.01 Hz at a strain of 0.02%. All gels were made using 200 mM calcium and 4 media washes. (B) Average measured elastic modulus ± standard deviation for 6 gels pooled from 2 independent repeats for the two gel compositions, 1 and 144 hrs after gelation at a frequency of 1 Hz. Each repeat is plotted in a different colour and the mean and standard deviation is plotted in black. **** indicates an ANOVA p-value of < 0.0001. (C) Measured elastic moduli of 1% and 2% alginate gels without cells and cultured with MCF-7 or MDA-MB-231 cells for 1 hr. Averages and standard deviations of 3 gels measured on one occasion for each condition. The stiffness of each gel is plotted in grey and the mean and standard deviation in black. Statistical significance was determined by an unpaired one-tailed Student's t-test.

We therefore considered the model with cells suitable for comparison of stiffnesses as discussed above.

5.2.3. Characterisation of the morphology of breast cancer cell lines in alginate gels of physiologically relevant stiffnesses.

As we observed changes in cellular morphology with stiffness in MCF-7 and MDA-MB-231 cells in our 2D polyacrylamide hydrogels we next investigated if the same changes were observed in our 3D alginate model. Initial bright field imaging showed that cells appeared to be clustered at both stiffnesses, although clusters did generally appear larger in 2% alginate (Figure 5.4.). However, single cells could not be distinguished via brightfield imaging to allow determination of individual cell size.

Therefore, we investigated cytoplasmic and nuclear area through immunofluorescence (Figure 5.5.). Cells were cultured for 24 hrs in alginate hydrogels prior to fixing and staining for actin using phalloidin and nuclear content using DAPI. Representative images are shown in Figure 5.5.a. The nuclear area of 30 cells pooled from 2 independent repeats was measured from the DAPI staining in FIJI.

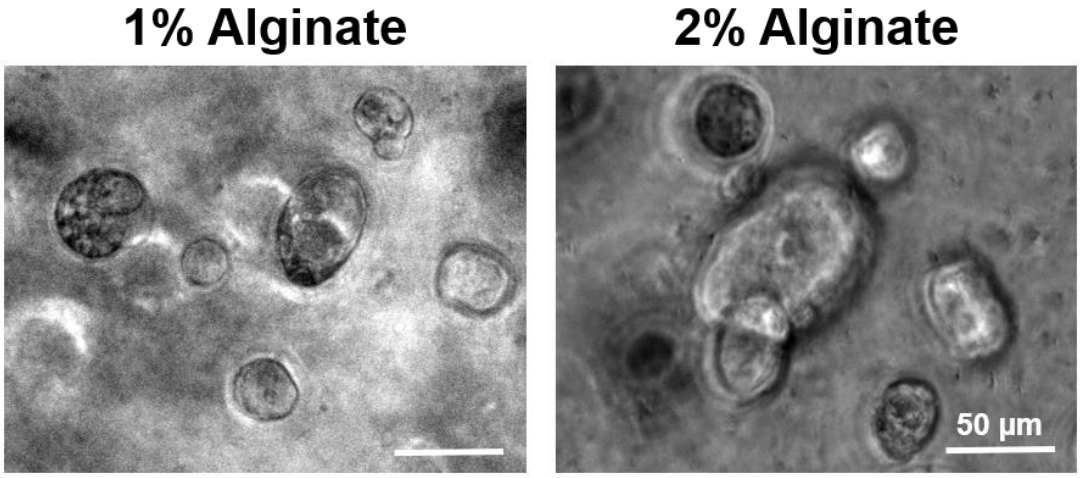

Figure 5.4. Representative brightfield images of the MCF-7 cell line cultured in alginate beads. The MCF-7 cell line was cultured in two alginate bead percentages as indicated. Representative brightfield images are shown from images taken on a Nikon TE200 inverted fluorescent microscope at a magnification of 20X, 96 hrs post alginate bead gelation.

The results are plotted in Figure 5.5.b. In the MCF-7 cell line we observed a significantly reduced nuclear area with increasing stiffness ($p = 0.0001$ by Mann-Whitney test). This result is opposite to the results observed in our polyacrylamide model and highlights a key difference between the 2D and 3D culture models. There was no difference in nuclear area with stiffness in MDA-MB-231 cells. Cytoplasmic area was measured from the actin stain in the same cells using FIJI. The results are plotted in Figure 5.5.c. Again, we observed a significant reduction in cytoplasmic area with increasing stiffness in the MCF-7 cell line ($p < 0.0001$ by Mann-Whitney test). There was no difference in cytoplasmic area with stiffness in the MDA-MB-231 cell line. Interestingly, we observed that cells were rounder in our 3D model compared to our 2D model regardless of stiffness.

Remarkably, attempts to use antibody stains in our alginate model produced a non-specific pan stain (data not shown). As a result, we were unable to compare the localisation of the stiffness specific proteins or investigate proliferative markers in this model as undertaken in chapter 3. Similarly, basal levels of replication stress and DNA damage could not be investigated. Therefore, we next chose to investigate if the relationship with gemcitabine was observed in this model.

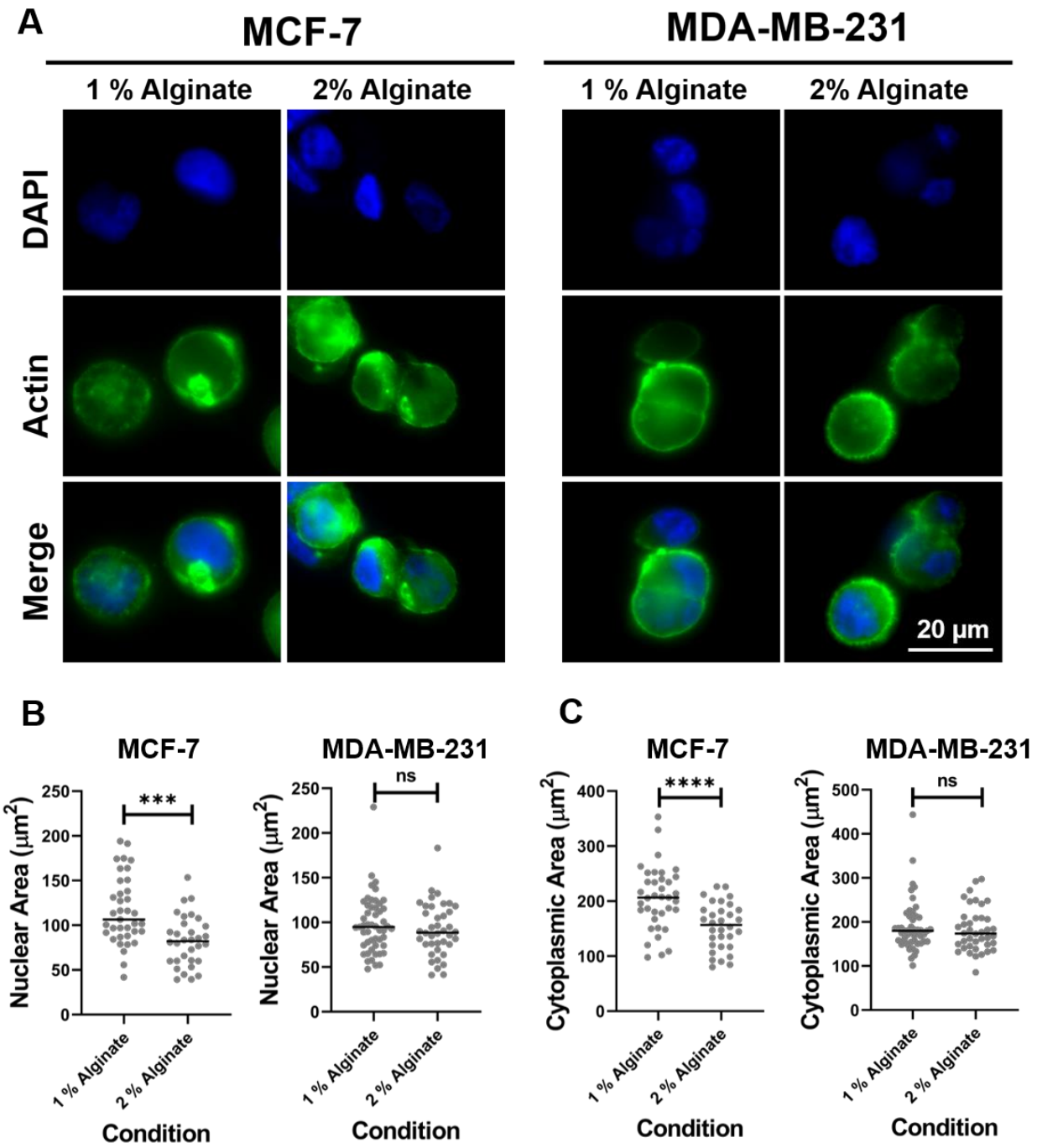

Figure 5.5. Nuclear and cytoplasmic area are reduced with higher alginate gel stiffness in the MCF-7 cell line but not in the MDA-MB-231 cell line.

(A) MCF-7 and MDA-MB-231 cell lines were cultured in 1% and 2% alginate beads for 24 hrs. Cells were then fixed and stained using immunofluorescence for actin and nuclear content. Representative images are shown from images taken on a Nikon TE200 inverted fluorescent microscope at a magnification of 60X. (B) Nuclear areas were measured in FIJI for at least 30 cells per condition pooled from 2 independent repeats. The data is plotted in grey and the median in black. *** indicates a one-tailed Mann-Whitney test p-value of <0.001. (C) Cytoplasmic areas were measured in FIJI for at least 30 cells per condition pooled from 2 independent repeats. The data is plotted in grey and the median in black. **** indicates a one-tailed Mann-Whitney test p-value of <0.0001. Images and measurements courtesy of Lucy Ginn.

5.2.4. Chemotherapeutic response in the alginate hydrogel model.

5.2.4.1. The stiffness relationship with gemcitabine is maintained in MCF-7 cells but not MDA-MB-231 cells in a 3D alginate model.

To compare the sensitivity of MCF-7 and MDA-MB-231 cells in our alginate stiffness model to gemcitabine, cells were cultured for 24 hrs in alginate beads prior to the addition of gemcitabine or a vehicle control for 72 hrs. The cell viability was measured by alamarBlue assay for 3 individual repeats and the averages are plotted in Figure 5.6. We observed that the MCF-7 cell line was resistant to gemcitabine at a higher alginate percentage of 2%. This was significant at a dose of 10 nM gemcitabine ($p = 0.0073$ by Student's t-test). It was not significant at 5 nM gemcitabine although the same trend was observed ($p = 0.0621$ by Student's t-test).

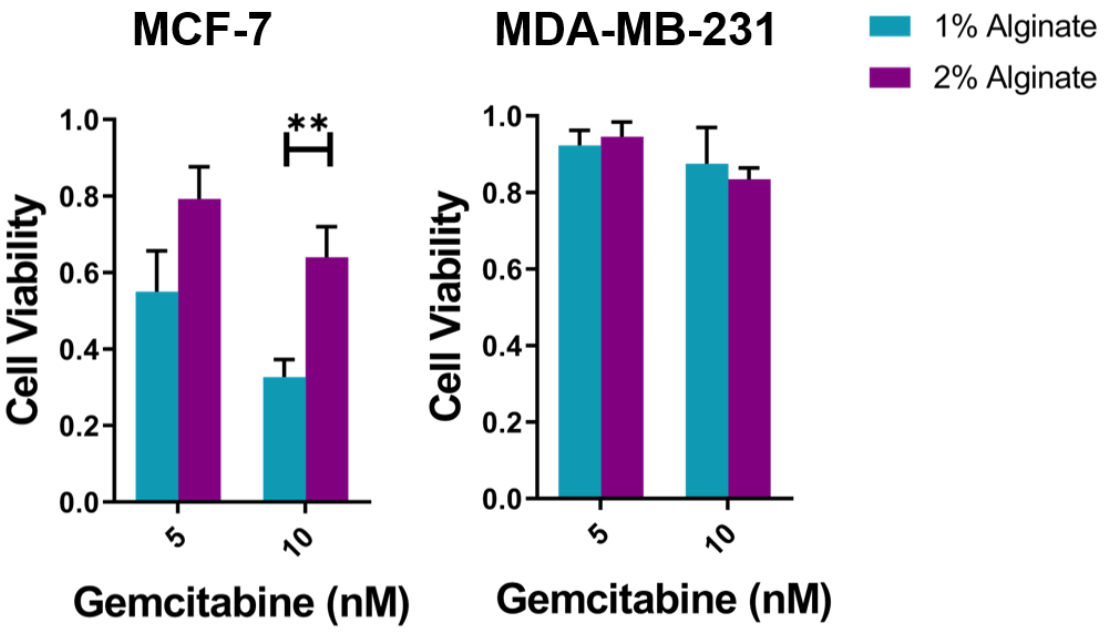

Figure 5.6. The MCF-7 cell line is resistant to gemcitabine at a higher stiffness in a 3D alginate model. MCF-7 and MDA-MB-231 cell lines were cultured in alginate beads of varying percentages as indicated for 24 hrs prior to the addition of gemcitabine or a vehicle control as indicated. After 72 hrs treatment cell metabolism was measured by alamarBlue assay. The cell viability for each condition was calculated by dividing the reading of the gemcitabine treated sample with that of the untreated vehicle control. Means and standard errors of the mean are plotted for 3 (MDA-MB-231) and 4 (MCF-7) independent repeats. ** indicates an unpaired one-tailed Student's t-test p-value of ≤0.01. MDA-MB-231 repeats and two of the MCF-7 repeats were produced with thanks to Lucy Ginn.

These results are in the same trend as observed in the polyacrylamide model, further validating our findings of this stiffness relationship with gemcitabine. A higher dose of gemcitabine may be required in the 3D model than 2D due to issues with diffusion of gemcitabine through the alginate matrix.

In the MDA-MB-231 cell line however we observed no difference in gemcitabine sensitivity between the two alginate percentages at either dosage. These results are not in agreement with the sensitivity differences observed in the 2D polyacrylamide model. Cells will need to be undergoing active DNA replication during cell growth to incorporate gemcitabine and therefore result in cell killing. As such, the small changes in cell viability following gemcitabine treatment in MDA-MB-231 cells may indicate that lack of cell growth in this cell line in alginate resulted in low levels of cell death.

As we observed the same sensitivity trend in the 3D alginate model with gemcitabine in MCF-7 cells, we next investigated if this could be reversed using pre-treatment with mifepristone as we observed in the 2D polyacrylamide model.

5.2.4.2. Pre-treatment with a high dose of mifepristone reduces gemcitabine resistance in MCF-7 cells at a higher stiffness in the alginate model.

In the polyacrylamide model, pre-treatment with the PR inhibitor mifepristone abolished resistance to gemcitabine at a higher stiffness. To investigate if the same was true in the alginate model we cultured cells in alginate beads for 24 hrs. We then added mifepristone or a vehicle control for a further 24 hrs, followed by the addition of gemcitabine or a vehicle control for a further 72 hrs. Cell viability was determined by alamarBlue assay for each condition. The means of 3 repeats are plotted in Figure 5.7. Cells were still more

resistant to 5 nM gemcitabine following pre-treatment with 0 and 10 µM mifepristone (p = 0.0482 and 0.0027 respectively by Student's t-test). However, at 15 µM mifepristone resistance to gemcitabine in cells cultured in 2% alginate was reduced and the difference between 1 and 2% was no longer significant (P = 0.0530 by Student's t-test). These data are in agreement with our 2D model. However, in our 2D model only 10 µM mifepristone was required to reverse resistance. Thus, again we observed that higher doses of drugs are required in 3D. Overall these data are suggestive of a role for PR function in resistance to gemcitabine. However, the effective dose of mifepristone in each model should be confirmed.

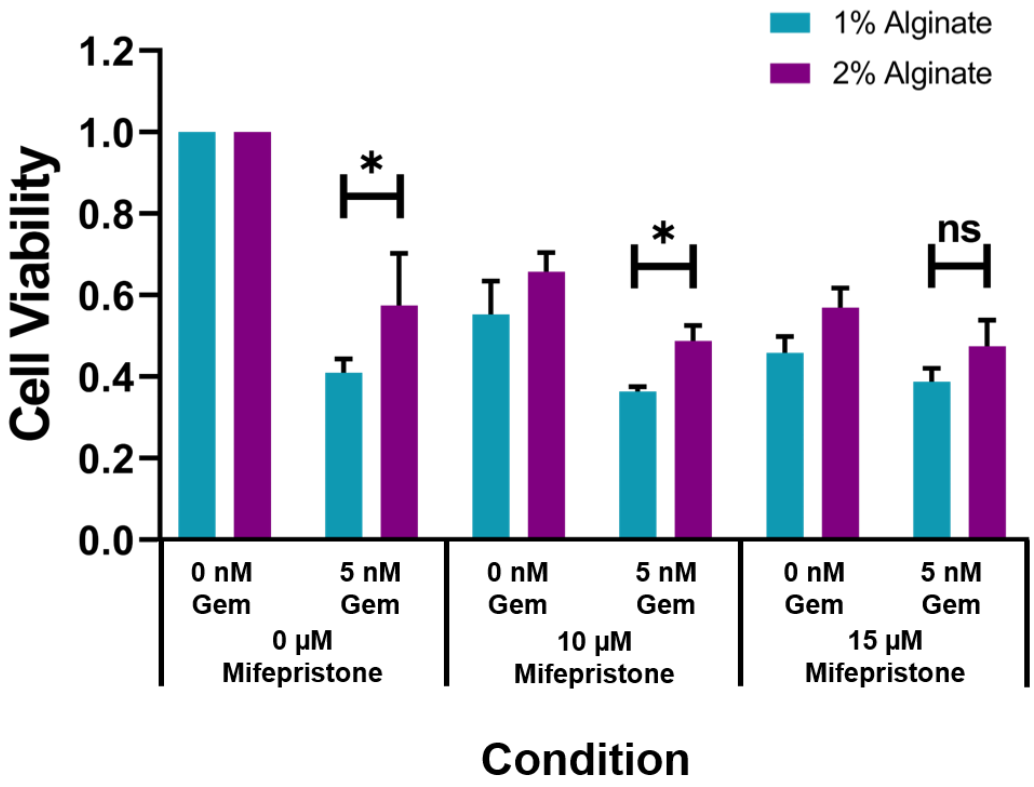

Figure 5.7. Pre-treatment of MCF-7 cells in alginate hydrogels with a high dose of mifepristone abolishes resistance to gemcitabine at a higher stiffness. MCF-7 cells were cultured in alginate hydrogels for 24 hrs prior to the addition of mifepristone or a vehicle control. After 24 hrs treatment with mifepristone, 5 nM gemcitabine (Gem) or a vehicle control was added. Cells were incubated for 72 hrs before cell metabolism was measured by alamarBlue assay. The cell viability for each condition was calculated by dividing the reading of the gemcitabine treated sample with that of the untreated vehicle control for each dose of mifepristone. Means and standard error of the means are plotted for 3 independent repeats. * indicates an unpaired one-tailed student's t-test p-value of ≤0.05.

5.2.4.3. Pre-treatment with other pathway inhibitors does not alter gemcitabine sensitivity in MCF-7 cells at a higher alginate percentage.

We observed that inhibition of PRs with only high doses of mifepristone reversed gemcitabine resistance at higher stiffnesses in our 3D alginate stiffness model. To determine if other stiffness related pathways could reverse gemcitabine resistance, we investigated other inhibitors. The four additional pathways chosen are shown at their sites of action in Figure 5.8.a.

Pazopanib is an inhibitor of YAP (Oku et al., 2015), a stiffness sensor that was described and investigated in chapter 4. FAKi 14 is an inhibitor of FAK, an enzyme which acts at mature FAs to facilitate cytoskeletal remodelling and downstream signalling associated with tumorgenicity (Mitra, Hanson, & Schlaepfer, 2005). Its activity is increased with increased stiffness (Provenzano, Inman, Eliceiri, & Keely, 2009). NVP-Bez 235 is an inhibitor which acts on the PI3K/mTOR pathway, downstream of FAK. Increased pathway activity has been reported with increased stiffness (You et al., 2016). Finally, Y-27632 is an inhibitor of the Rho-associated coiled coil-containing protein kinase (ROCK) pathway (Riento & Ridley, 2003), which is activated upon increased matrix stiffness facilitating cellular contractility (Provenzano et al., 2009). Dosages were optimised for the inhibitors using MCF-7 cells cultured on TCP. To do this a dosage range was chosen based on the active doses reported in the literature and the cell viability calculated after 72 hrs exposure. The cell viabilities are displayed in Figure 5.8.b for the 4 new inhibitors.

A

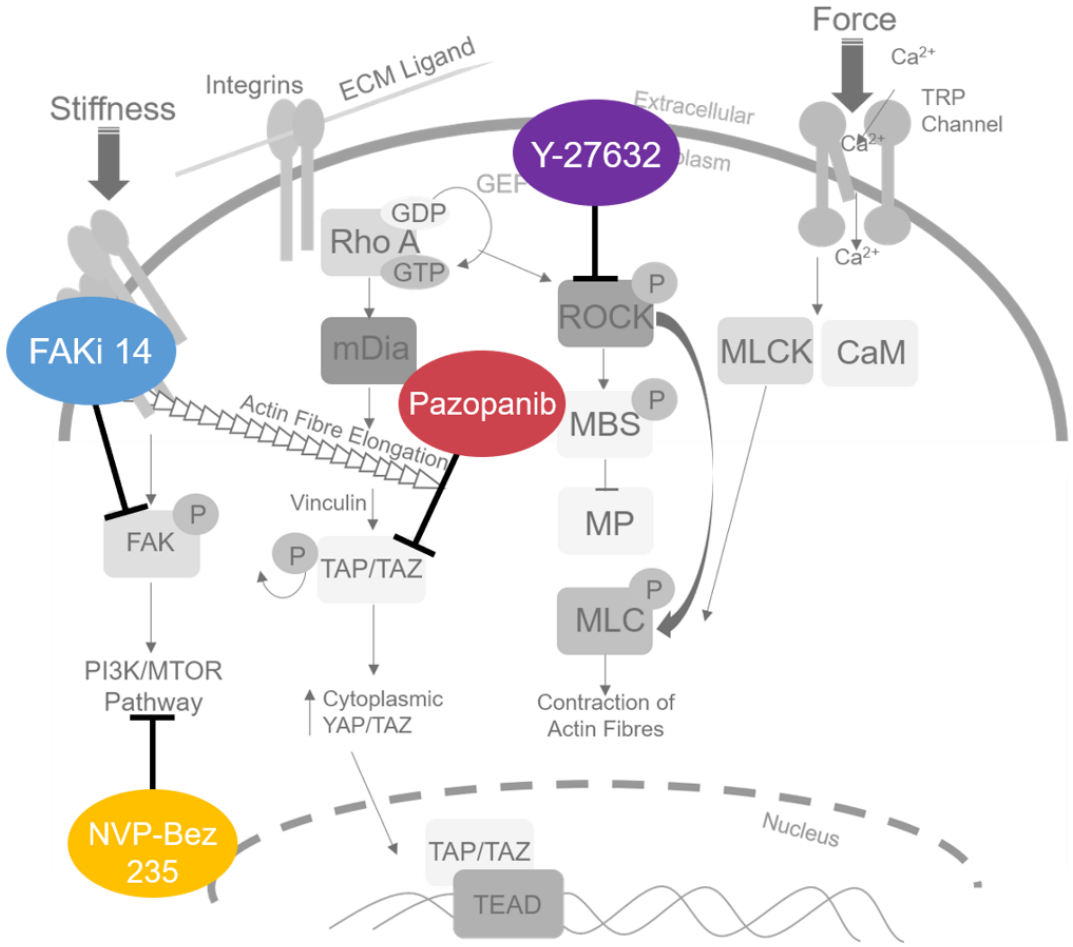

B

Pazopanib (μM)	Cell Viability
0	1
1	1.29
5	0.98
7.5	0.81
10	0.51

Y-27632 (μM)	Cell Viability
0	1
1	1.10
5	1.31
10	1.26
20	0.88

NVP-Bez 235 (nM)	Cell Viability
0	1
0.5	0.85
1	0.76
2.5	0.64
5	0.53

FAKi 14 (μM)	Cell Viability
0	1
0.1	0.12
0.5	0.11
1	0.11
2.5	0.11
5	0.12

Figure 5.8. Details and dose optimisation of alternative inhibitors investigated for combination treatment with gemcitabine in alginate. (A) Simplified diagram detailing the targets of the inhibitors investigated in relation to stiffness altered pathways. (B) Dosage optimisation of the 4 inhibitors investigated. The MCF-7 cell line was plated on plastic for 24 hrs prior to treatment with the inhibitors at the dosages as indicated. After 72 hrs incubation cell metabolism was measured by alamarBlue assay and the cell viability for each condition was calculated by dividing the reading of the treated sample with that of the vehicle control.

Dosages which induced around 20% death were chosen as an indication of activity and to allow for any sensitivity changes to be observed in combination with gemcitabine. However, it should be noted that formal demonstration of inhibition of the pathway was not obtained. FAKi 14 led to cell detachment at all the dosages examined, resulting in cell death. Therefore, we chose not to take this inhibitor forward.

Having decided upon inhibitor dosages on TCP we began trials in alginate beads. MCF-7 cells were cultured in 1 and 2% alginate beads for 24 hrs prior to the addition of 7.5 µM pazopanib, 20 µM Y-27632, 0.75 nM NVP-Bez 235 or a vehicle control for a further 24 hrs. Gemcitabine or a vehicle control was then added alongside the inhibitors for a further 72 hrs. Cell viability was measured using the alamarBlue assay. The results are plotted in Figure 5.9. Pre-treatment with pazopanib (Figure 5.9.a) resulted in an increase in cell viability in both percentages of alginate in combination with gemcitabine compared to gemcitabine alone, suggesting it was not suitable as a combination treatment. Likewise, Y-27632 (Figure 5.9.b), caused resistance to gemcitabine in cells cultured at both stiffnesses albeit more extreme in 1% alginate indicating it would also not be useful as a combination therapy. Pre-treatment with NVP-Bez 235 (Figure 5.9.c) had no effect on gemcitabine sensitivity at either stiffness. As we observed no clear sensitivity differences with any inhibitors, we decided not to undertake further repeats.

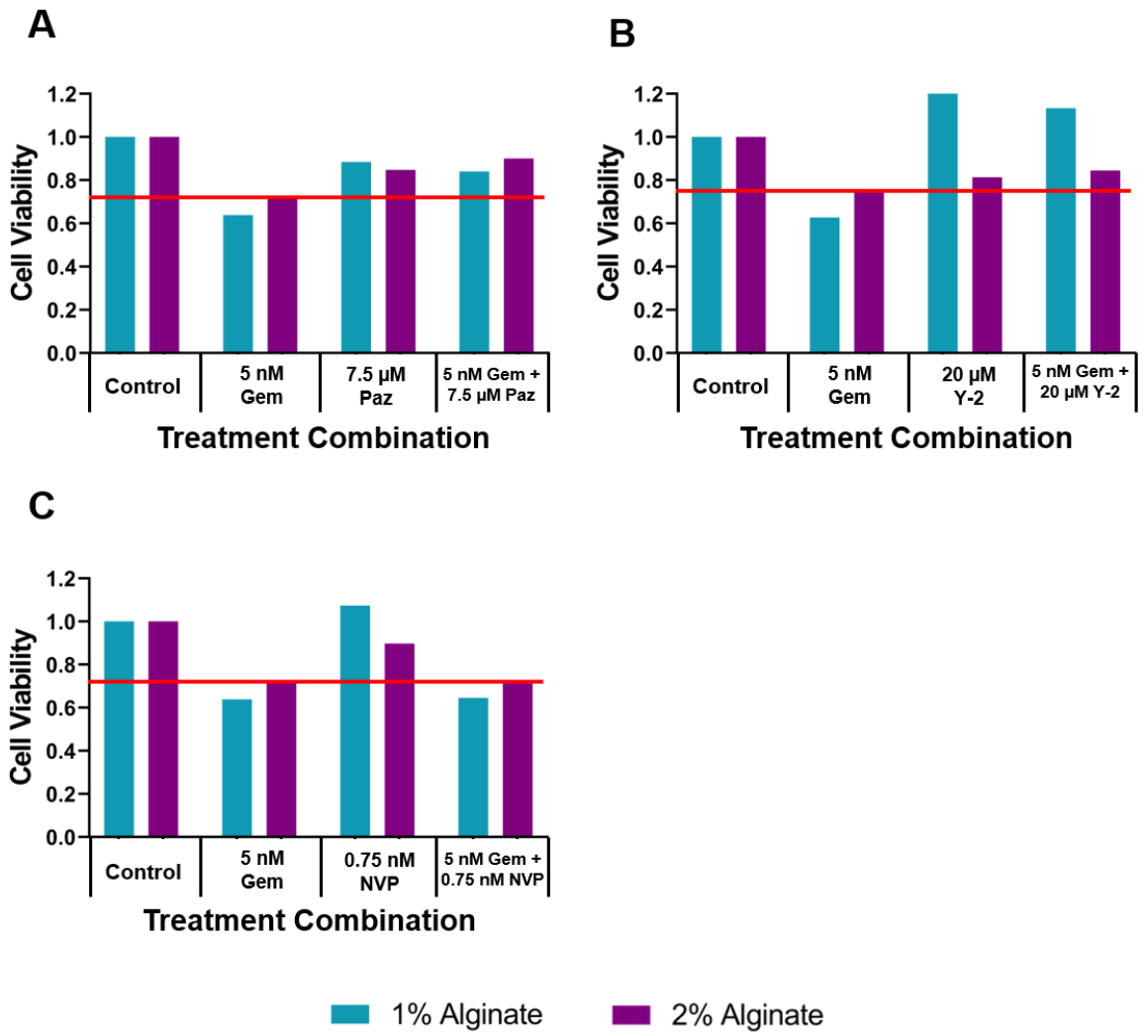

Figure 5.9. Pre-treatment of alginate hydrogels with selected pathway inhibitors prior to gemcitabine treatment does not increase gemcitabine sensitivity. MCF-7 cells were cultured in alginate hydrogels for 24 hrs prior to the addition of inhibitors or a vehicle control. Cell were pre-treated with the inhibitors (A) pazopanib (Paz), (B) Y-27632 (Y-2) or (C) NVP-Bez 235 (NVP) or a vehicle control. After 24 hrs treatment with inhibitors, 5 nM gemcitabine (Gem) or a vehicle control was added. Cells were incubated for 72 hrs before cell metabolism was measured by alamarBlue assay. The cell viability for each condition was calculated by dividing the reading of the treated sample with that of the vehicle control. Means are plotted from 1 independent repeat. A red line is drawn at the cell viability for 2% alginate hydrogels treated with 5 nM gemcitabine alone to show how pre-treatment with each inhibitor altered survival.

Despite the similarities with our 2D model there are limitations to the alginate 3D model. It was not possible to produce an alginate gel that matched the higher stiffnesses observed in breast cancer (4 kPa) as we did in 2D. Secondly, gel stiffness reduced with time,

further reducing the stiffness ranges compared. Growth was limited in the MDA-MB-231 cell line, which may account for the lack of cell death following gemcitabine treatment. We did not observe the same changes in cytoplasmic and nuclear area as in our 2D model which may have been limited by lack of cellular attachment. Immunofluorescence staining also proved unsuccessful which limited downstream assays. Therefore, we decided to investigate the design of another 3D model which may be more comparable to the 2D polyacrylamide model.

5.2.5. Investigations into a 3-D polyacrylamide stiffness model.

To overcome the problems above we decided to create an acrylamide based HIPE under the guidance of Dr Frederik Claeyssens (University of Sheffield). Use of polyacrylamide for a 3D model would allow direct comparison to our 2D polyacrylamide model and may allow for issues of cell attachment to be overcome through conjugation of collagen I, similar to our 2D model.

A polyHIPE is named so as it is a polymer formed from a high ratio of internal phase, in this case the oil phase, to the external (aqueous) phase, the acrylamide solution in our model. A detergent is added to the external phase to create an emulsified solution that can be set into a solid mesh (Silverstein & Cameron, 2010). Toluene, the oil phase in our experiment is slowly dripped into an un-polymerised solution of acrylamide and bis-acrylamide and an added detergent. With gentle mixing, an emulsion is formed (Figure 5.10.a). Once the emulsion is formed the gel can be set. We attempted this with the addition of the catalyst TEMED and heat or the photoinitiator diphenyl(2,4,6-trimethylbenzoyl)phosphine oxide/2-hydroxy-2-methylpropiophenone blend and UV light. The oil phase can then be removed leaving a fine meshwork suitable for the culture of

cells. We began with the same polyacrylamide mixture, minus the TEMED that we used for our stiffest 4 kPa 2D hydrogels. We were able to successfully form an emulsion as shown by the formation of a thick white liquid (Figure 5.10.b) which we transferred to a Petri dish (Figure 5.10.c). We then attempted to polymerise the polyacrylamide first with the addition of TEMED and heat (Figure 5.10.d) however, we did not observe formation of a solid white polyHIPE as expected. Instead we observed evaporation of the toluene and the production of a clear waxy solid. We therefore attempted to use a photoinitiator and UV light as this produces a quicker reaction which we hoped would prevent evaporation prior to setting. However, as can be seen in Figure 5.10.d, we did not observe setting of the polyHIPE as it still remained liquid and, when left for longer, evaporation occurred. This suggests that at the stiffnesses required we could not achieve setting of the polyHIPE. Indeed polyacrylamide polyHIPEs are typically reported in the megapascal range (Kovačič & Silverstein, 2017; Madhusudhana Rao, Anbananthan, & Varada Rajulu, 2011), suggesting polyacrylamide polyHIPEs may not be suitable for use as a breast cancer stiffness model.

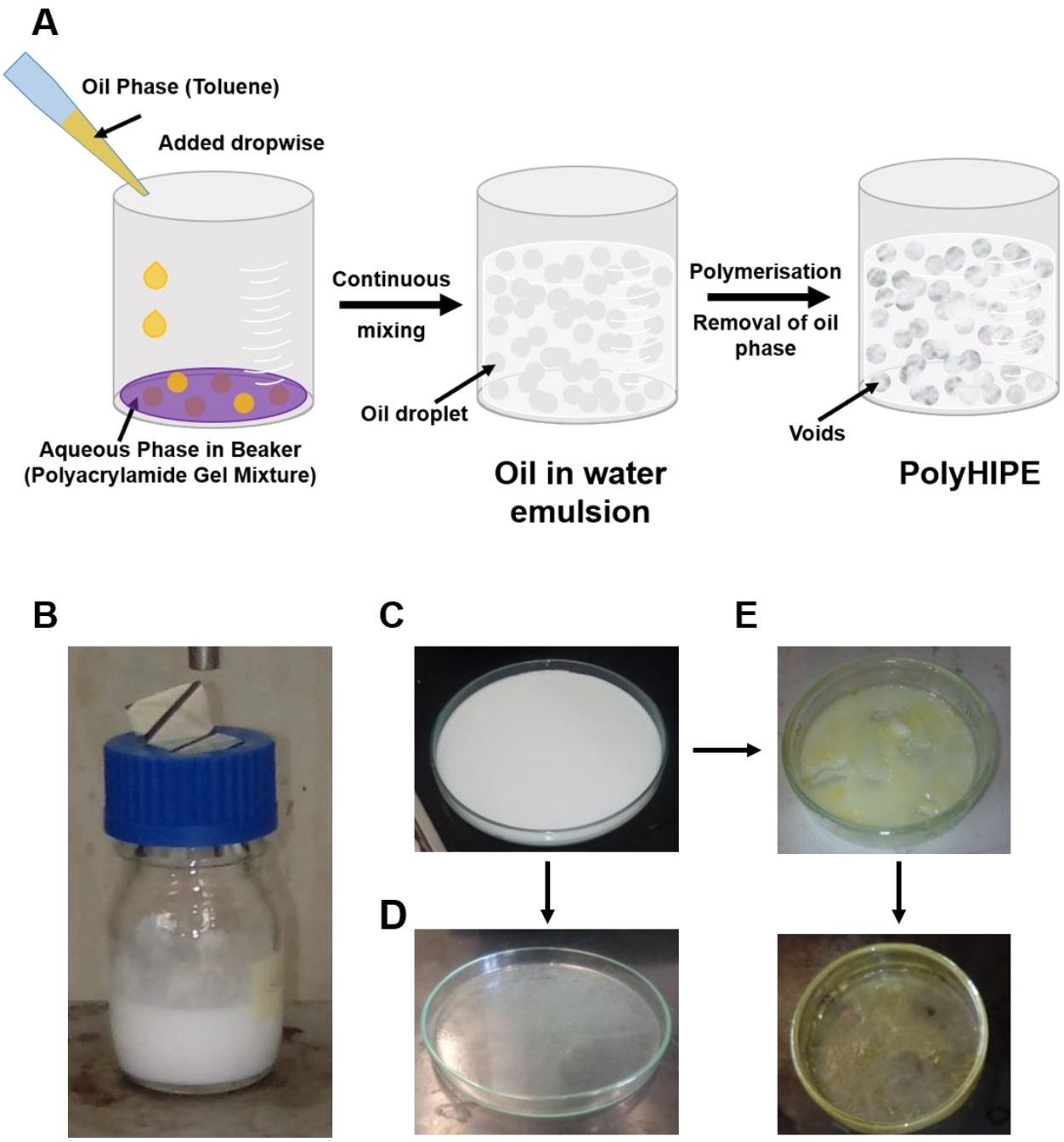

Figure 5.10. Methodology for formation of polyacrylamide high internal phase emulsions. (A) Simplified schematic for the methodology used to form polyacrylamide high internal phase emulsions (PolyHIPEs). (B) Picture showing successful formation of toluene and acrylamide emulsion as depicted in the second stage of Figure 5.10.a. This solution was then transferred to a glass Petri dish (C). Attempts were made to set the polyacrylamide gel component by using both heat and TEMED (D) and by addition of a photoinitiator and UV light (E) however these both resulted in formation of a clear waxy solid.

5.3. Discussion.

In this chapter evidence has been presented for the optimisation of a 3D alginate stiffness model, representative of the stiffnesses observed in breast tissue and cancer. Similarities in the response of MCF-7 cells to gemcitabine in this model are observed in comparison to the 2D polyacrylamide model. Differences are observed in the MDA-MB-231 cell line. Finally, we compared the response to gemcitabine in MCF-7 cells following pre-treatment with several pathway inhibitors, including mifepristone. Several similarities and differences were observed in comparison to our 2D polyacrylamide model which are discussed below.

5.3.1. A normal breast and breast cancer specific stiffness range can be achieved with alginate hydrogels.

We discussed in chapter 3 that *in vivo* measurements of the normal mouse mammary gland are reported to have an elastic modulus of around 170 Pa and established breast tumours measured around 4 kPa (Paszek et al., 2005). The stroma around the tumour is reported to have a lower stiffness of around 900 Pa (Paszek et al., 2005). Here we were able to produce alginate hydrogels of 300 Pa (1%) and 1.9 kPa (2%). Lower percentages of alginate resulted in a hydrogel bead that degraded during the wash and incubation steps. Thus, we chose 300 Pa as the stiffness representative of the normal breast. Whilst higher percentages of alginate did allow for an increase in stiffness, they also resulted in a huge loss of cell viability. We also attempted to use a higher viscosity of alginate; however, this did not correlate to an increased stiffness. Therefore, we chose to use 1.9 kPa as the stiffness representative of the cancerous breast. Indeed, this value is closer to the stiffnesses observed in the stroma surrounding the tumour. However, it is still significantly increased from 300 Pa and will therefore allow for an interesting comparison between the two alginate percentages.

It has been reported that an increase in calcium chloride concentration up to 1 M can provide an increased stiffness up to 2.5-4 kPa (Cavo et al., 2016), which would warrant further investigation in our model. Secondly increased gel setting times of up to 4 hrs have been shown to produce stiffer gels of up to 5.5 kPa (Khavari et al., 2016). Although a lower concentration of calcium (carbonate in this report) was used of around 30 mM the impact on cell viability for such a lengthy incubation would require investigation. Indeed the reported cell growth rate was low although did improve with the addition of collagen in the alginate (Khavari et al., 2016). Advanced alginate technologies have reported that incorporation of liposomes containing infrared activated nanorods and calcium ions into alginate gels allowed for further stiffening following gel setting through the release of additional calcium ions from the liposomes (Joyce et al., 2018). Such technologies may be suitable for systems such as ours to allow for higher stiffness to be achieved, where Joyce et al., (2018) achieved values up to 3 kPa.

Efforts were undertaken to optimise a new 3D hydrogel stiffness model based upon polyacrylamide. This may have allowed for coating with collagen, to allow for comparison to our first 2D model. However, we were not able to set the gels at the stiffnesses required and therefore we were not able to continue with this model. Use of other 3D hydrogels formed from biological components of the ECM such as collagen and hyaluronic acid do allow for physiologically similar stiffnesses to be observed of around 4 kPa (Duan, Hockaday, Kapetanovic, Kang, & Butcher, 2013). Though variation in stiffness due to the non-permanency of bonding can negate this improvement in stiffness. However, it is reported that chemical modifications of such components can allow for permanent crosslinking (Caliari & Burdick, 2016). Indeed, in our model, we did observe gel softening over time which correlated with a reduced stiffness from 319 to 275 Pa in the 1% alginate gels and from 1919 Pa to 1175 Pa in the 2% gels. The reduction in

stiffness observed was of almost half in the 2% gels, which is not ideal. If we had more time, we would have investigated other 3D hydrogels as discussed above that allowed for increased gel stability and stiffness. However, there was still a significant difference in stiffness between the 1 and 2% alginate hydrogels at 144 hrs and thus we decided to continue investigating our alginate model.

5.3.2. An increased stiffness results in reduced cytoplasmic and nuclear areas in MCF-7 cells but not MDA-MB-231 cells.

We observed in our 3D alginate model that cytoplasmic and nuclear area is reduced with increasing stiffness in MCF-7 cells. However, the opposite was observed in our 2D polyacrylamide model. Indeed it has been reported that cells in 3D alginate hydrogels are observed to be rounder than cells cultured on 2D alginate hydrogels or on plastic (Cavo et al., 2016). In higher stiffness (higher percentage) alginate matrices it is observed that pore size is smaller (Leal-Egaña, Dietrich-Braumann, Díaz-Cuenca, Nowicki, & Bader, 2011; Swioklo, Ding, Pacek, & Connon, 2017), which may account for the smaller cell size at higher stiffnesses. Secondly, we also observed that cells were rounder in our 3D model compared to our 2D model regardless of stiffness. As the cells only have one direction of contact in 2D they are likely to spread further on this one surface, compared to 3D where cells are in contact with the matrices in all directions. As such, the increased area of cell to ECM contacts in 3D may contribute to a rounder cell phenotype as cells spread between all ECM contacts within the alginate pores.

It has been observed in a 3D alginate model that nuclei are smaller and more deformed in larger cell clusters resulting in an elliptical shape (Khavari et al., 2016). This was not reported in relation to stiffness, however it was reported that the size of cell clusters

increased with stiffness thus suggestive of the same relationship observed in our model (Khavari et al., 2016). It would be interesting to investigate cell cluster size further in our model, although preliminary imaging of cells in Figure 5.4. is indicative of this relationship.

Whilst we observed a reduction in nuclear and cytoplasmic area in the MCF-7 cell line we observed no differences in the MDA-MB-231 cell line. This is contrary to our 2D model where, like the MCF-7 cell line, we observed an increase in the area of both the nucleus and cytoplasm with increasing stiffness. This may be owed to the lack of cell adhesion molecules in the gel which would allow for more cellular interaction with the matrix and therefore stiffness sensing. ECM components were not added to the beads because our collaborator, Dr Nick Peake, had successfully grown cells without and we wanted a cheap, quick and stable system. In addition, MCF-7 cells grew sufficiently without the addition of ECM ligands. However, in retrospect the addition of collagen or Matrigel to the gel mixture or modification to the alginate structure to add adhesive RGD ligands may have overcome some of our problems. The addition of adhesive ligands would allow for improved cell-ECM attachments which may provide a more responsive change to cell shape in regard to stiffness.

5.3.3. The gemcitabine response is conserved in alginate for only MCF-7 cells and extends to mifepristone pre-treatment at higher doses.

In our 3D alginate stiffness model, we observed that MCF-7 cells were more resistant to gemcitabine at a higher stiffness of 1.9 kPa compared to 300 Pa. This finding agrees with the stiffness relationship observed in our 2D polyacrylamide model at 4 kPa in comparison to 500 Pa. This relationship with gemcitabine and stiffness was also

observed in a 3D oligomer model in pancreatic cancer cell lines between 1 kPa and 500 Pa (Puls et al., 2017), further validating our findings.

However, in our 3D alginate model we observed no difference in gemcitabine response in the MDA-MB-231 cell line at either stiffness. Whereas in our 2D model we saw resistance to gemcitabine at a lower stiffness of 500 Pa in comparison to 4 kPa in this cell line. It is not uncommon for chemotherapeutic responses to be different in a 2D model compared to a 3D model. Joyce et al., (2018) observed that MDA-MB-231 cells were more resistant to doxorubicin when cultured in 2D than when cultured in a 3D alginate-based hydrogel. They also reported that MDA-MB-231 cells were more resistant to doxorubicin when cultured in a 2 kPa 3D alginate model than at 200 Pa (Joyce et al., 2018). These results are contrary to our results in MDA-MB-231 cells with gemcitabine, which may be owed to the use of Matrigel by Joyce et al., (2018). Matrigel contains many biological ECM components to mimic the natural environment cells would encounter *in vivo*. As such cell to ECM connections will be much more likely in an alginate gel containing Matrigel. This may explain why we saw lower growth in MDA-MB-231 cells in comparison to MCF-7 cells during the optimisation stage, as MCF-7 cells, unlike the MDA-MB-231 cell line, can form cell to cell connections through E-cadherin to allow for proliferation to occur. Use of Matrigel or collagen in our alginate model warrants further investigation in respect to gemcitabine response. Secondly modification of alginate to add RGD ligands has also shown to improve cellular adhesion and growth (K. Y. Lee & Mooney, 2012) which is another aspect which would be interesting to explore in our model.

Joyce et al., (2018) linked the resistance observed in MDA-MB-231 cells to EMT, however we could not observe this in our 3D model as immunofluorescent staining

proved unsuccessful. It would be interesting to investigate this and other changes in the DNA damage response in 2D further in our alginate model through the use of PCR had time been permitting.

In agreement with our 2D model, pre-treatment with mifepristone did abolish gemcitabine resistance in MCF-7 cells in 3D. However, a higher dose of mifepristone was required. As we did not include ECM ligands in the 3D model it may suggest that PRs require engagement with the ECM to elicit more resistance to gemcitabine at higher stiffnesses. It would be interesting to investigate this in other breast cancer cell lines including the PR positive T-47D cell line to see if the same result was observed as in our 2D model.

We also investigated the use of other stiffness related pathway inhibitors but did not find any differences in gemcitabine resistance. Therefore, it may be likely that the resistances observed at higher alginate percentages may instead be due to the ability of gemcitabine or inhibitors to permeate the gel and reach the cells. As discussed previously the use of antibodies in immunofluorescent staining proved unsuccessful perhaps due to the larger size of antibodies in comparison to DAPI and phalloidin. However, gemcitabine is not as large as an antibody (263 g/mol compared to 150,000 g/mol (Janeway, Travers, Walport, & Shlomchik, 2001)) and is also smaller than DAPI (350 g/mol) and phalloidin (789 g/mol), which we observed were able to reach cells. This indicates that gemcitabine is likely to have been able to access the cells, but it does not rule out that diffusion of compounds in and out of the alginate bead may compromise experiments. Similarly, the inhibitors used are also smaller than phalloidin where mifepristone is 429.6 g/mol, Y-27632 is 320.26 g/mol, NVP-Bez 235 is 469.5 g/mol and pazopanib 437.517 g/mol therefore suggesting that they were able to permeate the alginate. This is further

confirmed by them alone resulting in a small amount of death in cells when cultured in alginate. This would need to be confirmed, by measuring the gemcitabine or inhibitor content of cells extracted from the alginate to indicate if an effective dose is reaching the cells. Measurement of pore size and investigations into increased permeability would be helpful for future alginate-based hydrogel experiments.

Secondly, the reduced nuclear size observed in MCF-7 cells cultured in 2% alginate compared to 1% may contribute to the differences in gemcitabine response. However, increased nuclear size is typically associated with cancer and has been linked to increased cell proliferation and poorer prognosis in ovarian cancer patients (Jevtić, Edens, Vuković, & Levy, 2014). A reduced nuclear size however is likely to contribute to increased DNA compaction which may allow some protection from gemcitabine incorporation. This would be interesting to investigate further in our model if issues with immunofluorescence could be resolved.

5.3.4. Summary.

Here we have shown that a 3D alginate hydrogel model of physiologically relevant stiffnesses shows the same gemcitabine resistance at a higher stiffness in MCF-7 cells in comparison to that of normal breast stiffness. This further validates our findings in the 2D polyacrylamide stiffness model. However, the same results were not observed with the use of MDA-MB-231 cells which suggests that cellular attachment is important in this cell line. This may be improved through incorporation of attachment ligands in the alginate model. Overall, given the limitations of the 3D model, the results are in agreement, or at least are not arguing against the results of the 2D model.

6. Discussion.

6.1. Validity of the stiffness models.

In this thesis 2D polyacrylamide and 3D alginate stiffness models have been investigated in the context of breast cancer. Gel stiffness was a compromise in both models, with the polyacrylamide model limited to higher stiffnesses (500 Pa to 4 kPa) and the alginate model limited to lower stiffnesses (300 Pa to 1.9 kPa). In other studies of stiffness in the breast, softer models are typically used including alginate (Joyce et al., 2018) and collagen hydrogels (Paszek et al., 2005), where stiffnesses as low as 200 and 170 Pa are achieved respectively, similar to those measured *in vivo* in normal breast tissue (170 Pa). For polyacrylamide hydrogels lower stiffnesses of 150 Pa are infrequently reported (Tilghman et al., 2010). More frequently the lower stiffness range used is around 500 Pa (Syed et al., 2017), 1 kPa (Zustiak et al., 2014) and 2 kPa (Ebata et al., 2017). Given our issues with soft 1 Pa (predicted to be 100 Pa) polyacrylamide gels, this indicates a common limitation of the polyacrylamide model in achieving a stable lower stiffness relative to normal breast tissue. However, despite our issues with stiffness, the same gemcitabine resistance and resistance reversal with mifepristone was observed in MCF-7 cells at higher stiffnesses in both models. Patients likely show heterogeneity in stiffness (Plodinec et al., 2012), so it is encouraging that the relationship is true in both stiffness ranges.

In our 2D model cell area was increased at higher stiffnesses, but it was reduced at higher stiffnesses in 3D. This may be due to the lack of cell adhesion molecules in the 3D model, as discussed previously. In clinical cancer samples an increase in heterogeneity of size is observed, not a global change in either direction (Kumar et al., 2015). This suggests that neither of the models are wholly accurate in depicting the morphology of cancer cells. The question arises as to whether the use of cancerous cells in the models

may contribute to this, as they are already transformed and selected for growth in 2D. Given that increased matrix stiffness contributes to a tumorigenic phenotype and breast cancer development (Cox & Erler, 2011; Levental et al., 2009), we can hypothesise that *in vivo*, normal cells would likely become tumorigenic alongside an increasing matrix stiffness, transforming in parallel. Growth of cancerous cells on a soft matrix is also not representative of normal cell growth in the breast. It is reported that cells have a memory of the surface they were previously cultured on, which indicates an issue for use of transformed cell lines that are adapted to culture on TCP. In our 2D model, MCF-7 cells showed differential growth between the two stiffness only for the first 72 hrs of culture, indicating that an adaption to the matrix may occur after this time. Similarly it is reported that MDA-MB-231 cells previously cultured on TCP required several passages on 1 and 103 kPa polyacrylamide hydrogels for cell proliferation to increase to a similar level as on TCP (Syed et al., 2017). Whereas they maintained a steady proliferation rate on TCP. This indicates that immortalised cancer cells can require time to adapt to a new matrix. The mechanical memory of pancreatic cells has been attributed to YAP (Carnevale, Capula, Giovannetti, Schmidt, & Coppola, 2019). In our models, the MCF-7 cell line, which expresses low levels of YAP and therefore theoretically little mechanical memory, showed sufficient cell growth in 2D and 3D when moved from stiff plastic to comparatively soft hydrogels. However, MDA-MB-231 cells, which have comparatively higher levels of YAP expression (Shen et al., 2018), showed low levels of cell growth in 3D, where the mechanical memory may slow adaptation.

Our models indicate that the response of cells grown at cancer vs normal tissue stiffness may be a chemotherapeutic window in PR positive breast cancer for combination gemcitabine and mifepristone treatment. However, patient heterogeneity in stiffness may limit this and therefore investigation is required *in vivo* to determine efficacy. The link

between clinical measures of stiffness such as breast density and elastography and *in vitro* measures of stiffness will also require investigation to determine the validity of *in vitro* models in recapitulation of the *in vivo* environment. It is indeed indicated that increased stiffness is associated with poor prognosis (Acerbi et al., 2015) and cancer risk (Boyd et al., 2014), which together with our findings further validates stiffness as a clinical marker for treatment response.

6.2. Potential mechanisms behind gemcitabine resistance at higher stiffnesses.

In this thesis the MCF-7 and T-47D PR positive cell lines were resistant to gemcitabine when cultured at higher stiffnesses compared to the same cells grown at lower stiffnesses. This was observed in 2D for both cell lines and in 3D for MCF-7 cells (not tested in T-47D cells).

There are many reported mechanisms of gemcitabine resistance (De Sousa Cavalcante & Monteiro, 2014), which reflects its complex and multifactorial nature. The MCF-7 cell line can become resistant to gemcitabine through overexpression of RNR (Jordheim et al., 2005). Increased expression of RNR subunits M1 and M2 (2.5 and 3.9 fold respectively) has been reported in NMuMG normal mouse breast epithelial cells cultured at higher stiffnesses in a collagen model (Provenzano et al., 2009). However, in our investigations gemcitabine treatment resulted in the same amount of replication stress and DNA damage at both stiffnesses. This indicates that resistance is not likely to be due to expressional changes in dNTP modulating proteins such as RNR.

Gemcitabine treatment can induce apoptosis mediated by p53 and bcl-2 family proteins in lung cancer cell lines (Tolis et al., 1999), pancreatic cancer cell lines (Schniewind et al.,

2004; Shi, Liu, Kleeff, Friess, & Buchler, 2002) and paired breast cancer cell lines derived from MCF-7 cells (Galmarini et al., 2002). It is reported that gemcitabine resistance can occur due to expression changes in these cell death pathways in pancreatic cancer cell lines (Shi et al., 2002). In our 2D model, following gemcitabine treatment, p53 only localised to the nucleus on glass and 500 Pa hydrogels but not on stiffer 4 kPa hydrogels, suggesting that increased stiffness may modulate p53 function. A similar relationship with chemoresistance and p53 nuclear localisation has been observed in MCF-7 cells previously. Ebata et al., (2017) reported that a low stiffness (2 kPa vs 30 kPa) reduced p53 nuclear localisation following treatment with doxorubicin via the downregulation of the ROCK pathway, mediating resistance to doxorubicin. However, the mechanisms behind this are not clear. Although the stiffness relationship to chemotherapeutics was inverse to our model, chemotherapeutic resistance and aberrant p53 subcellular location did correlate. The lowest stiffness used in this paper (2 kPa), is more physiologically relevant to breast cancer which may also explain why we observed a similar affect at 4 kPa. Secondly, a relationship between p53 and the stiffness sensor YAP has recently been identified, where YAP can inhibit p53 acetylation and promote its deacetylation (Yuan et al., 2019), which is required for its function sensing DNA damage and inhibition of cell growth (Reed & Quelle, 2014). Thus, it is indicated that stiffness modulates p53 tumour suppressor function, and we can postulate that altered p53 function may explain the resistance to gemcitabine observed here.

The TNBC cell line, MDA-MB-231, was resistant to gemcitabine on softer matrices in our 2D model, however no difference was observed in the 3D model. Chemotherapy response differences between 2D and 3D culture have been observed previously in other alginate models (Joyce et al., 2018). However, in contrast to our results this study reported a differential effect in MDA-MB-231 but not MCF-7 cells. As Joyce et al., (2018)

used Matrigel in their model, this suggests that in stiffness models cell adhesions may impact chemotherapeutic response in a cell line specific manner. Indeed, it is reported that inhibition of cell adhesion improved inhibition of hepatic tumour growth by gemcitabine compared to gemcitabine or adhesion inhibitor alone (Seulki Cho et al., 2017). This indicates that claudin-low cell lines such as MDA-MB-231 which have low expression of cell-cell adhesion proteins (Prat et al., 2010), are therefore likely to be highly reliant on adhesion to the matrix for growth. Whereas MCF-7 cells which express higher levels of cell-cell adhesion proteins (Prat et al., 2010) may not be as reliant on adhesion to the matrix for growth. Consistent with this we observed low levels of cell growth in MDA-MB-231 cells in alginate. Active replication is required for incorporation of gemcitabine into DNA and therefore for induction of cell killing. We therefore propose that the limited growth of MDA-MB-231 cells due to lack of adhesion in 3D may explain their lack of sensitivity to gemcitabine at either stiffness.

In MCF-7 cells in our 2D model cell growth rate was greater at 4 kPa vs 500 Pa within the first 72 hrs of culture. This increase in cell growth rate at higher stiffnesses likely contributed to the increased replication stress observed. The question arises; why does increased stiffness increase cell growth rate and therefore DNA replication rate, replication stress and DNA damage. An increased expression in ‘proliferation signature genes’ (Whitfield, George, Grant, & Perou, 2006), including checkpoint kinases, cyclins and aurora kinases is reported in NMuMG breast cells cultured at higher stiffnesses (Provenzano et al., 2009). This implicates stiffness in the direct upregulation of cellular proliferation. Also upregulated at increased stiffnesses was expression of survivin (Provenzano et al., 2009), which has been implicated in gemcitabine resistance (Yoon et al., 2012). Whilst it is predicted that increased replication and replication stress would increase sensitivity to gemcitabine, the upregulation of other proliferation signatures

which act to prevent cell death, such as survivin, may protect the cell from the increased stress and lead to avoidance of cell death.

Another factor to consider in resistance to gemcitabine is its metabolism within the cell. Increased cellular export of gemcitabine is attributed to its resistance (Adamska et al., 2018). It has been reported that culture of immortalised breast cancer cell lines onto soft polyacrylamide hydrogels (5 kPa) vs stiff gels (30 kPa) or glass resulted in increased expression of multi-drug efflux ATP-binding cassette transporter (ABC transporter) genes (*Abcb9* and *Abcc3)* which act to remove chemotherapeutics from the cell (Medina et al., 2019). Overexpression of ABC transporters are attributed to gemcitabine resistance in pancreatic cancer (Hagmann, Jesnowski, & Löhr, 2010). However, as the lowest stiffness used by Medina et al., (2019) (5 kPa) is similar to the stiffnesses observed in breast cancer it is hard to determine what this means in comparison to cells cultured at the lower normal breast stiffnesses (170 Pa). It does however indicate that culture of cancer cells at physiologically relevant stiffnesses is vital for determining chemotherapy resistance.

EMT has also been implicated in contribution to chemoresistance to doxorubicin at increased stiffnesses in breast cancer cells (Joyce et al., 2018). However, this was not indicated in our 2D model where we saw that MCF-7 cells also exhibited a stiffness responsive resistance. Gemcitabine resistance is frequently investigated in triple negative cell lines in the context of breast cancer. Further investigations into gemcitabine mediated cell death and resistance in receptor positive cell lines are warranted as evidenced by our findings. Together, our findings in combination with other studies as discussed above indicate a clear link between stiffness and resistance to gemcitabine, as summarised in Figure 6.1.

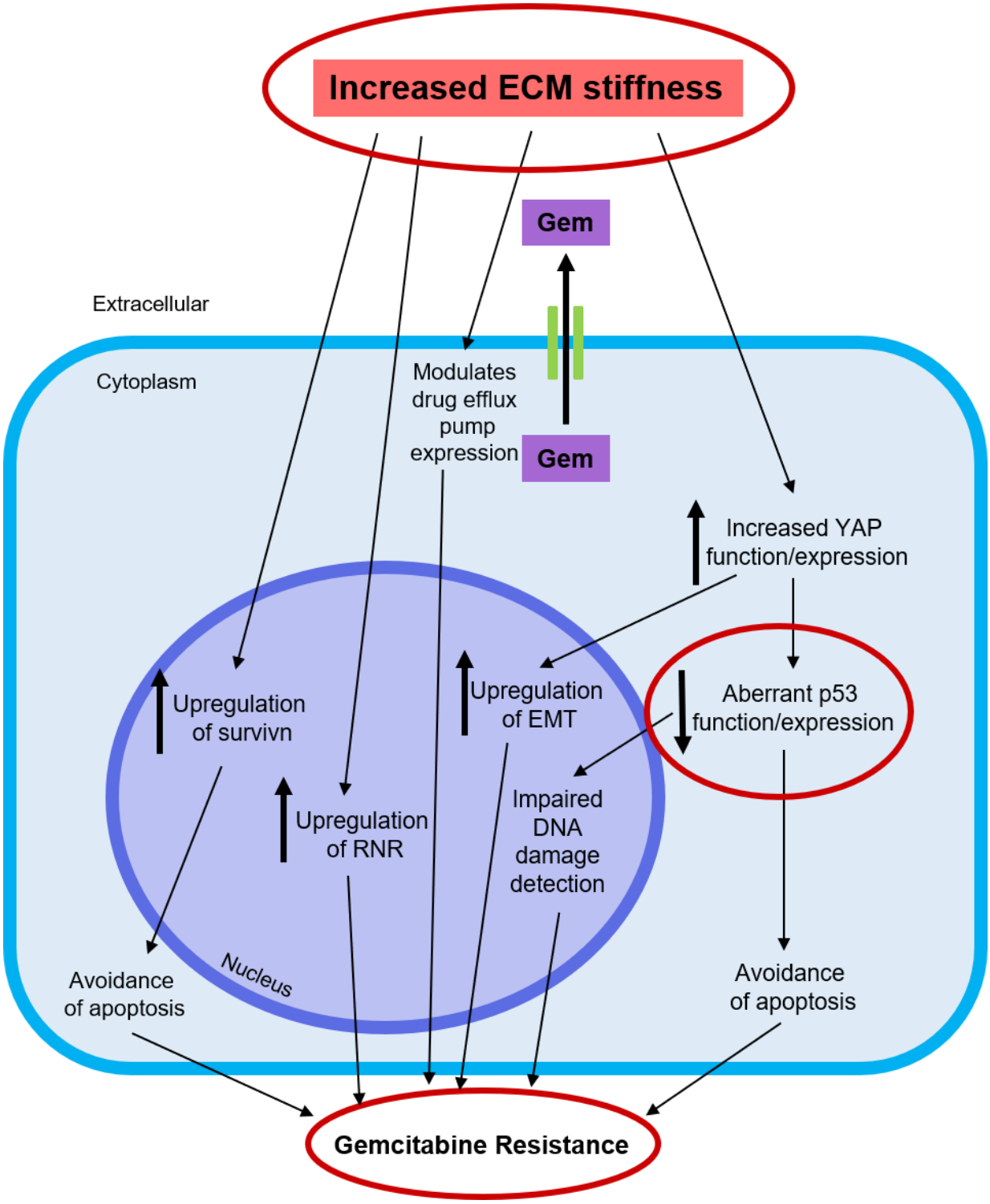

Figure 6.1. Mechanisms of gemcitabine resistance associated with increased ECM stiffness. Schematic representation of the connections between increased extracellular matrix (ECM) stiffness and resistance to gemcitabine (Gem). The connections contributed to by our models are circled in red.

6.3. Connection between gemcitabine resistance and progesterone receptor inhibition.

In our 2D and 3D models, inhibition of PRs abolished the resistance to gemcitabine seen at higher stiffnesses in MCF-7 cells. To my knowledge this is the first time a link between PR expression, matrix stiffness and gemcitabine resistance has been determined. Progesterone signalling has been linked to stiffness previously, where increased tension during pregnancy results in an increase in production of basal ECM components and reduces levels of progesterone (Shynlova et al., 2004). Conversely, addition of progesterone reduced production of other ECM components (fibronectin and laminin) (Shynlova et al., 2004), suggesting that PR signalling modulates ECM composition. Secondly PR expression is modulated by YAP (Lehn et al., 2014), further linking stiffness to PR signalling. However, in our 2D model a significant nuclear movement of YAP was not observed in MCF-7 cells suggesting that other mechanisms are responsible.

In 2D, mifepristone alone resulted in low levels of cell death and showed an additive effect when combined with gemcitabine. This suggests an underlying mechanism for PR function in gemcitabine resistance at increased stiffnesses in 2D.

In 3D, the relationship with PR inhibition was only observed at higher concentrations of mifepristone. Higher doses of drugs (both gemcitabine and mifepristone) may be required in 3D due to issues with diffusion through the alginate. Secondly, the lower levels of cell growth in 3D vs 2D (Chitcholtan, Asselin, Parent, Sykes, & Evans, 2013; Riedl et al., 2017) may limit drug effectiveness in 3D such that a higher dose of mifepristone is needed. Finally, the lack of effect in 3D could be due to the stiffnesses differences in 3D vs 2D at the cancer relative stiffnesses (2 vs 4 kPa).

The smaller effect/lack of effect in 3D could also provide clues as to why mifepristone reverses resistance. As the 3D model did not incorporate adhesion molecules it is suggestive of an interaction between PR and cellular adhesion. In regards to cell membrane connections and growth, mPR promotes cellular growth through increased EGFR stabilisation (Ahmed, Rohe, Twist, & Craven, 2010). This may contribute to the effectiveness of replication dependant chemotherapeutics such as gemcitabine. In modified T-47D cell lines PR-A has been over expressed to levels relative to clinical breast cancer (PR-A/B ratio of 1.8 to 5.1) (Graham et al., 1995). The expression profiles after progestin treatment revealed the down regulation of cell-cell adhesion proteins Br-cadherin and Protocadherin 43 but upregulation of the cell-ECM protein vinculin (Graham et al., 2005). This suggests the promotion of an EMT phenotype by PR-A which is likely to promote chemotherapeutic resistance. It also implicates PR signalling in increased FA signalling via vinculin, which would also likely be increased via stiffness. As discussed in section 6.2., increased cellular adhesion is associated with decreased tumour response to gemcitabine (Seulki Cho et al., 2017). In relation to cell adhesion progesterone signalling has also been shown to enhance cellular migration in MCF-7 and T-47D cells through activation of c-Src/AKT signalling (Wang & Lee, 2016), further implicating its role in modulating cancer phenotype and reducing cellular adhesion in breast cancer.

As we observed an abolished gemcitabine resistance at higher stiffnesses following PR inhibition it indicates that PR signalling may be increased at higher stiffnesses. PR signalling modulates expression of various target proteins such as Cyclin D1 and Wnt (Faivre & Lange, 2007) and also acts within the cytoplasm together with other proteins such as c-Src to activate proliferative pathways such as MAPK (Kariagina, Aupperlee, & Haslam, 2008). Linked to this, gemcitabine treatment also activates MAPK in pancreatic cancer cell lines (Habiro et al., 2004) and Wnt signalling has been linked to gemcitabine

resistance in pancreatic cancer (Jia & Xie, 2015). Secondly it has been reported that both PR-A and PR-B can alter the expression of a different array of genes (Richer et al., 2002). Of note is the specific PR-A-induced overexpression of the bcl-2 family protein, Bcl-xL. Theoretically, the increase in PR-A expression observed at higher stiffnesses in our 2D model following gemcitabine treatment may lead to an increase in Bcl-xL which may contribute to resistance to gemcitabine. Secondly, an increase in Bcl-xL may hold p53 in the cytoplasm which may explain the reduced p53 nuclear accumulation in MCF-7 cells cultured at higher stiffnesses (4 kPa) in our 2D model. Bcl-xL can also be upregulated by STAT3 (Al Zaid Siddiquee & Turkson, 2008), a protein also upregulated by PR signalling (Proietti et al., 2005) and attributed to gemcitabine resistance (Ioannou et al., 2016).

The convergence of gemcitabine resistance, PR signalling and increased stiffness is illustrated in Figure 6.2. Our findings indicate that further investigations are warranted to establish mechanisms of gemcitabine resistance in PR positive breast cancer in relation to stiffness.

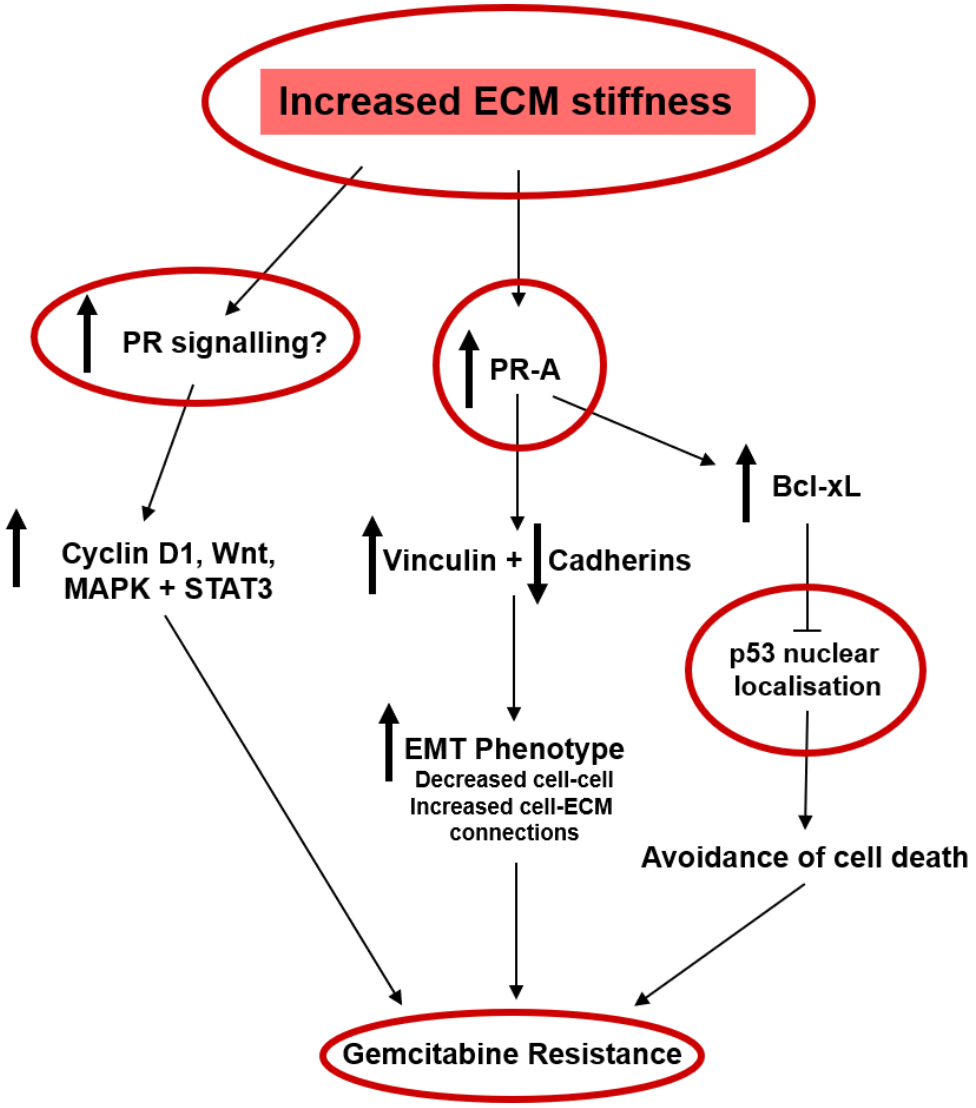

Figure 6.2. Convergence of matrix stiffness, progesterone signalling and resistance to gemcitabine. Schematic representation of the connections between increased extracellular matrix (ECM) stiffness, progesterone receptor (PR) signalling and resistance to gemcitabine. The connections contributed by our models are circled in red. Increased PR signalling may be indicated due to the abolished gemcitabine resistance following PR inhibition, although this would require confirmation.

6.4. Future work.

This thesis demonstrates that resistance to gemcitabine is observed at higher stiffnesses in 2D and 3D *in vitro* models in breast cancer cell lines expressing PRs. Resistance can be abolished with pre-treatment with the PR inhibitor mifepristone, indicating its potential as new treatment strategy in stiff PR+ breast tumours. It is important to confirm inhibition

of PR by mifepristone to verify this relationship. Further development of the 3D model using modified alginate to improve cell attachment, model stability and stiffness would be advantageous to confirm our findings. It would be interesting to investigate if the effect is continued into 3D with the T-47D cell line and with other PR+ cancer cell lines. It would also be interesting to determine the expression of PR in clinical samples of stiffer breast tumours and gemcitabine resistant breast tumours to elucidate the relationship *in vivo*.

In our 2D model p53 nuclear localisation was reduced at higher stiffnesses following gemcitabine treatment in p53-wt MCF-7 cells. This could be due to an increase in Bcl-xL (Figure 6.2.). However, T-47D cells continued the PR and gemcitabine relationship despite lack of p53 expression. It would therefore be interesting to investigate the response to gemcitabine in a range of PR+ and p53 wt or mutant cell lines to determine if p53 expression altered the severity of response. Further, the increase in PR-A expression at higher stiffnesses following gemcitabine treatment would need to be confirmed with further repeats. If found to be significant, investigations into the expression of PR-A affected genes including Bcl-xL and cellular adhesion proteins (Figure 6.2.) may be probative in determining the mechanisms behind PR and gemcitabine mediated signalling.

The relationship between PR and gemcitabine resistance at increased ECM stiffness holds great therapeutic potential. *In vivo* trials of stiffer tumours with and without mifepristone pre-treatment would provide further insight into the use of the combination clinically. This could be investigated using biocompatible 3D models such as alginate (K. Y. Lee & Mooney, 2012) that allow implantation into mice allowing further control of stiffness. Mifepristone is approved clinically for unwanted pregnancy and is currently in

clinical trials for use as a monotherapy in breast cancers with higher PR-A expression indicating its potential for other chemotherapeutic uses. Determining its toxicity for longer term treatment of cancers will therefore be required to observe its efficacy.

7. Bibliography.

Abal, M., Andreu, J. M., & Barasoain, I. (2003). Taxanes: microtubule and centrosome targets, and cell cycle dependent mechanisms of action. *Curr Cancer Drug Targets, 3*(3), 193-203. doi:10.2174/1568009033481967

Abylkassov, R., & Xie, Y. (2016). Role of Yes-associated protein in cancer: An update. *Oncology Letters, 12*(4), 2277-2282. doi:10.3892/ol.2016.4955

Acerbi, I., Cassereau, L., Dean, I., Shi, Q., Au, A., Park, C., . . . Weaver, V. M. (2015). Human breast cancer invasion and aggression correlates with ECM stiffening and immune cell infiltration. *Integrative Biology, 7*(10), 1120-1134. doi:10.1039/c5ib00040h

Acevedo-Acevedo, S., & Crone, W. C. (2015). Substrate stiffness effect and chromosome missegregation in hIPS cells. *Journal of Negative Results in BioMedicine, 14*(1). doi:10.1186/s12952-015-0042-8

Adamska, A., Elaskalani, O., Emmanouilidi, A., Kim, M., Abdol Razak, N. B., Metharom, P., & Falasca, M. (2018). Molecular and cellular mechanisms of chemoresistance in pancreatic cancer. *Adv Biol Regul, 68*, 77-87. doi:10.1016/j.jbior.2017.11.007

Agache, P. G., Monneur, C., Leveque, J. L., & De Rigal, J. (1980). Mechanical properties and Young's modulus of human skin in vivo. *Archives of Dermatological Research, 269*(3), 221-232. doi:10.1007/bf00406415

Ahmed, I. S., Rohe, H. J., Twist, K. E., & Craven, R. J. (2010). Pgrmc1 (Progesterone Receptor Membrane Component 1) Associates with Epidermal Growth Factor Receptor and Regulates Erlotinib Sensitivity. *Journal of Biological Chemistry, 285*(32), 24775-24782. doi:10.1074/jbc.m110.134585

Allison, K. H., Hammond, M. E. H., Dowsett, M., Mckernin, S. E., Carey, L. A., Fitzgibbons, P. L., . . . Wolff, A. C. (2020). Estrogen and Progesterone Receptor Testing in Breast Cancer: ASCO/CAP Guideline Update. *Journal of Clinical Oncology, 38*(12), 1346-1366. doi:10.1200/jco.19.02309

Amaral, J. D., Xavier, J. M., Steer, C. J., & Rodrigues, C. M. (2010). The role of p53 in apoptosis. *Discov Med, 9*(45), 145-152.

Aponte, P. M., & Caicedo, A. (2017). Stemness in Cancer: Stem Cells, Cancer Stem Cells, and Their Microenvironment. *Stem Cells International, 2017*, 5619472. doi:10.1155/2017/5619472

Araki, K., Ebata, T., Guo, A. K., Tobiume, K., Wolf, S. J., & Kawauchi, K. (2015). p53 regulates cytoskeleton remodeling to suppress tumor progression. *Cellular and Molecular Life Sciences, 72*(21), 4077-4094. doi:10.1007/s00018-015-1989-9

Bae, Y. H., Mui, K. L., Hsu, B. Y., Liu, S. L., Cretu, A., Razinia, Z., . . . Assoian, R. K. (2014). A FAK-Cas-Rac-lamellipodin signaling module transduces extracellular matrix stiffness into mechanosensitive cell cycling. *Sci Signal, 7*(330), ra57. doi:10.1126/scisignal.2004838

Barnes, J. M., Przybyla, L., & Weaver, V. M. (2017). Tissue mechanics regulate brain development, homeostasis and disease. *Journal of Cell Science, 130*(1), 71-82. doi:10.1242/jcs.191742

Barney, L. E., Jansen, L. E., Polio, S. R., Galarza, S., Lynch, M. E., & Peyton, S. R. (2016). The Predictive Link between Matrix and Metastasis. *Curr Opin Chem Eng, 11*, 85-93. doi:10.1016/j.coche.2016.01.001

Bell, S., Redmann, A.-L., & Terentjev, E. M. (2019). Universal Kinetics of the Onset of Cell Spreading on Substrates of Different Stiffness. *Biophysical Journal, 116*(3), 551-559. doi:10.1016/j.bpj.2018.12.020

Benad, P., Rauner, M., Rachner, T. D., & Hofbauer, L. C. (2011). The anti-progestin RU-486 inhibits viability of MCF-7 breast cancer cells by suppressing WNT1. *Cancer Letters, 312*(1), 101-108. doi:10.1016/j.canlet.2011.08.006

Bentley, K., Franco, C. A., Philippides, A., Blanco, R., Dierkes, M., Gebala, V., . . . Gerhardt, H. (2014). The role of differential VE-cadherin dynamics in cell rearrangement during angiogenesis. *Nature Cell Biology, 16*(4), 309-321. doi:10.1038/ncb2926

Beretta, G. L., & Zunino, F. (2008). Molecular mechanisms of anthracycline activity. *Top Curr Chem, 283*, 1-19. doi:10.1007/128_2007_3

Berns, E. M. J. J., Foekens, J. A., Van Staveren, I. L., Van Putten, W. L. J., De Koning, H. Y. W. C. M., Portengen, H., & Klijn, J. G. M. (1995). Oncogene amplification and prognosis in breast cancer: Relationship with systemic treatment. *Gene, 159*(1), 11-18. doi:10.1016/0378-1119(94)00534-y

Biscardi, J. S., Ishizawar, R. C., Silva, C. M., & Parsons, S. J. (2000). Tyrosine kinase signalling in breast cancer: Epidermal growth factor receptor and c-Src interactions in breast cancer. *Breast Cancer Research, 2*(3). doi:10.1186/bcr55

Boehm, T. L., Kreis, W., & Drahovsky, D. (1982). Inhibition of thymidylate synthase by hydroxyurea in rapidly proliferating P815 mastocytoma cells. *Biochim Biophys Acta, 696*(1), 52-56. doi:10.1016/0167-4781(82)90009-4

Bonnans, C., Chou, J., & Werb, Z. (2014). Remodelling the extracellular matrix in development and disease. *Nature Reviews Molecular Cell Biology, 15*(12), 786-801. doi:10.1038/nrm3904

Boonyaratanakornkit, V., Mcgowan, E., Sherman, L., Mancini, M. A., Cheskis, B. J., & Edwards, D. P. (2007). The Role of Extranuclear Signaling Actions of Progesterone Receptor in Mediating Progesterone Regulation of Gene Expression and the Cell Cycle. *Molecular Endocrinology, 21*(2), 359-375. doi:10.1210/me.2006-0337

Boonyaratanakornkit, V., Scott, M. P., Ribon, V., Sherman, L., Anderson, S. M., Maller, J. L., . . . Edwards, D. P. (2001). Progesterone Receptor Contains a Proline-Rich Motif that Directly Interacts with SH3 Domains and Activates c-Src Family Tyrosine Kinases. *Molecular Cell, 8*(2), 269-280. doi:10.1016/s1097-2765(01)00304-5

Bordeleau, F., Mason, B. N., Lollis, E. M., Mazzola, M., Zanotelli, M. R., Somasegar, S., . . . Reinhart-King, C. A. (2017). Matrix stiffening promotes a tumor vasculature phenotype. *Proceedings of the National Academy of Sciences, 114*(3), 492-497. doi:10.1073/pnas.1613855114

Borrego-Soto, G., Ortiz-Lopez, R., & Rojas-Martinez, A. (2015). Ionizing radiation-induced DNA injury and damage detection in patients with breast cancer. *Genet Mol Biol, 38*(4), 420-432. doi:10.1590/s1415-475738420150019

Bottino, M. C., Cerliani, J. P., Rojas, P., Giulianelli, S., Soldati, R., Mondillo, C., . . . Lanari, C. (2011). Classical membrane progesterone receptors in murine mammary carcinomas: agonistic effects of progestins and RU-486 mediating rapid non-genomic effects. *Breast Cancer Research and Treatment, 126*(3), 621-636. doi:10.1007/s10549-010-0971-3

Boyd, N. F., Li, Q., Melnichouk, O., Huszti, E., Martin, L. J., Gunasekara, A., . . . Minkin, S. (2014). Evidence That Breast Tissue Stiffness Is Associated with Risk of Breast Cancer. *PLoS ONE, 9*(7), e100937. doi:10.1371/journal.pone.0100937

Bray, F., Ferlay, J., Soerjomataram, I., Siegel, R. L., Torre, L. A., & Jemal, A. (2018). Global cancer statistics 2018: GLOBOCAN estimates of incidence and mortality worldwide for 36 cancers in 185 countries. *68*, 394-424. doi:10.3322/caac.21492

Breslin, S., & O'Driscoll, L. (2013). Three-dimensional cell culture: the missing link in drug discovery. *18*, 240-249. doi:10.1016/j.drudis.2012.10.003

Bruce, A., Alexander, J., Julian, L., Martin, R., Keith, R., & Peter, W. (2002). The Extracellular Matrix of Animals. In *Molecular Biology of the Cell*: Garland Science.

Bryant, H. E., Petermann, E., Schultz, N., Jemth, A.-S., Loseva, O., Issaeva, N., . . . Helleday, T. (2009). PARP is activated at stalled forks to mediate Mre11-

dependent replication restart and recombination. *The EMBO Journal, 28*(17), 2601-2615. doi:10.1038/emboj.2009.206

Bryant, H. E., Schultz, N., Thomas, H. D., Parker, K. M., Flower, D., Lopez, E., . . . Helleday, T. (2005). Specific killing of BRCA2-deficient tumours with inhibitors of poly(ADP-ribose) polymerase. *Nature, 434*(7035), 913-917. doi:10.1038/nature03443

Buehler, M. J. (2006). Nature designs tough collagen: Explaining the nanostructure of collagen fibrils. *Proceedings of the National Academy of Sciences, 103*(33), 12285-12290. doi:10.1073/pnas.0603216103

Burridge, K., & Guilluy, C. (2016). Focal adhesions, stress fibers and mechanical tension. *Experimental Cell Research, 343*(1), 14-20. doi:10.1016/j.yexcr.2015.10.029

Butcher, D. T., Alliston, T., & Weaver, V. M. (2009). A tense situation: forcing tumour progression. *Nature Reviews Cancer, 9*(2), 108-122. doi:10.1038/nrc2544

Buxboim, A., Irianto, J., Swift, J., Athirasala, A., Shin, J. W., Rehfeldt, F., & Discher, D. E. (2017). Coordinated increase of nuclear tension and lamin-A with matrix stiffness outcompetes lamin-B receptor that favors soft tissue phenotypes. *Mol Biol Cell, 28*(23), 3333-3348. doi:10.1091/mbc.E17-06-0393

Caliari, S. R., & Burdick, J. A. (2016). A practical guide to hydrogels for cell culture. *Nature Methods, 13*(5), 405-414. doi:10.1038/nmeth.3839

Capo-chichi, C. D., Cai, K. Q., Smedberg, J., Ganjei-Azar, P., Godwin, A. K., & Xu, X. X. (2011). Loss of A-type lamin expression compromises nuclear envelope integrity in breast cancer. *Chin J Cancer, 30*(6), 415-425. doi:10.5732/cjc.010.10566

Carnevale, I., Capula, M., Giovannetti, E., Schmidt, T., & Coppola, S. (2019). *A mechanical memory of pancreatic cancer cells*. Cold Spring Harbor Laboratory.

Caulfield, S. E., Davis, C. C., & Byers, K. F. (2019). Olaparib: A Novel Therapy for Metastatic Breast Cancer in Patients With a BRCA1/2 Mutation. *J Adv Pract Oncol, 10*(2), 167-174.

Cavo, M., Fato, M., Leonardo, P., Beltrame, F., Raiteri, R., & Scaglione, S. (2016). Microenvironment complexity and matrix stiffness regulate breast cancer cell activity in a 3D in vitro model. *Scientific Reports, 6*. doi:10.1038/srep35367

Chandler, N., Canete, J., & Callery, M. (2004). Caspase-3 drives apoptosis in pancreatic cancer cells after treatment with gemcitabine. *Journal of Gastrointestinal Surgery, 8*(8), 1072-1078. doi:10.1016/j.gassur.2004.09.054

Charles A Janeway, J., Travers, P., Walport, M., & Shlomchik, M. J. (2001). The structure of a typical antibody molecule. In *Immunobiology: The Immune System in Health and Disease*: Garland Science.

Chen, J.-H., Chan, S., Zhang, Y., Li, S., Chang, R.-F., & Su, M.-Y. (2019). Evaluation of breast stiffness measured by ultrasound and breast density measured by MRI using a prone-supine deformation model. *Biomarker Research, 7*(1). doi:10.1186/s40364-019-0171-1

Chen, M., He, M., Song, Y., Chen, L., Xiao, P., Wan, X., . . . Shen, P. (2014). The cytoprotective role of gemcitabine-induced autophagy associated with apoptosis inhibition in triple-negative MDA-MB-231 breast cancer cells. *International Journal of Molecular Medicine, 34*(1), 276-282. doi:10.3892/ijmm.2014.1772

Chen, M., Hough, A. M., & Lawrence, T. S. (2000). The role of p53 in gemcitabine-mediated cytotoxicity and radiosensitization. *45*(5), 369-374. doi:10.1007/s002800051004

Cheng, D., Jin, L., Chen, Y., Xi, X., & Guo, Y. (2020). YAP promotes epithelial mesenchymal transition by upregulating Slug expression in human colorectal cancer cells. *Int J Clin Exp Pathol, 13*(4), 701-710.

Chitcholtan, K., Asselin, E., Parent, S., Sykes, P. H., & Evans, J. J. (2013). Differences in growth properties of endometrial cancer in three dimensional (3D) culture and 2D

cell monolayer. *Experimental Cell Research, 319*(1), 75-87. doi:10.1016/j.yexcr.2012.09.012
Cho, S., Irianto, J., & Discher, D. E. (2017). Mechanosensing by the nucleus: From pathways to scaling relationships. *Journal of Cell Biology, 216*(2), 305-315. doi:10.1083/jcb.201610042
Cho, S., Lee, T. S., Song, I. H., Kim, A.-R., Lee, Y.-J., Kim, H., . . . Hong, H. J. (2017). Combination of anti-L1 cell adhesion molecule antibody and gemcitabine or cisplatin improves the therapeutic response of intrahepatic cholangiocarcinoma. *PLOS ONE, 12*(2), e0170078. doi:10.1371/journal.pone.0170078
Chondrou, V., Stavrou, E. F., Markopoulos, G., Kouraklis-Symeonidis, A., Fotopoulos, V., Symeonidis, A., . . . Sgourou, A. (2018). Impact of ZBTB7A hypomethylation and expression patterns on treatment response to hydroxyurea. *Human Genomics, 12*(1). doi:10.1186/s40246-018-0177-z
Chuang, C.-H., Lin, R.-Z., Melero-Martin, J. M., & Chen, Y.-C. (2018). Comparison of covalently and physically cross-linked collagen hydrogels on mediating vascular network formation for engineering adipose tissue. *Artificial Cells, Nanomedicine, and Biotechnology, 46*(sup3), S434-S447. doi:10.1080/21691401.2018.1499660
ClinicalTrials.gov. (2020). Mifepristone for Breast Cancer Patients With Higher Levels of Progesterone Receptor Isoform A Than Isoform B. Retrieved from https://clinicaltrials.gov/ct2/show/NCT02651844
Colvin, M. (2003). Alkylating Agents. In *Holland-Frei Cancer Medicine* (6 ed.): BC Decker.
Conneely, O. M., Mulac-Jericevic, B., Lydon, J. P., & De Mayo, F. J. (2001). Reproductive functions of the progesterone receptor isoforms: lessons from knock-out mice. *Mol Cell Endocrinol, 179*(1-2), 97-103. doi:10.1016/s0303-7207(01)00465-8
Conway, D. E., Breckenridge, M. T., Hinde, E., Gratton, E., Chen, C. S., & Schwartz, M. A. (2013). Fluid Shear Stress on Endothelial Cells Modulates Mechanical Tension across VE-Cadherin and PECAM-1. *Current Biology, 23*(11), 1024-1030. doi:10.1016/j.cub.2013.04.049
Coon, B. G., Baeyens, N., Han, J., Budatha, M., Ross, T. D., Fang, J. S., . . . Schwartz, M. A. (2015). Intramembrane binding of VE-cadherin to VEGFR2 and VEGFR3 assembles the endothelial mechanosensory complex. *J Cell Biol, 208*(7), 975-986. doi:10.1083/jcb.201408103
Cox, T. R., & Erler, J. T. (2011). Remodeling and homeostasis of the extracellular matrix: implications for fibrotic diseases and cancer. *Disease Models & Mechanisms, 4*(2), 165-178. doi:10.1242/dmm.004077
De Sousa Cavalcante, L., & Monteiro, G. (2014). Gemcitabine: Metabolism and molecular mechanisms of action, sensitivity and chemoresistance in pancreatic cancer. *European Journal of Pharmacology, 741*, 8-16. doi:10.1016/j.ejphar.2014.07.041
Demarzo, A. M., Beck, C. A., Onate, S. A., & Edwards, D. P. (1991). Dimerization of mammalian progesterone receptors occurs in the absence of DNA and is related to the release of the 90-kDa heat shock protein. *Proceedings of the National Academy of Sciences, 88*(1), 72-76. doi:10.1073/pnas.88.1.72
Denais, C. M., Gilbert, R. M., Isermann, P., McGregor, A. L., Te Lindert, M., Weigelin, B., . . . Lammerding, J. (2016). Nuclear envelope rupture and repair during cancer cell migration. *Science (New York, N.Y.), 352*(6283), 353. doi:10.1126/science.aad7297
Denisin, A. K., & Pruitt, B. L. (2016). Tuning the Range of Polyacrylamide Gel Stiffness for Mechanobiology Applications. *ACS Applied Materials & Interfaces, 8*(34), 21893-21902. doi:10.1021/acsami.5b09344
Desai, R. M., Koshy, S. T., Hilderbrand, S. A., Mooney, D. J., & Joshi, N. S. (2015). Versatile click alginate hydrogels crosslinked via tetrazine–norbornene chemistry. *Biomaterials, 50*, 30-37. doi:10.1016/j.biomaterials.2015.01.048

Dhananjayan, S. C., Ramamoorthy, S., Khan, O. Y., Ismail, A., Sun, J., Slingerland, J., . . . Nawaz, Z. (2006). WW Domain Binding Protein-2, an E6-Associated Protein Interacting Protein, Acts as a Coactivator of Estrogen and Progesterone Receptors. *Molecular Endocrinology, 20*(10), 2343-2354. doi:10.1210/me.2005-0533

Diaz Flaqué, M. C., Vicario, R., Proietti, C. J., Izzo, F., Schillaci, R., & Elizalde, P. V. (2013). Progestin drives breast cancer growth by inducing p21CIP1 expression through the assembly of a transcriptional complex among Stat3, progesterone receptor and ErbB-2. *Steroids, 78*(6), 559-567. doi:10.1016/j.steroids.2012.11.003

Ding, W., Li, Z., Wang, C., Dai, J., Ruan, G., & Tu, C. (2018). Anthracycline versus nonanthracycline adjuvant therapy for early breast cancer. *Medicine, 97*(42), e12908. doi:10.1097/md.0000000000012908

Domura, R., Sasaki, R., Ishikawa, Y., & Okamoto, M. (2017). Cellular Morphology-Mediated Proliferation and Drug Sensitivity of Breast Cancer Cells. *J Funct Biomater, 8*(2). doi:10.3390/jfb8020018

Duan, B., Hockaday, L. A., Kapetanovic, E., Kang, K. H., & Butcher, J. T. (2013). Stiffness and adhesivity control aortic valve interstitial cell behavior within hyaluronic acid based hydrogels. *Acta Biomaterialia, 9*(8), 7640-7650. doi:10.1016/j.actbio.2013.04.050

Dube, S., Thomas, A., Abbott, L., Benz, P., Mitschow, C., Dube, D. K., & Poiesz, B. J. (2016). Expression of tropomyosin 2 gene isoforms in human breast cancer cell lines. *Oncology Reports, 35*(6), 3143-3150. doi:10.3892/or.2016.4732

Dupont, S., Morsut, L., Aragona, M., Enzo, E., Giulitti, S., Cordenonsi, M., . . . Piccolo, S. (2011). Role of YAP/TAZ in mechanotransduction. *Nature, 474*(7350), 179-183. doi:10.1038/nature10137

Dybdal-Hargreaves, N. F., Risinger, A. L., & Mooberry, S. L. (2018). Regulation of E-cadherin localization by microtubule targeting agents: rapid promotion of cortical E-cadherin through p130Cas/Src inhibition by eribulin. *Oncotarget, 9*(5), 5545-5561. doi:10.18632/oncotarget.23798

Ebata, T., Mitsui, Y., Sugimoto, W., Maeda, M., Araki, K., Machiyama, H., . . . Kawauchi, K. (2017). Substrate Stiffness Influences Doxorubicin-Induced p53 Activation via ROCK2 Expression. *BioMed Research International, 2017*, 1-10. doi:10.1155/2017/5158961

Effler, J. C., Kee, Y.-S., Berk, J. M., Tran, M. N., Iglesias, P. A., & Douglas. (2006). Mitosis-Specific Mechanosensing and Contractile-Protein Redistribution Control Cell Shape. *Current Biology, 16*(19), 1962-1967. doi:10.1016/j.cub.2006.08.027

Evans, A., Armstrong, S., Whelehan, P., Thomson, K., Rauchhaus, P., Purdie, C., . . . Vinnicombe, S. (2013). Can shear-wave elastography predict response to neoadjuvant chemotherapy in women with invasive breast cancer? *British Journal of Cancer, 109*(11), 2798-2802. doi:10.1038/bjc.2013.660

Ewald, B., Sampath, D., & Plunkett, W. (2007). H2AX phosphorylation marks gemcitabine-induced stalled replication forks and their collapse upon S-phase checkpoint abrogation. *Molecular Cancer Therapeutics, 6*(4), 1239-1248. doi:10.1158/1535-7163.mct-06-0633

Faivre, E. J., & Lange, C. A. (2007). Progesterone Receptors Upregulate Wnt-1 To Induce Epidermal Growth Factor Receptor Transactivation and c-Src-Dependent Sustained Activation of Erk1/2 Mitogen-Activated Protein Kinase in Breast Cancer Cells. *Molecular and Cellular Biology, 27*(2), 466-480. doi:10.1128/mcb.01539-06

Falou, O., Sadeghi-Naini, A., Prematilake, S., Sofroni, E., Papanicolau, N., Iradji, S., . . . Czarnota, G. J. (2013). Evaluation of Neoadjuvant Chemotherapy Response in Women with Locally Advanced Breast Cancer Using Ultrasound Elastography. *Translational Oncology, 6*(1), 17-24. doi:10.1593/tlo.12412

Fang, C., & Yang, T. (2019). Value of tissue elastography in the prediction of efficacy of neoadjuvant chemotherapy in breast cancer. *J buon, 24*(2), 555-559.
Felipe Lima, J., Nofech-Mozes, S., Bayani, J., & Bartlett, J. (2016). EMT in Breast Carcinoma—A Review. *Journal of Clinical Medicine, 5*(7), 65. doi:10.3390/jcm5070065
Feng, Y., Spezia, M., Huang, S., Yuan, C., Zeng, Z., Zhang, L., . . . Ren, G. (2018). Breast cancer development and progression: Risk factors, cancer stem cells, signaling pathways, genomics, and molecular pathogenesis. *Genes & Diseases, 5*(2), 77-106. doi:10.1016/j.gendis.2018.05.001
Fernandes, J., Sannachi, L., Tran, W. T., Koven, A., Watkins, E., Hadizad, F., . . . Czarnota, G. (2019). Monitoring Breast Cancer Response to Neoadjuvant Chemotherapy Using Ultrasound Strain Elastography. *Transl Oncol, 12*(9), 1177-1184. doi:10.1016/j.tranon.2019.05.004
Ferreira, C. G., Span, S. W., Peters, G. J., Kruyt, F. A., & Giaccone, G. (2000). Chemotherapy triggers apoptosis in a caspase-8-dependent and mitochondria-controlled manner in the non-small cell lung cancer cell line NCI-H460. *Cancer Res, 60*(24), 7133-7141.
Fischer, R. S., Myers, K. A., Gardel, M. L., & Waterman, C. M. (2012). Stiffness-controlled three-dimensional extracellular matrices for high-resolution imaging of cell behavior. *Nature Protocols, 7*(11), 2056-2066. doi:10.1038/nprot.2012.127
Fleseriu, M., Biller, B. M. K., Findling, J. W., Molitch, M. E., Schteingart, D. E., Gross, C., . . . Weiss, R. (2012). Mifepristone, a Glucocorticoid Receptor Antagonist, Produces Clinical and Metabolic Benefits in Patients with Cushing's Syndrome. *The Journal of Clinical Endocrinology & Metabolism, 97*(6), 2039-2049. doi:10.1210/jc.2011-3350
Fortuny, A., & Polo, S. E. (2018). The response to DNA damage in heterochromatin domains. *Chromosoma, 127*(3), 291-300. doi:10.1007/s00412-018-0669-6
Fouad, M. A., Salem, S. E., Hussein, M. M., Zekri, A. R. N., Hafez, H. F., El Desouky, E. D., & Shouman, S. A. (2018). Impact of Global DNA Methylation in Treatment Outcome of Colorectal Cancer Patients. *Frontiers in Pharmacology, 9*. doi:10.3389/fphar.2018.01173
Fragomeni, S. M., Sciallis, A., & Jeruss, J. S. (2018). Molecular Subtypes and Local-Regional Control of Breast Cancer. *27*, 95-120. doi:10.1016/j.soc.2017.08.005
Frantz, C., Stewart, K. M., & Weaver, V. M. (2010). The extracellular matrix at a glance. *Journal of Cell Science, 123*(24), 4195-4200. doi:10.1242/jcs.023820
Gallant, N. D., Michael, K. E., & García, A. J. (2005). Cell Adhesion Strengthening: Contributions of Adhesive Area, Integrin Binding, and Focal Adhesion Assembly. *Molecular Biology of the Cell, 16*(9), 4329-4340. doi:10.1091/mbc.e05-02-0170
Galmarini, C. M. A., Clarke, M. L., Falette, N., Puisieux, A., Mackey, J. R., & Dumontet, C. (2002). Expression of a non-functional p53 affects the sensitivity of cancer cells to gemcitabine. *International Journal of Cancer, 97*(4), 439-445. doi:10.1002/ijc.1628
Gandhi, V., & Plunkett, W. (1990). Modulatory activity of 2',2'-difluorodeoxycytidine on the phosphorylation and cytotoxicity of arabinosyl nucleosides. *Cancer Res, 50*(12), 3675-3680.
Garg, D., Ng, S. S. M., Baig, K. M., Driggers, P., & Segars, J. (2017). Progesterone-Mediated Non-Classical Signaling. *Trends in Endocrinology & Metabolism, 28*(9), 656-668. doi:10.1016/j.tem.2017.05.006
Gavard, J. (2014). Endothelial permeability and VE-cadherin. *Cell Adhesion & Migration, 8*(2), 158-164. doi:10.4161/cam.29026
Goodin, S. (2008). Ixabepilone: A novel microtubule-stabilizing agent for the treatment of metastatic breast cancer. *American Journal of Health-System Pharmacy, 65*(21), 2017-2026. doi:10.2146/ajhp070628

Graham, J. D., Yager, M. L., Hill, H. D., Byth, K., O'Neill, G. M., & Clarke, C. L. (2005). Altered Progesterone Receptor Isoform Expression Remodels Progestin Responsiveness of Breast Cancer Cells. *Molecular Endocrinology, 19*(11), 2713-2735. doi:10.1210/me.2005-0126

Graham, J. D., Yeates, C., Balleine, R. L., Harvey, S. S., Milliken, J. S., Bilous, A. M., & Clarke, C. L. (1995). Characterization of progesterone receptor A and B expression in human breast cancer. *Cancer Res, 55*(21), 5063-5068.

Griguolo, G., Dieci, M. V., Guarneri, V., & Conte, P. (2018). Olaparib for the treatment of breast cancer. *Expert Rev Anticancer Ther, 18*(6), 519-530. doi:10.1080/14737140.2018.1458613

Habiro, A., Tanno, S., Koizumi, K., Izawa, T., Nakano, Y., Osanai, M., . . . Kohgo, Y. (2004). Involvement of p38 mitogen-activated protein kinase in gemcitabine-induced apoptosis in human pancreatic cancer cells. *Biochem Biophys Res Commun, 316*(1), 71-77. doi:10.1016/j.bbrc.2004.02.017

Hagmann, W., Jesnowski, R., & Löhr, J. M. (2010). Interdependence of gemcitabine treatment, transporter expression, and resistance in human pancreatic carcinoma cells. *Neoplasia, 12*(9), 740-747. doi:10.1593/neo.10576

Hamid, R., Rotshteyn, Y., Rabadi, L., Parikh, R., & Bullock, P. (2004). Comparison of alamar blue and MTT assays for high through-put screening. *Toxicol In Vitro, 18*(5), 703-710. doi:10.1016/j.tiv.2004.03.012

Harada, T., Swift, J., Irianto, J., Shin, J.-W., Spinler, K. R., Athirasala, A., . . . Discher, D. E. (2014). Nuclear lamin stiffness is a barrier to 3D migration, but softness can limit survival. *The Journal of Cell Biology, 204*(5), 669-682. doi:10.1083/jcb.201308029

Hartsock, A., & Nelson, W. J. (2008). Adherens and tight junctions: Structure, function and connections to the actin cytoskeleton. *Biochimica et Biophysica Acta (BBA) - Biomembranes, 1778*(3), 660-669. doi:10.1016/j.bbamem.2007.07.012

Hasty, P., & Montagna, C. (2014). Chromosomal rearrangements in cancer. *Molecular & Cellular Oncology, 1*(1), e29904. doi:10.4161/mco.29904

Hayashi, M., Yamamoto, Y., Ibusuki, M., Fujiwara, S., Yamamoto, S., Tomita, S., . . . Iwase, H. (2012). Evaluation of Tumor Stiffness by Elastography Is Predictive for Pathologic Complete Response to Neoadjuvant Chemotherapy in Patients with Breast Cancer. *Annals of Surgical Oncology, 19*(9), 3042-3049. doi:10.1245/s10434-012-2343-1

Heinemann, V., Xu, Y. Z., Chubb, S., Sen, A., Hertel, L. W., Grindey, G. B., & Plunkett, W. (1990). Inhibition of ribonucleotide reduction in CCRF-CEM cells by 2',2'-difluorodeoxycytidine. *Mol Pharmacol, 38*(4), 567-572.

Hertel, L. W., Kroin, J. S., Misner, J. W., & Tustin, J. M. (1988). Synthesis of 2-deoxy-2,2-difluoro-D-ribose and 2-deoxy-2,2'-difluoro-D-ribofuranosyl nucleosides. *The Journal of Organic Chemistry, 53*(11), 2406-2409. doi:10.1021/jo00246a002

Higa, G. M., & Abraham, J. (2007). Lapatinib in the treatment of breast cancer. *Expert Rev Anticancer Ther, 7*(9), 1183-1192. doi:10.1586/14737140.7.9.1183

Hill, K. K., Roemer, S. C., Churchill, M. E. A., & Edwards, D. P. (2012). Structural and functional analysis of domains of the progesterone receptor. *Molecular and Cellular Endocrinology, 348*(2), 418-429. doi:10.1016/j.mce.2011.07.017

Honeywell, R. J., Ruiz Van Haperen, V. W. T., Veerman, G., Smid, K., & Peters, G. J. (2015). Inhibition of thymidylate synthase by 2′,2′-difluoro-2′-deoxycytidine (Gemcitabine) and its metabolite 2′,2′-difluoro-2′-deoxyuridine. *The International Journal of Biochemistry & Cell Biology, 60*, 73-81. doi:10.1016/j.biocel.2014.12.010

Hopp, T. A. (2004). Breast Cancer Patients with Progesterone Receptor PR-A-Rich Tumors Have Poorer Disease-Free Survival Rates. *Clinical Cancer Research, 10*(8), 2751-2760. doi:10.1158/1078-0432.ccr-03-0141

Horwitz, S. B. (1994). Taxol (paclitaxel): mechanisms of action. *Ann Oncol, 5 Suppl 6*, S3-6.

Huang, L., Ma, M., Du, Z., Liu, Z., & Gong, X. (2019). Quantitative evaluation of tissue stiffness around lesion by sound touch elastography in the diagnosis of benign and malignant breast lesions. *PLOS ONE, 14*(7), e0219943. doi:10.1371/journal.pone.0219943

Huang, P., Chubb, S., Hertel, L. W., Grindey, G. B., & Plunkett, W. (1991). Action of 2',2'-difluorodeoxycytidine on DNA synthesis. *Cancer Res, 51*(22), 6110-6117.

Hui, L., Zhang, J., Ding, X., Guo, X., & Jiang, X. (2017). Matrix stiffness regulates the proliferation, stemness and chemoresistance of laryngeal squamous cancer cells. *International Journal of Oncology, 50*(4), 1439-1447. doi:10.3892/ijo.2017.3877

Ioannou, N., Seddon, A. M., Dalgleish, A., Mackintosh, D., Solca, F., & Modjtahedi, H. (2016). Acquired resistance of pancreatic cancer cells to treatment with gemcitabine and HER-inhibitors is accompanied by increased sensitivity to STAT3 inhibition. *International Journal of Oncology, 48*(3), 908-918. doi:10.3892/ijo.2016.3320

Isono, S., Fujishima, M., Azumi, T., Hashimoto, Y., Komoike, Y., Yukawa, M., & Watatani, M. (2014). O6-methylguanine-DNA methyltransferase as a prognostic and predictive marker for basal-like breast cancer treated with cyclophosphamide-based chemotherapy. *Oncology Letters, 7*(6), 1778-1784. doi:10.3892/ol.2014.1985

Jacobsen, B. M., & Horwitz, K. B. (2012). Progesterone receptors, their isoforms and progesterone regulated transcription. *Mol Cell Endocrinol, 357*(1-2), 18-29. doi:10.1016/j.mce.2011.09.016

Janeway, C. A. J., Travers, P., Walport, M., & Shlomchik, M. J. (2001). The structure of a typical antibody molecule. In *Immunobiology: The Immune System in Health and Disease*: Garland Science.

Janmey, P. A., Georges, P. C., & Hvidt, S. (2007). Basic rheology for biologists. *Methods Cell Biol, 83*, 3-27. doi:10.1016/s0091-679x(07)83001-9

Jevtić, P., Edens, L. J., Vuković, L. D., & Levy, D. L. (2014). Sizing and shaping the nucleus: mechanisms and significance. *Current Opinion in Cell Biology, 28*, 16-27. doi:10.1016/j.ceb.2014.01.003

Jia, Y., & Xie, J. (2015). Promising molecular mechanisms responsible for gemcitabine resistance in cancer. *Genes & Diseases, 2*(4), 299-306. doi:10.1016/j.gendis.2015.07.003

Jing, H., Cheng, W., Li, Z.-Y., Ying, L., Wang, Q.-C., Wu, T., & Tian, J.-W. (2016). Early Evaluation of Relative Changes in Tumor Stiffness by Shear Wave Elastography Predicts the Response to Neoadjuvant Chemotherapy in Patients With Breast Cancer. *Journal of Ultrasound in Medicine, 35*(8), 1619-1627. doi:10.7863/ultra.15.08052

Jones, R. M., Kotsantis, P., Stewart, G. S., Groth, P., & Petermann, E. (2014). BRCA2 and RAD51 Promote Double-Strand Break Formation and Cell Death in Response to Gemcitabine. *Molecular Cancer Therapeutics, 13*(10), 2412-2421. doi:10.1158/1535-7163.mct-13-0862

Jordheim, L. P., Guittet, O., Lepoivre, M., Galmarini, C. M., & Dumontet, C. (2005). Increased expression of the large subunit of ribonucleotide reductase is involved in resistance to gemcitabine in human mammary adenocarcinoma cells. *Mol Cancer Ther, 4*(8), 1268-1276. doi:10.1158/1535-7163.mct-05-0121

Joyce, M. H., Lu, C., James, E. R., Hegab, R., Allen, S. C., Suggs, L. J., & Brock, A. (2018). Phenotypic Basis for Matrix Stiffness-Dependent Chemoresistance of Breast Cancer Cells to Doxorubicin. *Frontiers in Oncology, 8*. doi:10.3389/fonc.2018.00337

Kam, Y., & Quaranta, V. (2009). Cadherin-Bound β-Catenin Feeds into the Wnt Pathway upon Adherens Junctions Dissociation: Evidence for an Intersection between β-Catenin Pools. *PLoS ONE, 4*(2), e4580. doi:10.1371/journal.pone.0004580
Kandoth, C., Mclellan, M. D., Vandin, F., Ye, K., Niu, B., Lu, C., . . . Ding, L. (2013). Mutational landscape and significance across 12 major cancer types. *Nature, 502*(7471), 333-339. doi:10.1038/nature12634
Kariagina, A., Aupperlee, M. D., & Haslam, S. Z. (2008). Progesterone receptor isoform functions in normal breast development and breast cancer. *Crit Rev Eukaryot Gene Expr, 18*(1), 11-33. doi:10.1615/critreveukargeneexpr.v18.i1.20
Kastner, P., Krust, A., Turcotte, B., Stropp, U., Tora, L., Gronemeyer, H., & Chambon, P. (1990). Two distinct estrogen-regulated promoters generate transcripts encoding the two functionally different human progesterone receptor forms A and B. *The EMBO Journal, 9*(5), 1603-1614. doi:10.1002/j.1460-2075.1990.tb08280.x
Katyan, A., Mittal, M. K., Mani, C., & Mandal, A. K. (2019). Strain wave elastography in response assessment to neo-adjuvant chemotherapy in patients with locally advanced breast cancer. *Br J Radiol, 92*(1099), 20180515. doi:10.1259/bjr.20180515
Kharbanda, S., Pandey, P., Schofield, L., Israels, S., Roncinske, R., Yoshida, K., . . . Kufe, D. (1997). Role for Bcl-xL as an inhibitor of cytosolic cytochrome C accumulation in DNA damage-induced apoptosis. *Proceedings of the National Academy of Sciences, 94*(13), 6939-6942. doi:10.1073/pnas.94.13.6939
Khavari, A., Nydén, M., Weitz, D. A., & Ehrlicher, A. J. (2016). Composite alginate gels for tunable cellular microenvironment mechanics. *Scientific Reports, 6*(1), 30854. doi:10.1038/srep30854
Kim, D. H., & Wirtz, D. (2013). Focal adhesion size uniquely predicts cell migration. *The FASEB Journal, 27*(4), 1351-1361. doi:10.1096/fj.12-220160
King, M. C., & Lusk, C. P. (2016). A model for coordinating nuclear mechanics and membrane remodeling to support nuclear integrity. *Curr Opin Cell Biol, 41*, 9-17. doi:10.1016/j.ceb.2016.03.009
Kitao, H., Iimori, M., Kataoka, Y., Wakasa, T., Tokunaga, E., Saeki, H., . . . Maehara, Y. (2018). DNA replication stress and cancer chemotherapy. *Cancer Science, 109*(2), 264-271. doi:10.1111/cas.13455
Klein, E. A., Yin, L., Kothapalli, D., Castagnino, P., Byfield, F. J., Xu, T., . . . Assoian, R. K. (2009). Cell-Cycle Control by Physiological Matrix Elasticity and In Vivo Tissue Stiffening. *Current Biology, 19*(18), 1511-1518. doi:10.1016/j.cub.2009.07.069
Kloxin, A. M., Kasko, A. M., Salinas, C. N., & Anseth, K. S. (2009). Photodegradable Hydrogels for Dynamic Tuning of Physical and Chemical Properties. *Science, 324*(5923), 59-63. doi:10.1126/science.1169494
Kocgozlu, L., Lavalle, P., Koenig, G., Senger, B., Haikel, Y., Schaaf, P., . . . Vautier, D. (2010). Selective and uncoupled role of substrate elasticity in the regulation of replication and transcription in epithelial cells. *Journal of Cell Science, 123*(1), 29-39. doi:10.1242/jcs.053520
Kocgozlu, L., Rabineau, M., Koenig, G., Haikel, Y., Schaaf, P., Freund, J.-N., . . . Vautier, D. (2012). The control of chromosome segregation during mitosis in epithelial cells by substrate elasticity. *Biomaterials, 33*(3), 798-809. doi:10.1016/j.biomaterials.2011.10.024
Kornmuller, A., Brown, C. F. C., Yu, C., & Flynn, L. E. (2017). Fabrication of Extracellular Matrix-derived Foams and Microcarriers as Tissue-specific Cell Culture and Delivery Platforms. *J Vis Exp*(122). doi:10.3791/55436
Kovačič, S., & Silverstein, M. S. (2017). Hydrogels through emulsion templating: sequential polymerization and double networks. *Polym. Chem., 8*(40), 6319-6328. doi:10.1039/c7py01305a

Kumar, R., Srivastava, R., & Srivastava, S. (2015). Detection and Classification of Cancer from Microscopic Biopsy Images Using Clinically Significant and Biologically Interpretable Features. *Journal of Medical Engineering, 2015*, 1-14. doi:10.1155/2015/457906

Lanari, C., Wargon, V., Rojas, P., & Molinolo, A. A. (2012). Antiprogestins in breast cancer treatment: are we ready? *Endocrine-Related Cancer, 19*(3), R35-R50. doi:10.1530/erc-11-0378

Larsen, B. E., Bjørnstad, J., Pettersen, E. O., Tønnesen, H. H., & Melvik, J. E. (2015). Rheological characterization of an injectable alginate gel system. *BMC biotechnology., 15*(1). doi:10.1186/s12896-015-0147-7

LaValley, D. J., Zanotelli, M. R., Bordeleau, F., Wang, W., Schwager, S. C., & Reinhart-King, C. A. (2017). Matrix Stiffness Enhances VEGFR-2 Internalization, Signaling, and Proliferation in Endothelial Cells. *Converg Sci Phys Oncol, 3*. doi:10.1088/2057-1739/aa9263

Lee, J. Y., Chang, J. K., Dominguez, A. A., Lee, H.-P., Nam, S., Chang, J., . . . Chaudhuri, O. (2019). YAP-independent mechanotransduction drives breast cancer progression. *Nature Communications, 10*(1). doi:10.1038/s41467-019-09755-0

Lee, K. Y., & Mooney, D. J. (2012). Alginate: Properties and biomedical applications. *37*, 106-126. doi:10.1016/j.progpolymsci.2011.06.003

Lehn, S., Tobin, N. P., Sims, A. H., Stål, O., Jirström, K., Axelson, H., & Landberg, G. (2014). Decreased expression of Yes-associated protein is associated with outcome in the luminal A breast cancer subgroup and with an impaired tamoxifen response. *BMC Cancer, 14*(1), 119. doi:10.1186/1471-2407-14-119

LeRoux, M. A., Guilak F Fau - Setton, L. A., & Setton, L. A. (1999). Compressive and shear properties of alginate gel: effects of sodium ions and alginate concentration. (0021-9304 (Print)).

Leroy, B., Fournier, J. L., Ishioka, C., Monti, P., Inga, A., Fronza, G., & Soussi, T. (2013). The TP53 website: an integrative resource centre for the TP53 mutation database and TP53 mutant analysis. *Nucleic Acids Res, 41*(Database issue), D962-969. doi:10.1093/nar/gks1033

Levental, K. R., Yu, H., Kass, L., Lakins, J. N., Egeblad, M., Erler, J. T., . . . Weaver, V. M. (2009). Matrix Crosslinking Forces Tumor Progression by Enhancing Integrin Signaling. *Cell, 139*(5), 891-906. doi:10.1016/j.cell.2009.10.027

Lilly, E. (1996). Gemzar (gemcitabine HCL). Retrieved from https://www.centerwatch.com/directories/1067-fda-approved-drugs/listing/3570-gemzar-gemcitabine-hcl

Lilly, E. (2004). FDA Grants Approval for Lilly's Gemzar in Combination with Taxol as First-Line Treatment for Metastatic Breast Cancer. Retrieved from https://investor.lilly.com/news-releases/news-release-details/fda-grants-approval-lillys-gemzar-combination-taxol-first-line

Lim, E., Palmieri, C., & Tilley, W. D. (2016). Renewed interest in the progesterone receptor in breast cancer. *British Journal of Cancer, 115*(8), 909-911. doi:10.1038/bjc.2016.303

Linwang, Y. Y., Jan, M. Y., Shyu, C. S., Chiang, C. A., & Wang, W. K. (2004). The Natural Frequencies of the Arterial System and Their Relation to the Heart Rate. *IEEE Transactions on Biomedical Engineering, 51*(1), 193-195. doi:10.1109/tbme.2003.820378

Lodish, H., Berk, A., Zipursky, S. L., Matsudaira, P., Baltimore, D., & Darnell, J. (2000). The Role of Topoisomerases in DNA Replication. In: W. H. Freeman.

Longley, D. B., Harkin, D. P., & Johnston, P. G. (2003). 5-Fluorouracil: mechanisms of action and clinical strategies. *Nature Reviews Cancer, 3*(5), 330-338. doi:10.1038/nrc1074

Louie, M. C., & Sevigny, M. B. (2017). Steroid hormone receptors as prognostic markers in breast cancer. *Am J Cancer Res, 7*(8), 1617-1636.

Lovett, D. B., Shekhar, N., Nickerson, J. A., Roux, K. J., & Lele, T. P. (2013). Modulation of Nuclear Shape by Substrate Rigidity. *6*(2), 230-238. doi:10.1007/s12195-013-0270-2

Lutolf, M. P., Lauer-Fields, J. L., Schmoekel, H. G., Metters, A. T., Weber, F. E., Fields, G. B., & Hubbell, J. A. (2003). Synthetic matrix metalloproteinase-sensitive hydrogels for the conduction of tissue regeneration: Engineering cell-invasion characteristics. *Proceedings of the National Academy of Sciences, 100*(9), 5413-5418. doi:10.1073/pnas.0737381100

Mackey, J. R., Mani, R. S., Selner, M., Mowles, D., Young, J. D., Belt, J. A., . . . Cass, C. E. (1998). Functional nucleoside transporters are required for gemcitabine influx and manifestation of toxicity in cancer cell lines. *Cancer Res, 58*(19), 4349-4357.

Madhusudhana Rao, K., Anbananthan, N., & Varada Rajulu, A. (2011). Bicontinuous highly cross-linked poly(acrylamide-co-ethyleneglycol dimethacrylate) porous materials synthesized within high internal phase emulsions. *Soft Matter, 7*(22), 10780. doi:10.1039/c1sm06084h

Maier, B., Bensimon, D., & Croquette, V. (2000). Replication by a single DNA polymerase of a stretched single-stranded DNA. *Proceedings of the National Academy of Sciences, 97*(22), 12002-12007. doi:10.1073/pnas.97.22.12002

Marsh, P., & Williamson, G. R. (2019). What is the Current Effectiveness of Olaparib for Breast Cancer Patients with a BRCA Mutation? A Systematic Review. *The Open Nursing Journal, 13*(1), 39-59. doi:10.2174/1874434601913010039

Martino, E., Casamassima, G., Castiglione, S., Cellupica, E., Pantalone, S., Papagni, F., . . . Collina, S. (2018). Vinca alkaloids and analogues as anti-cancer agents: Looking back, peering ahead. *Bioorg Med Chem Lett, 28*(17), 2816-2826. doi:10.1016/j.bmcl.2018.06.044

Maya-Mendoza, A., Moudry, P., Merchut-Maya, J. M., Lee, M., Strauss, R., & Bartek, J. (2018). High speed of fork progression induces DNA replication stress and genomic instability. *Nature, 559*(7713), 279-284. doi:10.1038/s41586-018-0261-5

Mayr, M., Hu, Y., Hainaut, P., & Xu, Q. (2002). Mechanical Stress-induced DNA damage and rac-p38MAPK Signal Pathways Mediate p53-dependent Apoptosis in Vascular Smooth Muscle Cells. *The FASEB Journal, 16*(11), 1423-1425. doi:10.1096/fj.02-0042fje

Mbalaviele, G., Dunstan, C. R., Sasaki, A., Williams, P. J., Mundy, G. R., & Yoneda, T. (1996). E-cadherin expression in human breast cancer cells suppresses the development of osteolytic bone metastases in an experimental metastasis model. *Cancer Res, 56*(17), 4063-4070.

McCluskey, G. D., Mohamady, S., Taylor, S. D., & Bearne, S. L. (2016). Exploring the Potent Inhibition of CTP Synthase by Gemcitabine-5'-Triphosphate. *Chembiochem, 17*(23), 2240-2249. doi:10.1002/cbic.201600405

McGowan, J. V., Chung, R., Maulik, A., Piotrowska, I., Walker, J. M., & Yellon, D. M. (2017). Anthracycline Chemotherapy and Cardiotoxicity. *Cardiovascular Drugs and Therapy, 31*(1), 63-75. doi:10.1007/s10557-016-6711-0

Medina, S. H., Bush, B., Cam, M., Sevcik, E., DelRio, F. W., Nandy, K., & Schneider, J. P. (2019). Identification of a mechanogenetic link between substrate stiffness and chemotherapeutic response in breast cancer. *Biomaterials, 202*, 1-11. doi:10.1016/j.biomaterials.2019.02.018

Mei, L., Zhang, J., He, K., & Zhang, J. (2019). Ataxia telangiectasia and Rad3-related inhibitors and cancer therapy: where we stand. *Journal of Hematology & Oncology, 12*(1). doi:10.1186/s13045-019-0733-6

Mih, J. D., Marinkovic, A., Liu, F., Sharif, A. S., & Tschumperlin, D. J. (2012). Matrix stiffness reverses the effect of actomyosin tension on cell proliferation. *Journal of Cell Science, 125*(24), 5974-5983. doi:10.1242/jcs.108886

Mini, E., Nobili, S., Caciagli, B., Landini, I., & Mazzei, T. (2006). Cellular pharmacology of gemcitabine. *Ann Oncol, 17 Suppl 5*, v7-12. doi:10.1093/annonc/mdj941

Misao, R., Nakanishi, Y., Iwagaki, S., Fujimoto, J., & Tamaya, T. (1998). Expression of progesterone receptor isoforms in corpora lutea of human subjects: correlation with serum oestrogen and progesterone concentrations. *Molecular Human Reproduction, 4*(11), 1045-1052. doi:10.1093/molehr/4.11.1045

Misrahi, M., Venencie, P.-Y., Saugier-Veber, P., Sar, S., Dessen, P., & Milgrom, E. (1993). Structure of the human progesterone receptor gene. *Biochimica et Biophysica Acta (BBA) - Gene Structure and Expression, 1216*(2), 289-292. doi:10.1016/0167-4781(93)90156-8

Mitra, S. K., Hanson, D. A., & Schlaepfer, D. D. (2005). Focal adhesion kinase: in command and control of cell motility. *Nature Reviews Molecular Cell Biology, 6*(1), 56-68. doi:10.1038/nrm1549

Moeglin, E., Desplancq, D., Conic, S., Oulad-Abdelghani, M., Stoessel, A., Chiper, M., . . . Weiss, E. (2019). Uniform Widespread Nuclear Phosphorylation of Histone H2AX Is an Indicator of Lethal DNA Replication Stress. *Cancers, 11*(3), 355. doi:10.3390/cancers11030355

Moorsel, C. J. A. V., Pinedo, H. M., Veerman, G., Bergman, A. M., Kuiper, C. M., Vermorken, J. B., . . . Peters, G. J. (1999). Mechanisms of synergism between cisplatin and gemcitabine in ovarian and non-small-cell lung cancer cell lines. *British Journal of Cancer, 80*(7), 981-990. doi:10.1038/sj.bjc.6690452

Moreno-Aspitia, A., & Perez, E. A. (2009). Treatment Options for Breast Cancer Resistant to Anthracycline and Taxane. *Mayo Clinic Proceedings, 84*(6), 533-545. doi:10.4065/84.6.533

Mote, P. A., Bartow, S., Tran, N., & Clarke, C. L. (2002). Loss of Co-ordinate Expression of Progesterone Receptors A and B is an Early Event in Breast Carcinogenesis. *Breast Cancer Research and Treatment, 72*(2), 163-172. doi:10.1023/a:1014820500738

Moudi, M., Go, R., Yien, C. Y., & Nazre, M. (2013). Vinca alkaloids. *Int J Prev Med, 4*(11), 1231-1235.

Muller, P. A. J., & Vousden, K. H. (2014). Mutant p53 in Cancer: New Functions and Therapeutic Opportunities. *Cancer cell., 25*(3), 304-317. doi:10.1016/j.ccr.2014.01.021

Murakami, Y. (2013). Heterochromatin and Euchromatin. In W. Dubitzky, O. Wolkenhauer, K.-H. Cho, & H. Yokota (Eds.), *Encyclopedia of Systems Biology* (pp. 881-884). New York, NY: Springer New York.

Nagano, M., Hoshino, D., Koshikawa, N., Akizawa, T., & Seiki, M. (2012). Turnover of Focal Adhesions and Cancer Cell Migration. *International Journal of Cell Biology, 2012*, 1-10. doi:10.1155/2012/310616

Nava, M. M., Miroshnikova, Y. A., Biggs, L. C., Whitefield, D. B., Metge, F., Boucas, J., . . . Wickström, S. A. (2020). Heterochromatin-Driven Nuclear Softening Protects the Genome against Mechanical Stress-Induced Damage. *Cell*. doi:10.1016/j.cell.2020.03.052

Nelli, F., Moscetti, L., Natoli, G., Massari, A., D'Auria, G., Chilelli, M., . . . Ruggeri, E. M. (2013). Gemcitabine and carboplatin for pretreated metastatic breast cancer: the

predictive value of immunohistochemically defined subtypes. *International Journal of Clinical Oncology, 18*(2), 343-349. doi:10.1007/s10147-012-0384-x
Noguchi, S., Saito, A., & Nagase, T. (2018). YAP/TAZ Signaling as a Molecular Link between Fibrosis and Cancer. *International Journal of Molecular Sciences, 19*(11), 3674. doi:10.3390/ijms19113674
Oku, Y., Nishiya, N., Shito, T., Yamamoto, R., Yamamoto, Y., Oyama, C., & Uehara, Y. (2015). Small molecules inhibiting the nuclear localization of YAP/TAZ for chemotherapeutics and chemosensitizers against breast cancers. *FEBS Open Bio, 5*(1), 542-549. doi:10.1016/j.fob.2015.06.007
Ospovat, I., Siegelmann-Danieli, N., Grenader, T., Hubert, A., Hamburger, T., & Peretz, T. (2009). Mitomycin C and vinblastine: an active regimen in previously treated breast cancer patients. *Tumori, 95*(6), 683-686.
Owen, R., Sherborne, C., Paterson, T., Green, N. H., Reilly, G. C., & Claeyssens, F. (2016). Emulsion templated scaffolds with tunable mechanical properties for bone tissue engineering. *Journal of the Mechanical Behavior of Biomedical Materials, 54*, 159-172. doi:10.1016/j.jmbbm.2015.09.019
Papademetrio, D. L., Cavaliere, V., Simunovich, T., Costantino, S., Campos, M. D., Lombardo, T., . . . Álvarez, É. (2014). Interplay between autophagy and apoptosis in pancreatic tumors in response to gemcitabine. *Targeted Oncology, 9*(2), 123-134. doi:10.1007/s11523-013-0278-5
Parise, C. A., & Caggiano, V. (2014). Breast Cancer Survival Defined by the ER/PR/HER2 Subtypes and a Surrogate Classification according to Tumor Grade and Immunohistochemical Biomarkers. *Journal of Cancer Epidemiology, 2014*, 469251. doi:10.1155/2014/469251
Paszek, M. J., Zahir, N., Johnson, K. R., Lakins, J. N., Rozenberg, G. I., Gefen, A., . . . Weaver, V. M. (2005). Tensional homeostasis and the malignant phenotype. *Cancer Cell, 8*(3), 241-254. doi:10.1016/j.ccr.2005.08.010
Pathak, M., Dwivedi, S. N., Deo, S. V. S., Thakur, B., Sreenivas, V., & Rath, G. K. (2018). Neoadjuvant chemotherapy regimens in treatment of breast cancer: a systematic review and network meta-analysis protocol. *Systematic Reviews, 7*(1). doi:10.1186/s13643-018-0754-1
Peters, G. J. (2014). Novel Developments in the Use of Antimetabolites. *Nucleosides, Nucleotides and Nucleic Acids, 33*(4-6), 358-374. doi:10.1080/15257770.2014.894197
Petrova, Y. I., Schecterson, L., & Gumbiner, B. M. (2016). Roles for E-cadherin cell surface regulation in cancer. *Mol Biol Cell, 27*(21), 3233-3244. doi:10.1091/mbc.E16-01-0058
Plodinec, M., Loparic, M., Monnier, C. A., Obermann, E. C., Zanetti-Dallenbach, R., Oertle, P., . . . Schoenenberger, C.-A. (2012). The nanomechanical signature of breast cancer. *Nature Nanotechnology, 7*(11), 757-765. doi:10.1038/nnano.2012.167
Poltavets, V., Kochetkova, M., Pitson, S. M., & Samuel, M. S. (2018). The Role of the Extracellular Matrix and Its Molecular and Cellular Regulators in Cancer Cell Plasticity. *Frontiers in Oncology, 8*. doi:10.3389/fonc.2018.00431
Prat, A., Parker, J. S., Karginova, O., Fan, C., Livasy, C., Herschkowitz, J. I., . . . Perou, C. M. (2010). Phenotypic and molecular characterization of the claudin-low intrinsic subtype of breast cancer. *Breast Cancer Research, 12*(5), R68. doi:10.1186/bcr2635
Primo, L. M. F., & Teixeira, L. K. (2020). DNA replication stress: oncogenes in the spotlight. *Genetics and Molecular Biology, 43*(1 suppl 1). doi:10.1590/1678-4685-gmb-2019-0138

Proietti, C., Salatino, M., Rosemblit, C., Carnevale, R., Pecci, A., Kornblihtt, A. R., . . . Elizalde, P. V. (2005). Progestins Induce Transcriptional Activation of Signal Transducer and Activator of Transcription 3 (Stat3) via a Jak- and Src-Dependent Mechanism in Breast Cancer Cells. *Molecular and Cellular Biology, 25*(12), 4826-4840. doi:10.1128/mcb.25.12.4826-4840.2005

Provenzano, P. P., Inman, D. R., Eliceiri, K. W., & Keely, P. J. (2009). Matrix density-induced mechanoregulation of breast cell phenotype, signaling and gene expression through a FAK–ERK linkage. *Oncogene, 28*(49), 4326-4343. doi:10.1038/onc.2009.299

Puls, T. J., Tan, X., Whittington, C. F., & Voytik-Harbin, S. L. (2017). 3D collagen fibrillar microstructure guides pancreatic cancer cell phenotype and serves as a critical design parameter for phenotypic models of EMT. *PLoS One, 12*(11), e0188870. doi:10.1371/journal.pone.0188870

Rabineau , M., Kocgozlu, L., Dujardin, D., Senger, B., Haikel, Y., Voegel, J.-C., . . . Vautier, D. (2013). Contribution of Soft Substrates to Malignancy and Tumor Suppression during Colon Cancer Cell Division. *PLoS ONE, 8*(10), e78468. doi:10.1371/journal.pone.0078468

Rakha, E. A., El-Sayed, M. E., Green, A. R., Paish, E. C., Powe, D. G., Gee, J., . . . Ellis, I. O. (2007). Biologic and Clinical Characteristics of Breast Cancer With Single Hormone Receptor–Positive Phenotype. *Journal of Clinical Oncology, 25*(30), 4772-4778. doi:10.1200/jco.2007.12.2747

Reed, S., & Quelle, D. (2014). p53 Acetylation: Regulation and Consequences. *Cancers, 7*(1), 30-69. doi:10.3390/cancers7010030

Rice, A. J., Cortes, E., Lachowski, D., Cheung, B. C. H., Karim, S. A., Morton, J. P., & Del Río Hernández, A. (2017). Matrix stiffness induces epithelial–mesenchymal transition and promotes chemoresistance in pancreatic cancer cells. *Oncogenesis, 6*(7), e352-e352. doi:10.1038/oncsis.2017.54

Richer, J. K., Jacobsen, B. M., Manning, N. G., Abel, M. G., Wolf, D. M., & Horwitz, K. B. (2002). Differential Gene Regulation by the Two Progesterone Receptor Isoforms in Human Breast Cancer Cells. *Journal of Biological Chemistry, 277*(7), 5209-5218. doi:10.1074/jbc.m110090200

Riedl, A., Schlederer, M., Pudelko, K., Stadler, M., Walter, S., Unterleuthner, D., . . . Dolznig, H. (2017). Comparison of cancer cells in 2D vs 3D culture reveals differences in AKT–mTOR–S6K signaling and drug responses. *Journal of Cell Science, 130*(1), 203-218. doi:10.1242/jcs.188102

Riento, K., & Ridley, A. J. (2003). ROCKs: multifunctional kinases in cell behaviour. *Nature Reviews Molecular Cell Biology, 4*(6), 446-456. doi:10.1038/nrm1128

Roche, J. (2018). The Epithelial-to-Mesenchymal Transition in Cancer. *Cancers, 10*(2), 52. doi:10.3390/cancers10020052

Rowley, J. A., Madlambayan, G., & Mooney, D. J. (1999). Alginate hydrogels as synthetic extracellular matrix materials. *Biomaterials, 20*(1), 45-53. doi:10.1016/s0142-9612(98)00107-0

Ruiz Van Haperen, V. W. T., Veerman, G., Vermorken, J. B., & Peters, G. J. (1993). 2′,2′-Difluoro-deoxycytidine (gemcitabine) incorporation into RNA and DNA of tumour cell lines. *Biochemical Pharmacology, 46*(4), 762-766. doi:10.1016/0006-2952(93)90566-f

Rękawiecki, R., Kowalik, M., & Kotwica, J. (2011). Nuclear progesterone receptor isoforms and their functions in the female reproductive tract. *Polish Journal of Veterinary Sciences, 14*(1), 149-158. doi:10.2478/v10181-011-0024-9

Saldivar, J. C., Cortez, D., & Cimprich, K. A. (2017). The essential kinase ATR: ensuring faithful duplication of a challenging genome. *Nature Reviews Molecular Cell Biology, 18*(10), 622-636. doi:10.1038/nrm.2017.67

Sansregret, L., & Swanton, C. (2017). The Role of Aneuploidy in Cancer Evolution. *Cold Spring Harbor Perspectives in Medicine, 7*(1), a028373. doi:10.1101/cshperspect.a028373

Schindelin, J., Arganda-Carreras, I., Frise, E., Kaynig, V., Longair, M., Pietzsch, T., . . . Cardona, A. (2012). Fiji: an open-source platform for biological-image analysis. *Nature Methods, 9*(7), 676-682. doi:10.1038/nmeth.2019

Schniewind, B., Christgen, M., Kurdow, R., Haye, S., Kremer, B., Kalthoff, H., & Ungefroren, H. (2004). Resistance of pancreatic cancer to gemcitabine treatment is dependent on mitochondria-mediated apoptosis. *International Journal of Cancer, 109*(2), 182-188. doi:10.1002/ijc.11679

Schrader, J., Gordon-Walker, T. T., Aucott, R. L., Van Deemter, M., Quaas, A., Walsh, S., . . . Iredale, J. P. (2011). Matrix stiffness modulates proliferation, chemotherapeutic response, and dormancy in hepatocellular carcinoma cells. *Hepatology, 53*(4), 1192-1205. doi:10.1002/hep.24108

Schäfer, A., Schomacher, L., Barreto, G., Döderlein, G., & Niehrs, C. (2010). Gemcitabine Functions Epigenetically by Inhibiting Repair Mediated DNA Demethylation. *PLoS ONE, 5*(11), e14060. doi:10.1371/journal.pone.0014060

Shahbandi, A., Nguyen, H. D., & Jackson, J. G. (2020). TP53 Mutations and Outcomes in Breast Cancer: Reading beyond the Headlines. *Trends in Cancer, 6*(2), 98-110. doi:10.1016/j.trecan.2020.01.007

Shaked, E., & Gefen, A. (2013). Modeling the Effects of Moisture-Related Skin-Support Friction on the Risk for Superficial Pressure Ulcers during Patient Repositioning in Bed. *Frontiers in Bioengineering and Biotechnology, 1*. doi:10.3389/fbioe.2013.00009

Sharma, A., Singh, K., & Almasan, A. (2012). Histone H2AX phosphorylation: a marker for DNA damage. *Methods Mol Biol, 920*, 613-626. doi:10.1007/978-1-61779-998-3_40

Shen, J., Cao, B., Wang, Y., Ma, C., Zeng, Z., Liu, L., . . . Xie, D. (2018). Hippo component YAP promotes focal adhesion and tumour aggressiveness via transcriptionally activating THBS1/FAK signalling in breast cancer. *Journal of Experimental & Clinical Cancer Research, 37*(1). doi:10.1186/s13046-018-0850-z

Shevelyov, Y. Y., & Ulianov, S. V. (2019). The Nuclear Lamina as an Organizer of Chromosome Architecture. *Cells, 8*(2), 136. doi:10.3390/cells8020136

Shi, X., Liu, S., Kleeff, J., Friess, H., & Buchler, M. W. (2002). Acquired resistance of pancreatic cancer cells towards 5-Fluorouracil and gemcitabine is associated with altered expression of apoptosis-regulating genes. *Oncology, 62*(4), 354-362. doi:10.1159/000065068

Shoulders, M. D., & Raines, R. T. (2009). Collagen Structure and Stability. *Annual Review of Biochemistry, 78*(1), 929-958. doi:10.1146/annurev.biochem.77.032207.120833

Shynlova, O., Mitchell, J. A., Tsampalieros, A., Langille, B. L., & Lye, S. J. (2004). Progesterone and Gravidity Differentially Regulate Expression of Extracellular Matrix Components in the Pregnant Rat Myometrium1. *Biology of Reproduction, 70*(4), 986-992. doi:10.1095/biolreprod.103.023648

Silverstein, M. S., & Cameron, N. R. (2010). PolyHIPEs — Porous Polymers from High Internal Phase Emulsions. *Encyclopedia of Polymer Science and Technology*. doi:10.1002/0471440264.pst571

Smith, M. L., Gourdon, D., Little, W. C., Kubow, K. E., Eguiluz, R. A., Luna-Morris, S., & Vogel, V. (2007). Force-Induced Unfolding of Fibronectin in the Extracellular Matrix of Living Cells. *PLoS Biology, 5*(10), e268. doi:10.1371/journal.pbio.0050268

Song, L.-N., Coghlan, M., & Gelmann, E. P. (2004). Antiandrogen Effects of Mifepristone on Coactivator and Corepressor Interactions with the Androgen Receptor. *Molecular Endocrinology, 18*(1), 70-85. doi:10.1210/me.2003-0189

Sormunen, R. T., Leong, A. S., Vääräniemi, J. P., Fernando, S. S., & Eskelinen, S. M. (1999). Immunolocalization of the fodrin, E-cadherin, and beta-catenin adhesion complex in infiltrating ductal carcinoma of the breast-comparison with an in vitro model. *J Pathol, 187*(4), 416-423. doi:10.1002/(sici)1096-9896(199903)187:4<416::aid-path255>3.0.co;2-d

Strasberg Rieber, M., Zangemeister-Wittke, U., & Rieber, M. (2001). p53-Independent induction of apoptosis in human melanoma cells by a bcl-2/bcl-xL bispecific antisense oligonucleotide. *Clin Cancer Res, 7*(5), 1446-1451.

Sun, H. (2019). *Understanding how extracellular matrix stiffness drives mammary epithelial cell transformation.* (Doctoral Doctoral). The University of Manchester, Retrieved from https://ethos.bl.uk/OrderDetails.do?uin=uk.bl.ethos.779673

Swift, J., Ivanovska, I. L., Buxboim, A., Harada, T., Dingal, P. C. D. P., Pinter, J., . . . Discher, D. E. (2013). Nuclear Lamin-A Scales with Tissue Stiffness and Enhances Matrix-Directed Differentiation. *Science, 341*(6149), 1240104-1240104. doi:10.1126/science.1240104

Syed, S., Schober, J., Blanco, A., & Zustiak, S. P. (2017). Morphological adaptations in breast cancer cells as a function of prolonged passaging on compliant substrates. *PLOS ONE, 12*(11), e0187853. doi:10.1371/journal.pone.0187853

Tabriz, A. G., Hermida, M. A., Leslie, N. R., & Shu, W. (2015). Three-dimensional bioprinting of complex cell laden alginate hydrogel structures. *Biofabrication, 7*(4), 045012. doi:10.1088/1758-5090/7/4/045012

Tajik, A., Zhang, Y., Wei, F., Sun, J., Jia, Q., Zhou, W., . . . Wang, N. (2016). Transcription upregulation via force-induced direct stretching of chromatin. *Nature Materials, 15*(12), 1287-1296. doi:10.1038/nmat4729

Tang, D., Mehta, D., & Gunst, S. J. (1999). Mechanosensitive tyrosine phosphorylation of paxillin and focal adhesion kinase in tracheal smooth muscle. *American Journal of Physiology-Cell Physiology, 276*(1), C250-C258. doi:10.1152/ajpcell.1999.276.1.c250

Taubenberger, A. V., Girardo, S., Träber, N., Fischer-Friedrich, E., Kräter, M., Wagner, K., . . . Guck, J. (2019). 3D Microenvironment Stiffness Regulates Tumor Spheroid Growth and Mechanics via p21 and ROCK. *Advanced Biosystems, 3*(9), 1900128. doi:10.1002/adbi.201900128

Taylor, A. H., McParland, P. C., Taylor, D. J., & Bell, S. C. (2009). The cytoplasmic 60 kDa progesterone receptor isoform predominates in the human amniochorion and placenta at term. *Reprod Biol Endocrinol, 7*, 22. doi:10.1186/1477-7827-7-22

Theocharis, A. D., Skandalis, S. S., Gialeli, C., & Karamanos, N. K. (2016). Extracellular matrix structure. *Advanced Drug Delivery Reviews, 97*, 4-27. doi:10.1016/j.addr.2015.11.001

ThePharmaLetter. (1998). FDA Approves Gemzar For NSC Lung Cancer - Pharmaceutical industry news. Retrieved from https://www.thepharmaletter.com/article/fda-approves-gemzar-for-nsc-lung-cancer

Thomas, A., Redon, C. E., Sciuto, L., Padiernos, E., Ji, J., Lee, M.-J., . . . Pommier, Y. (2018). Phase I Study of ATR Inhibitor M6620 in Combination With Topotecan in Patients With Advanced Solid Tumors. *Journal of Clinical Oncology, 36*(16), 1594-1602. doi:10.1200/jco.2017.76.6915

Théry, M., & Bornens, M. (2008). Get round and stiff for mitosis. *HFSP Journal, 2*(2), 65-71. doi:10.2976/1.2895661

Tian, X., Liu, Z., Niu, B., Zhang, J., Tan, T. K., Lee, S. R., . . . Zheng, G. (2011). E-Cadherin/β-Catenin Complex and the Epithelial Barrier. *Journal of Biomedicine and Biotechnology, 2011*, 1-6. doi:10.1155/2011/567305

Tieszen, C. R., Goyeneche, A. A., Brandhagen, B. N., Ortbahn, C. T., & Telleria, C. M. (2011). Antiprogestin mifepristone inhibits the growth of cancer cells of reproductive and non-reproductive origin regardless of progesterone receptor expression. *BMC Cancer, 11*(1), 207. doi:10.1186/1471-2407-11-207

Tilghman, R. W., Cowan, C. R., Mih, J. D., Koryakina, Y., Gioeli, D., Slack-Davis, J. K., . . . Parsons, J. T. (2010). Matrix Rigidity Regulates Cancer Cell Growth and Cellular Phenotype. *PLoS ONE, 5*(9), e12905. doi:10.1371/journal.pone.0012905

Tiwari, M. (2012). Antimetabolites: established cancer therapy. *J Cancer Res Ther, 8*(4), 510-519. doi:10.4103/0973-1482.106526

Tolis, C., Peters, G. J., Ferreira, C. G., Pinedo, H. M., & Giaccone, G. (1999). Cell cycle disturbances and apoptosis induced by topotecan and gemcitabine on human lung cancer cell lines. *Eur J Cancer, 35*(5), 796-807. doi:10.1016/s0959-8049(98)00425-0

Toschi, L., Finocchiaro, G., Bartolini, S., Gioia, V., & Cappuzzo, F. (2005). Role of gemcitabine in cancer therapy. *Future Oncol, 1*(1), 7-17. doi:10.1517/14796694.1.1.7

Trabert, B., Sherman, M. E., Kannan, N., & Stanczyk, F. Z. (2020). Progesterone and Breast Cancer. *Endocrine Reviews, 41*(2), 320-344. doi:10.1210/endrev/bnz001

Tu, X., Kahila, M. M., Zhou, Q., Yu, J., Kalari, K. R., Wang, L., . . . Mutter, R. W. (2018). ATR Inhibition Is a Promising Radiosensitizing Strategy for Triple-Negative Breast Cancer. *Molecular Cancer Therapeutics, 17*(11), 2462-2472. doi:10.1158/1535-7163.mct-18-0470

Tung, L., Abdel-Hafiz, H., Shen, T., Harvell, D. M. E., Nitao, L. K., Richer, J. K., . . . Horwitz, K. B. (2006). Progesterone Receptors (PR)-B and -A Regulate Transcription by Different Mechanisms: AF-3 Exerts Regulatory Control over Coactivator Binding to PR-B. *Molecular Endocrinology, 20*(11), 2656-2670. doi:10.1210/me.2006-0105

Ubhi, T., & Brown, G. W. (2019). Exploiting DNA Replication Stress for Cancer Treatment. *Cancer Research, 79*(8), 1730-1739. doi:10.1158/0008-5472.can-18-3631

Urruticoechea, A., Archer, C. D., Assersohn, L. A., Gregory, R. K., Verrill, M., Mendes, R., . . . Johnston, S. R. D. (2005). Mitomycin C, vinblastine and cisplatin (MVP): an active and well-tolerated salvage regimen for advanced breast cancer. *British Journal of Cancer, 92*(3), 475-479. doi:10.1038/sj.bjc.6602367

Vendetti, F. P., Lau, A., Schamus, S., Conrads, T. P., O'Connor, M. J., & Bakkenist, C. J. (2015). The orally active and bioavailable ATR kinase inhibitor AZD6738 potentiates the anti-tumor effects of cisplatin to resolve ATM-deficient non-small cell lung cancer in vivo. *Oncotarget, 6*(42), 44289-44305. doi:10.18632/oncotarget.6247

Vienonen, A., Syvälä, H., Miettinen, S., Tuohimaa, P., & Ylikomi, T. (2002). Expression of progesterone receptor isoforms A and B is differentially regulated by estrogen in different breast cancer cell lines. *The Journal of Steroid Biochemistry and Molecular Biology, 80*(3), 307-313. doi:10.1016/s0960-0760(02)00027-4

Visconti, R., Monica, R. D., & Grieco, D. (2016). Cell cycle checkpoint in cancer: a therapeutically targetable double-edged sword. *Journal of Experimental & Clinical Cancer Research, 35*(1). doi:10.1186/s13046-016-0433-9

Waks, A. G., & Winer, E. P. (2019). Breast Cancer Treatment: A Review. *JAMA, 321*(3), 288-300. doi:10.1001/jama.2018.19323

Walters, B. D., & Stegemann, J. P. (2014). Strategies for directing the structure and function of three-dimensional collagen biomaterials across length scales. *Acta Biomater, 10*(4), 1488-1501. doi:10.1016/j.actbio.2013.08.038
Wang, H.-C., & Lee, W.-S. (2016). Molecular mechanisms underlying progesterone-enhanced breast cancer cell migration. *Scientific Reports, 6*(1), 31509. doi:10.1038/srep31509
Wang, L.-M., Chang, H., Zhang, H., Ren, K.-F., Li, H., Hu, M., . . . Ji, J. (2015). Dynamic stiffness of polyelectrolyte multilayer films based on disulfide bonds for in situ control of cell adhesion. *Journal of Materials Chemistry B, 3*(38), 7546-7553. doi:10.1039/c5tb01151e
Wazir, U., Ahmed, M. H., Bridger, J. M., Harvey, A., Jiang, W. G., Sharma, A. K., & Mokbel, K. (2013). The clinicopathological significance of lamin A/C, lamin B1 and lamin B receptor mRNA expression in human breast cancer. *Cell Mol Biol Lett, 18*(4), 595-611. doi:10.2478/s11658-013-0109-9
Wei, L. L., Norris, B. M., & Baker, C. J. (1997). An N-terminally truncated third progesterone receptor protein, PRC, forms heterodimers with PRB but interferes in PRB-DNA binding. *The journal of steroid biochemistry and molecular biology., 62*(4), 287-297. doi:10.1016/S0960-0760(97)00044-7
Whitfield, M. L., George, L. K., Grant, G. D., & Perou, C. M. (2006). Common markers of proliferation. *Nature Reviews Cancer, 6*(2), 99-106. doi:10.1038/nrc1802
Willis, N., & Rhind, N. (2009). Regulation of DNA replication by the S-phase DNA damage checkpoint. *Cell Division, 4*(1), 13. doi:10.1186/1747-1028-4-13
Willson, M. L., Burke, L., Ferguson, T., Ghersi, D., Nowak, A. K., & Wilcken, N. (2019). Taxanes for adjuvant treatment of early breast cancer. *Cochrane Database of Systematic Reviews*. doi:10.1002/14651858.cd004421.pub3
Xie, Z., Zhang, Y., Jin, C., & Fu, D. (2018). Gemcitabine-based chemotherapy as a viable option for treatment of advanced breast cancer patients: a meta-analysis and literature review. *Oncotarget, 9*(6), 7148-7161. doi:10.18632/oncotarget.23426
Xu, B., Sun, Z., Liu, Z., Guo, H., Liu, Q., Jiang, H., . . . Shao, C. (2011). Replication Stress Induces Micronuclei Comprising of Aggregated DNA Double-Strand Breaks. *PLoS ONE, 6*(4), e18618. doi:10.1371/journal.pone.0018618
Yano, Y., Geibel, J., & Sumpio, B. E. (1996). Tyrosine phosphorylation of pp125FAK and paxillin in aortic endothelial cells induced by mechanical strain. *Am J Physiol, 271*(2 Pt 1), C635-649. doi:10.1152/ajpcell.1996.271.2.C635
Yarbro, J. W. (1992). Mechanism of action of hydroxyurea. *Semin Oncol, 19*(3 Suppl 9), 1-10.
Yeh, Y.-C., Ling, J.-Y., Chen, W.-C., Lin, H.-H., & Tang, M.-J. (2017). Mechanotransduction of matrix stiffness in regulation of focal adhesion size and number: reciprocal regulation of caveolin-1 and β1 integrin. *Scientific Reports, 7*(1). doi:10.1038/s41598-017-14932-6
Yeung, T., Georges, P. C., Flanagan, L. A., Marg, B., Ortiz, M., Funaki, M., . . . Janmey, P. A. (2005). Effects of substrate stiffness on cell morphology, cytoskeletal structure, and adhesion. *Cell Motil Cytoskeleton, 60*(1), 24-34. doi:10.1002/cm.20041
Yoon, D. H., Shin, J. S., Jin, D. H., Hong, S. W., Jung, K. A., Kim, S. M., . . . Kim, T. W. (2012). The survivin suppressant YM155 potentiates chemosensitivity to gemcitabine in the human pancreatic cancer cell line MiaPaCa-2. *Anticancer Res, 32*(5), 1681-1688.
You, Y., Zheng, Q., Dong, Y., Xie, X., Wang, Y., Wu, S., . . . Ren, Z. (2016). Matrix stiffness-mediated effects on stemness characteristics occurring in HCC cells. *Oncotarget, 7*(22), 32221-32231. doi:10.18632/oncotarget.8515

Yuan, F., Wang, J., Li, R., Zhao, X., Zhang, Y., Liu, B., . . . Hu, Y. (2019). A New Regulatory Mechanism Between P53 And YAP Crosstalk By SIRT1 Mediated Deacetylation To Regulate Cell Cycle And Apoptosis In A549 Cell Lines. *Cancer Manag Res, 11*, 8619-8633. doi:10.2147/cmar.s214826

Zanotelli, M. R., & Reinhart-King, C. A. (2018). Mechanical Forces in Tumor Angiogenesis. *Adv Exp Med Biol, 1092*, 91-112. doi:10.1007/978-3-319-95294-9_6

Zhang, B., Luo, Q., Chen, Z., Shi, Y., Ju, Y., Yang, L., & Song, G. (2016). Increased nuclear stiffness via FAK-ERK1/2 signaling is necessary for synthetic mechano-growth factor E peptide-induced tenocyte migration. *Scientific Reports, 6*(1), 18809. doi:10.1038/srep18809

Zhang, C.-Z., Spektor, A., Cornils, H., Francis, J. M., Jackson, E. K., Liu, S., . . . Pellman, D. (2015). Chromothripsis from DNA damage in micronuclei. *Nature, 522*(7555), 179-184. doi:10.1038/nature14493

Zhang, J., Dai, Q., Park, D., & Deng, X. (2016). Targeting DNA Replication Stress for Cancer Therapy. *Genes, 7*(8), 51. doi:10.3390/genes7080051

Zhang, J., Wang, Z., Hu, X., Wang, B., Wang, L., Yang, W., . . . Shao, Z. (2015). Cisplatin and gemcitabine as the first line therapy in metastatic triple negative breast cancer. *International Journal of Cancer, 136*(1), 204-211. doi:10.1002/ijc.28966

Zheng, R.-R., Hu, W., Sui, C.-G., Ma, N., & Jiang, Y.-H. (2014). Effects of doxorubicin and gemcitabine on the induction of apoptosis in breast cancer cells. *Oncology Reports, 32*(6), 2719-2725. doi:10.3892/or.2014.3513

Zou, Y., Liu, Y., Wu, X., & Shell, S. M. (2006). Functions of human replication protein A (RPA): From DNA replication to DNA damage and stress responses. *Journal of Cellular Physiology, 208*(2), 267-273. doi:10.1002/jcp.20622

Zustiak, S., Nossal, R., & Sackett, D. L. (2014). Multiwell stiffness assay for the study of cell responsiveness to cytotoxic drugs. *Biotechnology and Bioengineering, 111*(2), 396-403. doi:10.1002/bit.25097

Zysset, P. K., Guo, X. E., Hoffler, C. E., Moore, K. E., & Goldstein, S. A. (1999). Elastic modulus and hardness of cortical and trabecular bone lamellae measured by nanoindentation in the human femur. *J Biomech, 32*(10), 1005-1012. doi:10.1016/s0021-9290(99)00111-6